Ollscoil na hÉireann, Corcaigh

National University of Ireland, Cork

Therapeutic Trials and Translational Gaps:

Respiratory Outcomes in the *mdx* mouse model of Duchenne Muscular Dystrophy

Michael N. Maxwell, BSc (Honours)

for the degree of

Doctor of Philosophy

University College Cork

Department of Physiology

Under the supervision of:

Professor Ken D. O'Halloran PhD

&

Dr. Fiona McDonald PhD

June 2025

Table of Contents

Declaration

"This is to certify that the work I am submitting is my own and has not been submitted for another degree, either at University College Cork or elsewhere. All external references and sources are clearly acknowledged and identified within the contents. I have read and understood the regulations of University College Cork concerning plagiarism and intellectual property."

Michael Maxwell June 2025

Acknowledgements

I would like to begin by expressing my appreciation to everyone in the lab and all members of the department of Physiology for their support, collaboration, and friendship. The positive and encouraging environment you created made this journey rewarding and enjoyable and years I will look back on fondly. I always knew that I had people I could count on if I needed help or support in any way.

I am profoundly grateful to my supervisor, Ken, for his unwavering support, kindness, and for always believing in me. His guidance and generosity have been instrumental in my academic and personal development, and I am truly fortunate to have had his mentorship. I have loved every second in the lab. From the challenges to the laughs and chats. I have thoroughly enjoyed every second that I spent over the last 4 years working in his lab. Thank you for taking a chance on a guy from Dublin that cold called about a position in your lab a year too early.

I would also like to express my deepest gratitude to my family for their unwavering support, encouragement and belief in me.

To Allyson, for your love, support, and patience. Your understanding and encouragement have meant the world to me, especially during the most challenging moments.

List of abbreviations

DMD	Duchenne Muscular Dystrophy
mdx	Dystrophin-deficient X-linked muscular dystrophy mouse model of DMD
NAC	N-acetylcysteine
AIH	Acute Intermittent Hypoxia
LTF	Long-Term Facilitation
EMG	Electromyogram
FVC	Forced Vital Capacity
MIP	Maximal Inspiratory Pressure
MEP	Maximal Expiratory Pressure
SNIP	Sniff Nasal Inspiratory Pressure
DGC	Dystrophin Glycoprotein Complex
ROS	Reactive Oxygen Species
EDL	Extensor Digitorum Longus
TGF-β	Transforming Growth Factor Beta
IL-6	Interleukin 6
TNF-α	Tumour Necrosis Factor Alpha
CoQ10	Coenzyme Q10
FDA	Food and Drug Administration
BMI	Body Mass Index
CSA	Cross-Sectional Area
V_T	Tidal Volume
$\dot{V}_I$	Minute Ventilation
$\dot{V}CO_2$	Metabolic CO_2 Production
H&E	Haematoxylin and Eosin (staining)
qPCR	Quantitative Polymerase Chain Reaction

L_o	Optimum Length (of muscle)
P_o	Tetanic Force
EIC	External Intercostal
PS	Parasternal Intercostal
SCAL	Scalene
CM	Cleidomastoid
SM	Sternomastoid
SH	Sternohyoid
TRAP	Trapezius
HcHx	Hypercapnic Hypoxia
SpO_2	Peripheral Capillary Oxygen Saturation
Ffar2	Free Fatty Acid Receptor 2
IGF	Insulin-like Growth Factor
IL1B	Interleukin 1 Beta
MEF2C	Myocyte Enhancer Factor 2C
Mstn	Myostatin
Murf-1	Muscle RING-finger Protein-1
MyoD	Myogenic Differentiation
MyoG	Myogenin
NFκB	Nuclear Factor Kappa-B
NOX	NADPH Oxidase
Nr1h4	Nuclear Receptor Subfamily 1 Group H Member 4
Nrf2	Nuclear Factor Erythroid 2-related Factor 2
PARK-2	Parkin RBR E3 Ubiquitin Protein Ligase
Pink1	PTEN-induced Kinase 1
Sirt1	Sirtuin-1

SOD1 Superoxide Dismutase 1

TGFβ-1 Transforming Growth Factor Beta-1

HDAC Histone Deacetylase

Thesis abstract

Duchenne muscular dystrophy (DMD) is a devastating X-linked neuromuscular disorder marked by progressive muscle degeneration and respiratory failure, primarily due to mutations in the *DMD* gene encoding dystrophin. The *mdx* mouse, which lacks functional dystrophin, is the most widely used preclinical model for DMD, but the trajectory of respiratory dysfunction and the effects of various interventions on respiratory musculature in this model remain incompletely defined. This thesis comprehensively investigates the impact of acute intermittent hypoxia (AIH), chronic N-acetylcysteine (NAC) administration, intermittent prednisone, and combined prednisone plus NAC treatment on respiratory system performance in the *mdx* mouse, while also evaluating the translational value of this model for studying respiratory decline in DMD.

The initial focus was on AIH, a therapeutic intervention that exposes subjects to repeated short bouts of hypoxia, which in other neuromuscular disorders has been shown to induce respiratory plasticity and enhanced ventilatory capacity. However, in *mdx* mice, AIH failed to elicit ventilatory long-term facilitation (LTF). While there was a significant increase in minute ventilation post-AIH, this was matched by a corresponding rise in metabolic CO_2 production, resulting in no net improvement in ventilatory efficiency. This suggests that AIH does not induce beneficial neural or muscular adaptations in the dystrophic respiratory system of *mdx* mice, limiting its therapeutic potential for DMD.

Chronic administration of NAC, a thiol-based antioxidant with anti-inflammatory and anti-fibrotic properties, was evaluated over a three-month period. Despite

its mechanistic promise, chronic NAC treatment did not improve diaphragm force generation, reduce fibrosis, or diminish immune cell infiltration in the *mdx* diaphragm. Respiratory parameters, including ventilatory responsiveness to hypercapnic hypoxia and peak inspiratory pressures, remained unaffected. These findings indicate that NAC monotherapy is insufficient to counteract the multifactorial dystropathology of DMD, at least in the context of the *mdx* mouse model.

Intermittent prednisone, the mainstay corticosteroid therapy in DMD, and its combination with NAC were also assessed. Neither regimen resulted in significant improvements in diaphragm specific force, respiratory muscle electromyogram (EMG) amplitudes, or overall respiratory system performance. The lack of additive or synergistic benefit from combining anti-inflammatory and antioxidant strategies further underscores the complexity of *mdx* pathology and the limitations of targeting isolated pathways.

A critical component of this thesis was the longitudinal characterization of respiratory function in *mdx* mice. Despite severe and progressive diaphragm pathology, including extensive fibrosis by 16 months of age, *mdx* mice maintained stable peak inspiratory pressures and ventilatory capacity until advanced age. This contrasts starkly with the human DMD phenotype, where respiratory decline is evident from early adolescence and progresses steadily. The data suggest that compensatory recruitment of accessory respiratory muscles in *mdx* mice masks respiratory insufficiency until late in the disease

course, thereby reducing the translational relevance of this model for studying early-stage respiratory decline and therapeutic intervention.

In summary, this thesis demonstrates that AIH, chronic NAC, intermittent prednisone, and their combination do not meaningfully preserve respiratory function in the *mdx* mouse model of DMD. The findings highlight the need for multitarget therapeutic strategies that concurrently address oxidative stress, inflammation, and fibrosis. Furthermore, the resilience of the *mdx* respiratory system limits its utility for preclinical studies aimed at early intervention to ameliorate ventilatory insufficiency, emphasizing the need for next-generation animal models that more faithfully recapitulate the human disease trajectory. The work also calls for the refinement of clinical biomarkers—to move beyond forced vital capacity (FVC) and maximal inspiratory pressure (MIP)—to enable earlier detection of respiratory compromise and more sensitive assessment of therapeutic efficacy. Collectively, this thesis provides a critical framework for reevaluating both therapeutic development and model selection in DMD research, advocating for approaches that prioritize human-relevant pathophysiological endpoints and combinatorial treatment strategies.

Chapter 1. Introduction

1.1 DMD and its clinical significance

Duchenne muscular dystrophy (DMD) is a life-limiting X-linked neuromuscular disease caused by a mutation on the *DMD* gene that encodes for the muscle isoform (Dp427m) of the structural protein dystrophin (Aartsma-Rus et al., 2006; Hoffman et al., 1987a). The *DMD* gene consists of 2.3 Mb of genomic DNA making it the largest known gene in humans (Ahn & Kunkel, 1993). Over 7,000 different mutations have been found with 80% of all mutations classed as large mutations (1 exon or larger, 86% deletions, 14% duplications), and 20% of all mutations considered small mutations (smaller than 1 exon, 25% small deletions, 9% small insertions, 14% affected the splice sites, 50% nonsense mutations, 2% missense mutations, 0.3% mid-intronic mutations)(Bladen et al., 2015). The most common mutations exist in hotspots located between exons 45-53 (Aartsma-Rus et al., 2006; Bladen et al., 2015).

Dystrophin is an essential part of the dystrophin glycoprotein complex (DGC), which serves as a structural link between the cytoskeleton inside muscle cells and the extracellular matrix, through the sarcolemma. For a detailed and clear schematic representation of dystrophin in the DGC in DMD, readers are referred to a recent open-access review from our laboratory (Delaney & O'Halloran, 2024). The DGC stabilizes muscle fibres during contraction and shields them from injury caused by mechanical stress (Gao & McNally, 2015). In DMD, the absence of dystrophin disrupts this protective mechanism, making muscle fibres susceptible to contraction-induced damage. Over time, this leads to progressive muscle degeneration, declining muscle function, infiltration by

immune cells, persistent inflammation, and eventual muscle wasting (Deconinck & Dan, 2007; Duan et al., 2021; McDouall et al., 1990; Schmalbruch, 1984).

DMD is the most common childhood muscular dystrophy. Approximately 1 in 3500 to 1 in 5000 boys are affected worldwide (Crisafulli et al., 2020). At the age of 2 to 3 years of age, DMD boys start to exhibit the initial motor deficit symptoms such as a waddling gait, trouble climbing stairs, and frequent falls (Emery, 2002). With the rapid nature of the disease, by the age of 9 DMD boys are wheelchair bound with additional loss of distal limb function (Emery, 2002). At the age of 10 years the sign of respiratory insufficiency due to respiratory muscle weakness begins with a reduction in pressure generating capacity and reduction in ventilatory capacity (Fauroux et al., 2015; Khirani et al., 2014). As DMD is a progressive disease, sleep disordered breathing such as obstructive sleep apnoea begins in the early teenage years and progressively worsens to the need for full-time assisted ventilation by the age of 20 years (Emery, 2002). With improvements in the standard of clinical care with the use of non-invasive mechanical ventilation, management of spinal deformities, and earlier treatment implementation, the median life expectancy has increased from late teens to late twenties (Broomfield et al., 2021; Passamano et al., 2012).

No curative therapies exist for Duchenne muscular dystrophy (DMD), and corticosteroids remain the primary pharmacological intervention. Drugs like prednisone, prednisolone, and deflazacort are routinely administered to mitigate disease progression and prolong ambulatory function (Birnkrant et al.,

2018) but ultimately these interventions are not curative. While these drugs provide initial improvements in mobility, their long-term efficacy is limited, as respiratory capacity continues to deteriorate at a consistent annual rate (Fauroux et al., 2015; Khirani et al., 2014).

Respiratory complications in DMD remain inadequately characterized, complicating therapeutic strategies. Conventional tools such as spirometry and respiratory muscle assessments lack the sensitivity to map the full spectrum of respiratory decline—from early-stage impairment to terminal respiratory failure. This gap hinders the development of targeted interventions to preserve pulmonary health in affected individuals (Finder, 2009; Finder et al., 2004; Hudson et al., 2025a; Sheehan et al., 2018).

1.2 Defining the Focus and Scope of the Thesis

1.2.1 The *mdx* mouse model of DMD

The dystrophin-deficient *mdx* mouse serves as a pivotal model for studying DMD. The *mdx* mouse has a naturally occurring point mutation in exon 23 of the *DMD* gene, as a result, it lacks the dystrophin protein isoform Dp427 and was identified on the C57BL/10ScSn genetic background (Bulfield et al., 1984). The mutation leads to a premature stop of protein translation, resulting in non-functional dystrophin (Sicinski et al., 1989). In the *mdx* mouse, as in human DMD patients, absence of dystrophin predisposes the sarcolemma to damage and degeneration during repeated cycles of muscle contraction (Burns, Drummond, et al., 2019; Burns et al., 2018; Burns, Murphy, et al., 2019; O'Halloran et al.,

2023). The pathophysiological consequences of dystrophin deficiency manifest differently across various muscle groups. Limb muscles in the *mdx* mouse model of DMD exhibit structural and functional anomalies characterized by early hypertrophy followed by progressive weakness (Massopust et al., 2020). While younger *mdx* mice display limb muscle hypertrophy due to fibre branching and regenerative hyperplasia, this increased size does not translate to greater strength (Lynch et al., 2001).

The diaphragm muscle in both human DMD patients and the *mdx* mouse model undergoes progressive fibrosis, which contributes substantially to respiratory insufficiency. Fibrosis arises as part of the chronic injury and repair process following repeated cycles of muscle fibre damage due to absent dystrophin, leading to extracellular matrix deposition and loss of functional muscle tissue (Mann et al., 2011). Histological studies of human DMD diaphragms consistently demonstrate fibrotic remodelling correlated with disease severity (Smith et al., 1989). In the *mdx* mouse diaphragm, fibrosis is evident by 3 to 6 months of age, representing an accelerated timeline relative to the progressive, years-long pathology observed in humans that often begins in early childhood (Massopust et al., 2020; O'Halloran et al., 2023; Slyne et al., 2025; Stedman et al., 1991).

The diaphragm exhibits severe muscle dysfunction and fibrosis like that observed in DMD patients. This makes the *mdx* mouse a valuable model for studying diaphragm remodelling as damage is prevalent in the first few weeks of life and significantly increased at 4 months of age (O'Halloran et al., 2023). Respiratory muscle pathology in *mdx* mice includes structural remodelling,

functional weakness, and disrupted respiratory regulation (Burns, Murphy, et al., 2019; Burns, Roy, et al., 2017; Mhandire et al., 2022; O'Halloran et al., 2023; Slyne et al., 2025). EMG analyses reveal diminished activity in obligatory muscles of breathing, pointing to neuromuscular deficits that may underlie impaired respiratory output (Burns, Murphy, et al., 2019; O'Halloran et al., 2023; Personius & Sawyer, 2006; Slyne et al., 2025). Longitudinal assessments of inspiratory pressure and EMG activity in wildtype and *mdx* mice aged 1–16 months demonstrates that peak inspiratory pressure remains stable until 8 months and deficits are seen at 12 months and a greater deficit at 16 months of age (O'Halloran et al., 2023).

Breathing is controlled by a distributed network of brainstem neurons that generate rhythmic output to the respiratory muscles, principally via the pre-Bötzinger complex and parafacial respiratory group, which serve as central pattern generators for inspiration and actively coordinate respiratory muscle activation across different phases of the breathing cycle (Del Negro et al., 2018; Prabhakar & Peng, 2004; J. C. Smith et al., 2009). Motor drive descends from these brainstem centres to phrenic and intercostal motor neurons in the spinal cord, enabling contraction of the diaphragm and intercostal muscles during inspiration (Fogarty et al., 2018). Expiration is typically passive but can involve active recruitment of abdominal and internal intercostal muscles under conditions of increased ventilatory demand (Abraham et al., 2002; Aliverti, 2016). Sensory feedback constantly modulates this motor output: peripheral chemoreceptors in the carotid bodies respond rapidly to decreased arterial

oxygen to augment ventilation, while central chemoreceptors in the brainstem are sensitive to CO_2-dependent changes in pH (Prabhakar & Peng, 2004). Additional afferents from pulmonary stretch receptors, airway mechanoreceptors, and muscle proprioceptors—largely conveyed via the vagus nerve and exemplified by the Breuer–Hering inflation reflex—further modulate respiratory pattern. This integration of central rhythm generation and peripheral/sensory feedback underpin the adaptability of breathing and is critically relevant to studies involving vagotomy, which disrupts vagal afferent input to the respiratory centres (Hayashi et al., 1996; Molkov et al., 2013; Simon et al., 1991).

Preservation of peak inspiratory pressure over much of the natural history of disease in *mdx* mice suggests compensatory mechanisms involving accessory respiratory muscles, and abdominal musculature, which may be enabled by a stiffened, remodelled diaphragm characteristic of DMD. Notably, this adaptation appears independent of heightened motor drive in accessory motor pathways, highlighting the diaphragm's altered biomechanical properties as a critical factor (O'Halloran et al., 2023). Complementary recordings of respiratory pressures and electromyography (EMG) can help chart the natural history of DMD by evaluating temporal progression of the disease (Fauroux et al., 2009, 2015; J. D. Finder, 2009; J. D. Finder et al., 2004; Hahn et al., 1997). Our group has contributed an in-depth characterisation of inspiratory pressure and eight respiratory muscles including obligatory and accessory muscles in the *mdx* mouse (O'Halloran et al., 2023).

1.2.2 Acute intermittent hypoxia and respiratory plasticity

Respiratory insufficiency is a leading cause of death in DMD patients. DMD is a progressive disorder and ventilatory capacity reduces annually after the age of 10 until premature death due to respiratory failure (Fauroux et al., 2015; Khirani et al., 2014). Acute intermittent hypoxia (AIH) is a therapeutic intervention involving repeated, brief exposures to low oxygen concentrations (hypoxia), each separated by periods of normal oxygen exposure (normoxia), over a short duration. Exposure to AIH elicits a form of respiratory plasticity known as long-term facilitation (LTF), which increases respiratory motor output via a central spinal mechanism (Bach & Mitchell, 1996). This process begins with episodic serotonin release in the spinal cord during hypoxic episodes, activating 5-HT2A receptors on phrenic motor neurons and initiating downstream protein kinase signalling cascades (Baker-Herman & Mitchell, 2002). An essential mediator of LTF is the generation of ROS, particularly superoxide, via NADPH oxidase localized in phrenic motor neurons (Macfarlane et al., 2009). The ROS produced during AIH act to shift the cellular balance toward protein kinase activation and inhibit phosphatase activity, favouring net phosphorylation and persistent plasticity in respiratory motor output (Macfarlane et al., 2009; MacFarlane & Mitchell, 2008). Thus, both serotonin-dependent signalling and ROS formation are required for AIH-induced LTF, with the central spinal cord serving as the primary anatomical site of integration for these molecular pathways (Baker-Herman & Mitchell, 2002; MacFarlane & Mitchell, 2008).

LTF is a form of neuroplasticity that is characterized by serotonin dependent signalling pathways that strengthen synaptic efficacy within spinal respiratory

networks leading to prolonged increases in phrenic nerve activity (Millhorn et al., 1980). LTF exemplifies the respiratory system's adaptive capacity to optimize ventilation in response to stressors, a process critical for maintaining homeostasis. Interest has grown in developing AIH interventions to treat ventilatory insufficiency, with promising results in spinal cord injury and amyotrophic lateral sclerosis (Golder & Mitchell, 2005; Nichols et al., 2017; Sajjadi et al., 2022; Sutor et al., 2021).

Golder and Mitchell (2005) demonstrated that acute intermittent hypoxia strengthens serotonin-dependent spinal synaptic plasticity (phrenic long-term facilitation) in rats with chronic cervical spinal cord injury, enhancing respiratory motor output via restored crossed-spinal pathways (Golder & Mitchell, 2005).

Sajjadi and colleagues (2022) demonstrated that acute intermittent hypoxia (AIH) enhances motor output to respiratory muscles in individuals with amyotrophic lateral sclerosis (ALS), resulting in improved tidal volume and heightened activation of respiratory musculature. This neuroplastic adaptation partially counteracts the progressive ventilatory decline characteristic of ALS (Sajjadi et al., 2022).

Nichols et al. (2017) demonstrated that enhanced phrenic long-term facilitation in end-stage SOD1^{G93A} rats, a model of ALS, arises from amplified signalling through the serotonin-dependent Q pathway (BDNF/MEK/ERK) rather than recruitment of alternative plasticity mechanisms, despite significant phrenic motor neuron loss (Nichols et al., 2017).

Sutor et al. (2021) found that a single session of AIH significantly increased maximal inspiratory pressure in adults with chronic spinal cord injury, without affecting other measures of breathing function, suggesting selective enhancement of inspiratory muscle strength through respiratory motor plasticity (Sutor et al., 2021).

In pathological states like DMD, where structural and functional deficits impair primary respiratory muscles, LTF may underpin compensatory mechanisms that temporarily stabilize breathing. However, the interplay between such plasticity and the progressive biomechanical constraints of dystrophic remodelling—such as diaphragm stiffening—remains poorly understood. Investigating LTF in models of neuromuscular disease could illuminate novel therapeutic targets to preserve respiratory autonomy in vulnerable populations.

1.2.3 Corticosteroids

1.2.3.1 Prednisone and Deflazacort

Corticosteroid therapy remains a cornerstone of disease management in DMD, yet its benefits and risks in the non-ambulatory phase have been less well characterized than in ambulatory patients and this tends to be around the time that respiratory decline begins. McDonald et al. (2023) addressed this gap by conducting a longitudinal cohort study of 86 non-ambulatory boys with DMD, comparing outcomes among those treated with deflazacort, prednisone, or no steroids (McDonald et al., 2023). Over an average follow-up of nearly two years, both deflazacort and prednisone were associated with significantly slower declines in pulmonary function (as measured by forced vital capacity percent-

predicted), cardiac function (left ventricular ejection fraction), and upper limb abilities compared to no steroid treatment. Notably, deflazacort was linked to even slower deterioration in upper limb function than prednisone, with patients on deflazacort experiencing a more gradual loss of hand-to-mouth function and the ability to eat independently or turn in bed unaided—milestones considered highly relevant to quality of life. Both steroids delayed the progression to clinically significant thresholds of respiratory and cardiac impairment and preserved important daily functions longer than in untreated patients (McDonald et al., 2023).

Despite these benefits, steroid therapy was not without drawbacks. Deflazacort use was associated with a more rapid decline in height, reflecting greater growth suppression compared to prednisone or no steroids, while both steroid groups experienced fewer rapid declines in body mass index than untreated patients. The study also highlighted variability in dosing regimens, with deflazacort more often administered daily and at higher relative doses than prednisone, potentially influencing the observed efficacy differences (McDonald et al., 2023).

Overall, the findings from McDonald et al. (2023) provide important evidence that continuing corticosteroid therapy after loss of ambulation in DMD can meaningfully slow the progression of respiratory, cardiac, and upper limb decline, with deflazacort potentially offering modest advantages over prednisone in preserving function. However, FVC% predicted demonstrates limited utility as a standalone respiratory biomarker in DMD patients, owing to its insufficient sensitivity for detecting functional decline (Trucco & O'Halloran,

2025). The dynamic and interconnected mechanisms of respiratory health cannot be fully captured by isolated metrics and necessitates a multimodal analysis across multiple factors (Trucco & O'Halloran, 2025). These results support the ongoing use of steroids in later disease stages, while underscoring the need for individualized risk–benefit assessment and further research to optimize long-term management strategies in non-ambulatory DMD patients (McDonald et al., 2023).

1.2.3.2 Vamorolone

Other corticosteroids have been developed and are suggested to be safer with fewer side effects such as vamorolone. First studied in the *mdx* mouse, it is now an FDA approved treatment (AGAMREE®) for DMD in patients 2 years of age or older. Vamorolone is a novel steroidal anti-inflammatory drug developed to address the limitations of traditional glucocorticoid therapy in DMD, particularly the significant adverse effects associated with long-term steroid use. Three key clinical studies have evaluated the efficacy and safety of vamorolone across short, medium, and long-term treatment periods.

Initial evidence from a 24-week open-label, dose-escalation trial demonstrated that vamorolone at doses of 2.0 mg/kg/day and above led to clinically meaningful improvements in motor function, including time to stand from supine, 6-minute walk distance, and other gross motor assessments. These benefits were dose-dependent and supported by secondary outcome measures (Hoffman et al., 2019). Importantly, vamorolone was generally well tolerated, with a lower

incidence of classic glucocorticoid-associated side effects such as growth stunting and bone morbidity. Adverse events were mostly mild or moderate, and the drug showed a favourable biomarker profile for bone health and adrenal function compared to standard glucocorticoids (Hoffman et al., 2019).

A subsequent 48-week randomized, double-blind trial confirmed and extended these findings. Vamorolone at 6 mg/kg/day maintained or improved motor function over 48 weeks, with efficacy comparable to prednisone but with a more favourable safety profile (Dang et al., 2024). Notably, vamorolone-treated participants exhibited normalized growth trajectories and reversal of prednisone-induced bone turnover suppression. The incidence of Cushingoid features, behavioural disturbances, and gastrointestinal symptoms was reduced compared to prednisone, and BMI increases stabilized after the initial treatment period. However, some degree of adrenal suppression persisted, and higher doses were occasionally associated with mild glucocorticoid-like side effects such as hypertrichosis and anxiety. Both studies highlighted the importance of dose selection and the need for ongoing monitoring of adrenal function and weight (Dang et al., 2024).

The long-term efficacy and safety of vamorolone have been evaluated in a 30-month open-label extension study involving boys who completed the initial dose-finding trial (Mah et al., 2022). Over 2.5 years of treatment at doses of 2.0 mg/kg/day or higher, vamorolone was associated with sustained maintenance of muscle strength and function, as measured by time to stand velocity, 6-minute walk test, and NorthStar Ambulatory Assessment. When compared with

matched historical cohorts treated with glucocorticoids, vamorolone demonstrated similar efficacy in disease modification but was associated with a significantly reduced risk of growth delay and other steroid-associated adverse outcomes. Height percentiles remained stable in the vamorolone group, in contrast to the growth deceleration observed with glucocorticoid therapy. The long-term safety profile remained favourable, with few discontinuations and no new safety concerns emerging over the extended treatment period (Mah et al., 2022).

Collectively, these studies suggest that vamorolone offers a disease-modifying effect in DMD that is comparable to standard glucocorticoids in terms of efficacy, while providing a more favourable safety and tolerability profile, particularly in relation to growth and bone health. The evidence from up to 30 months of treatment supports vamorolone as a promising candidate for standard of care in DMD, though ongoing surveillance for adrenal suppression and individualized dose optimization remain important considerations (Mah et al., 2022). However, there are no respiratory outcome measures stated within the studies highlighting the gap in assessment of respiratory system performance that is commonplace within clinical trials of DMD.

1.2.3.3 Dosing strategies

The FOR-DMD trial, as reported by Guglieri et al. (2022), represents the largest and most rigorous randomized clinical trial to date comparing the three most widely used corticosteroid regimens in boys with DMD who were corticosteroid-naïve at study entry (Guglieri et al., 2022). In this double-blind, multicentre study,

196 boys aged 4 to 7 years were randomized to receive either daily prednisone (0.75 mg/kg), daily deflazacort (0.9 mg/kg), or intermittent prednisone (0.75 mg/kg for 10 days on, 10 days off) and were followed for a minimum of three years. The primary composite outcome incorporated measures of motor function (rise from floor velocity), pulmonary function (forced vital capacity percent predicted), and participant or parent satisfaction with treatment (Guglieri et al., 2022).

Both daily prednisone and daily deflazacort regimens resulted in significantly better outcomes on the primary composite measure compared to intermittent prednisone, with no significant difference between the two daily regimens (Guglieri et al., 2022). The superiority of the daily regimens was primarily attributable to improvements in motor function, particularly the ability to rise from the floor. The primary driver of this difference was improvement in motor function; however, the pulmonary function component (FVC) did not show a statistically significant difference between groups, although all regimens maintained FVC at similar levels over the study period.

Secondary outcomes, such as 10-meter walk/run velocity, North Star Ambulatory Assessment, and 6-minute walk test, also favoured daily dosing over intermittent prednisone, reinforcing the superiority of daily regimens in preserving motor abilities. Importantly, while the composite primary outcome included FVC as a measure of respiratory function, individual comparisons of FVC between groups did not reach statistical significance, indicating that all

three regimens were similarly effective in maintaining pulmonary function over three years in this relatively young, ambulant cohort (Guglieri et al., 2022).

In terms of safety and tolerability, adverse events such as abnormal behaviour, infections, and gastrointestinal symptoms were common across all groups and distributed similarly. However, growth stunting was less severe with intermittent prednisone, while daily deflazacort was associated with the greatest slowing of growth (Guglieri et al., 2022). Weight gain was more pronounced in the daily prednisone group compared to daily deflazacort, and the increase in body mass index was also highest with daily prednisone. Cushingoid appearance and bone fractures were observed in all groups, but no significant differences in serious adverse events attributable to corticosteroids were detected. Cataracts were more frequent in the daily deflazacort group, though none required treatment (Guglieri et al., 2022).

The choice between daily prednisone and daily deflazacort may be guided by differences in side-effect profiles, particularly regarding growth and weight gain, but both are effective options for long-term disease management when considering the motor outcomes (Guglieri et al., 2022). Respiratory measures of FVC% predicted decline may not manifest before the loss of ambulation and the spinal abnormalities that occur thereafter so investigation of intermittent corticosteroid treatment after loss of ambulation and the decline in respiratory outcomes is necessary.

1.2.4 Antioxidants as a potential adjunct therapy for DMD

Oxidative stress and chronic inflammation are hallmark features of dystrophin-deficient muscle pathology, contributing to skeletal and respiratory muscle dysfunction in DMD (Burns, Drummond, et al., 2019; Choi et al., 2016; O'Halloran et al., 2023). The absence of dystrophin disrupts membrane integrity, leading to calcium dysregulation, mitochondrial dysfunction, and elevated reactive oxygen species (ROS) production, which exacerbate muscle fibre necrosis and fibrosis.

N-Acetylcysteine (NAC) is a thiol-containing compound that serves as a direct scavenger of ROS and a precursor for glutathione synthesis, the body's primary endogenous antioxidant (Halasi et al., 2013). By replenishing glutathione stores and modulating redox-sensitive signalling pathways, NAC mitigates oxidative stress, suppresses pro-inflammatory cytokines (e.g., IL-6, TNF-α), and inhibits fibrotic mediators like TGF-β in the *mdx* mouse model of DMD (Burns, Drummond, et al., 2019). Approved by regulatory agencies for treating acetaminophen overdose and chronic respiratory conditions, NAC has a well-established safety profile in humans, making it a viable candidate for repurposing in disorders characterized by oxidative imbalance (M. C. D. S. Tenório et al., 2021). In DMD, where dystrophin loss exacerbates ROS-driven damage and inflammation, NAC's multi-target action—addressing antioxidant depletion, calcium dyshomeostasis, and mitochondrial dysfunction, positions it as a theoretically promising adjunct therapy (Bellissimo et al., 2022; Burns, Drummond, et al., 2019; Casati et al., 2024).

Preclinical studies in the *mdx* model have explored these mechanisms, though clinical translation to human DMD remains unexplored. Administering 2% NAC to *mdx* mice over a six-week period led to notable improvements in grip strength and extensor digitorum longus (EDL) muscle force, and a reduction in markers of muscle inflammation and oxidative stress (Pinniger et al., 2017). A one-week regimen of 1% NAC was effective in protecting *mdx* mice from exercise-induced myofibre necrosis and in lowering post-exercise blood creatine kinase levels, indicating reduced muscle damage (Terrill et al., 2012). Six weeks of 1% NAC supplementation diminished ROS in muscle, as shown by reduced dihydroethidium fluorescence, and lessened EDL muscle pathology, evidenced by fewer centrally nucleated fibres in *mdx* mice (Whitehead et al., 2008). Six weeks of 2% NAC treatment significantly decreased EDL muscle mass and reduced the prevalence of abnormal fibre branching and splitting, phenomena that typically contribute to hypertrophy in dystrophic EDL muscles (Redwan et al., 2023). Two weeks of 1% NAC administration in drinking water improved diaphragm force generation, reduced fibrosis, and lowered inflammatory markers such as IL-1β and KC/GRO (Burns, Drummond, et al., 2019). While these studies showed benefits short term, there are no longer-term studies of NAC treatment in *mdx* mice and there are no published studies on NAC in human DMD patients, but other antioxidants have been studied clinically showing some potentially positive results.

Clinical studies in DMD found that idebenone significantly improved pulmonary function (Buyse et al., 2017; Meier et al., 2016), FLAVOMEGA enhanced muscle

strength (Sitzia et al., 2019), and CoQ10 was associated with better physical activity (Spurney et al., 2011). Antioxidant treatments were generally well tolerated, with mostly mild side effects and low rates of serious adverse events or dropouts. While idebenone demonstrates efficacy in preserving pulmonary function (Buyse et al., 2017; Meier et al., 2016), CoQ10 and FLAVOMEGA may enhance muscle-related outcomes (Sitzia et al., 2019), but larger-scale trials are needed. These findings support the hypothesis that NAC treatment could preserve respiratory muscle function and delay disease progression.

However, the translational potential of antioxidants remains contested. Idebenone showed modest reductions in FVC decline but did not alter overall disease trajectory or quality of life (Buyse et al., 2017; Meier et al., 2016). Combinatorial therapies may be necessary to address both primary dystropathology and secondary oxidative injury. While antioxidants hold mechanistic promise for mitigating redox imbalance in DMD, their standalone application may be insufficient to meaningfully alter respiratory system deterioration. Future research should explore synergistic approaches pairing antioxidants with anti-inflammatory or fibrosis-targeting agents to address the interconnected pathways driving dystrophic muscle failure.

1.2.5 Combination therapies for DMD

DMD is characterized by a complex pathophysiology involving not only the primary loss of dystrophin but also secondary processes such as chronic inflammation, oxidative stress, fibrosis, and progressive muscle degeneration.

While corticosteroids remain the mainstay of pharmacological management and antioxidants have shown promise in preclinical models, both approaches have limitations when used as monotherapies. Corticosteroids, though effective in slowing disease progression and preserving muscle and respiratory function, are associated with significant adverse effects and do not fully address the multifactorial nature of DMD pathology. Similarly, antioxidant therapies such as NAC and idebenone target oxidative damage and inflammation but have demonstrated only modest benefits in clinical settings, and their ability to alter the overall disease trajectory remains uncertain.

In response to these challenges, there is growing interest in combination therapy strategies that simultaneously target multiple pathogenic pathways in DMD. The rationale for such approaches is grounded in the recognition that the secondary consequences of dystrophin deficiency—such as inflammation, oxidative injury, and fibrosis—can diminish the effectiveness of single-agent therapies. By combining agents with complementary mechanisms of action, it is hoped that synergistic effects can be achieved, leading to improved muscle phenotype, enhanced respiratory function, and potentially greater preservation of quality of life for patients.

Kendall and colleagues identified dantrolene, a drug traditionally used to treat malignant hyperthermia, as a pharmacological enhancer of antisense oligonucleotide (AON)-mediated exon skipping. When administered to *mdx* mice, dantrolene increased the efficiency of exon skipping, resulting in

greater dystrophin production and improved muscle strength (Kendall et al., 2012).

Abmayr et al. demonstrated that co-expressing insulin-like growth factor-1 (IGF-1), known to induce muscle hypertrophy and regeneration, alongside micro-dystrophin in *mdx* mice resulted in increased muscle mass and specific force compared to micro-dystrophin alone (Abmayr et al., 2005).

Heller and colleagues investigated the combined overexpression of microRNA-29, which is associated with anti-fibrotic effects, and micro-dystrophin delivery in dystrophic mice. This combination led to reduced fibrosis, increased muscle strength, and improved muscle size, demonstrating that targeting both the genetic defect and secondary pathological features like fibrosis can produce additive therapeutic benefits (Heller et al., 2017).

Morales and colleagues showed that genetically reducing Connective Tissue Growth Factor (CTGF) expression or blocking it with neutralizing antibodies decreased fibrosis and improved the success of cell therapy in *mdx* mice. This combined approach led to more dystrophin-positive fibres and enhanced muscle strength, highlighting the importance of addressing fibrosis to boost the effectiveness of regenerative therapies (Morales et al., 2013).

Cabrera and colleagues tested the anti-inflammatory compound andrographolide in *mdx* mice, finding that it reduced fibrotic factors and extracellular matrix proteins, increased muscle strength, and improved the efficacy of cell therapy. Their results suggest that anti-inflammatory and anti-

fibrotic agents can be valuable adjuncts to cell-based treatments in DMD (Cabrera et al., 2014).

Brunelli and colleagues combined mesoangioblast cell therapy with HCT 1026, a nitric oxide-releasing non-steroidal anti-inflammatory drug (NSAID), in dystrophic mice. This combination increased the efficiency of cell therapy, improved muscle force, and enhanced animal performance. The study demonstrates that correcting nitric oxide deficiency and inflammation can synergize with regenerative treatments (Brunelli et al., 2006).

Verhaart and colleagues explored the effect of combining the anti-inflammatory steroid prednisolone with AON-mediated exon skipping in *mdx* mice. Their results indicated that prednisolone did not interfere with exon skipping and increased dystrophin expression, supporting the safety and potential benefit of combining corticosteroids with genetic therapies (Verhaart et al., 2012).

These studies collectively illustrate the promise of combination therapies in DMD, where addressing both the primary genetic defect and secondary pathological features such as inflammation, fibrosis, and muscle atrophy can yield synergistic improvements in muscle function and therapeutic efficacy.

Clinical discussions increasingly emphasize the need for multidrug regimens that balance efficacy and safety, particularly as new agents such as vamorolone and gene-targeted therapies become available. The goal of combination therapy is to slow disease progression at multiple levels, improve functional outcomes, and reduce the burden of side effects associated with long-term single-agent

use (Cordova et al., 2018). As research advances, future clinical trials will be essential to determine the optimal combinations, dosing strategies, and timing of interventions to maximize therapeutic benefit for individuals with DMD.

Combination therapy represents a promising and rational evolution in the treatment of DMD, aiming to address the complex and multifactorial nature of the disease more effectively than monotherapies alone. Ongoing research into synergistic strategies holds the potential to transform the standard of care and improve long-term outcomes for people with DMD.

1.2.6 Current clinical evaluation standards

1.2.6.1 Forced vital capacity (FVC) measurement in DMD care

Forced vital capacity (FVC) is a spirometry measurement that quantifies the maximum volume of air a person can forcibly exhale after a full inhalation. It serves as a critical biomarker in the assessment and monitoring of various pulmonary diseases. FVC is a pivotal spirometry measure in DMD, serving as a key prognostic indicator and monitoring tool for respiratory decline clinically (Childs et al., 2024). In DMD, progressive respiratory muscle weakness leads to a restrictive pattern characterized by reduced FVC, which typically increases until around age 10–12 before declining at an average rate of 5-8% annually (Khirani et al., 2014; Machado et al., 2012). This decline accelerates in adolescence, with FVC trajectories varying significantly between individuals (Khirani et al., 2014; Phillips et al., 2001).

An FVC below 1 L is strongly associated with mortality, correlating with a 5-year survival rate of just 8% (Phillips et al., 2001). Similarly, FVC <40–50% of predicted values predict nocturnal hypoventilation and increased need for non-invasive ventilation (Bourke & Gibson, 2002). Longitudinal studies highlight that the rate of FVC decline itself is predictive of survival, with faster declines linked to shorter lifespans (Phillips et al., 2001). A decline in FVC to <50% of predicted values in DMD marks a critical threshold for heightened respiratory vulnerability, while values below 30% predict severe insufficiency and elevated mortality risk (Childs et al., 2024). At less than 50% predicted FVC, patients face increased susceptibility to sleep-disordered breathing, nocturnal hypoventilation, and post-procedural respiratory complications, even in the absence of overt symptoms. This stage necessitates intensified monitoring and often prompts initiation of non-invasive ventilation to mitigate risks (Childs et al., 2024). Less than 30% predicted FVC correlates with severe respiratory insufficiency, characterized by pronounced hypoventilation, frequent respiratory infections, and a 5-year survival rate of just 8%. At this advanced stage, patients typically require continuous ventilatory support and exhibit markedly reduced cough efficacy, increasing hospitalization risks. These thresholds guide clinical decisions, with FVC trajectories serving as key predictors for interventions like lung volume recruitment manoeuvres or surgical risk assessments. FVC remains one of the key biomarkers for evaluating disease progression, stratifying risk, and optimizing therapeutic strategies in DMD, with ongoing research refining its role in personalized care.

1.2.6.2 Pressure measurements in DMD care

Pressure measurements, including maximal inspiratory pressure (MIP), maximal expiratory pressure (MEP), and sniff nasal inspiratory pressure (SNIP), are critical tools for assessing respiratory muscle strength and predicting clinical outcomes in DMD (Delaney & O'Halloran, 2024; J. Finder et al., 2017; Yuksel Kalyoncu et al., 2024). These metrics indirectly quantify the force generated by respiratory muscles during inhalation and exhalation, reflecting progressive diaphragm and intercostal muscle weakness. MIP, which measures inspiratory effort, typically declines to less than 60 cmH_2O in early adolescence, signalling diminished diaphragmatic function (Delaney & O'Halloran, 2024; J. Finder et al., 2017; Yuksel Kalyoncu et al., 2024). A MIP below 30 cmH_2O is strongly associated with nocturnal hypoventilation and predicts imminent respiratory failure, often necessitating non-invasive ventilation (J. Finder et al., 2017). Similarly, MEP, which evaluates expiratory muscle strength, correlates with cough efficacy; values less than 60 cmH_2O are associated with loss of effective cough and values below 40 cmH_2O indicate impaired airway clearance and heightened risk of recurrent infections (J. Finder et al., 2017; Yuksel Kalyoncu et al., 2024).

SNIP, a non-invasive measure of inspiratory sniff pressure, provides complementary data, with values below 40 cmH_2O serving as a threshold for initiating nocturnal ventilatory support (J. Finder et al., 2017). A significant annual decline in SNIP predicts rapid disease progression and reduced survival (J. Finder et al., 2017). Furthermore, steroid therapy has been shown to attenuate

the decline in MIP and MEP, preserving respiratory function compared to untreated patients (J. Finder et al., 2017).

Clinically, pressure thresholds inform risk stratification. A MIP below 25 cmH_2O or SNIP below 30 cmH_2O predicts severe respiratory insufficiency, with a high proportion of patients requiring continuous non-invasive ventilation within two years (J. Finder et al., 2017). These measurements also aid in surgical planning, as preoperative MIP below 40 cmH_2O increases post-anaesthesia complication risks (J. Finder et al., 2017). Emerging biomarkers, such as serum creatine kinase levels, correlate weakly with pressure declines, underscoring the need for direct respiratory monitoring (Yuksel Kalyoncu et al., 2024).

Pressure measurements are indispensable for evaluating respiratory muscle deterioration, guiding ventilatory support, and optimizing therapeutic strategies in DMD. Their prognostic precision and responsiveness to interventions make them vital for personalized care and clinical trial design.

1.2.6.3 EMG in DMD care

EMG offers insights into neuromuscular degeneration and therapeutic responses in various neuromuscular diseases. As a diagnostic tool, EMG detects myopathic changes through abnormalities in motor unit action potentials (MUAPs), such as increased polyphasic potentials and reduced duration/amplitude, even in subclinical stages and has been investigated in the limb muscles of DMD boys (Emeryk-Szajewska & Kopeć, 2008; Lobo-Prat et al.,

2017; Verma et al., 2017). Surface EMG (sEMG) has demonstrated utility in late-stage DMD, where measurable signals from atrophied muscles enable control interfaces for robotic assistive devices, despite amplitudes 100-fold lower than healthy individuals (Lobo-Prat et al., 2017).

Quantitative EMG reveals disease progression through parameters like MUAP duration and amplitude. Early-stage DMD shows increased polyphasic potentials (>25%), while advanced stages exhibit profound reductions in MUAP amplitude and density (Emeryk-Szajewska & Kopeć, 2008; Verma et al., 2017). Longitudinal quantitative EMG studies in ambulatory patients demonstrate stable MUAP duration over six months, suggesting its sensitivity to chronic myopathic processes rather than short-term fluctuations (Verma et al., 2017). EMG also correlates with functional decline: reduced MUAP complexity predicts loss of ambulation, while sEMG-derived co-activation ratios in antagonistic muscles reflect compensatory mechanisms during motor task attempts (Emeryk-Szajewska & Kopeć, 2008; Lobo-Prat et al., 2017).

EMG serves as a biomarker for evaluating novel therapies. In clinical trials of DT-DEC01 cell therapy, limb muscle EMG detected increased MUAP duration (12–18%) and amplitude (15–22%) at 12 months post-treatment, indicating improved muscle electrophysiology (Niezgoda et al., 2023). Similarly, EMG-guided interventions like robotic arm supports leverage residual sEMG signals to restore functional movements, even in non-ambulatory patients with Brooke scale 6 disability (Lobo-Prat et al., 2017).

Emerging research highlights the potential of EMG screening in personalized care, where machine learning analyses of sEMG trajectories optimize assistive device responsiveness (Lobo-Prat et al., 2017). Despite muscle fibrosis and fatty infiltration, EMG remains a critical tool for capturing residual neuromuscular function, guiding interventions from robotic arm support to experimental gene therapies (Lobo-Prat et al., 2017; Niezgoda et al., 2023). Its non-invasive nature and sensitivity to subclinical changes position sEMG as an indispensable component of multidisciplinary DMD management. However, this technology and the use of EMG as a biomarker for DMD has not been utilised to investigate the respiratory natural history of the disease.

1.3 Objectives and hypotheses of the thesis

The primary objective of this thesis is to comprehensively evaluate the effects of several therapeutic interventions—namely, AIH, chronic NAC administration, intermittent prednisone, and combined prednisone plus NAC treatment—on respiratory system performance in the *mdx* mouse model of DMD. This work also aims to characterize clinically relevant respiratory parameters across the natural history of disease in the *mdx* mouse, thereby assessing the translational value of this preclinical model for studying respiratory decline in DMD to inform future therapeutic strategies. The research is structured to determine whether these interventions can induce beneficial changes in respiratory muscle structure and function, improve ventilatory parameters, and ultimately preserve respiratory capacity in the context of dystrophin deficiency.

The central hypotheses are as follows: First, it is hypothesized that AIH will induce respiratory plasticity, specifically ventilatory LTF, leading to sustained improvements in respiratory output and efficiency in *mdx* mice (Chapter 2). Second, chronic NAC administration is expected to ameliorate respiratory muscle pathology by reducing oxidative stress, inflammation, and fibrosis, thereby enhancing diaphragm force generation and overall respiratory function (Chapter 3). Third, it is proposed that intermittent prednisone, either alone or in combination with NAC, will improve respiratory muscle strength and delay the progression of respiratory dysfunction in the *mdx* model (Chapter 4). Finally, it is hypothesized that the *mdx* mouse will exhibit a progressive decline in respiratory system performance, revealed in neuromuscular and neuromechanical assessments that parallel key clinical features of human DMD, validating its use for preclinical studies of respiratory interventions (Chapter 5). Should these interventions fail to demonstrate efficacy, the findings will underscore the need for new therapeutic strategies and the development of more clinically relevant animal models. Together, these objectives and hypotheses provide a focused framework for the experimental work presented in this thesis, ensuring a systematic exploration of both the efficacy of potential interventions and the suitability of the *mdx* model for translational DMD research.

1.4 References

Aartsma-Rus, A., Van Deutekom, J. C. T., Fokkema, I. F., Van Ommen, G. B., & Den Dunnen, J. T. (2006). Entries in the Leiden Duchenne muscular dystrophy mutation database: An overview of mutation types and paradoxical cases that confirm the reading-frame rule. Muscle & Nerve, 34(2), 135–144. https://doi.org/10.1002/mus.20586

Abmayr, S., Gregorevic, P., Allen, J. M., & Chamberlain, J. S. (2005). Phenotypic improvement of dystrophic muscles by rAAV/microdystrophin vectors is augmented by Igf1 codelivery. Molecular Therapy, 12(3), 441–450. https://doi.org/10.1016/j.ymthe.2005.04.001

Abraham, K. A., Feingold, H., Fuller, D. D., Jenkins, M., Mateika, J. H., & Fregosi, R. F. (2002). Respiratory-related activation of human abdominal muscles during exercise. Journal of Physiology, 541(2). https://doi.org/10.1113/jphysiol.2001.013462

Ahn, A. H., & Kunkel, L. M. (1993). The structural and functional diversity of dystrophin. In Nature Genetics (Vol. 3, Issue 4). https://doi.org/10.1038/ng0493-283

Aliverti, A. (2016). The respiratory muscles during exercise. Breathe, 12(2). https://doi.org/10.1183/20734735.008116

Bach, K. B., & Mitchell, G. S. (1996). Hypoxia-induced long-term facilitation of respiratory activity is serotonin dependent. Respiration Physiology, 104(2–3), 251–260. https://doi.org/10.1016/0034-5687(96)00017-5

Baker-Herman, T. L., & Mitchell, G. S. (2002). Phrenic long-term facilitation requires spinal serotonin receptor activation and protein synthesis. Journal of Neuroscience, 22(14). https://doi.org/10.1523/jneurosci.22-14-06239.2002

Bellissimo, C. A., Garibotti, M. C., & Perry, C. G. R. (2022). Mitochondrial stress responses in Duchenne muscular dystrophy: metabolic dysfunction or adaptive reprogramming? In American Journal of Physiology - Cell Physiology (Vol. 323, Issue 3, pp. C718–C730). American Physiological Society. https://doi.org/10.1152/ajpcell.00249.2022

Birnkrant, D. J., Bushby, K., Bann, C. M., Apkon, S. D., Blackwell, A., Brumbaugh, D., Case, L. E., Clemens, P. R., Hadjiyannakis, S., Pandya, S., Street, N., Tomezsko, J., Wagner, K. R., Ward, L. M., & Weber, D. R. (2018). Diagnosis and management of Duchenne muscular dystrophy, part 1: diagnosis, and neuromuscular, rehabilitation, endocrine, and gastrointestinal and nutritional management. In The Lancet Neurology (Vol. 17, Issue 3). https://doi.org/10.1016/S1474-4422(18)30024-3

Bladen, C. L., Salgado, D., Monges, S., Foncuberta, M. E., Kekou, K., Kosma, K., Dawkins, H., Lamont, L., Roy, A. J., Chamova, T., Guergueltcheva, V., Chan, S., Korngut, L., Campbell, C., Dai, Y., Wang, J., Barišić, N., Brabec, P., Lahdetie, J., … Lochmüller, H. (2015). The TREAT-NMD DMD global database: Analysis of more than 7,000 duchenne muscular dystrophy mutations. Human Mutation, 36(4). https://doi.org/10.1002/humu.22758

Bourke, S. C., & Gibson, G. J. (2002). Sleep and breathing in neuromuscular disease. In European Respiratory Journal (Vol. 19, Issue 6, pp. 1194–1201).

European Respiratory Society.
https://doi.org/10.1183/09031936.02.01302001a

Broomfield, J., Hill, M., Guglieri, M., Crowther, M., & Abrams, K. (2021). Life Expectancy in Duchenne Muscular Dystrophy: Reproduced Individual Patient Data Meta-analysis. Neurology, 97(23), e2304. https://doi.org/10.1212/WNL.0000000000012910

Brunelli, S., Sciorati, C., D'antona, G., Innocenzi, A., Covarello, D., Galvez, B. G., Perrotta, C., Monopoli, A., Sanvito, F., Bottinelli, R., Ongini, E., Cossu, G., & Clementi, E. (2006). Nitric oxide release combined with nonsteroidal antiinflammatory activity prevents muscular dystrophy pathology and enhances stem cell therapy. www.pnas.orgcgidoi10.1073pnas.0608277104

Bulfield, G., Siller, W. G., Wight, P. A., & Moore, K. J. (1984). X chromosome-linked muscular dystrophy (mdx) in the mouse. Proceedings of the National Academy of Sciences, 81(4), 1189–1192. https://doi.org/10.1073/pnas.81.4.1189

Burns, D. P., Canavan, L., Rowland, J., O'Flaherty, R., Brannock, M., Drummond, S. E., O'Malley, D., Edge, D., & O'Halloran, K. D. (2018). Recovery of respiratory function in mdx mice co-treated with neutralizing interleukin-6 receptor antibodies and urocortin-2. The Journal of Physiology, 596(21), 5175–5197. https://doi.org/10.1113/JP276954

Burns, D. P., Drummond, S. E., Bolger, D., Coiscaud, A., Murphy, K. H., Edge, D., & O'Halloran, K. D. (2019). N-acetylcysteine Decreases Fibrosis and

Increases Force-Generating Capacity of mdx Diaphragm. Antioxidants, 8(12), 581. https://doi.org/10.3390/antiox8120581

Burns, D. P., Murphy, K. H., Lucking, E. F., & O'Halloran, K. D. (2019). Inspiratory pressure-generating capacity is preserved during ventilatory and non-ventilatory behaviours in young dystrophic mdx mice despite profound diaphragm muscle weakness. The Journal of Physiology, 597(3), 831–848. https://doi.org/10.1113/JP277443

Burns, D. P., Roy, A., Lucking, E. F., McDonald, F. B., Gray, S., Wilson, R. J., Edge, D., & O'Halloran, K. D. (2017). Sensorimotor control of breathing in the mdx mouse model of Duchenne muscular dystrophy. The Journal of Physiology, 595(21), 6653–6672. https://doi.org/10.1113/JP274792

Buyse, G. M., Voit, T., Schara, U., Straathof, C. S. M., D'Angelo, M. G., Bernert, G., Cuisset, J. M., Finkel, R. S., Goemans, N., Rummey, C., Leinonen, M., Mayer, O. H., Spagnolo, P., Meier, T., McDonald, C. M., Knipp, F., Van den Hauwe, M., Doppler, V., Gidaro, T., … Richardson, R. C. (2017). Treatment effect of idebenone on inspiratory function in patients with Duchenne muscular dystrophy. Pediatric Pulmonology, 52(4), 508–515. https://doi.org/10.1002/ppul.23547

Cabrera, D., Gutiérrez, J., Cabello-Verrugio, C., Morales, M. G., Mezzano, S., Fadic, R., Casar, J. C., Hancke, J. L., & Brandan, E. (2014). Andrographolide attenuates skeletal muscle dystrophy in mdx mice and increases efficiency of cell therapy by reducing fibrosis. Skeletal Muscle, 4(1). https://doi.org/10.1186/2044-5040-4-6

Casati, S. R., Cervia, D., Roux-Biejat, P., Moscheni, C., Perrotta, C., & De Palma, C. (2024). Mitochondria and Reactive Oxygen Species: The Therapeutic Balance of Powers for Duchenne Muscular Dystrophy. In Cells (Vol. 13, Issue 7). Multidisciplinary Digital Publishing Institute (MDPI). https://doi.org/10.3390/cells13070574

Childs, A. M., Turner, C., Astin, R., Bianchi, S., Bourke, J., Cunningham, V., Edel, L., Edwards, C., Farrant, P., Heraghty, J., James, M., Massey, C., Messer, B., Sodhi, J. M., Murphy, P. B., Schiava, M., Thomas, A., Trucco, F., & Guglieri, M. (2024). Development of respiratory care guidelines for Duchenne muscular dystrophy in the UK: key recommendations for clinical practice. In Thorax (Vol. 79, Issue 5, pp. 476–485). BMJ Publishing Group. https://doi.org/10.1136/thorax-2023-220811

Choi, M. H., Ow, J. R., Yang, N. Di, & Taneja, R. (2016). Oxidative Stress-Mediated Skeletal Muscle Degeneration: Molecules, Mechanisms, and Therapies. In Oxidative Medicine and Cellular Longevity (Vol. 2016). https://doi.org/10.1155/2016/6842568

Cordova, G., Negroni, E., Cabello-Verrugio, C., Mouly, V., & Trollet, C. (2018). Combined therapies for Duchenne muscular dystrophy to optimize treatment efficacy. In Frontiers in Genetics (Vol. 9, Issue APR). Frontiers Media S.A. https://doi.org/10.3389/fgene.2018.00114

Crisafulli, S., Sultana, J., Fontana, A., Salvo, F., Messina, S., Messina, S., & Trifirò, G. (2020). Global epidemiology of Duchenne muscular dystrophy: An updated systematic review and meta-analysis. In Orphanet Journal of Rare

Diseases (Vol. 15, Issue 1). BioMed Central Ltd. https://doi.org/10.1186/s13023-020-01430-8

Dang, U. J., Damsker, J. M., Guglieri, M., Clemens, P. R., Perlman, S. J., Smith, E. C., Horrocks, I., Finkel, R. S., Mah, J. K., Deconinck, N., Goemans, N. M., Haberlová, J., Straub, V., Mengle-Gaw, L., Schwartz, B. D., Harper, A., Shieh, P. B., De Waele, L., Castro, D., … Hoffman, E. P. (2024). Efficacy and Safety of Vamorolone Over 48 Weeks in Boys With Duchenne Muscular Dystrophy. Neurology, 102(5). https://doi.org/10.1212/wnl.0000000000208112

Deconinck, N., & Dan, B. (2007). Pathophysiology of Duchenne Muscular Dystrophy: Current Hypotheses. In Pediatric Neurology (Vol. 36, Issue 1). https://doi.org/10.1016/j.pediatrneurol.2006.09.016

Del Negro, C. A., Funk, G. D., & Feldman, J. L. (2018). Breathing matters. In Nature Reviews Neuroscience (Vol. 19, Issue 6). https://doi.org/10.1038/s41583-018-0003-6

Delaney, R., & O'Halloran, K. D. (2024). Respiratory performance in Duchenne muscular dystrophy: Clinical manifestations and lessons from animal models. In Experimental Physiology (Vol. 109, Issue 9, pp. 1426–1445). John Wiley and Sons Inc. https://doi.org/10.1113/EP091967

Duan, D., Goemans, N., Takeda, S., Mercuri, E., & Aartsma-Rus, A. (2021). Duchenne muscular dystrophy. In Nature Reviews Disease Primers (Vol. 7, Issue 1). https://doi.org/10.1038/s41572-021-00248-3

Emery, A. E. (2002). The muscular dystrophies. The Lancet, 359(9307), 687–695. https://doi.org/10.1016/S0140-6736(02)07815-7

Emeryk-Szajewska, B., & Kopeć, J. (2008). Electromyographic pattern in Duchenne and Becker muscular dystrophy. Part I: Electromyographic pattern in subsequent stages of muscle lesion in Duchenne muscular dystrophy. Electromyography and Clinical Neurophysiology, 48(6–7).

Fauroux, B., Aubertin, G., Clément, A., Lofaso, F., & Bonora, M. (2009). Which tests may predict the need for noninvasive ventilation in children with neuromuscular disease? Respiratory Medicine, 103(4). https://doi.org/10.1016/j.rmed.2008.10.023

Fauroux, B., Quijano-Roy, S., Desguerre, I., & Khirani, S. (2015). The Value of Respiratory Muscle Testing in Children With Neuromuscular Disease. Chest, 147(2), 552–559. https://doi.org/10.1378/chest.14-0819

Finder, J. D. (2009). A 2009 perspective on the 2004 American thoracic society statement, “respiratory care of the patient with Duchenne muscular dystrophy.” Pediatrics, 123(SUPPL. 4). https://doi.org/10.1542/peds.2008-2952I

Finder, J. D., Birnkrant, D., Carl, J., Farber, H. J., Gozal, D., Iannaccone, S. T., Kovesi, T., Kravitz, R. M., Panitch, H., Schramm, C., Schroth, M., Sharma, G., Sievers, L., Silvestri, J. M., & Sterni, L. (2004). Respiratory care of the patient with duchenne muscular dystrophy: ATS consensus statement. American

Journal of Respiratory and Critical Care Medicine, 170(4). https://doi.org/10.1164/rccm.200307-885ST

Finder, J., Mayer, O. H., Sheehan, D., Sawnani, H., Abresch, R. T., Benditt, J., Birnkrant, D. J., Duong, T., Henricson, E., Kinnett, K., McDonald, C. M., & Connolly, A. M. (2017). Pulmonary endpoints in duchenne muscular dystrophy a workshop summary. American Journal of Respiratory and Critical Care Medicine, 196(4), 512–519. https://doi.org/10.1164/rccm.201703-0507WS

Fogarty, M. J., Mantilla, C. B., & Sieck, G. C. (2018). Breathing: Motor control of diaphragm muscle. In Physiology (Vol. 33, Issue 2). https://doi.org/10.1152/physiol.00002.2018

Gao, Q. Q., & McNally, E. M. (2015). The Dystrophin Complex: Structure, Function, and Implications for Therapy. In Comprehensive Physiology (Vol. 5, Issue 3, pp. 1223–1239). Wiley. https://doi.org/10.1002/cphy.c140048

Golder, F. J., & Mitchell, G. S. (2005). Spinal synaptic enhancement with acute intermittent hypoxia improves respiratory function after chronic cervical spinal cord injury. Journal of Neuroscience, 25(11), 2925–2932. https://doi.org/10.1523/JNEUROSCI.0148-05.2005

Guglieri, M., Bushby, K., McDermott, M. P., Hart, K. A., Tawil, R., Martens, W. B., Herr, B. E., McColl, E., Speed, C., Wilkinson, J., Kirschner, J., King, W. M., Eagle, M., Brown, M. W., Willis, T., Griggs, R. C., Straub, V., van Ruiten, H., Childs, A.-M., … Chang, T. (2022). Effect of Different Corticosteroid Dosing Regimens on

Clinical Outcomes in Boys With Duchenne Muscular Dystrophy. JAMA, 327(15), 1456. https://doi.org/10.1001/jama.2022.4315

Hahn, A., Bach, J. R., Delaubier, A., Renardel-Irani, A., Guillou, C., & Rideau, Y. (1997). Clinical implications of maximal respiratory pressure determinations for individuals with Duchenne muscular dystrophy. Archives of Physical Medicine and Rehabilitation, 78(1). https://doi.org/10.1016/S0003-9993(97)90001-0

Halasi, M., Wang, M., Chavan, T. S., Gaponenko, V., Hay, N., & Gartel, A. L. (2013). ROS inhibitor N-acetyl-L-cysteine antagonizes the activity of proteasome inhibitors. Biochemical Journal, 454(2), 201–208. https://doi.org/10.1042/BJ20130282

Hayashi, F., Coles, S. K., & McCrimmon, D. R. (1996). Respiratory neurons mediating the Breuer-Hering reflex prolongation of expiration in rat. Journal of Neuroscience, 16(20). https://doi.org/10.1523/jneurosci.16-20-06526.1996

Heller, K. N., Mendell, J. T., Mendell, J. R., & Rodino-Klapac, L. R. (2017). MicroRNA-29 overexpression by adeno-associated virus suppresses fibrosis and restores muscle function in combination with micro-dystrophin. JCI Insight, 2(9). https://doi.org/10.1172/jci.insight.93309

Hoffman, E. P., Brown, R. H., & Kunkel, L. M. (1987). Dystrophin: The protein product of the duchenne muscular dystrophy locus. Cell, 51(6), 919–928. https://doi.org/10.1016/0092-8674(87)90579-4

Hoffman, E. P., Schwartz, B. D., Mengle-Gaw, L. J., Smith, E. C., Castro, D., Mah, J. K., Mcdonald, C. M., Kuntz, N. L., Finkel, R. S., Guglieri, M., Bushby, K.,

Tulinius, M., Nevo, Y., Ryan, M. M., Webster, R., Smith, A. L., Morgenroth, L. P., Arrieta, A., Shimony, M., … Clemens, P. R. (2019). Vamorolone trial in Duchenne muscular dystrophy shows dose-related improvement of muscle function. Neurology, 93(13), E1312–E1323. https://doi.org/10.1212/WNL.0000000000008168

Hudson, A. L., Jolley, C. J., Gandevia, S. C., & Butler, J. E. (2025). Myths and methodologies: Invasive and non-invasive assessment of respiratory muscle activity in humans. Experimental Physiology. https://doi.org/10.1113/EP091526

Kendall, G. C., Mokhonova, E. I., Moran, M., Sejbuk, N. E., Wang, D. W., Silva, O., Wang, R. T., Martinez, L., Lu, Q. L., Damoiseaux, R., Spencer, M. J., Nelson, S. F., & Miceli, M. C. (2012). Dantrolene enhances antisense-mediated exon skipping in human and mouse models of Duchenne muscular dystrophy. Science Translational Medicine, 4(164). https://doi.org/10.1126/scitranslmed.3005054

Khirani, S., Ramirez, A., Aubertin, G., Boulé, M., Chemouny, C., Forin, V., & Fauroux, B. (2014). Respiratory muscle decline in duchenne muscular dystrophy. Pediatric Pulmonology, 49(5), 473–481. https://doi.org/10.1002/ppul.22847

Lobo-Prat, J., Janssen, M. M. H. P., Koopman, B. F. J. M., Stienen, A. H. A., & De Groot, I. J. M. (2017). Surface EMG signals in very late-stage of Duchenne muscular dystrophy: A case study. Journal of NeuroEngineering and Rehabilitation, 14(1). https://doi.org/10.1186/s12984-017-0292-4

Lynch, G. S., Hinkle, R. T., Chamberlain, J. S., Brooks, S. V., & Faulkner, J. A. (2001). Force and power output of fast and slow skeletal muscles from mdx mice 6-28 months old. The Journal of Physiology, 535(2), 591–600. https://doi.org/10.1111/j.1469-7793.2001.00591.x

MacFarlane, P. M., & Mitchell, G. S. (2008). Respiratory long-term facilitation following intermittent hypoxia requires reactive oxygen species formation. Neuroscience, 152(1), 189–197. https://doi.org/10.1016/j.neuroscience.2007.12.003

Macfarlane, P. M., Satriotomo, I., Windelborn, J. A., & Mitchell, G. S. (2009). NADPH oxidase activity is necessary for acute intermittent hypoxia-induced phrenic long-term facilitation. Journal of Physiology, 587(9). https://doi.org/10.1113/jphysiol.2008.165597

Machado, D. L., Silva, E. C., Resende, M. B. D., Carvalho, C. R. F., Zanoteli, E., & Reed, U. C. (2012). Lung function monitoring in patients with duchenne muscular dystrophy on steroid therapy. BMC Research Notes, 5(1), 435. https://doi.org/10.1186/1756-0500-5-435

Mah, J. K., Clemens, P. R., Guglieri, M., Smith, E. C., Finkel, R. S., Tulinius, M., Nevo, Y., Ryan, M. M., Webster, R., Castro, D., Kuntz, N. L., McDonald, C. M., Damsker, J. M., Schwartz, B. D., Mengle-Gaw, L. J., Jackowski, S., Stimpson, G., Ridout, D. A., Ayyar-Gupta, V., … Karachunski, P. (2022). Efficacy and Safety of Vamorolone in Duchenne Muscular Dystrophy. JAMA Network Open, 5(1), e2144178. https://doi.org/10.1001/jamanetworkopen.2021.44178

Mann, C. J., Perdiguero, E., Kharraz, Y., Aguilar, S., Pessina, P., Serrano, A. L., & Muñoz-Cánoves, P. (2011). Aberrant repair and fibrosis development in skeletal muscle. In Skeletal Muscle (Vol. 1, Issue 1). https://doi.org/10.1186/2044-5040-1-21

Massopust, R. T., Lee, Y. il, Pritchard, A. L., Nguyen, V. K. M., McCreedy, D. A., & Thompson, W. J. (2020). Lifetime analysis of mdx skeletal muscle reveals a progressive pathology that leads to myofiber loss. Scientific Reports, 10(1). https://doi.org/10.1038/s41598-020-74192-9

McDonald, C. M., Mayer, O. H., Hor, K. N., Miller, D., Goemans, N., Henricson, E. K., Marden, J. R., Freimark, J., Lane, H., Zhang, A., Frean, M., Trifillis, P., Koladicz, K., & Signorovitch, J. (2023). Functional and Clinical Outcomes Associated with Steroid Treatment among Non-ambulatory Patients with Duchenne Muscular Dystrophy. Journal of Neuromuscular Diseases, 10(1), 67–79. https://doi.org/10.3233/JND-221575

McDouall, R. M., Dunn, M. J., & Dubowitz, V. (1990). Nature of the mononuclear infiltrate and the mechanism of muscle damage in juvenile dermatomyositis and Duchenne muscular dystrophy. Journal of the Neurological Sciences, 99(2–3). https://doi.org/10.1016/0022-510X(90)90156-H

Meier, T., Voit, T., Schara, U., Straathof, C. S. M., D'Angelo, M. G., Bernert, G., Cuisset, J. M., Finkel, R. S., Goemans, N., Rummey, C., Leinonen, M., Spagnolo, P., Buyse, G. M., Knipp, F., van den Hauwe, M., Doppler, V., Gidaro, T., Coopman, S., Lutz, S., … Richardson, R. C. (2016). Idebenone reduces respiratory complications in patients with Duchenne muscular dystrophy.

Neuromuscular Disorders, 26(8), 473–480. https://doi.org/10.1016/j.nmd.2016.05.008

Mhandire, D. Z., Burns, D. P., Roger, A. L., O'Halloran, K. D., & ElMallah, M. K. (2022). Breathing in Duchenne muscular dystrophy: translation to therapy. The Journal of Physiology, 600(15), 3465–3482. https://doi.org/10.1113/JP281671

Millhorn, D. E., Eldridge, F. L., & Waldrop, R. G. (1980). Prolonged stimulation for respiration by endogenous central serotonin. Respiration Physiology, 42(3). https://doi.org/10.1016/0034-5687(80)90113-9

Molkov, Y. I., Bacak, B. J., Dick, T. E., & Rybak, I. A. (2013). Control of breathing by interacting pontine and pulmonary feedback loops. Frontiers in Neural Circuits, JAN. https://doi.org/10.3389/fncir.2013.00016

Morales, M. G., Gutierrez, J., Cabello-Verrugio, C., Cabrera, D., Lipson, K. E., Goldschmeding, R., & Brandan, E. (2013). Reducing CTGF/CCN2 slows down mdx muscle dystrophy and improves cell therapy. Human Molecular Genetics, 22(24), 4938–4951. https://doi.org/10.1093/hmg/ddt352

Nichols, N. L., Satriotomo, I., Allen, L. L., Grebe, A. M., & Mitchell, G. S. (2017). Mechanisms of enhanced phrenic long-term facilitation in SOD1G93a rats. Journal of Neuroscience, 37(24), 5834–5845. https://doi.org/10.1523/JNEUROSCI.3680-16.2017

Niezgoda, A., Biegański, G., Wachowiak, J., Czarnota, J., Siemionow, K., Heydemann, A., Ziemiecka, A., Sikorska, M. H., Bożyk, K., & Siemionow, M. (2023). Assessment of Motor Unit Potentials Duration as the Biomarker of DT-

DEC01 Cell Therapy Efficacy in Duchenne Muscular Dystrophy Patients up to 12 Months After Systemic–Intraosseous Administration. Archivum Immunologiae et Therapiae Experimentalis, 71(1). https://doi.org/10.1007/s00005-023-00691-y

O'Halloran, K. D., Maxwell, M. N., Marullo, A. L., Hamilton, C. P., Ó Murchú, S. C., Burns, D. P., Mahony, C. M., Slyne, A. D., & Drummond, S. E. (2023). Loss of compensation afforded by accessory muscles of breathing leads to respiratory system compromise in the mdx mouse model of Duchenne muscular dystrophy. The Journal of Physiology, 601(19), 4441–4467. https://doi.org/10.1113/JP285203

Passamano, L., Taglia, A., Palladino, A., Viggiano, E., D'Ambrosio, P., Scutifero, M., Cecio, M. R., Torre, V., De Luca, F., Picillo, E., Paciello, O., Piluso, G., Nigro, G., & Politano, L. (2012). Improvement of survival in Duchenne Muscular Dystrophy: Retrospective analysis of 835 patients. In Acta Myologica (Vol. 31, Issue OCTOBER).

Personius, K. E., & Sawyer, R. P. (2006). Variability and failure of neurotransmission in the diaphragm of mdx mice. Neuromuscular Disorders, 16(3), 168–177. https://doi.org/10.1016/j.nmd.2006.01.002

Phillips, M. F., Quinlivan, R. C. M., Edwards, R. H. T., & Calverley, P. M. A. (2001). Changes in Spirometry Over Time as a Prognostic Marker in Patients with Duchenne Muscular Dystrophy. Am J Respir Crit Care Med, 164, 2191–2194. https://doi.org/10.1164/rccm2103052

Prabhakar, N. R., & Peng, Y. J. (2004). Peripheral chemoreceptors in health and disease. In Journal of Applied Physiology (Vol. 96, Issue 1). https://doi.org/10.1152/japplphysiol.00809.2003

Redwan, A., Kiriaev, L., Kueh, S., Morley, J. W., Houweling, P., Perry, B. D., & Head, S. I. (2023). Six weeks of N-acetylcysteine antioxidant in drinking water decreases pathological fiber branching in MDX mouse dystrophic fast-twitch skeletal muscle. Frontiers in Physiology, 14. https://doi.org/10.3389/fphys.2023.1109587

Sajjadi, E., Seven, Y. B., Ehrbar, J. G., Wymer, J. P., Mitchell, G. S., & Smith, B. K. (2022). Acute intermittent hypoxia and respiratory muscle recruitment in people with amyotrophic lateral sclerosis: A preliminary study. In Experimental Neurology (Vol. 347). Academic Press Inc. https://doi.org/10.1016/j.expneurol.2021.113890

Schmalbruch, H. (1984). Regenerated muscle fibers in duchenne muscular dystrophy: A serial section study. Neurology, 34(1). https://doi.org/10.1212/wnl.34.1.60

Sheehan, D. W., Birnkrant, D. J., Benditt, J. O., Eagle, M., Finder, J. D., Kissel, J., Kravitz, R. M., Sawnani, H., Shell, R., Sussman, M. D., & Wolfe, L. F. (2018). Respiratory management of the patient with Duchenne muscular dystrophy. Pediatrics, 142. https://doi.org/10.1542/peds.2018-0333H

Sicinski, P., Geng, Y., Ryder-Cook, A. S., Barnard, E. A., Darlison, M. G., & Barnard, P. J. (1989). The Molecular Basis of Muscular Dystrophy in the mdx

Mouse: a Point Mutation. Science, 244(4912), 1578–1580. https://doi.org/10.1126/science.2662404

Simon, P. M., Skatrud, J. B., Badr, M. S., Griffin, D. M., Iber, C., & Dempsey, J. A. (1991). Role of airway mechanoreceptors in the inhibition of inspiration during mechanical ventilation in humans. American Review of Respiratory Disease, 144(5). https://doi.org/10.1164/ajrccm/144.5.1033

Sitzia, C., Meregalli, M., Belicchi, M., Farini, A., Arosio, M., Bestetti, D., Villa, C., Valenti, L., Brambilla, P., & Torrente, Y. (2019). Preliminary evidences of safety and efficacy of flavonoids- And omega 3-based compound for muscular dystrophies treatment: A randomized double-blind placebo controlled pilot clinical trial. Frontiers in Neurology, 10(JUL). https://doi.org/10.3389/fneur.2019.00755

Slyne, A. D., Burns, D. P., Wöller, K., May, A., Dowd, R., Drummond, S. E., Jasionek, G., & O'Halloran, K. D. (2025). Obligatory and accessory respiratory muscle structure, function and control in early and advanced disease in the mdx mouse model of Duchenne muscular dystrophy Corresponding author. The Journal of Physiology, 1–40. https://doi.org/10.1113/JP288709#support-information-section

Smith, J. C., Abdala, A. P. L., Rybak, I. A., & Paton, J. F. R. (2009). Structural and functional architecture of respiratory networks in the mammalian brainstem. In Philosophical Transactions of the Royal Society B: Biological Sciences (Vol. 364, Issue 1529). https://doi.org/10.1098/rstb.2009.0081

Smith, P. E. M., Edwards, R. H. T., & Calverley, P. M. A. (1989). Ventilation and Breathing Pattern during Sleep in Duchenne Muscular Dystrophy. Chest, 96(6), 1346–1351. https://doi.org/10.1378/chest.96.6.1346

Spurney, C. F., Carolina, T. R., Henricson, E., Florence, J., Mayhew, J., Gorni, K., Pasquali, L., Pestronk, A., Martin, G. R., Hu, F., Nie, L., Connolly, A. M., & Escolar, D. M. (2011). CINRG pilot trial of coenzyme Q10 in Steroid-Treated duchenne muscular dystrophy. Muscle and Nerve, 44(2), 174–178. https://doi.org/10.1002/mus.22047

Stedman, H. H., Sweeney, H. L., Shrager, J. B., Maguire, H. C., Panettieri, R. A., Petrof, B., Narusawa, M., Leferovich, J. M., Sladky, J. T., & Kelly, A. M. (1991). The mdx mouse diaphragm reproduces the degenerative changes of Duchenne muscular dystrophy. Nature, 352(6335), 536–539. https://doi.org/10.1038/352536a0

Sutor, T., Cavka, K., Vose, A. K., Welch, J. F., Davenport, P., Fuller, D. D., Mitchell, G. S., & Fox, E. J. (2021). Single-session effects of acute intermittent hypoxia on breathing function after human spinal cord injury. In Experimental Neurology (Vol. 342). https://doi.org/10.1016/j.expneurol.2021.113735

Tenório, M. C. D. S., Graciliano, N. G., Moura, F. A., de Oliveira, A. C. M., & Goulart, M. O. F. (2021). N-acetylcysteine (Nac): Impacts on human health. In Antioxidants (Vol. 10, Issue 6). MDPI. https://doi.org/10.3390/antiox10060967

Terrill, J. R., Radley-Crabb, H. G., Grounds, M. D., & Arthur, P. G. (2012). N-Acetylcysteine treatment of dystrophic mdx mice results in protein thiol

modifications and inhibition of exercise induced myofibre necrosis. Neuromuscular Disorders, 22(5), 427–434. https://doi.org/10.1016/j.nmd.2011.11.007

Trucco, F., & O'Halloran, K. D. (2025). The Journal of Physiology Unravelling the complexity of respiratory involvement in Duchenne muscular dystrophy: An urgent call for a collective translational approach. J Physiol, 603, 3263–3267. https://doi.org/10.1113/JP288810#support-information-section

Verhaart, I. E. C., Heemskerk, H., Karnaoukh, T. G., Kolfschoten, I. G. M., Vroon, A., Van Ommen, G. J. B., Van Deutekom, J. C. T., & Aartsma-Rus, A. (2012). Prednisolone treatment does not interfere with 2'-O-methyl phosphorothioate antisense-mediated exon skipping in duchenne muscular dystrophy. Human Gene Therapy, 23(3), 262–273. https://doi.org/10.1089/hum.2011.127

Verma, S., Lin, J., Travers, C., McCracken, C., & Shah, D. (2017). Quantitative electromyography in ambulatory boys with Duchenne muscular dystrophy. Muscle and Nerve, 56(6), 1168–1171. https://doi.org/10.1002/mus.25678

Whitehead, N. P., Pham, C., Gervasio, O. L., & Allen, D. G. (2008). N - Acetylcysteine ameliorates skeletal muscle pathophysiology in mdx mice. The Journal of Physiology, 586(7), 2003–2014. https://doi.org/10.1113/jphysiol.2007.148338

Yuksel Kalyoncu, M., Gokdemir, Y., Yilmaz Yegit, C., Yanaz, M., Gulieva, A., Selcuk, M., Karabulut, Ş., Metin Çakar, N., Ergenekon, P., Erdem Eralp, E., Öztürk, G., Unver, O., Turkdogan, D., Sahbat, Y., Akgülle, A. H., Karakoç, F., &

Karadag, B. (2024). Unveiling the Respiratory Muscle Strength in Duchenne Muscular Dystrophy: The Impact of Nutrition and Thoracic Deformities, Beyond Spirometry. Children, 11(8). https://doi.org/10.3390/children11080994

Chapter 2. Ventilatory Effects of Acute Intermittent Hypoxia in Conscious Dystrophic Mice

2.1 Publication information

Published in:	Advances in Experimental Medicine and Biology
Article type:	Research article
Title:	**Ventilatory Effects of Acute Intermittent Hypoxia in Conscious Dystrophic Mice**

Authors:	Michael N. Maxwell[1]
	Anthony L. Marullo[1]
	Aoife D. Slyne[1]
	Eric F. Lucking[1]
	Ken D. O'Halloran[1]
Affiliations:	[1]Department of Physiology, University College Cork.

Key words:	Acute intermittent hypoxia, Long term facilitation, Duchenne muscular dystrophy, *mdx*, whole-body plethysmography.

2.2 Abstract

Exposure to acute intermittent hypoxia (AIH) elicits a form of respiratory plasticity known as long-term facilitation (LTF). Interest has grown in developing AIH interventions to treat ventilatory insufficiency, with promising results in spinal cord injury and amyotrophic lateral sclerosis. Therapeutic AIH may have application in neuromuscular disorders including muscular dystrophies. We sought to establish hypoxic ventilatory responsiveness and the expression of ventilatory LTF in X-linked muscular dystrophy (*mdx*) mice.

Experiments were performed in 15 male wild-type (BL10) and 15 male *mdx* mice at 4 months of age. Ventilation was assessed using whole-body plethysmography. Baseline measures of ventilation and metabolism were established. Mice were exposed to 10 successive bouts of hypoxia, each lasting 5 min, interspersed with 5-min bouts of normoxia. Measurements were taken for 60 min following termination of AIH.

In *mdx* mice, ventilation was significantly increased 60 min post-AIH compared to baseline. However, metabolic CO_2 production was also increased. Therefore, ventilatory equivalent was unaffected by AIH exposure, i.e., no ventilatory LTF manifestation. In wild-type mice, ventilation and metabolism were not affected by AIH.

Eliciting ventilatory LTF is dependent on many factors and may require concomitant isocapnia or hypercapnia during AIH exposures and/or repeated daily AIH exposures, which is worthy of further pursuit.

2.3 Introduction

Duchenne muscular dystrophy (DMD) is a severe monogenic neuromuscular disease caused by secondary consequences arising due to the absence of the structural protein dystrophin. Muscle contraction without dystrophin mechanically strains the plasma membrane, causing injury to the myofibres and subsequent skeletal muscle degeneration, which leads to a profound loss of function (Gumerson & Michele, 2011; Manning & O'Malley, 2015). Dysfunction extends to the respiratory musculature (Sawnani et al., 2015).

In infancy, people with DMD present with symptoms such as frequent falls and a waddling gate, culminating in wheelchair dependency by about 10–12 years of age. Most DMD patients require assisted ventilation in some capacity around the age of 20 years. Advances in cardiorespiratory care have increased patients' life expectancy from early 20s to 30s with some living until the age of ~40 (Broomfield et al., 2021). There is continued interest in the development of novel therapeutic strategies.

Progressive DMD is characterised by ventilatory insufficiency. People with DMD hypoventilate, especially during sleep (Sawnani et al., 2015). Exposure to acute intermittent hypoxia (AIH) elicits a form of respiratory plasticity known as long-term facilitation (LTF), which increases respiratory motor output. Following decades of basic fundamental research in animal models, therapeutic intermittent hypoxia is now an established modality with proven capacity to increase ventilation in various disease states characterised by ventilatory

compromise including amyotrophic lateral sclerosis and incomplete spinal cord injury, restoring normal or near-normal levels of breathing (Golder & Mitchell, 2005; Nichols et al., 2017; Sajjadi et al., 2022; Sutor et al., 2021).

Therapeutic intermittent hypoxia may be useful as an adjunctive therapy in the treatment of DMD. The aim of this study was to establish the capacity for the expression of ventilatory LTF in X-linked muscular dystrophy using *mdx* mice.

2.4 Materials and Methods

2.4.1 Ethical approval

Procedures on live animals were performed under authorisation from the Health Products Regulatory Authority in accordance with Irish and European law following approval by University College Cork's ethics committee (AEEC no. 2021/019). Experiments were carried out in accordance with guidelines laid down by University College Cork's Animal Welfare Body.

2.4.2 Experimental Animals

Male wild-type (C57BL/10; n = 15) and *mdx* (C57BL/10ScSn-Dmd*mdx*/J; n = 15) mice were bred in our institution's animal housing facility and were studied at 4 months of age. Animals were housed in individually ventilated cages in temperature- and humidity-controlled rooms, operating under a 12:12 h light/dark cycle with food and water available ad libitum.

2.4.3 Whole-Body Plethysmography

Whole-body plethysmography was used to assess respiratory flow in unrestrained, unanaesthetised mice. Mice were introduced into plethysmograph chambers (Model PLY4211; volume 600 mL; Buxco Research Systems, Wilmington, NC, USA) and allowed to acclimate to the chamber environment for ~2 h. Following completion of exploration and grooming behaviours, mice settled and were studied during quiet rest.

2.4.4 Experimental Protocol

Following acclimation and a settling period, a 30-min baseline recording was performed in normoxia. This was followed by 10 successive bouts of hypoxia ($FiO_2 = 0.10$), lasting 5 min, interspersed with 5-min bouts of normoxia ($FiO_2 = 0.21$). Measurements were taken for 60 min following termination of AIH. Following the experimental protocol, mice were anaesthetised using 5% isoflurane in air and killed by cervical dislocation.

2.4.5 Data and Statistical Analysis

Minute ventilation ($\dot{V}_I$) and metabolic CO_2 production ($\dot{V}CO_2$) were normalised for body mass (g). Data are shown as individual data points in box and whisker plots with median, interquartile ranges and maximum and minimum values. The ventilatory equivalent ($\dot{V}_I/\dot{V}CO_2$) was determined. One-way ANOVA was

performed with Bonferroni post hoc comparisons. $P < 0.05$ was considered statistically significant.

2.5 Results

2.5.1 Effect of AIH on Ventilation

In wild-type mice, there was no significant difference in minute ventilation at either 30 min (p = 0.4355) or 60 min (p = 0.8310) compared with the initial baseline pre-AIH (Fig. 1A). In *mdx* mice, there was no significant difference between the initial baseline values and 30 min post-AIH (p = 0.1167); however, a significant increase was observed at 60 min post-AIH (p = 0.0124) (Fig. 1B).

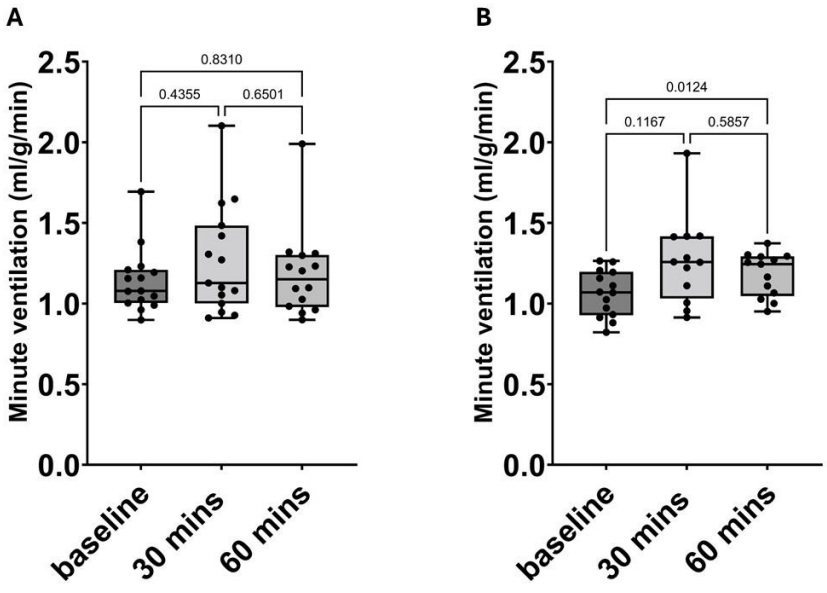

Fig. 2.1: Ventilation following exposure to AIH. Minute ventilation during baseline (pre-AIH), and 30- and 60-minutes post AIH for (A) wild-type and (B) mdx mice.

2.5.2 Effect of AIH on Metabolism

In wild-type mice, there was no significant difference in metabolic CO_2 production at either 30 min ($p = 0.9766$) or 60 min ($p = 0.1964$) compared with the initial baseline pre-AIH (Fig. 2A). In *mdx* mice, there was a significant increase in metabolic CO_2 production at 30 min post-AIH ($p = 0.0019$) and 60 min post-AIH ($p = 0.0122$) (Fig. 2B).

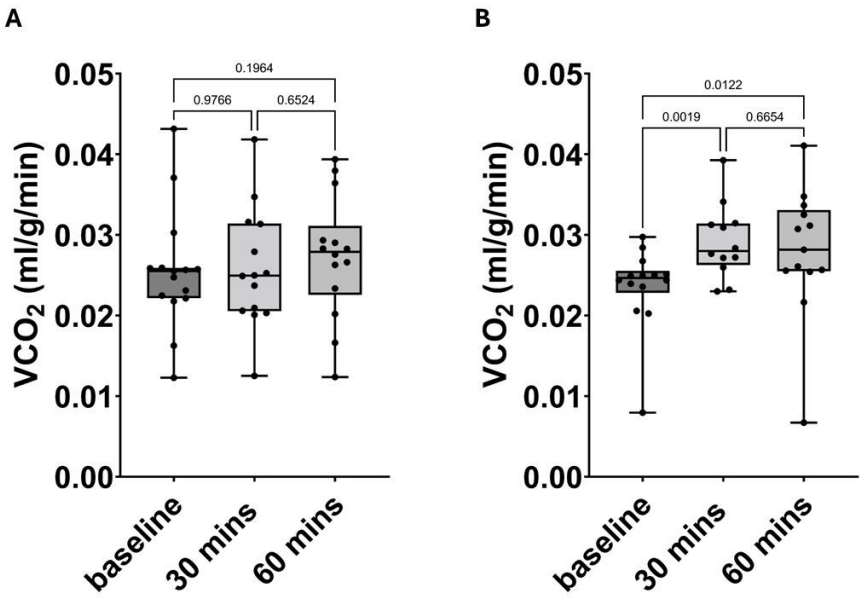

Fig. 2.2: Metabolism following exposure to AIH. Metabolic CO_2 production during baseline (pre-AIH), and 30- and 60-minutes post AIH for (A) wild-type and (B) mdx mice.

2.5.3 Effect of AIH on the ventilatory equivalent

In wild-type mice, the ventilatory equivalent ($\dot{V}_I/\dot{V}CO_2$) was comparable to baseline at 30 min ($p = 0.6557$) and 60 min ($p = 0.7626$) (Fig. 3A). Similarly,

in *mdx* mice, there was no significant difference in the ventilatory equivalent comparing the initial baseline values and values at 30 min post-AIH (p = 0.8315) and 60 min post-AIH (p = 0.7447) (Fig. 3B).

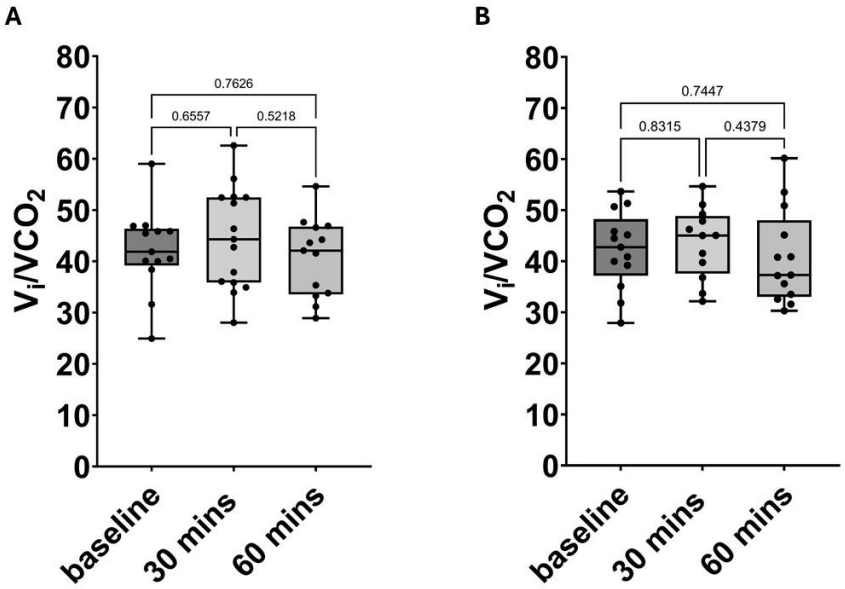

Figure 2.3: Ventilatory equivalent following exposure to AIH. Ventilatory equivalent pre-AIH, and 30- and 60-minutes post AIH for (A) wild-type and (B) mdx mice.

2.5.4 Effect of AIH on Breathing frequency

In wild-type mice, the breathing frequency was comparable to baseline at 30 min (p = 0.1312) and 60 min (p = 0.2180) (Fig. 4A). In *mdx* mice, there was a significant difference in the breathing frequency comparing the initial baseline values and values at 30 min post-AIH (p = 0.0414) but no significant difference at 60 min post-AIH (p = 0.1592) (Fig. 4B).

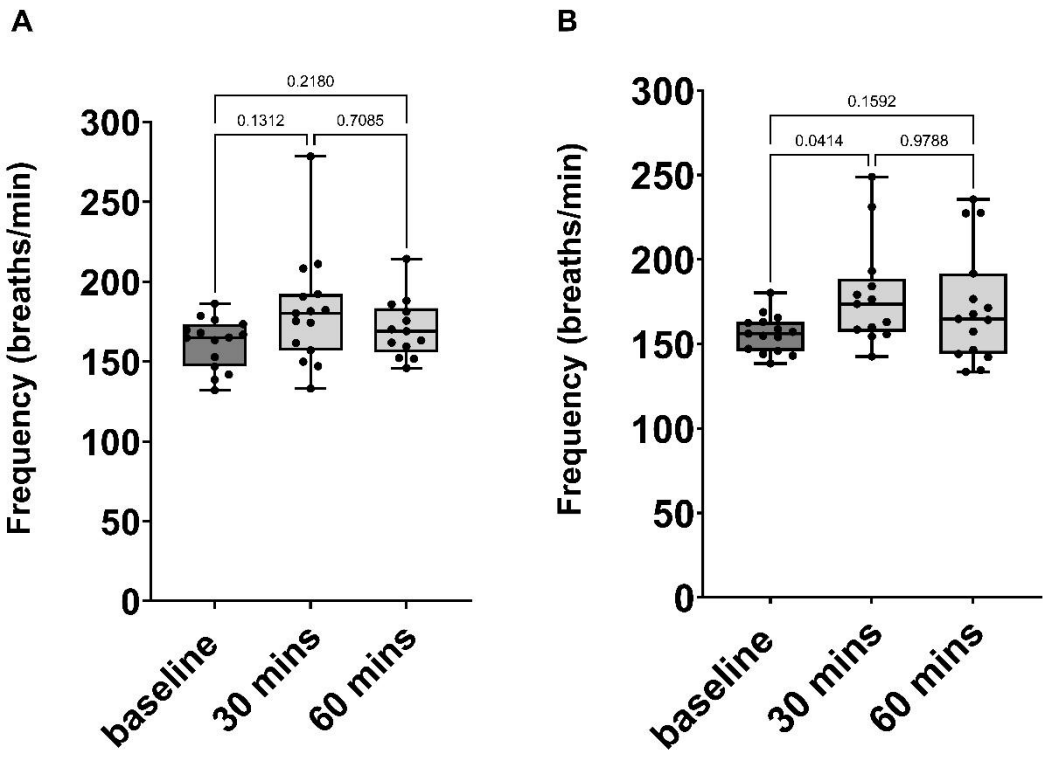

Figure 2.4: Breathing frequency following exposure to AIH. Breathing frequency pre-AIH, and 30- and 60-minutes post AIH for (A) wild-type and (B) mdx mice.

2.5.5 Effect of AIH on Tidal Volume

In wild-type mice, the tidal volume was comparable to baseline at 30 min (p = 0.9918) and 60 min (p = 0.9058) (Fig. 5A). Similarly, in *mdx* mice, there was no significant difference in tidal volume comparing the initial baseline values and values at 30 min post-AIH (p = 0.0746) and 60 min post-AIH (p = 0.1915) (Fig. 5B).

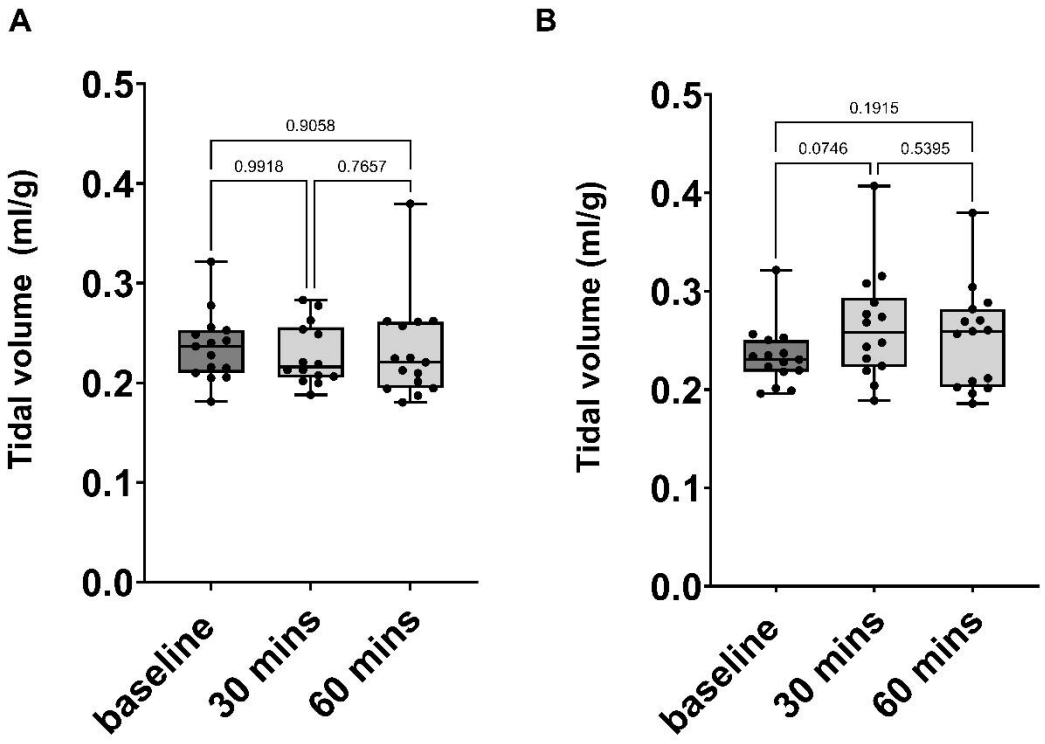

Figure 2.5: Tidal volume following exposure to AIH. Tidal volume pre-AIH, and 30- and 60-minutes post AIH for (A) wild-type and (B) mdx mice.

2.6 Discussion

We sought to establish the capacity for the expression of ventilatory LTF in X-linked muscular dystrophy using *mdx* mice. Ventilation, metabolism and the ventilatory equivalent were examined at baseline and for 60 min following AIH. We fully anticipated that the AIH protocol employed in the study would elicit LTF in wild-type mice, based upon prior literature, albeit mostly in rats (M. S. Hoffman & Mitchell, 2013; Mendonça-Junior et al., 2021). Whether AIH would elicit LTF in *mdx* mice was an open question given that there are impairments at several sites of the respiratory network in *mdx* mice (Burns, Drummond, et al., 2019; Burns et al., 2018; Burns, Murphy, et al., 2019; Burns, Roy, et al., 2017;

Lovering et al., 2020; Mhandire et al., 2022), which could conceivably limit the capacity to elicit LTF.

In *mdx* mice, upon examination of the data for frequency, tidal volume and ventilation, it is evident that minute ventilation was significantly increased 60 min following exposure to AIH compared to the initial baseline period despite no statistically significant increase in frequency or tidal volume. On the face of it, this is suggestive of the expression of LTF of breathing. However, upon examination of the metabolic CO_2 production at the same timepoints, we determined that there were also significant increases in metabolism at both 30 and 60 min compared with baseline values. There was no overt difference in animal activity or behaviour between the respective timepoints suggesting that the metabolic effect may have been a direct effect of exposure to AIH. However, as illustrated by the data for ventilatory equivalent ($\dot{V}_I/\dot{V}CO_2$), it is clear that the increase in ventilation following AIH was an appropriate adjustment for the increase in metabolism. As such, there was no expression of ventilatory LTF in dystrophic mice.

Surprisingly, LTF did not manifest in wild-type mice also. Indeed, neither frequency, tidal volume, ventilation nor metabolism were affected by exposure to AIH in wild-type mice. As such, given this unexpected finding, the issue as to whether LTF can be expressed in muscular dystrophy remains inconclusive. Further studies are required to establish a model of LTF in conscious BL-10 mice that can be applied to the *mdx* mouse model of muscular dystrophy.

The capacity to elicit ventilatory LTF is dependent on many factors and future experimental studies could consider the following modifications to the current study. First, it may be necessary to employ concomitant isocapnia or hypercapnia during AIH exposure. The combined effect of hypoxia and CO_2 to enhance chemoreceptor activation of breathing may be required to elicit long-lasting robust facilitation of breathing (Wakai et al., 2015). Second, daily AIH exposure to elicit metaplasticity may be required for sustained functional gains and will be important to establish in the context of chronic rehabilitative therapy for DMD (Hickner et al., 2014). Third, pharmacological co-treatment could be applied in tandem with AIH, for example, the use of adenosine receptor blockade to avoid cross-talk inhibition of serotonergic mechanisms contributing to LTF (M. S. Hoffman et al., 2010). And finally, albeit more readily applicable to the clinical scenario, task-specific co-treatment such as exposure to AIH in tandem with ventilatory-specific exercises might amplify the plasticity priming effects of AIH to drive ventilatory LTF (Welch et al., 2020).

We acknowledge too that whereas our study was an attempt at proof of principle, to consider the manifestation of LTF in a mouse model of DMD, and our single exposure AIH paradigm did not evoke a sustained change in ventilation that was independent of VCO_2, whether AIH can be safely and effectively applied in human DMD is an issue requiring careful consideration. Whereas DMD is characterised by ventilatory insufficiency, interventions that increase neural drive to recruit respiratory muscles could potentially exacerbate muscle dysfunction through enhanced contraction-induced injury. Interestingly,

however, repeated exposure to AIH has the potential to influence many other aspects of the respiratory system including respiratory muscles. Whereas chronic intermittent hypoxia modelling human sleep apnoea results in respiratory dysfunction, including respiratory muscle weakness (Drummond et al., 2021, 2022; O'Halloran, 2016; O'Halloran et al., 2017; Shortt et al., 2014) that must clearly be avoided in therapeutic strategies for muscle weakness disorders, there is scope for modest application of AIH paradigms to evoke muscle plasticity in favour of improved functional outcomes and/or resilience to stressors associated with disease. We suggest that further study of the potential benefits of AIH for the treatment of muscular dystrophy is worthy of pursuit.

2.7 References

Broomfield, J., Hill, M., Guglieri, M., Crowther, M., & Abrams, K. (2021). Life Expectancy in Duchenne Muscular Dystrophy: Reproduced Individual Patient Data Meta-analysis. Neurology, 97(23), e2304. https://doi.org/10.1212/WNL.0000000000012910

Burns, D. P., Canavan, L., Rowland, J., O'Flaherty, R., Brannock, M., Drummond, S. E., O'Malley, D., Edge, D., & O'Halloran, K. D. (2018). Recovery of respiratory function in mdx mice co-treated with neutralizing interleukin-6 receptor antibodies and urocortin-2. The Journal of Physiology, 596(21), 5175–5197. https://doi.org/10.1113/JP276954

Burns, D. P., Drummond, S. E., Bolger, D., Coiscaud, A., Murphy, K. H., Edge, D., & O'Halloran, K. D. (2019). N-acetylcysteine Decreases Fibrosis and Increases Force-Generating Capacity of mdx Diaphragm. Antioxidants, 8(12), 581. https://doi.org/10.3390/antiox8120581

Burns, D. P., Murphy, K. H., Lucking, E. F., & O'Halloran, K. D. (2019). Inspiratory pressure-generating capacity is preserved during ventilatory and non-ventilatory behaviours in young dystrophic mdx mice despite profound diaphragm muscle weakness. The Journal of Physiology, 597(3), 831–848. https://doi.org/10.1113/JP277443

Burns, D. P., Roy, A., Lucking, E. F., McDonald, F. B., Gray, S., Wilson, R. J., Edge, D., & O'Halloran, K. D. (2017). Sensorimotor control of breathing in the mdx mouse model of Duchenne muscular dystrophy. The Journal of Physiology, 595(21), 6653–6672. https://doi.org/10.1113/JP274792

Drummond, S. E., Burns, D. P., Maghrani, S. El, Ziegler, O., Healy, V., & O'Halloran, K. D. (2022). NADPH oxidase 2 is necessary for chronic intermittent hypoxia-induced sternohyoid muscle weakness in adult male mice. Experimental Physiology, 107(8), 946–964. https://doi.org/10.1113/EP090536

Drummond, S. E., Burns, D. P., O'Connor, K. M., Clarke, G., & O'Halloran, K. D. (2021). The role of NADPH oxidase in chronic intermittent hypoxia-induced respiratory plasticity in adult male mice. Respiratory Physiology & Neurobiology, 292, 103713. https://doi.org/10.1016/J.RESP.2021.103713

Golder, F. J., & Mitchell, G. S. (2005). Spinal synaptic enhancement with acute intermittent hypoxia improves respiratory function after chronic cervical spinal cord injury. Journal of Neuroscience, 25(11), 2925–2932. https://doi.org/10.1523/JNEUROSCI.0148-05.2005

Gumerson, J. D., & Michele, D. E. (2011). The Dystrophin-Glycoprotein Complex in the Prevention of Muscle Damage. Journal of Biomedicine and Biotechnology, 2011, 13. https://doi.org/10.1155/2011/210797

Hickner, S., Hussain, N., Angoa-Perez, M., Francescutti, D. M., Kuhn, D. M., & Mateika, J. H. (2014). Ventilatory long-term facilitation is evident after initial and repeated exposure to intermittent hypoxia in mice genetically depleted of brain

serotonin. Journal of Applied Physiology, 116(3), 240–250. https://doi.org/10.1152/japplphysiol.01197.2013

Hoffman, M. S., Golder, F. J., Mahamed, S., & Mitchell, G. S. (2010). Spinal adenosine A2A receptor inhibition enhances phrenic long term facilitation following acute intermittent hypoxia. Journal of Physiology, 588(1), 255–266. https://doi.org/10.1113/jphysiol.2009.180075

Hoffman, M. S., & Mitchell, G. S. (2013). Spinal 5-HT7 receptors and protein kinase A constrain intermittent hypoxia-induced phrenic long-term facilitation. Neuroscience, 250. https://doi.org/10.1016/j.neuroscience.2013.06.068

Lovering, R. M., Iyer, S. R., Edwards, B., & Davies, K. E. (2020). Alterations of neuromuscular junctions in Duchenne muscular dystrophy. In Neuroscience Letters (Vol. 737). Elsevier Ireland Ltd. https://doi.org/10.1016/j.neulet.2020.135304

Manning, J., & O'Malley, D. (2015). What has the mdx mouse model of duchenne muscular dystrophy contributed to our understanding of this disease? Journal of Muscle Research and Cell Motility, 36(2), 155–167. https://doi.org/10.1007/S10974-015-9406-4/FIGURES/2

Mendonça-Junior, B. A., V. Fernandes, M., & Zoccal, D. B. (2021). Acute intermittent hypoxia evokes ventilatory long-term facilitation and active expiration in unanesthetized rats. Respiratory Physiology and Neurobiology, 294. https://doi.org/10.1016/j.resp.2021.103768

Mhandire, D. Z., Burns, D. P., Roger, A. L., O'Halloran, K. D., & ElMallah, M. K. (2022). Breathing in Duchenne muscular dystrophy: translation to therapy. The Journal of Physiology, 600(15), 3465–3482. https://doi.org/10.1113/JP281671

Nichols, N. L., Satriotomo, I., Allen, L. L., Grebe, A. M., & Mitchell, G. S. (2017). Mechanisms of enhanced phrenic long-term facilitation in SOD1G93a rats. Journal of Neuroscience, 37(24), 5834–5845. https://doi.org/10.1523/JNEUROSCI.3680-16.2017

O'Halloran, K. D. (2016). Chronic intermittent hypoxia creates the perfect storm with calamitous consequences for respiratory control. Respiratory Physiology and Neurobiology, 226. https://doi.org/10.1016/j.resp.2015.10.013

O'Halloran, K. D., Lewis, P., & McDonald, F. (2017). Sex, stress and sleep apnoea: Decreased susceptibility to upper airway muscle dysfunction following intermittent hypoxia in females. Respiratory Physiology & Neurobiology, 245, 76–82. https://doi.org/10.1016/J.RESP.2016.11.009

Sajjadi, E., Seven, Y. B., Ehrbar, J. G., Wymer, J. P., Mitchell, G. S., & Smith, B. K. (2022). Acute intermittent hypoxia and respiratory muscle recruitment in people with amyotrophic lateral sclerosis: A preliminary study. In Experimental Neurology (Vol. 347). Academic Press Inc. https://doi.org/10.1016/j.expneurol.2021.113890

Sawnani, H., Thampratankul, L., Szczesniak, R. D., Fenchel, M. C., & Simakajornboon, N. (2015). Sleep disordered breathing in young boys with duchenne muscular dystrophy. Journal of Pediatrics, 166(3). https://doi.org/10.1016/j.jpeds.2014.12.006

Shortt, C. M., Fredsted, A., Chow, H. B., Williams, R., Skelly, J. R., Edge, D., Bradford, A., & O'Halloran, K. D. (2014). Reactive oxygen species mediated diaphragm fatigue in a rat model of chronic intermittent hypoxia. Experimental Physiology, 99(4). https://doi.org/10.1113/expphysiol.2013.076828

Sutor, T., Cavka, K., Vose, A. K., Welch, J. F., Davenport, P., Fuller, D. D., Mitchell, G. S., & Fox, E. J. (2021). Single-session effects of acute intermittent hypoxia on breathing function after human spinal cord injury. In Experimental Neurology (Vol. 342). https://doi.org/10.1016/j.expneurol.2021.113735

Wakai, J., Takamura, D., Morinaga, R., Nakamuta, N., & Yamamoto, Y. (2015). Differences in respiratory changes and Fos expression in the ventrolateral medulla of rats exposed to hypoxia, hypercapnia, and hypercapnic hypoxia.

Respiratory Physiology and Neurobiology, 215. https://doi.org/10.1016/j.resp.2015.05.008

Welch, J. F., Sutor, T. W., Vose, A. K., Perim, R. R., Fox, E. J., & Mitchell, G. S. (2020). Synergy between Acute Intermittent Hypoxia and Task-Specific Training. Exercise and Sport Sciences Reviews, 48(3), 125–132. https://doi.org/10.1249/JES.0000000000000222

Chapter 3. Chronic N-acetyl cysteine treatment does not improve respiratory system performance in the *mdx* mouse model of Duchenne muscular dystrophy

3.1 Publication information

Published in:	Experimental Physiology
Article type:	Research article
Title:	**Chronic *N*-acetyl cysteine treatment does not improve respiratory system performance in the *mdx* mouse model of Duchenne muscular dystrophy**

Authors:	Michael N. Maxwell[1]
	Anthony L. Marullo[1]
	Esther Valverde-Pérez[2,3]
	Aoife D. Slyne[1]
	Ben T. Murphy[1]
	Ken D. O'Halloran[1]
Affiliations:	[1]Department of Physiology, University College Cork, Ireland
	[2] Departamento de Bioquímica y Biología Molecular y Fisiología, Facultad de Medicina, Universidad de Valladolid, Valladolid, Spain
	[3]Unidad de Excelencia Instituto Biomedicina y Genética Molecular (IBGM), Universidad de Valladolid-CSIC, Valladolid, Spain

Key words:	antioxidant, diaphragm, inspiratory pressure, muscular dystrophy, respiratory EMGs

3.2 Abstract

Duchenne muscular dystrophy (DMD) is characterised by respiratory muscle injury, inflammation, fibrosis and weakness, ultimately culminating in respiratory failure. The dystrophin-deficient mouse model of DMD (*mdx*) shows evidence of respiratory muscle remodelling and dysfunction contributing to impaired respiratory system performance. The antioxidant N-acetylcysteine (NAC) has been shown to exert anti-inflammatory and anti-fibrotic effects leading to improved respiratory muscle performance in a range of animal models of muscle dysfunction, including *mdx* mice, following short-term administration (2 weeks). We sought to build on previous work by exploring the effects of chronic NAC administration (3 months) on respiratory system performance in *mdx* mice. One-month-old male *mdx* mice were randomised to receive normal drinking water (n = 30) or 1% NAC in the drinking water (n = 30) for 3 months. At 4 months of age, we assessed breathing in conscious mice by plethysmography followed by ex vivo assessment of diaphragm force-generating capacity. Additionally, diaphragm histology was performed. In separate studies, in anaesthetised mice, respiratory electromyogram (EMG) activity and inspiratory pressure across a range of behaviours were determined, including assessment of peak inspiratory pressure-generating capacity. NAC treatment did not affect force-generating capacity of the *mdx* diaphragm. Collagen content and immune cell infiltration were unchanged in *mdx* + NAC compared with *mdx* diaphragms. Additionally, there was no significant effect of NAC on breathing, ventilatory responsiveness, inspiratory EMG activity or inspiratory pressure across the range of behaviours from basal conditions to peak system performance. We conclude that chronic

NAC treatment has no apparent beneficial effects on respiratory system performance in the *mdx* mouse model of DMD suggesting limited potential of NAC treatment alone for human DMD.

3.2.1 Highlights

3.2.1.1 What is the central question of this study?

Does chronic treatment with the antioxidant, anti-inflammatory, and anti-fibrotic dietary supplement N-acetyl cysteine (NAC) improve respiratory system performance in the *mdx* mouse model of Duchenne muscular dystrophy?

3.2.1.2 What is the main finding and its importance?

Chronic treatment with NAC does not improve a range of respiratory-related parameters in *mdx* mice suggesting limited potential for NAC alone as an intervention in Duchenne muscular dystrophy.

3.3 Introduction

Duchenne muscular dystrophy (DMD) is a fatal neuromuscular disease caused by mutations in the *DMD* gene, which results in the absence of the muscle isoform of the protein dystrophin (Dp427m) (Aartsma-Rus et al., 2006; E. P. Hoffman et al., 1987a). Dystrophin is part of the dystrophin glycoprotein complex (DGC), a structure that connects the myocellular cytoskeleton to the extracellular matrix via the sarcolemma, providing support during recurring contractions, and thus protecting muscle fibres (Gao & McNally, 2015).

In the absence of dystrophin, during contraction, damage occurs to muscle fibres leading to muscle deterioration and degeneration, which is a primary phenotype of DMD (Burns, Drummond, et al., 2019; Burns et al., 2018; Burns, Murphy, et al., 2019; O'Halloran et al., 2023). As a result, the DGC and its function is lost and inflammation and fibrosis ensue with attendant respiratory muscle weakness, which is evident in reductions in ventilatory capacity, and eventual respiratory failure and death (De Bruin et al., 1997; Evans et al., 2009; Khirani et al., 2014; P. E. M. Smith et al., 1989). To date, there is no cure for people with DMD. Therapies for the improvement of respiratory muscle strength in DMD are necessary, to delay or prevent respiratory muscle failure, protecting respiratory system capacity.

The dystrophin-deficient mouse model of DMD (*mdx*) exhibits impaired respiratory muscle performance like that observed in human DMD. Studies of the respiratory system of the *mdx* mouse have shown severe muscle weakness in conjunction with structural remodelling of the diaphragm (Burns, Drummond,

et al., 2019; Burns et al., 2018; Burns, Murphy, et al., 2019; Burns, Roy, et al., 2017; Mhandire et al., 2022; O'Halloran et al., 2023). Markers of inflammation including immune cell infiltration, elevated cytokine concentrations, elevated levels of reactive oxygen species and collagen deposition are evident in the *mdx* diaphragm (Burns, Drummond, et al., 2019; Choi et al., 2016; O'Halloran et al., 2023). It has also been established that electromyogram (EMG) activity in the principal muscles of breathing is reduced, most likely reflecting impaired neuromuscular transmission of central respiratory neural activation critical for respiratory performance (Burns, Murphy, et al., 2019; O'Halloran et al., 2023; Personius & Sawyer, 2006).

Antioxidants have been proposed as a potential therapy for respiratory muscle dysfunction, and several studies have yielded promising results in animal models including animal models of muscular dystrophy (Burns, Ali, et al., 2017; Burns et al., 2018; Garegnani et al., 2021; Lewis et al., 2015, 2016; Lewis & O'Halloran, 2016; O'Halloran et al., 2017). *N*-acetyl cysteine (NAC) is a dietary antioxidant, a precursor to glutathione, which is safe for use in humans. NAC exerts antioxidant, anti-inflammatory and anti-fibrotic effects leading to improved muscle performance in a range of animal models of muscular dystrophy (Burns, Drummond, et al., 2019; Pinniger et al., 2017; Redwan et al., 2023; Terrill et al., 2012; Whitehead et al., 2008). Pinniger et al. (2017) showed an increase in *mdx* mouse grip strength and extensor digitorum longus (EDL) muscle force after 6 weeks of 2% NAC treatment. Furthermore, the authors showed evidence of a reduction in muscle inflammation and oxidative stress

(Pinniger et al., 2017). Terrill et al. (2012) showed that 1% NAC treatment for 1 week prevented exercise-induced myofibre necrosis and reduced blood creatine kinase activity after exercise. Whitehead et al. (2008) showed that 6 weeks of 1% NAC treatment resulted in a reduction in reactive oxygen species by reduced fluorescence in muscle tissue stained for dihydroethidium, and a reduction of damage in the *mdx* EDL evidenced by a decrease in centrally nucleated muscle fibres. Redwan et al. (2023) reported that 2% NAC administration for 6 weeks significantly reduced EDL muscle mass and abnormal fibre branching and splitting, which causes dystrophic EDL muscle hypertrophy (Redwan et al., 2023). Previously our research group investigated the effects of acute NAC treatment on respiratory performance in the *mdx* mouse. Burns, Drummond et al. (2019) showed that 1% NAC treatment for 2 weeks rescued *mdx* diaphragm function by increasing force-generating capacity, associated with a decrease in diaphragm fibrosis and immune cell infiltration compared to untreated *mdx* mice. However, short-term NAC treatment did not recover impaired respiratory EMG activity in diaphragm and external intercostal muscles of breathing. Collectively, these studies suggest that NAC administration may be a promising therapeutic for the treatment of skeletal muscle dysfunction in the *mdx* model of DMD with potential application to human DMD.

DMD is a progressive muscle wasting disorder with temporal decline in respiratory system performance. It is important to consider the efficacy of longer-term pharmacotherapies for DMD over time domains that reflect

progressive deterioration in muscle performance due to persistent dystropathology. In the current study, we sought to assess the effects of chronic NAC treatment (1% NAC for 3 months) on respiratory system performance in *mdx* mice starting at 1 month of age. We hypothesised that NAC would have beneficial effects on dystrophic respiratory muscle structure and function and would improve respiratory EMG activity leading to preservation of respiratory performance.

3.4 Methods

3.4.1 Ethical approval

Procedures on live animals were performed under project authorisation (AE19130/P117) from the Health Products Regulatory Authority in accordance with Irish and European law with prior ethical approval by University College Cork (AEEC 2019/013). Experiments were carried out in accordance with guidelines and requirements laid down by University College Cork's Animal Welfare Body.

3.4.2 Experimental animals and NAC treatment

Breeding pairs (homozygous females with hemizygous males) for *mdx* mice (C57BL/10ScSn-Dmd*mdx*/J) were purchased from The Jackson Laboratory (Bar Harbor, ME, USA) and a colony was established at University College Cork's specific pathogen-free facility. Animals were housed in individually ventilated cages in temperature- and humidity-controlled rooms, operating on a 12 h

light:12 h dark cycle with food and water available ad libitum. Studies were performed in 60 male *mdx* mice. Mice were randomly assigned to two different experimental groups: *mdx* (*n* = 30) and *mdx* + NAC (*n* = 30). The *mdx* + NAC group received 1% NAC (Sigma-Aldrich, Wicklow, Ireland) in the drinking water for 3 months, beginning at 1 month of age. Drinking water containing NAC was pH matched to control water and prepared fresh each day to mitigate any potential degradation and ensure maximal bioavailability. For the *mdx* + NAC group, water bottles were weighed daily. Estimated fluid intake was normal and stable over the 3-month intervention, averaging 4–5 mL per mouse per day. Mice were studied at 4 months of age. A thorough assessment of respiratory performance was made, with measurements of breathing and ventilatory capacity in response to chemoactivation, recordings of thoracic inspiratory pressure and respiratory muscle electromyography (EMG) in anaesthetised animals and respiratory muscle function tests *ex vivo*. Diaphragm muscle tissue was collected for structural and molecular analysis using standard histological techniques and qPCR.

3.4.3 Plethysmography

Whole-body plethysmography was used to assess respiratory flow in unrestrained, unanaesthetised *mdx* (*n* = 15) and *mdx* + NAC (*n* = 15) mice. Mice were introduced into plethysmograph chambers (Model PLY4211; volume 600 mL, Buxco Research Systems, Wilmington, NC, USA) and were allowed an

acclimation period (~2 h) with room air passing through each chamber (0.85 L min^{-1}).

3.4.3.1 Experimental protocol

Following acclimation, during confirmed periods of quiet rest, a 10-min baseline recording was performed in normoxia. This was followed by combined central and peripheral chemoreceptor stimulation with hypercapnic hypoxia (10% O_2 and 6% CO_2) for 10 min, to examine maximum chemoactivated breathing. Respiratory parameters including respiratory frequency (*f*), tidal volume (V_T) and minute ventilation ($\dot{V}_I$) were recorded on a breath-by-breath basis for analysis offline. A gas analyser (AD Instruments, Colorado Springs, CO, USA) was used to measure oxygen consumption ($\dot{V}O_2$) and carbon dioxide production ($\dot{V}CO_2$).

3.4.3.2 Data analysis

Baseline normoxic ventilation was determined as an average of the baseline period. For hypercapnic hypoxia, ventilatory measurements were taken during the final 5 min of the challenge to ensure steady-state changes. V_T and $\dot{V}_I$ were normalised for body mass (g).

3.4.4 Ex vivo diaphragm muscle function

Following plethysmography measurements, mice were killed by cervical dislocation under 5% isoflurane anaesthesia, and diaphragm muscle (rib and central tendon intact) was immediately excised and placed in a tissue bath at

room temperature containing continuously gassed hyperoxic (95% O_2/5% CO_2) Krebs solution (in mM: NaCl, 120; KCl, 5; calcium gluconate, 2.5; $MgSO_4$, 1.2; NaH_2PO_4, 1.2; $NaHCO_3$, 25; and glucose, 11.5) and d-tubocurarine (25 μM) prior to functional analysis. Thin strips of diaphragm muscle were prepared from the mid-costal section of the right hemidiaphragm. Diaphragm muscle preparations were suspended vertically between two platinum plate electrodes in a water-jacketed tissue bath at 35°C containing Krebs solution and were continuously gassed with carbogen (95% O_2 and 5% CO_2). The rib was sutured to an immobile hook and remained in a fixed position for the duration of the experiment. Using non-elastic string, the central tendon was attached to a lever connected to a dual-mode force transducer (Aurora Scientific Inc., Aurora, ON, Canada). To determine muscle optimum length (L_o), the length of the muscle preparations was adjusted using a micro-positioner between intermittent twitch contractions. The muscle length which revealed maximal isometric twitch force for a single isometric twitch stimulation (supramaximal stimulation, 1 ms duration) was considered L_o. Diaphragm preparations were maintained at L_o for the duration of the protocol.

3.4.4.1 Experimental protocol

First, a single isometric twitch contraction was measured and tetanic force at 100 Hz (Po), time to peak (TTP) and half-relaxation time were assessed. To examine the force–frequency relationship, muscle bundles were stimulated

sequentially at 25, 50, 75 and 150 Hz (300 ms train duration). Contractions were interspersed by a 1 min interval.

3.4.4.2 Data analysis

Muscle bundle cross-sectional area (CSA) was determined for the purpose of normalising muscle force to bundle size. CSA was calculated by dividing muscle mass (weight in grams) by the product of muscle L_o (cm) and muscle density (assumed to be 1.06 g cm^{-3}). Muscle force was divided by bundle CSA and expressed as specific force (N cm^{-2}). TTP and half-relaxation time were measured as indices of isometric twitch kinetics and were expressed in milliseconds.

3.4.5 Respiratory EMGs and inspiratory pressure recordings

In separate studies, *mdx* (*n* = 15) and *mdx* + NAC mice (*n* = 15), anaesthesia was induced with 5% isoflurane in 60% O_2 (balance N_2) in an induction chamber. Mice were subsequently placed in the supine position and received 2% isoflurane in 60% O_2 (balance N_2) by nose-cone delivery. Mice were gradually transitioned from isoflurane to urethane anaesthesia (1.7 g kg^{-1} i.p. in total given in three injections) over a 25-min period. Body temperature was maintained at 37°C via a rectal probe and thermostatically controlled heating blanket (Harvard Apparatus, Holliston, MA, USA). We established an acceptable surgical plane of anaesthesia, determined by an absent pedal withdrawal reflex and no somatic

motor response to noxious pinch. Supplemental anaesthetic was administered as required. A pulse oximeter clip (MouseOx™, Starr Life Sciences Corp., Oakmount, PA, USA) was placed on a shaved thigh for the measurement of peripheral capillary O_2 saturation (SpO_2). A mid-cervical tracheotomy was performed. All animals were maintained with a bias flow of supplemental O_2 (FiO_2 = 0.60) under baseline conditions. Oesophageal pressure was measured using a pressure-tip catheter (Mikro-Tip, Millar Inc., Houston, TX, USA), which was positioned in the thoracic oesophagus through the mouth. The catheter was advanced into the stomach to record positive pressure swings during inspiration and then withdrawn into the lower oesophagus where stable phasic sub-atmospheric pressure swings during inspiration were observed. Concentric needle monopolar recording electrodes (26G; Natus Manufacturing Ltd, Gort, Ireland) were inserted into the middle costal region of the diaphragm on the right-hand side for the continuous measurement of diaphragm EMG activity. In addition, concentric needle monopolar electrodes were inserted into an external intercostal (EIC), in the second to fourth rostro-ventral intercostal space, for the measurement of EIC EMG and into the parasternal intercostal (PS) (second or third space) for the measurement of PS EMG. In addition, concentric needle monopolar electrodes were used to record scalene (SCAL), cleidomastoid (CM), sternomastoid (SM), sternohyoid (SH) (all mid-belly insertions) and trapezius (TRAP) (superficial insertion in the upper region on either side) with contemporaneous recordings of eight EMG signals in each mouse. EMG signals were amplified (×5000), filtered (350 Hz low cut-off to 5000 Hz high cut-off) and integrated (50 ms time constant; Neurolog system,

Digitimer Ltd, Welwyn Garden City, UK). All signals were passed through an analog-to-digital converter (Powerlab r8/30; ADInstruments) and were acquired using LabChart 8 (ADInstruments) sampled at 20 kHz (EMG) and 1 kHz for other parameters (tracheal airflow and pressure, and SpO_2).

3.4.5.1 Experimental protocol

Following instrumentation, animals were allowed to stabilise before baseline parameters were measured. Next, animals were challenged with a single sustained tracheal occlusion until peak inspiratory efforts (identified as stable, maximal successive efforts often until task failure) were observed in the inspiratory pressure recordings during sustained maximum non-ventilatory efforts. Following recovery, animals were instrumented for the measurement of tracheal airflow, and parameters were recorded during a newly established second baseline (pre-vagotomy) period. Subsequently, the vagi were sectioned bilaterally at the cervical level. Respiratory parameters were recorded under steady-state conditions for a minimum of 10 min following vagotomy. Next, animals were challenged with hypercapnic hypoxia (FiO_2 = 0.15/$FiCO_2$ = 0.06; 2 min) to examine the effects of chemostimulation on diaphragm, EIC, PS, CM, SM, SH, SCAL and TRAP EMG activity and ventilatory parameters. Following the experimental protocol, anaesthetised mice were killed by cervical dislocation and death was confirmed by the absence of cardiac rhythm.

3.4.5.2 Data analysis

The amplitudes of absolute integrated inspiratory diaphragm, EIC, PS, CM, SM, SH, SCAL and TRAP EMG activity and peak inspiratory sub-atmospheric oesophageal pressure change from baseline were measured and averaged under steady-state basal conditions (typically over 1 min) and averaged for the five successive maximal sustained efforts (maximal response) of the single airway occlusion challenge (Burns, Murphy, et al., 2019). During baseline breathing and chemoactivation, peak inspiratory and expiratory flows were measured, and inspiratory tidal volume was derived from the integral of tracheal airflow measurements.

3.4.6 Muscle Histology

3.4.6.1 Tissue preparation

Sections of hemidiaphragm from *mdx* (n = 8) and *mdx* + NAC mice (n = 8) were mounted on cubes of liver. Diaphragm samples were embedded in optimum cutting temperature embedding medium (OCT; VWR International, Dublin, Ireland) for cryoprotection and then frozen in isopentane (Sigma-Aldrich) cooled on dry ice. Samples were then stored at −80°C for subsequent structural analysis. Serial transverse muscle sections (10 μm) were cut using a cryostat (Leica CM3050; Leica Biosystems, Nußloch, Germany) at −20°C and mounted across polylysine-coated glass slides (VWR International) allowing for a distribution of tissue on a given slide.

3.4.6.2 Histological analysis

To examine putative inflammatory cell infiltration of muscle, tissue sections were stained with haematoxylin and eosin (H&E) using an autostainer (Leica ST5010 Autostainer XL, Leica Biosystems). For percentage collagen deposition, picro-sirius red (Leica Biosystems) staining was completed. Slides were mounted using DPX mounting medium (Sigma-Aldrich), air-dried and visualised on a bright field microscope (Olympus BX51, Hamburg, Germany) at ×10 magnification.

3.4.6.3 Data analysis

A total of four tissue sections per animal were examined. Muscle histology was scored using ImageJ software. Putative inflammatory cell infiltration (the presence of cells in the extracellular matrix) was scored and expressed as a percentage of the total area of muscle. For slides stained with picro-sirius red, the microscope lighting exposure was standardised during imaging. Images were analysed using a colour balance threshold and the area of collagen was expressed as a percentage of the total area of muscle. Data generated from multiple images with varying regions of interest per muscle were averaged per animal before computing group means.

3.4.7 Muscle Histology

3.4.7.1 RNA extraction and quantification

Diaphragm muscle samples were stored at −80°C. Ten to twenty milligrams per sample was homogenised on ice in Tripure Isolation Reagent (Roche Diagnostics, Ltd, Burgess Hill, UK) using a bead homogeniser (Thermo Fisher Scientific, Waltham, MA, USA). Two chloroform-phase separation steps were performed followed by 100% isopropanol precipitation of the RNA pellet and 70% ethanol wash. Isolated RNA was quantified by NeoDot (Neo Biotech, Nanterre, France). The integrity of isolated RNA was qualitatively assessed via gel electrophoresis (E-gel, Thermo Fisher Scientific).

3.4.7.2 Reverse transcription

Diaphragm muscle RNA was reverse transcribed into cDNA using a Transcriptor First Strand cDNA synthesis Kit (Roche Diagnostics Ltd) according to manufacturer's protocols.

3.4.7.3 Quantification of gene expression by qPCR

cDNA was amplified using TaqMan Gene Expression Assays (FAM; Thermo Fisher Scientific) and Fast Start Essential Probe Master Mix (Roche Diagnostics) as per the manufacturer's instructions. All reactions were carried out on a 96-well plate with a ratio of 5 µL (500 ng) cDNA/15 µL master mix using the Lightcycler 96 (Roche Diagnostics). Cycle threshold (C_T) values were normalised to the

reference gene, *Hprt1*. We have previously demonstrated that *Hprt1* is a suitable housekeeping reference gene in *mdx* diaphragm (Burns, Drummond, et al., 2019). The relative gene expression was calculated as $\Delta\Delta C_T$ between normalised expression of the gene of interest to the reference gene (*Hprt1*). Changes in genes expression were calculated as a fold change relative to the control group (*mdx*).

3.4.7 Statistical analysis

Values are expressed as box and whisker plots (median, interquartile range (IQR) and individual data scatter plot) in graphs. Data were statistically compared by repeated measures two-way ANOVA (or mixed model when occasional data points were missing for technical reasons) with Šidák's multiple comparisons *post hoc* test (Prism 10.2.0; GraphPad Software, Boston, MA, USA). Exact *P*-values are reported for all comparisons. $P < 0.05$ was considered statistically significant.

3.5 Results

3.5.1 Body mass and tibia length and mass measurements

Figure 1 compares body mass and tibia length and mass between *mdx* and *mdx* + NAC groups. Body mass was unaffected by NAC administration. Tibia length and mass were also unaffected by NAC administration. Chronic NAC treatment

had no effect on somatic growth and body mass in the *mdx* mouse model of DMD.

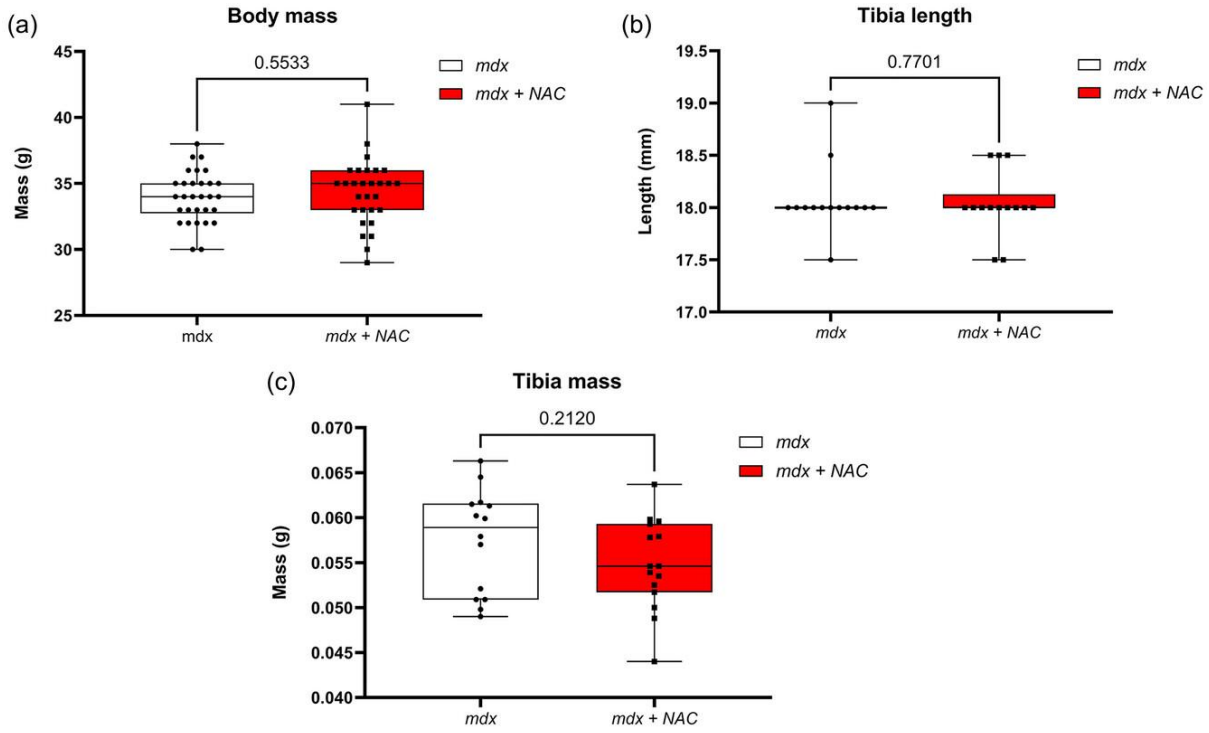

Figure 3.1: Body mass (A), tibia length (B), and tibia mass (C) in mdx and mdx + NAC mice. Values are expressed as box and whisker plots (median, 25–75 percentile and scatter plot) and were statistically compared using unpaired two-tailed t tests. Exact P-values are reported.

3.5.2 Baseline ventilation and ventilatory responsiveness to hypercapnic hypoxia in conscious mice

Respiratory frequency, tidal volume (V_T), minute ventilation ($\dot{V}_I$), metabolic CO_2 production ($\dot{V}CO_2$) and the ventilatory equivalent ($\dot{V}_I/\dot{V}CO_2$) during baseline

(20.9% O_2) and hypercapnic hypoxia (FiO_2 0.10 and $FiCO_2$ 0.06) are shown in Figure 2. All parameters were equivalent between *mdx* and *mdx* + NAC mice. Chronic NAC treatment had no effect on ventilatory performance in the *mdx* mouse model of DMD.

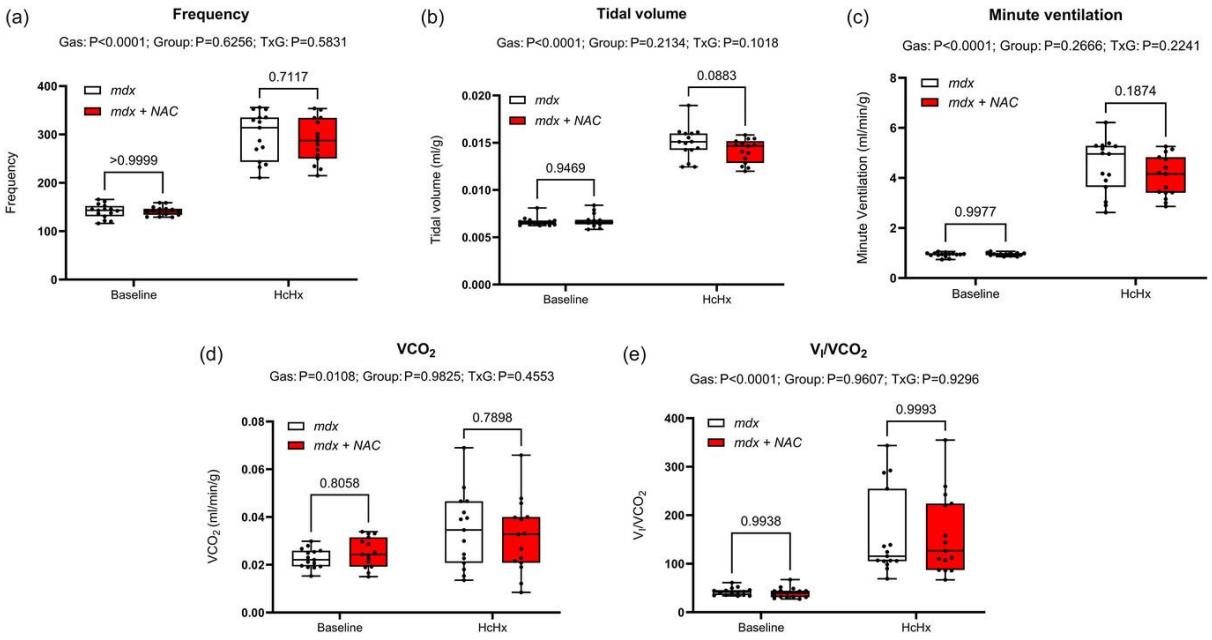

Figure 3.2: Assessment of breathing and metabolism during baseline and exposure to hypercapnic hypoxia (HcHx) in conscious mdx and mdx + NAC mice. Frequency (a), tidal volume (b) and minute ventilation (c) were determined from measurement of respiratory airflow. $\dot{V}_I/\dot{V}CO_2$ (d) was measured, and the ventilatory equivalent ($\dot{V}_I/\dot{V}CO_2$) (e) was determined offline. Data were statistically compared by repeated measures two-way ANOVA (or mixed model when occasional data points were missing for technical reasons) with Šidák's multiple comparisons post hoc test (Prism 10.2.0). Exact P-values are reported for all comparisons.

3.5.3 Diaphragm muscle contractile function ex vivo

Figure 3 shows summary data for diaphragm muscle twitch and tetanic contractions, time to peak, half-relaxation time, and the force–frequency relationships in *mdx* and *mdx* + NAC mice. Twitch force, tetanic force, time to peak, half-relaxation time, and the force–frequency relationship were equivalent between *mdx* and *mdx* + NAC mice. Chronic NAC treatment had no effect on diaphragm muscle function in the *mdx* mouse model of DMD.

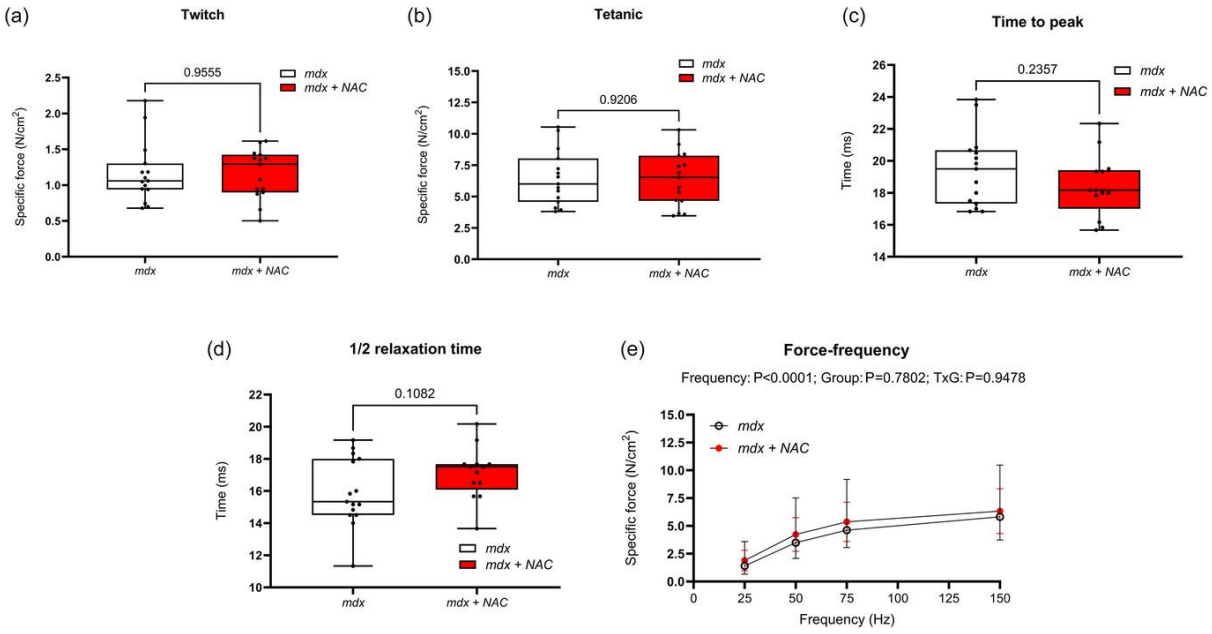

Figure 3.3: Ex vivo assessment of diaphragm twitch force (a), tetanic force (b), time to peak (TTP) (c), half-relaxation time (d) and force–frequency relationship (e) in mdx and mdx + NAC mice. Values are expressed as box and whisker plots (median, 25–75 percentile and scatter plot) or mean ± SD (force–frequency plots). Force and contractile kinetics data were statistically compared using an unpaired two-tailed t-test. The force-frequency relationships were compared by repeated measures two-way ANOVA with Šidák's multiple comparisons post hoc test (Prism 10.2.0). Exact P-values are reported for all comparisons.

3.5.4 Inspiratory pressure and obligatory and accessory muscle EMGs and ventilation in anaesthetised mice

Representative original traces of diaphragm electromyogram activity, tracheal airflow and tidal volume in an anaesthetised *mdx* mouse across a range of behaviours—baseline, following vagotomy (increased central respiratory drive) and during exposure to hypercapnic hypoxia (further increase in central respiratory drive)—are shown in Figure 4. Table 1 shows summary data for ventilatory parameters measured directly in anaesthetised *mdx* and *mdx* + NAC mice. There were no significant differences between *mdx* and *mdx* + NAC for respiratory frequency, tidal volume, minute ventilation, and peak inspiratory and expiratory flows across all behaviours. Consistent with observations in conscious mice, NAC treatment had no effect on ventilatory performance in the *mdx* mouse model of DMD.

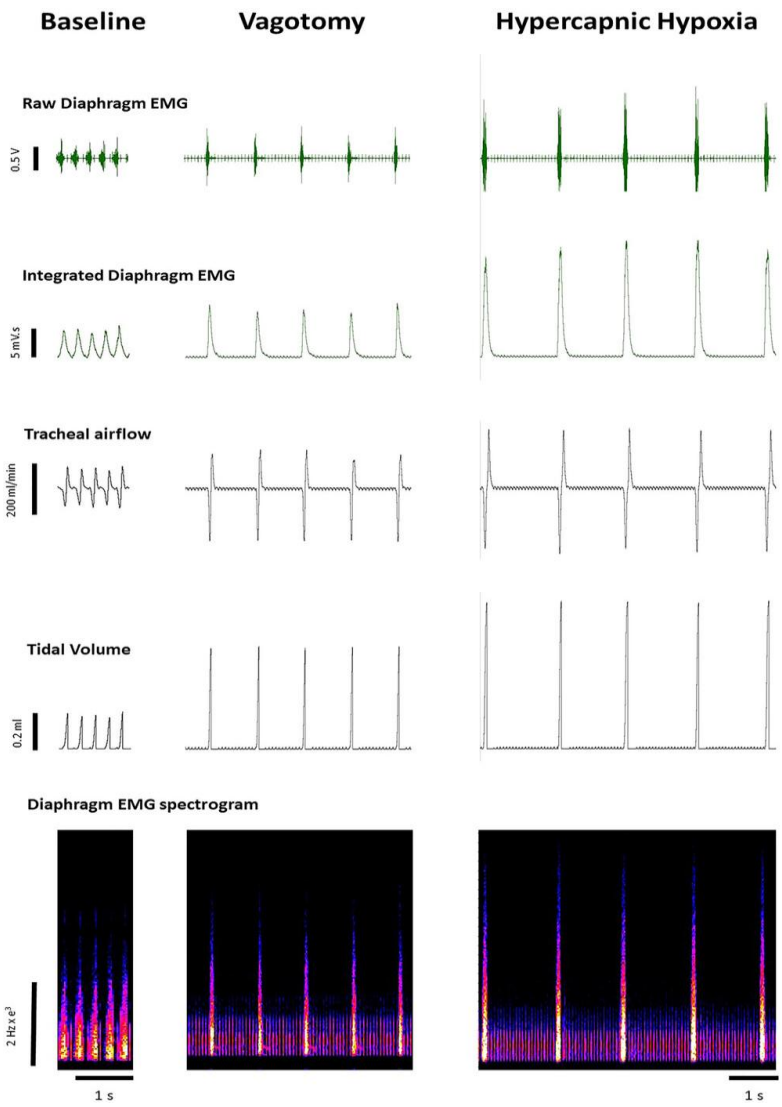

Figure 3.4: Original traces of respiratory parameters across the ventilatory range in an anaesthetised mdx mouse. Diaphragm electromyogram activity including raw, integrated and spectrogram traces, tracheal airflow and tidal volume in an anaesthetised mdx mouse during baseline, following vagotomy and during hypercapnic hypoxia.

Table 1: Respiratory parameters during baseline, following vagotomy and during exposure to hypercapnic hypoxia (HcHx) in mdx and mdx + NAC mice. Values are expressed as means ± standard deviation (SD) and were statistically compared by repeated measures two-way ANOVA (or mixed model when occasional data points were missing for technical reasons) with Šidák's multiple comparisons post hoc test (Prism 10.2.0). HcHx, hypercapnic hypoxia. Exact P-values are reported for all comparisons.

Baseline	***mdx* (n = 15)**	***mdx* + NAC (n=13)**	**adjusted P-value**
Respiratory frequency (breaths/min)	191 ± 39	196 ± 36	0.9849
Tidal Volume (µl/g)	5.8 ± 1.3	5.1 ± 1.5	0.5162
Minute Ventilation (ml/g/min)	1.08 ± 0.19	0.98 ± 0.23	0.5710
Peak inspiratory flow (ml/s)	2.94 ± 0.51	2.82 ± 0.55	0.9309
Peak expiratory flow (ml/s)	4.61 ± 0.65	5.05± 0.61	0.2216
Vagotomy			
Respiratory frequency (breaths/min)	48 ± 7	42 ± 7	0.0888
Tidal Volume (µl/g)	15.0 ± 6.0	15.3 ± 6.6	0.9989
Minute Ventilation (ml/g/min)	0.70± 0.25	0.63 ± 0.25	0.8402
Peak inspiratory flow (ml/s)	7.68 ± 1.49	8.57 ± 1.75	0.4169
Peak expiratory flow (ml/s)	6.89 ± 1.32	7.84 ± 1.55	0.2613
HcHx			
Respiratory frequency (breaths/min)	35 ± 8	32 ± 4	0.4617
Tidal Volume (µl/g)	21.6 ± 6.6	21.3 ± 8.8	0.9994
Minute Ventilation (ml/g/min)	0.75 ± 0.24	0.67 ± 0.25	0.7965
Peak inspiratory flow (ml/s)	9.43 ± 2.27	10.71 ± 1.2	0.1967
Peak expiratory flow (ml/s)	9.38 ± 1.88	10.12 ± 1.41	0.5754

Representative original traces of inspiratory pressure and diaphragm EMG activity at baseline and during tracheal occlusion are shown in Figure 5. Table 1 and Figure 6 illustrate the inspiratory pressure and EMG activity of obligatory and accessory muscles of breathing during baseline conditions, following bilateral vagotomy, during hypercapnic hypoxia and during sustained tracheal airway occlusion. There were no significant differences between *mdx* and *mdx* + NAC mice across all behaviours. Chronic NAC treatment had no effect on inspiratory pressure generating capacity in the *mdx* mouse model of DMD.

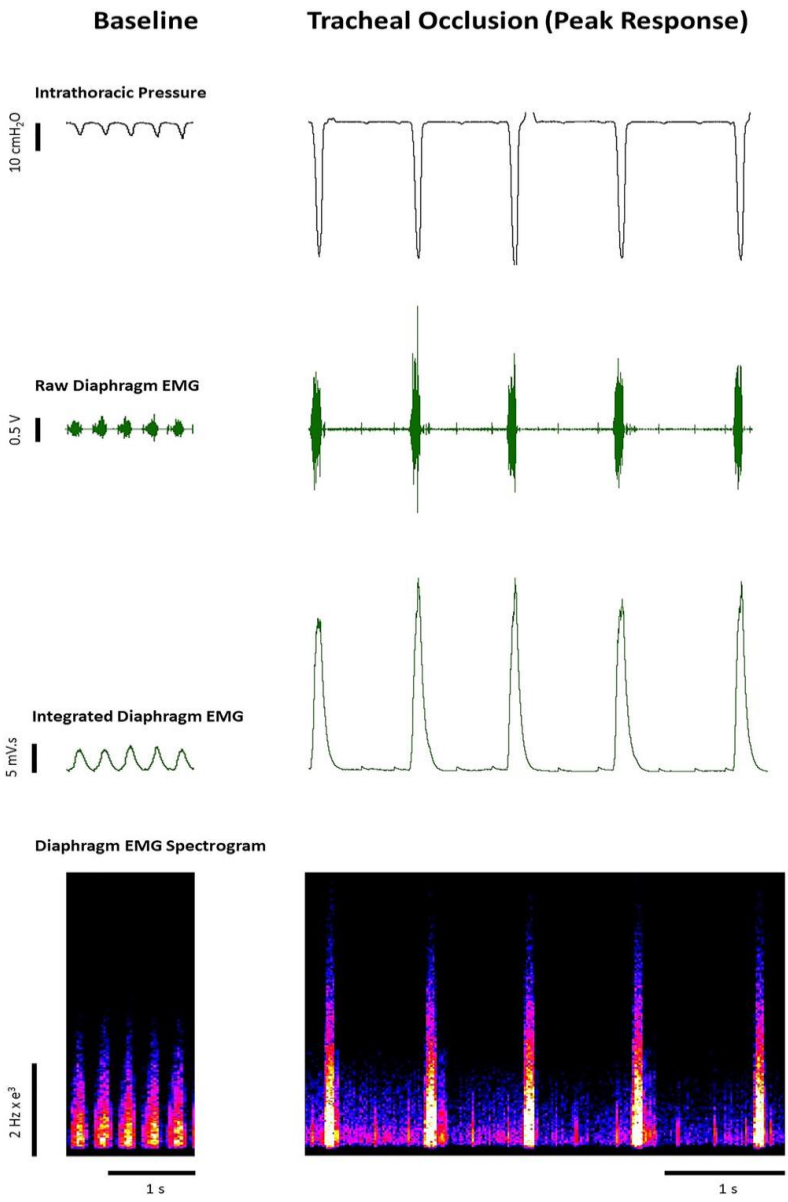

Figure 3.5: Original traces of respiratory parameters during baseline and tracheal occlusion in an anaesthetised mdx mouse. Diaphragm electromyogram activity including raw, integrated and spectrogram traces, together with tracheal airflow and tidal volume in an anaesthetised mdx mouse during baseline and sustained tracheal occlusion.

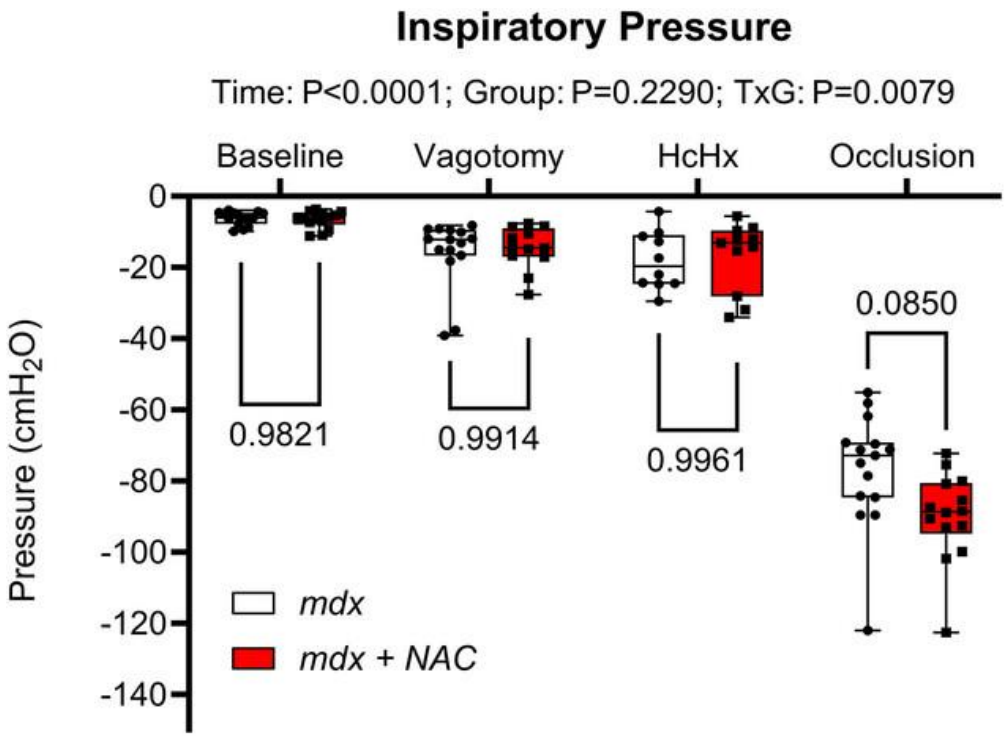

Figure 3.6: Inspiratory pressure during baseline, following vagotomy, during hypercapnic hypoxia (HcHx) exposure and tracheal occlusion in mdx and mdx + NAC mice. Values are expressed as box and whisker plots (median, 25–75 percentile and scatter plot) and were statistically compared by repeated measures two-way ANOVA (or mixed model when occasional data points were missing for technical reasons) with Šidák's multiple comparisons post hoc test (Prism 10.2.0). Exact P-values are reported for all comparisons.

Figure 7 shows EMG activity of the obligatory muscles of breathing (diaphragm, external intercostal and parasternal intercostal muscles) during baseline, following bilateral vagotomy, during hypercapnic hypoxia exposure and during sustained tracheal airway occlusion. Chronic NAC treatment had no effect on the amplitude of obligatory respiratory muscle EMG activity of the *mdx* mouse model of DMD.

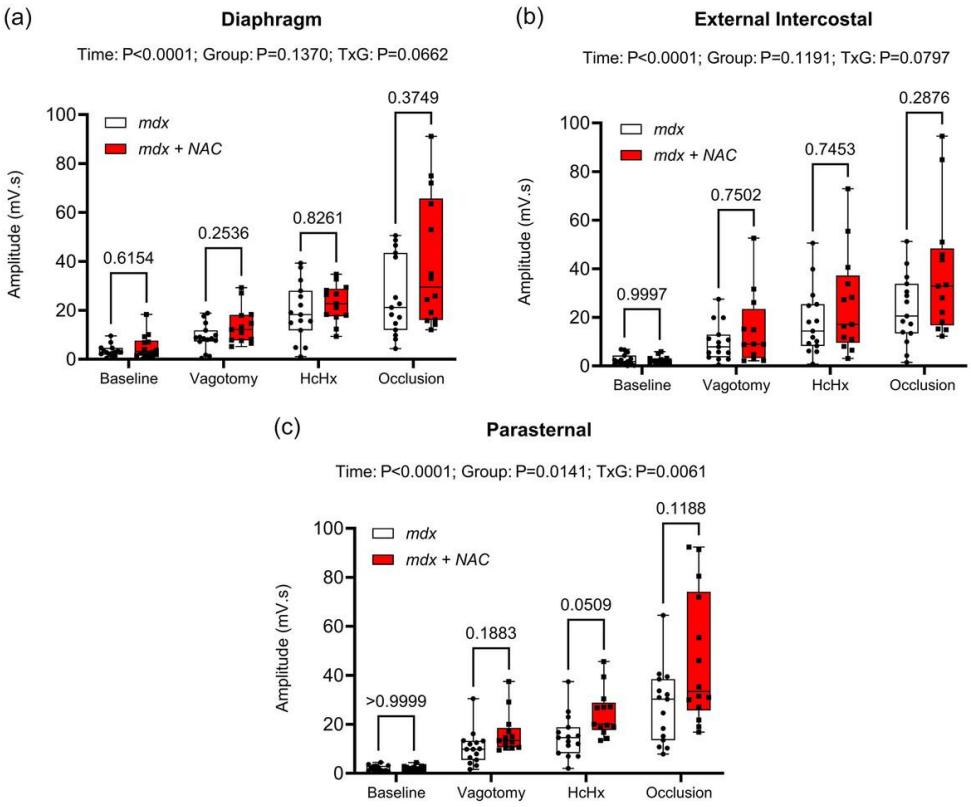

Figure 3.7: Diaphragm (a), external intercostal (b) and parasternal (c) respiratory EMG activity during baseline, following vagotomy, during hypercapnic hypoxia (HcHx) exposure and during tracheal occlusion in mdx and mdx + NAC mice. Values are expressed as box and whisker plots (median, 25–75 percentile and scatter plot) and were statistically compared by repeated measures two-way ANOVA (or mixed model when occasional data points were missing for technical reasons) with Šidák's multiple comparisons post hoc test (Prism 10.2.0). Exact P-values are reported for all comparisons.

Figure 8 shows summary data for EMG activity of the accessory muscles of breathing (cleidomastoid, scalene, sternomastoid, trapezius and sternohyoid) during baseline, following bilateral vagotomy, during hypercapnic hypoxia

exposure and during sustained tracheal airway occlusion. Chronic NAC treatment had no effect on EMG activity of the accessory muscles of breathing across a range of behaviours in the *mdx* mouse model of DMD.

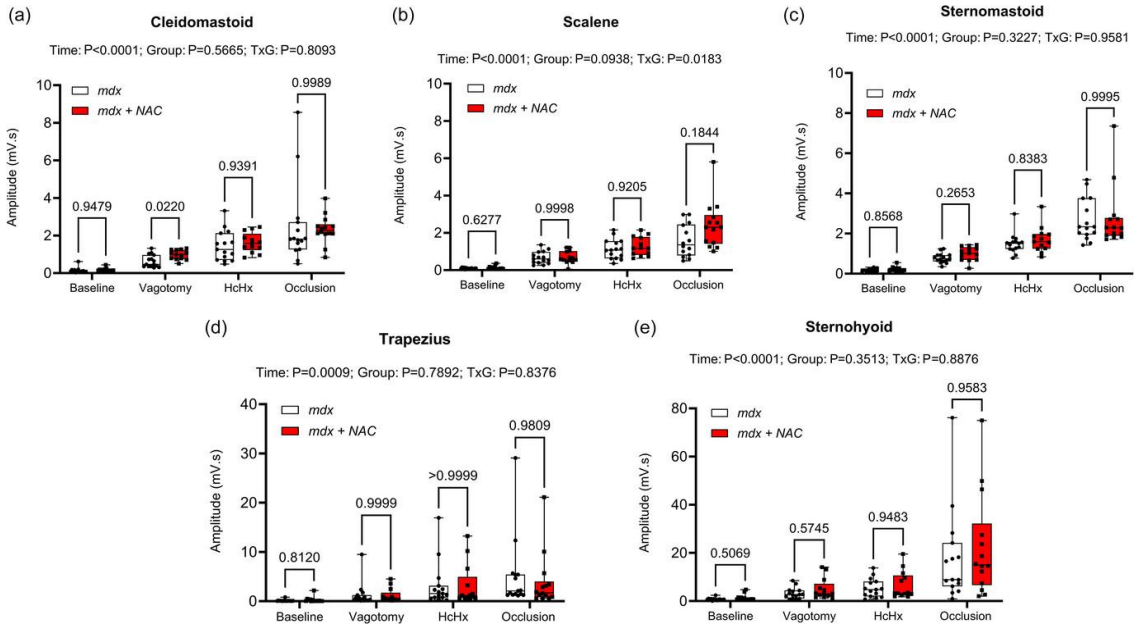

Figure 3.8: Cleidomastoid (a), scalene (b), sternomastoid (c), trapezius (d) and sternohyoid (e) respiratory EMG activity during baseline, following vagotomy, during hypercapnic hypoxia (HcHx) exposure and during tracheal airway occlusion in mdx and mdx + NAC mice. Values are expressed as box and whisker plots (median, 25–75 percentile and scatter plot) and were statistically compared by repeated measures two-way ANOVA (or mixed model when occasional data points were missing for technical reasons) with Šidák's multiple comparisons post hoc test (Prism 10.2.0). Exact P-values are reported for all comparisons.

3.5.5 Inflammatory cell infiltration and collagen deposition in diaphragm muscle

Figure 9 shows representative histological images for diaphragm muscle from *mdx* and *mdx* + NAC groups. Collagen deposition in *mdx* and *mdx* + NAC diaphragms is equivalent. Similarly, percentage area of immune cell infiltration was equivalent between *mdx* and *mdx* + NAC. Chronic NAC treatment had no effect on immune cell infiltration or collagen deposition (fibrosis) in the *mdx* mouse model of DMD.

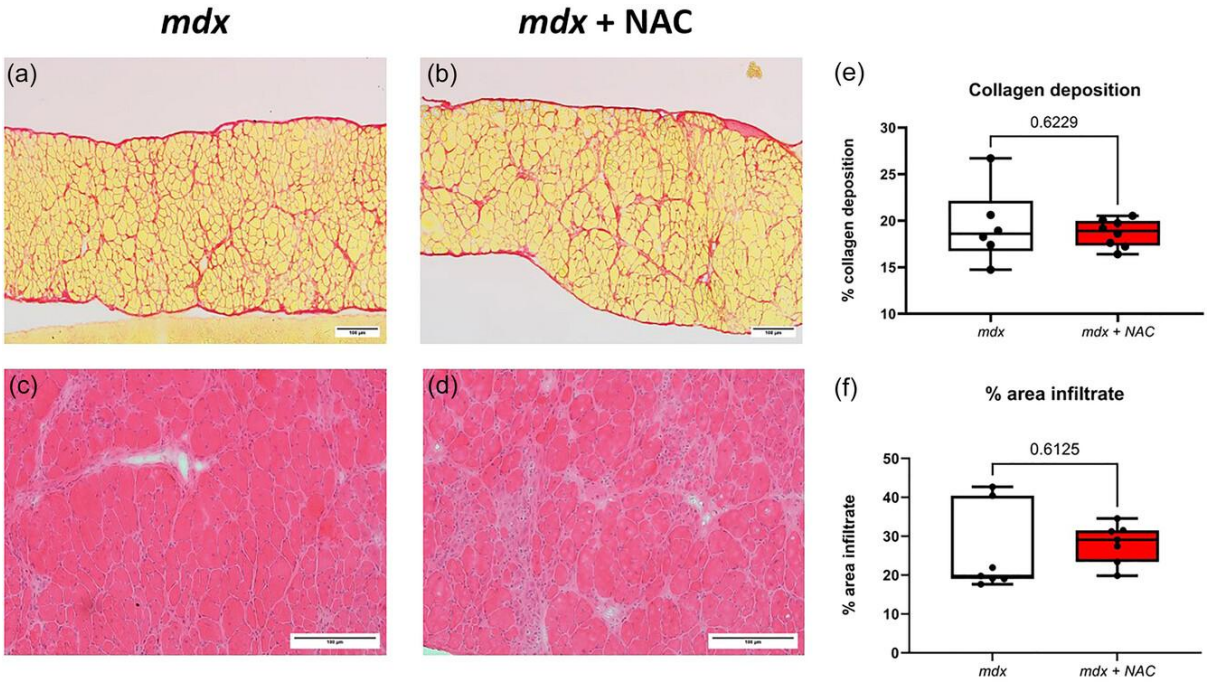

Figure 3.9: Collagen deposition and immune cell infiltration in diaphragm muscle of mdx and mdx + NAC mice. Representative histological images of transverse sections of diaphragm muscle stained with Sirius red (a, b), and haematoxylin and eosin (c, d) in mdx and mdx + NAC mice. Group data showing the relative area of collagen deposition (e), and relative area of infiltration of inflammatory cells (f). Values are expressed as box and whisker plots (median, 25–75 percentile and scatter plot) and were statistically compared using unpaired two-tailed t tests. Exact P-values are reported for comparisons between groups.

3.5.6 Diaphragm muscle mRNA expression

Figure 10 shows mRNA expression of genes related to antioxidant capacity, autophagy, mitophagy, muscle repair and inflammation from diaphragm samples of *mdx* and *mdx* + NAC mice. There was a significant decrease in *SOD1* in the *mdx* + NAC group compared to the *mdx* group. There were no significant differences in mRNA fold change for any other genes tested.

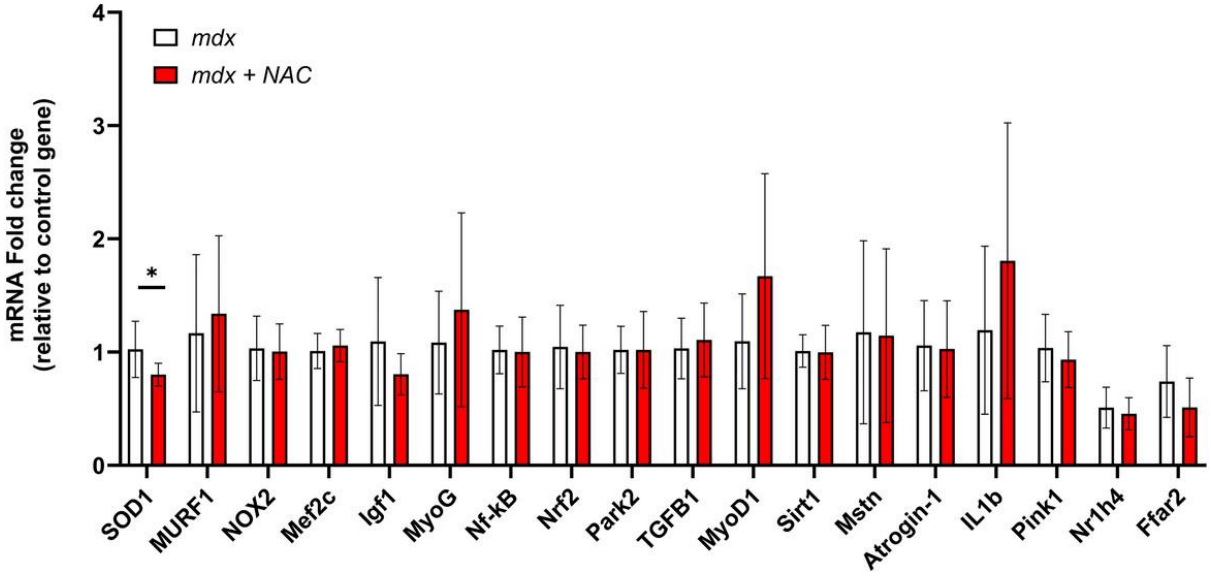

Figure 3.10: Diaphragm muscle mRNA expression. Group data for mRNA expression

of SOD1, MURF1, NOX2, Mef2c, Igf1, MyoG, NfkB, Nrf2, Park2, TGFB1, MyoD1, S irt1, Mstn, Atrogin-1, IL1b, Pink1, Nr1h4, Ffar2 in diaphragm muscle from mdx (n = 10) and mdx + NAC (n = 10) groups. Data are shown as means ± SD and were statistically compared using two-tailed, unpaired Mann–Whitney tests. Ffar2, free fatty acid receptor 2; IGF, insulin-like growth factor; IL1B, interleukin 1 beta; MEF2C, myocyte enhancer factor 2C; Mstn, myostatin; Murf-1, muscle RING-finger protein-1; MyoD, myogenic differentiation; MyoG, myogenin; NFκB, nuclear factor kappa-B; NOX, NADPH oxidase; Nr1h4, nuclear receptor subfamily 1 group H member 4; Nrf2, nuclear factor erythroid 2-related factor 2; PARK-2, parkin RBR E3 ubiquitin protein ligase; Pink1, phosphatase and

*tensin homolog (PTEN)-induced kinase 1; Sirt1, sirtuin-1; SOD1, superoxide dismutase 1; TGFB-1, transforming growth factor-B. *represents P = 0.022.*

3.6 Discussion

The major findings of this study are: (i) chronic NAC treatment did not improve *mdx* diaphragm functional capacity; (ii) chronic NAC treatment did not reduce collagen deposition (fibrosis) and immune cell infiltration in *mdx* diaphragm; (iii) chronic NAC had no effect on ventilation and ventilatory responsiveness in *mdx* mice; (iv) chronic NAC did not improve respiratory muscle EMG activity in *mdx* mice across a range of behaviours from basal to peak activity.

Previous studies have shown that diaphragm muscle force is reduced in the *mdx* model when compared to wild-type mice, equating to 40%–50% loss of peak force by 4 months of age (Burns, Drummond, et al., 2019; Burns et al., 2018; O'Halloran et al., 2023). The present study demonstrates that chronic NAC treatment (1% NAC for 3 months) does not rescue diaphragm muscle force-generating capacity, such that *mdx* + NAC treated mice generated forces equivalent to *mdx*, which are considerably lower than wild-type values (Burns, Drummond, et al., 2019; Burns et al., 2018; O'Halloran et al., 2023). NAC was ineffective in improving diaphragm muscle force across a range of stimulus intensities, demonstrating a lack of effect on muscle force relevant to basal, sub-maximal and maximal behaviours, that is, resting breathing, peak ventilatory capacity and peak respiratory system performance.

Structural remodelling is evident in dystrophic muscle, including increased central nucleation (indicative of fibre regeneration following damage), immune cell infiltration (inflammatory response) and collagen content (fibrosis) (Burns, Drummond, et al., 2019; O'Halloran et al., 2023). Our study revealed that chronic NAC treatment did not ameliorate canonical dystropathology in the *mdx* mouse over the period of 1– 4 months of age.

We investigated the effects of NAC treatment on ventilation and ventilatory responsiveness to hypercapnic hypoxia in conscious and anaesthetised mice, and inspiratory pressure and respiratory (obligatory and accessory) EMG activity in anaesthetised mice. These assessments confirmed the capacity for *mdx* mice to maintain basal breathing similar to wild-type mice and enhance ventilation in response to ventilatory challenges as previously described (Burns, Murphy, et al., 2019); NAC treatment had no effect on breathing. Respiratory airflow and volumes were measured in anaesthetised mice during baseline, following bilateral vagotomy and with superimposed chemo-activation to maximally activate ventilation. Tidal volume, peak inspiratory and expiratory flow rates and minute ventilation were equivalent between groups. Considering respiratory parameters are generally well protected in *mdx* mice at 4 months of age (O'Halloran et al., 2023), these data are unsurprising yet nevertheless demonstrate no adverse effects of NAC treatment on breathing in early dystrophic disease.

We have previously described reduced respiratory EMG activity during maximum activation in anaesthetised *mdx* mice compared with age-matched wild-type

mice (Burns, Drummond, et al., 2019; O'Halloran et al., 2023). Decreased respiratory EMG activity evident as reduced motor unit potential amplitudes most likely reflects impaired neuromuscular transmission due to neuromuscular junction dysfunction in muscular dystrophy and/or loss of large motor units (Carlson & Roshek, 2001; Personius & Sawyer, 2006). The present study demonstrates that chronic NAC treatment does not rescue impaired respiratory EMG activity, further illustrating no apparent benefit of chronic administration of NAC during the progression from early to established muscular dystrophy. While the statistical analyses did not reach the conventional threshold for significance, several observable trends in the data suggest potential biological effects of NAC treatment in the *mdx* mouse model. These trends, evident in measures of respiratory muscle EMG and inspiratory pressure during occlusion, may reflect subtle treatment impacts that warrant further investigation, especially given the inherent variability and small sample sizes typical in physiological studies with animal models. It is important to emphasize that these findings are exploratory and should not be over-interpreted as definitive evidence of efficacy. These exploratory findings highlight areas of possible therapeutic benefit and justify further investigation with larger sample sizes or complementary methodologies to confirm and extend the understanding of NAC's impact on respiratory function in dystrophic muscle.

Our examination of diaphragm mRNA expression indicated a decrease in the expression levels of *SOD1* in *mdx* + NAC presumably related to the antioxidant effects of NAC. However, transcriptional responses in *mdx* diaphragm,

characterised by increased pro-oxidant, pro-inflammatory and pro-fibrotic factors, in addition to those associated with increased muscle regeneration (Burns, Drummond, et al., 2019) were unaffected by chronic NAC treatment.

A comparison of the present study to our previous report (Burns, Drummond, et al., 2019) reveals that short-term beneficial effects of NAC on diaphragm function (principally related to positive inotropic effects on healthy fibres) is not maintained over a longer time course of disease, albeit that measures following short-term NAC administration were not performed in the present study to confirm our previous finding. A significant increase in dystropathology of the *mdx* diaphragm manifests in the period from 1 to 4 months of age, including the emergence of increased fibrosis (O'Halloran et al., 2023). It is evident that NAC treatment alone is inadequate to ameliorate the pathophysiological changes that ensue due to injury and inflammation in the principal muscle of breathing. We acknowledge that other studies have employed higher concentrations of NAC, and such studies are required to fully comprehend the potential efficacy of NAC treatment alone for DMD, although chronic treatment with high concentrations of NAC may have side effects (Head, 2017; Pinniger et al., 2017). Sex differences in the efficacy of NAC are reported (Bushana et al., 2023; Goenaga et al., 2020) with potentially greater efficacy in males. All mice in our study were male given that DMD is X-linked.

The gold standard treatment for DMD is the use of glucocorticoids such as prednisone or deflazacort, which aim to slow disease progression by anti-inflammatory action (Gloss et al., 2016). Their benefits are well known, but so too

are their side effects. Chronic use of steroids is associated with deleterious effects including muscle atrophy (Quattrocelli et al., 2017). Various strategies are undertaken to offset these effects in pre-clinical trials with a view to translation to human DMD. For example, it has been successfully shown that weekly treatment rather than daily treatment with prednisone is effective and can offset the negative side effects of chronic use of steroidal treatment (Quattrocelli et al., 2017). Quattrocelli et al. (2017) compared weekly versus daily prednisone and deflazacort over a 4-week period. Weekly treatment with glucocorticoids showed an increase in functional measures including grip strength, run to exhaustion and tetanic force in the tibialis anterior (Quattrocelli et al., 2017). Furthermore, weekly treatment increased gastrocnemius and diaphragm muscle cross-sectional areas, whereas these measures were decreased following chronic daily treatment (Quattrocelli et al., 2017). We acknowledge that promising emerging therapies will likely be administered as adjunctive therapies in human DMD. It would be interesting to determine if co-administration of NAC and prednisone exerted beneficial effects on respiratory muscle over prednisone alone.

Notwithstanding the observations of the present study, which may suggest limited application for NAC in the treatment of DMD, we conclude that further studies are warranted to fully investigate the potential beneficial effects of NAC as an adjunctive treatment for muscular dystrophy.

3.7 Author contributions

Michael N. Maxwell: administration of NAC; acquisition of whole-body plethysmography data; acquisition of diaphragm histology data; data and statistical analysis and interpretation of data; preparation of figures and drafting of the manuscript. Anthony L. Marullo: administration of NAC; acquisition of force data; data and statistical analysis; preparation of figures; drafting of the manuscript. Ben T. Murphy: administration of NAC; critical review of the manuscript. Esther Valverde-Pérez: acquisition of gene expression data; data and statistical analysis and interpretation of the data. Aoife D. Slyne: administration of NAC; acquisition of tissue and growth data; critical review of the manuscript. Ken D. O'Halloran: experimental design; acquisition of EMG and pressure data; data and statistical analysis and interpretation of data; preparation of figures and drafting and critical review of the manuscript. Authors have approved the final version of the manuscript and agree to be accountable for all aspects of the work in ensuring that questions related to the accuracy or integrity of any part of the work are appropriately investigated and resolved. All persons designated as authors qualify for authorship, and all those who qualify for authorship are listed.

3.8 Acknowledgements

We are grateful to staff of the Biological Services Unit, University College Cork for excellent service in the management of the mouse colony and animal care.

3.9 Conflict of Interest

None.

3.10 References

Aartsma-Rus, A., Van Deutekom, J. C. T., Fokkema, I. F., Van Ommen, G. B., & Den Dunnen, J. T. (2006). Entries in the Leiden Duchenne muscular dystrophy mutation database: An overview of mutation types and paradoxical cases that confirm the reading-frame rule. Muscle & Nerve, 34(2), 135–144. https://doi.org/10.1002/mus.20586

Burns, D. P., Ali, I., Rieux, C., Healy, J., Jasionek, G., & O'Halloran, K. D. (2017). Tempol supplementation restores diaphragm force and metabolic enzyme activities in mdx mice. Antioxidants, 6(4). https://doi.org/10.3390/antiox6040101

Burns, D. P., Canavan, L., Rowland, J., O'Flaherty, R., Brannock, M., Drummond, S. E., O'Malley, D., Edge, D., & O'Halloran, K. D. (2018). Recovery of respiratory function in mdx mice co-treated with neutralizing interleukin-6 receptor antibodies and urocortin-2. The Journal of Physiology, 596(21), 5175–5197. https://doi.org/10.1113/JP276954

Burns, D. P., Drummond, S. E., Bolger, D., Coiscaud, A., Murphy, K. H., Edge, D., & O'Halloran, K. D. (2019). N-acetylcysteine Decreases Fibrosis and Increases Force-Generating Capacity of mdx Diaphragm. Antioxidants, 8(12), 581. https://doi.org/10.3390/antiox8120581

Burns, D. P., Murphy, K. H., Lucking, E. F., & O'Halloran, K. D. (2019). Inspiratory pressure-generating capacity is preserved during ventilatory and non-ventilatory behaviours in young dystrophic mdx mice despite profound diaphragm muscle

weakness. The Journal of Physiology, 597(3), 831–848. https://doi.org/10.1113/JP277443

Burns, D. P., Roy, A., Lucking, E. F., McDonald, F. B., Gray, S., Wilson, R. J., Edge, D., & O'Halloran, K. D. (2017). Sensorimotor control of breathing in the mdx mouse model of Duchenne muscular dystrophy. The Journal of Physiology, 595(21), 6653–6672. https://doi.org/10.1113/JP274792

Bushana, P. N., Schmidt, M. A., Chang, K. M., Vuong, T., Sorg, B. A., & Wisor, J. P. (2023). Effect of N-Acetylcysteine on Sleep: Impacts of Sex and Time of Day. Antioxidants, 12(5). https://doi.org/10.3390/antiox12051124

Carlson, C. G., & Roshek, D. M. (2001). Adult dystrophic (mdx) endplates exhibit reduced quantal size and enhanced quantal variation. Pflugers Archiv European Journal of Physiology, 442(3). https://doi.org/10.1007/s004240100561

Choi, M. H., Ow, J. R., Yang, N. Di, & Taneja, R. (2016). Oxidative Stress-Mediated Skeletal Muscle Degeneration: Molecules, Mechanisms, and Therapies. In Oxidative Medicine and Cellular Longevity (Vol. 2016). https://doi.org/10.1155/2016/6842568

De Bruin, P. F., Ueki, J., Bush, A., Khan, Y., Watson, A., & Pride, N. B. (1997). Diaphragm thickness and inspiratory strength in patients with Duchenne muscular dystrophy. Thorax, 52(5), 472–475. https://doi.org/10.1136/thx.52.5.472

Evans, N. P., Misyak, S. A., Robertson, J. L., Bassaganya-Riera, J., & Grange, R. W. (2009). Immune-Mediated Mechanisms Potentially Regulate the Disease Time-Course of Duchenne Muscular Dystrophy and Provide Targets for Therapeutic Intervention. PM&R, 1(8), 755–768. https://doi.org/10.1016/j.pmrj.2009.04.010

Gao, Q. Q., & McNally, E. M. (2015). The Dystrophin Complex: Structure, Function, and Implications for Therapy. In Comprehensive Physiology (Vol. 5, Issue 3, pp. 1223–1239). Wiley. https://doi.org/10.1002/cphy.c140048

Garegnani, L., Hyland, M., Rodriguez, P. R., Liquitay, C. M. E., & Franco, J. V. (2021). Antioxidants to prevent respiratory decline in people with Duchenne muscular dystrophy and progressive respiratory decline. The Cochrane Database of Systematic Reviews, 2021(12). https://doi.org/10.1002/14651858.CD013720.PUB3

Gloss, D., Moxley, R. T., Ashwal, S., & Oskoui, M. (2016). Practice guideline update summary: Corticosteroid treatment of Duchenne muscular dystrophy. Neurology, 86(5), 465–472. https://doi.org/10.1212/WNL.0000000000002337

Goenaga, J., Powell, G. L., Leyrer-Jackson, J. M., Piña, J., Phan, S., Prakapenka, A. V., Koebele, S. V., Namba, M. D., McClure, E. A., Bimonte-Nelson, H. A., & Gipson, C. D. (2020). N-acetylcysteine yields sex-specific efficacy for cue-induced reinstatement of nicotine seeking. Addiction Biology, 25(1). https://doi.org/10.1111/adb.12711

Head, S. I. (2017). Antioxidant therapy in a mouse model of Duchenne muscular dystrophy: some promising results but with a weighty caveat. In Journal of Physiology (Vol. 595, Issue 23). https://doi.org/10.1113/JP275232

Hoffman, E. P., Brown, R. H., & Kunkel, L. M. (1987). Dystrophin: The protein product of the duchenne muscular dystrophy locus. Cell, 51(6), 919–928. https://doi.org/10.1016/0092-8674(87)90579-4

Khirani, S., Ramirez, A., Aubertin, G., Boulé, M., Chemouny, C., Forin, V., & Fauroux, B. (2014). Respiratory muscle decline in duchenne muscular dystrophy. Pediatric Pulmonology, 49(5), 473–481. https://doi.org/10.1002/ppul.22847

Lewis, P., & O'Halloran, K. D. (2016). Diaphragm muscle adaptation to sustained hypoxia: Lessons from animal models with relevance to high altitude and chronic respiratory diseases. Frontiers in Physiology, 7(DEC), 232066. https://doi.org/10.3389/FPHYS.2016.00623/BIBTEX

Lewis, P., Sheehan, D., Soares, R., Coelho, A. V., & O'Halloran, K. D. (2015). Chronic sustained hypoxia-induced redox remodeling causes contractile dysfunction in mouse sternohyoid muscle. Frontiers in Physiology, 6(APR). https://doi.org/10.3389/fphys.2015.00122

Lewis, P., Sheehan, D., Soares, R., Coelho, A. V., & O'Halloran, K. D. (2016). Redox remodeling is pivotal in murine diaphragm muscle adaptation to chronic sustained hypoxia. American Journal of Respiratory Cell and Molecular Biology, 55(1). https://doi.org/10.1165/rcmb.2015-0272OC

Mhandire, D. Z., Burns, D. P., Roger, A. L., O'Halloran, K. D., & ElMallah, M. K. (2022). Breathing in Duchenne muscular dystrophy: translation to therapy. The Journal of Physiology, 600(15), 3465–3482. https://doi.org/10.1113/JP281671

O'Halloran, K. D., Lewis, P., & McDonald, F. (2017). Sex, stress and sleep apnoea: Decreased susceptibility to upper airway muscle dysfunction following intermittent hypoxia in females. Respiratory Physiology & Neurobiology, 245, 76–82. https://doi.org/10.1016/J.RESP.2016.11.009

O'Halloran, K. D., Maxwell, M. N., Marullo, A. L., Hamilton, C. P., Ó Murchú, S. C., Burns, D. P., Mahony, C. M., Slyne, A. D., & Drummond, S. E. (2023). Loss of compensation afforded by accessory muscles of breathing leads to respiratory system compromise in the mdx mouse model of Duchenne muscular dystrophy. The Journal of Physiology, 601(19), 4441–4467. https://doi.org/10.1113/JP285203

Personius, K. E., & Sawyer, R. P. (2006). Variability and failure of neurotransmission in the diaphragm of mdx mice. Neuromuscular Disorders, 16(3), 168–177. https://doi.org/10.1016/j.nmd.2006.01.002

Pinniger, G. J., Terrill, J. R., Assan, E. B., Grounds, M. D., & Arthur, P. G. (2017). Pre-clinical evaluation of N -acetylcysteine reveals side effects in the mdx mouse model of Duchenne muscular dystrophy. The Journal of Physiology, 595(23), 7093–7107. https://doi.org/10.1113/JP274229

Quattrocelli, M., Barefield, D. Y., Warner, J. L., Vo, A. H., Hadhazy, M., Earley, J. U., Demonbreun, A. R., & McNally, E. M. (2017). Intermittent glucocorticoid steroid dosing enhances muscle repair without eliciting muscle atrophy. Journal of Clinical Investigation, 127(6). https://doi.org/10.1172/JCI91445

Redwan, A., Kiriaev, L., Kueh, S., Morley, J. W., Houweling, P., Perry, B. D., & Head, S. I. (2023). Six weeks of N-acetylcysteine antioxidant in drinking water decreases pathological fiber branching in MDX mouse dystrophic fast-twitch skeletal muscle. Frontiers in Physiology, 14. https://doi.org/10.3389/fphys.2023.1109587

Smith, P. E. M., Edwards, R. H. T., & Calverley, P. M. A. (1989). Ventilation and Breathing Pattern during Sleep in Duchenne Muscular Dystrophy. Chest, 96(6), 1346–1351. https://doi.org/10.1378/chest.96.6.1346

Terrill, J. R., Radley-Crabb, H. G., Grounds, M. D., & Arthur, P. G. (2012). N-Acetylcysteine treatment of dystrophic mdx mice results in protein thiol modifications and inhibition of exercise induced myofibre necrosis. Neuromuscular Disorders, 22(5), 427–434. https://doi.org/10.1016/j.nmd.2011.11.007

Whitehead, N. P., Pham, C., Gervasio, O. L., & Allen, D. G. (2008). N - Acetylcysteine ameliorates skeletal muscle pathophysiology in mdx mice. The Journal of Physiology, 586(7), 2003–2014. https://doi.org/10.1113/jphysiol.2007.148338

Chapter 4. Exploring the respiratory efficacy of combined chronic glucocorticoid and antioxidant interventions in the *mdx* mouse: the PREDNAC trial

4.1 Publication information

Published in:	Experimental Physiology
Article type:	Research article
Title:	**Exploring the respiratory efficacy of combined chronic glucocorticoid and antioxidant interventions in the *mdx* mouse: the PREDNAC trial**
Authors:	Michael N. Maxwell[1]
	Ben T. Murphy[1]
	Fiona B. McDonald[1]
	Ken D. O'Halloran[1]
Affiliations: Cork, Ireland	[1]Department of Physiology, University College Cork,
Key words:	Glucocorticoid; Diaphragm; *mdx*; Inspiratory pressure; Muscular dystrophy; Respiratory EMGs

4.2 Abstract

Duchenne muscular dystrophy (DMD) is characterized by respiratory muscle injury and weakness, ultimately leading to respiratory failure. Impaired respiratory muscle performance, fibrosis and inflammation in early disease are evident in the dystrophin-deficient *mdx* mouse model of DMD. Prednisone or similar treatment is the current standard of care for DMD and exerts its benefits via an anti-inflammatory action, but chronic treatment is associated with side-effects. A recent study demonstrated improved function in *mdx* limb muscle with weekly glucocorticoid treatment compared with daily treatment. Herein, we investigated the effect of weekly α-methylprednisolone (PRED) treatment alone and the effect of PRED in combination with daily intake of the antioxidant *N*-acetyl cysteine, NAC (PREDNAC) on respiratory performance. One-month-old male *mdx* mice received PRED (0.8 mg/kg methylprednisolone i.p. weekly) or PREDNAC (0.8 mg/kg methylprednisolone i.p. weekly and 1% NAC in drinking water daily) for 3 months. At 4 months of age, conscious breathing was measured in vivo by whole-body plethysmography. Under urethane general anaesthesia, respiratory EMG and inspiratory pressure were measured at baseline and during maximal activity. The intrinsic force-generating capacity of the diaphragm was determined *ex vivo*. Neither PRED nor PREDNAC influenced breathing or diaphragm force-generating capacity in *mdx* mice. There was a significant increase in diaphragm and parasternal EMG activity, but inspiratory pressure was unchanged with treatment. We conclude that neither PRED nor PREDNAC has a major beneficial effect on respiratory system performance in the *mdx* mouse model of DMD. Weekly administration of glucocorticoids is

inadequate to protect respiratory performance in *mdx* mice, which might reflect the higher duty cycle of respiratory muscles compared with limb muscles.

Highlights

What is the central question of this study?

Does combined chronic glucocorticoid and antioxidant treatment improve respiratory system performance in the *mdx* mouse model of Duchenne muscular dystrophy?

What is the main finding and its importance?

We determined that combined glucocorticoid and antioxidant treatment for 3 months exerted an anti-inflammatory effect on the *mdx* diaphragm and modestly increased diaphragm peak EMG activity. However, combined therapy did not improve a range of respiratory-related parameters in *mdx* mice, suggesting that at the doses used in this study there is limited potential for weekly glucocorticoid treatment with or without antioxidant supplementation as an intervention to support respiratory performance in Duchenne muscular dystrophy.

4.3 Introduction

Duchenne muscular dystrophy (DMD) is a life-limiting X-linked neuromuscular disease arising from mutations in the *DMD* gene, leading to the absence of the structural protein dystrophin (Aartsma-Rus et al., 2006; E. P. Hoffman et al., 1987a). Dystrophin is integral to the dystrophin glycoprotein complex, a

structure that links F-actin in the myocellular cytoskeleton to the extracellular matrix via the sarcolemma, thus offering structural support during repetitive contraction and protecting muscle fibres (Gao & McNally, 2015). In DMD, there is a complete absence of dystrophin in skeletal muscles and evidence of contraction-induced muscle injury from early life, leading to muscle degeneration and functional deterioration, which constitutes a fundamental phenotype of DMD (Burns, Drummond, et al., 2019; Burns et al., 2018; Burns, Murphy, et al., 2019; O'Halloran et al., 2023). Consequently, the dystrophin glycoprotein complex and its associated functionality are compromised, resulting in inflammation within skeletal muscle and the development of fibrosis. Functional respiratory muscle weakness is accompanied by diminished ventilatory capacity, ultimately leading to respiratory failure (De Bruin et al., 1997; Evans et al., 2009; Khirani et al., 2014; P. E. M. Smith et al., 1989). Currently, no cure exists for boys with DMD. Therefore, interventions aimed at enhancing respiratory muscle strength in DMD are important in attempting to delay respiratory muscle failure, thereby preserving respiratory system efficacy.

Damage and degeneration in human DMD starts early in the disease, with children exhibiting motor deficits at ~2–3 years of age. The initial symptoms include challenges in climbing stairs, a distinctive waddling gait and recurrent falls (Emery, 2002). As the disease progresses rapidly, the muscle phenotype becomes more apparent. Patients as early as 9 years of age are wheelchair dependent; they experience loss of upper limb function and respiratory insufficiency, which requires assisted ventilation by 20 years of age (Emery, 2002). Improvements in the standards of clinical care, such as non-invasive

support with mechanical ventilation, ongoing management of deformities in the spine and earlier implementation of therapies, have translated into the extension of median life expectancy for patients with DMD from late teens to late twenties (Broomfield et al., 2021; Passamano et al., 2012).

One of the most widely studied models of DMD is the dystrophin-deficient *mdx* mouse. Studies by our group have illustrated compromised respiratory muscle function in the *mdx* mouse, which models the human DMD condition. Specifically, investigations into the respiratory system of the *mdx* mouse model have revealed pronounced muscle weakness alongside structural remodelling of the diaphragm, the primary muscle of breathing (Burns, Drummond, et al., 2019; Burns et al., 2018; Burns, Murphy, et al., 2019; Burns, Roy, et al., 2017; Mhandire et al., 2022; O'Halloran et al., 2023). Inflammatory markers, such as immune cell infiltration, increased cytokine concentrations, elevated levels of reactive oxygen species and collagen deposition, are evident in the *mdx* diaphragm (Burns, Drummond, et al., 2019; Choi et al., 2016; O'Halloran et al., 2023). EMG activity of the obligatory muscles of breathing in the *mdx* model of DMD is reduced, which most probably reflects impaired neuromuscular function pertinent to respiratory performance (Burns, Murphy, et al., 2019; O'Halloran et al., 2023; Personius & Sawyer, 2006).

Glucocorticoids, such as prednisone/prednisolone or deflazacort, are the standard treatment of care for boys with DMD, which aims to offset the progression of the disease by promoting anti-inflammatory pathways. Although glucocorticoids have benefits, their chronic use is also associated with adverse side-effects that can decrease quality of life, including muscle fibre atrophy,

decreased muscle force, weight gain and bone loss. Interestingly, patients can also develop resistance to glucocorticoids. Numerous strategies are being explored in preclinical investigations to mitigate these adverse effects, with the aim of translation to humans. Quattrocelli, Barefield et al. (2017) demonstrated that administering glucocorticoids on a weekly basis, as opposed to a daily regimen, for 4 weeks, is effective in diminishing the harmful consequences associated with chronic glucocorticoid treatment in the D2.*mdx* mouse model of DMD. Their findings indicated that weekly glucocorticoid treatment resulted in improved functional outcomes, including enhanced grip strength, extended endurance and increased tetanic force in the tibialis anterior muscle (Quattrocelli et al., 2017). Additionally, the weekly regimen was associated with an increase in the cross-sectional areas of the gastrocnemius and diaphragm muscles, whereas these measures were found to be reduced following chronic daily administration, indicating that daily steroid dosing elicits an atrophic effect (Quattrocelli et al., 2017).

The antioxidant *N*-acetylcysteine (NAC) has been shown to exert anti-inflammatory and anti-fibrotic effects (Tenório et al., 2021), improving respiratory muscle performance in a range of animal models of muscle dysfunction, including *mdx* mice (Burns, Drummond, et al., 2019; Redwan et al., 2023; Terrill et al., 2012). Although 1% NAC was ineffective in supporting respiratory system performance in *mdx* mice (Maxwell et al., 2024), which was disappointing and surprising based upon our previous findings over a shorter time frame of 2 weeks of treatment (Burns, Drummond, et al., 2019) and prior findings of a range of improvements in *mdx* limb muscle, including increased

force generation (Pinniger et al., 2017) also after 2 weeks of treatment, we nevertheless sought value in considering the potential benefit of co-administration of NAC and PRED. We reasoned that combined treatment might be superior considering the potential for PRED administered chronically (albeit weekly for 3 months in this study) to drive adverse outcomes for muscle per se and active respiratory muscles in particular, since chronic PRED treatment can lead to muscle wasting (Danon & Carpenter, 1991; Quattrocelli et al., 2017). We have previously shown that NAC prevents respiratory muscle atrophy and weakness in chronically hypoxic mice (Lewis et al., 2016) and prevents diaphragm dysfunction in rats exposed to chronic intermittent hypoxia (Shortt et al., 2014). Therefore, NAC has the capacity to prevent stress-induced muscle wasting and weakness, and although NAC alone does not improve *mdx* diaphragm function, combination therapy (PREDNAC) could conceivably be superior to PRED in improving *mdx* diaphragm function, acknowledging too that this is speculative.

In the present study, we sought to assess the effects of PRED once weekly and a combination therapy of PRED and NAC (PREDNAC) on respiratory system performance in the *mdx* mouse model of DMD starting at 1 month of age for a duration of 3 months. We hypothesized that both PRED treatment and the combination therapy (PREDNAC) would be beneficial to *mdx* diaphragm muscle form, improve *mdx* diaphragm force generation and rescue impaired *mdx* respiratory EMG activity (O'Halloran et al., 2023).

4.4 Methods

4.4.1 Ethical approval

Procedures on live animals were performed under project authorization (AE19130/P117) from the Health Products Regulatory Authority in accordance with Irish and European law, with prior ethical approval by University College Cork (AEEC 2019/013). Experiments were carried out in accordance with guidelines and requirements laid down by University College Cork's Animal Welfare Body. We adhered to *Experimental Physiology*'s policies regarding animal experiments.

4.4.2 Experimental animals, PRED and PREDNAC treatment

Breeding pairs for wild-type (C57BL/10ScSnJ) and *mdx* mice (C57BL/10ScSn-Dmd*mdx*/J) were purchased from the Jackson Laboratory (Bar Harbor, ME, USA), and colonies were established at University College Cork's specific pathogen-free facility. Animals were group housed in individually ventilated cages in temperature- and humidity-controlled rooms, operating on a 12 h light–12 h dark cycle, with food and water available ad libitum. Studies were performed on 60 male mice. Wild-type mice were randomly selected from our colony (n = 15); *mdx* mice were randomly assigned to one of three groups: *mdx* (n = 15); *mdx* + PRED (n = 15); and *mdx* + PREDNAC (n = 15). A schematic timeline of the study protocol is shown in Figure 1.

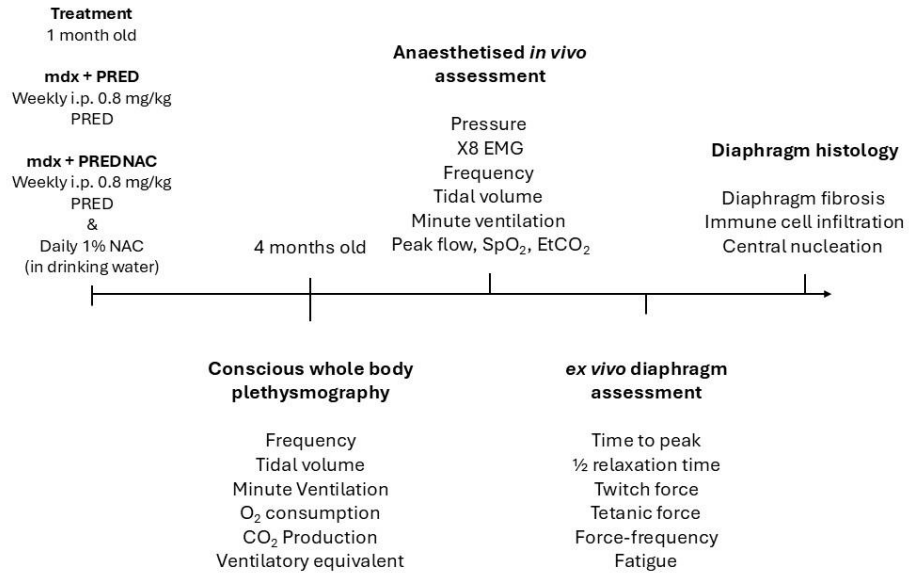

Figure 4.1: Schematic diagram of the timeline of the experimental protocol, experimental groups and parameters measured. Abbreviations: $EtCO_2$, end-tidal CO_2; PRED, α-methylprednisolone; PREDNAC, α-methylprednisolone plus N-acetyl cysteine.

The *mdx* + PRED group received 0.8 mg/kg of α-methylprednisolone once weekly i.p. for 3 months, beginning at 1 month of age. The 0.8 mg/kg dose of α-methylprednisolone administered once weekly intraperitoneally was recommended by a veterinarian as equivalent to the more commonly employed 1 mg/kg dose of prednisone, which we were unable to obtain. This substitution allowed us to maintain the weekly glucocorticoid administration strategy shown to reduce side effects and improve muscle function in DMD mouse models (Quattrocelli et al., 2017). Thus, the dose selection was pragmatically based on expert guidance to approximate the established effective dose for prednisone in this model.

The *mdx* + PREDNAC group received 0.8 mg/kg of α-methylprednisolone once weekly i.p. and 1% *N*-acetyl cysteine daily (Sigma-Aldrich, Wicklow, Ireland) in the drinking water for 3 months, beginning at 1 month of age.

α-Methylprednisolone was prepared fresh on the day of injection. Drinking water containing NAC was pH matched to control water and prepared fresh each day. For both treatment groups, fluid intake was estimated by weighing water bottles daily and estimating fluid intake per mouse. Fluid intake was normal and stable over the 3-month intervention, averaging 4–5 mL per mouse per day. Mice were studied at 4 months of age. A thorough assessment of respiratory performance was made, with measurements of breathing and ventilatory capacity in response to chemo-activation in conscious animals, recordings of thoracic inspiratory pressure and respiratory muscle EMG in anaesthetized animals, and respiratory muscle function tests *ex vivo*. Diaphragm muscle tissue was collected for structural analysis using standard histological techniques.

4.4.3 Plethysmography

Whole-body plethysmography was used to assess respiratory flow in unrestrained, conscious wild-type (n = 13), *mdx* (n = 13), *mdx* + PRED (n = 12) and *mdx* + PREDNAC (n = 12) mice. Mice were introduced into plethysmography chambers (model PLY4211; volume 600 mL; Buxco Research Systems, Wilmington, NC, USA) and were allowed an acclimation period (~30 min) with room air passing through each chamber (0.85 L/min).

4.4.3.1 Experimental protocol

Following acclimation, combined central and peripheral chemoreceptor stimulation with hypercapnic hypoxia (HcHx; 10% O_2 and 6% CO_2) was performed for 10 min, to examine maximum chemoactivated breathing. Following a 20 min wash-out period, during confirmed periods of quiet rest, a 10 min baseline recording was performed in room air to measure normal tidal breathing. Respiratory parameters, including respiratory frequency (*f*), tidal volume (V_T) and minute ventilation ($\dot{V}_I$), were recorded on a breath-by-breath basis for analysis offline. A gas analyser (AD Instruments, Colorado Springs, CO, USA) was used to determine oxygen consumption ($\dot{V}_{O_2}$) and carbon dioxide production ($\dot{V}_{CO_2}$).

4.4.3.2 Data analysis

Baseline normoxic ventilation was determined as an average of the 10 min baseline period during a continuous period of confirmed quiet rest. For HcHx, ventilatory measurements were taken during the final 5 min of the challenge to ensure steady-state changes. The V_T and $\dot{V}_I$ were normalized for body mass (in grams). The ventilatory equivalents for oxygen ($\dot{V}_I/\dot{V}_{O_2}$) and carbon dioxide ($\dot{V}_I/\dot{V}_{CO_2}$) were determined.

4.4.4 Respiratory EMGs and inspiratory pressure recordings

Following plethysmography measurements and with additional animals [wild-type (*n* = 15), *mdx* (*n* = 15), *mdx* + PRED (*n* = 13) and *mdx* + PREDNAC (*n* = 14) mice], anaesthesia was induced with 5% isoflurane (Vetflurane, VIRBAC Ltd.,

Suffolk, UK) in 60% O_2 (balance N_2) in an induction chamber. Mice were subsequently placed in the supine position and received 2% isoflurane in 60% O_2 (balance N_2) by nose-cone delivery. Mice were gradually transitioned from isoflurane to urethane anaesthesia (1.7 g/kg i.p. in total given in three injections) over a 25 min period. Urethane was purchased from Sigma-Aldrich, Wicklow, Ireland. Body temperature was maintained at 37°C–38°C via a rectal probe and thermostatically controlled heating blanket (Harvard Apparatus, Holliston, MA, USA). We established an acceptable surgical plane of anaesthesia, determined by an absent pedal withdrawal reflex and no somatic motor response to noxious pinch. Supplemental anaesthetic was administered as required. A pulse oximeter clip (MouseOx™; Starr Life Sciences Corporation, Oakmount, PA, USA) was placed on a shaved thigh for the measurement of peripheral capillary O_2 saturation (S_{pO_2}). A mid-cervical tracheotomy was performed. All animals were maintained with a bias flow of supplemental O_2 [fraction of inspired oxygen (F_{IO_2}) = 0.60] in baseline conditions. Oesophageal pressure was measured using a pressure-tip catheter (Mikro-Tip; Millar Inc., Houston, TX, USA), which was positioned in the thoracic oesophagus through the mouth. The catheter was advanced into the stomach to record positive pressure swings during inspiration, then withdrawn into the lower oesophagus, where stable phasic sub-atmospheric pressure swings during inspiration were observed. Concentric needle monopolar recording electrodes (26 gauge; Natus Manufacturing Ltd, Ireland) were inserted into the middle costal region of the diaphragm on the right-hand side for the continuous measurement of diaphragm EMG activity, into an external intercostal, in the second to fourth rostroventral intercostal space, for

the measurement of external intercostal EMG, and into the parasternal intercostal (second or third space) for the measurement of parasternal intercostal EMG. In addition, concentric needle monopolar electrodes were used to record scalene, cleidomastoid, sternomastoid, sternohyoid (all mid-belly insertions) and trapezius (superficial insertion in the upper region on either side) with contemporaneous recordings of eight EMG signals in each mouse. EMG signals were amplified (×5000), filtered (500 Hz low cut-off to 5000 Hz high cut-off) and integrated (50 ms time constant; Neurolog system; Digitimer Ltd, UK). All signals were passed through an analog-to-digital converter (Powerlab r8/30; ADInstruments, Colorado Springs, CO, USA) and were acquired using LabChart 8 (ADInstruments) sampled at 20 kHz (EMG) and 1 kHz for other parameters (tracheal airflow and pressure, and S_{pO_2}).

4.4.4.1 Experimental protocol

Following instrumentation, animals were allowed to stabilize before baseline parameters were measured. Next, animals were challenged with a single sustained tracheal occlusion until peak inspiratory efforts (identified as stable, maximal successive efforts, often until task failure) were observed in the inspiratory pressure recordings during sustained maximum non-ventilatory efforts. Following recovery, animals were instrumented for the measurement of tracheal airflow, and parameters were recorded during a newly established second baseline (prevagotomy) period. Subsequently, the vagi were sectioned bilaterally at the cervical level. Respiratory parameters were recorded in steady-state conditions for a minimum of 10 min following vagotomy. Next, animals

were challenged with HcHx [F_{IO_2} = 0.15 and fraction of inspired carbon dioxide (F_{ICO_2}) = 0.06; 2 min] to examine the effects of chemostimulation on the diaphragm, external intercostal, parasternal intercostal, cleidomastoid, sternomastoid, sternohyoid, scalene and trapezius EMG activities and ventilatory parameters. After the experimental protocol, anaesthetized mice were killed by cervical dislocation, and death was confirmed by the absence of cardiac rhythm.

4.4.4.2 Data analysis

The amplitudes of integrated inspiratory diaphragm, external intercostal, parasternal intercostal, cleidomastoid, sternomastoid, sternohyoid, scalene and trapezius EMG activities and peak inspiratory sub-atmospheric oesophageal pressure change from baseline were measured and averaged in steady-state basal conditions (typically over 1 min) and averaged for the five successive maximal sustained efforts (maximal response) of the single airway occlusion challenge (Burns, Murphy, et al., 2019). During baseline breathing and chemo-activation, peak inspiratory and expiratory flows were measured, and inspiratory tidal volume was derived from the integral of tracheal airflow measurements.

4.4.5 Ex vivo Diaphragm Muscle function

Following in vivo pressure and EMG measurements mice were killed by cervical dislocation, and the diaphragm muscle (rib and central tendon intact) was immediately excised and placed in a tissue bath at room temperature containing

continuously gassed hyperoxic (95% O_2–5% CO_2) Krebs solution (mM: NaCl, 120; KCl, 5; calcium gluconate, 2.5; $MgSO_4$, 1.2; NaH_2PO_4, 1.2; $NaHCO_3$, 25; and glucose, 11.5) and *d*-tubocurarine (25 μM) prior to functional analysis. Thin strips of diaphragm muscle were prepared from the mid-costal section of the right hemidiaphragm. Diaphragm muscle preparations were suspended vertically between two platinum plate electrodes in a water-jacketed tissue bath at 35°C containing Krebs solution and were continuously gassed with carbogen (95% O_2–5% CO_2). The rib was sutured to an immobile hook and remained in a fixed position for the duration of the experiment. Using non-elastic string, the central tendon was attached to a lever connected to a dual-mode force transducer (Aurora Scientific Inc., Aurora, ON, Canada). To determine muscle optimum length (L_o), the length of the muscle preparations was adjusted using a micro-positioner between intermittent twitch contractions. The muscle length that revealed maximal isometric twitch force for a single isometric twitch stimulation (supramaximal stimulation, 1 ms duration) was considered L_o. Diaphragm preparations were maintained at L_o for the duration of the protocol.

4.4.5.1Experimental protocol

First, peak isometric twitch force was measured via stimulation of the muscle preparation at 100 Hz for 1 ms duration. Time-to-peak force and half-relaxation time parameters were derived from resultant twitch contractions. Isometric tetanic force was assessed via stimulation of the muscle preparation at 100 Hz for 300 ms duration. To examine the force–frequency relationship, the muscle preparation was stimulated sequentially at 25, 50, 75, 100, 125 and 150 Hz

(300 ms train duration), interspersed by 1 min intervals. Finally, a fatiguing protocol was run involving 150 sequential submaximal contractions at 40 Hz, separated by 2 s intervals.

4.4.5.2 Data analysis

Muscle bundle cross-sectional area was determined for the purpose of normalizing muscle force to bundle size. Cross-sectional area was calculated by dividing muscle mass (weight, in grams) by the product of muscle L_o (in centimetres) and muscle density (assumed to be 1.06 g/cm^3). Muscle force was divided by bundle cross-sectional area and expressed as a specific force (in newtons per centimetre squared). Time-to-peak force and half-relaxation time were measured as indices of isometric twitch kinetics and were expressed in milliseconds.

4.4.6 Muscle histology

4.4.6.1 Tissue preparation

Sections of hemidiaphragm from wild-type (n = 10), *mdx* (n = 10), *mdx* + PRED (n = 10) and *mdx* + PREDNAC (n = 10) mice were mounted on cubes of liver. Diaphragm samples were embedded in optimum cutting temperature embedding medium (OCT; VWR International, Dublin, Ireland) for cryoprotection, then frozen in isopentane (Sigma–Aldrich, Wicklow, Ireland) cooled on dry ice. Samples were then stored at −80°C for subsequent structural analysis. Serial transverse muscle sections (10 μm thick) were cut using a

cryostat (Leica CM1950; Leica Microsystems, Nussloch, Germany) at −20°C and mounted across polylysine-coated glass slides (VWR International, Dublin, Ireland) allowing for a distribution of tissue on a given slide.

4.4.6.2 Histological Analysis

To examine putative inflammatory cell infiltration and the relative density of centrally nucleated myofibres in diaphragm, tissue sections were stained with Haematoxylin and Eosin using an autostainer (Leica ST5010 Autostainer XL; Leica Microsystems, Nussloch, Germany). Slides were mounted using DPX mounting medium (Sigma–Aldrich, Wicklow, Ireland), air-dried and visualized on a bright field microscope (Olympus BX51) at ×20 magnification.

To determine the relative area of collagen deposition, Picrosirius Red (Leica Biosystems, Wetzlar, Germany) staining was completed. Slides were mounted using DPX mounting medium (Sigma–Aldrich, Wicklow, Ireland), air-dried and visualized on a bright field microscope (Olympus BX51) at ×10 magnification.

4.4.6.3 Data analysis

A total of four tissue sections per animal were examined. Muscle histology was scored using ImageJ software. Putative inflammatory cell infiltration (the presence of nucleated cells in the extracellular matrix) was scored and expressed as a percentage of the total area of muscle within the area randomly selected. The number of centrally nucleated cells (the presence of cells where the nuclei are located centrally and not peripherally in the muscle cell) was

scored and expressed as a percentage of the total muscle cells within the area randomly selected. For slides stained with Picrosirius Red, the microscope lighting exposure was standardized during imaging. Images were analysed using a colour balance threshold, and the area of collagen was expressed as a percentage of the total area of muscle. Data generated from multiple images with varying regions of interest per muscle were averaged per animal before computing group means.

4.4.7 Statistical Analysis

Values are expressed as box and whisker plots (median, interquartile range and individual data scatter plot) in graphs. One-way ANOVA was used statistically to compare body mass, inflammatory cell infiltrate, collagen deposition, diaphragm muscle contractile function and respiratory parameters (Table 1). All other data were compared statistically by two-way ANOVA (or mixed model when occasional data points were missing for technical reasons) with Tukey's multiple comparisons *post hoc* test (Prism v.10.3.1). Values of $p < 0.05$ are reported, and $p < 0.05$ was considered statistically significant.

4.5 Results

4.5.1 Effect of PRED and PREDNAC on body mass

Body mass was reduced in *mdx* mice compared with wild-type control mice ($p = 0.011$). Both PRED ($p = 0.0355$) and PREDNAC ($p = 0.0017$) treatments

recovered body mass in the *mdx* mouse model of DMD such that it was equivalent to wild type (Figure 4.2).

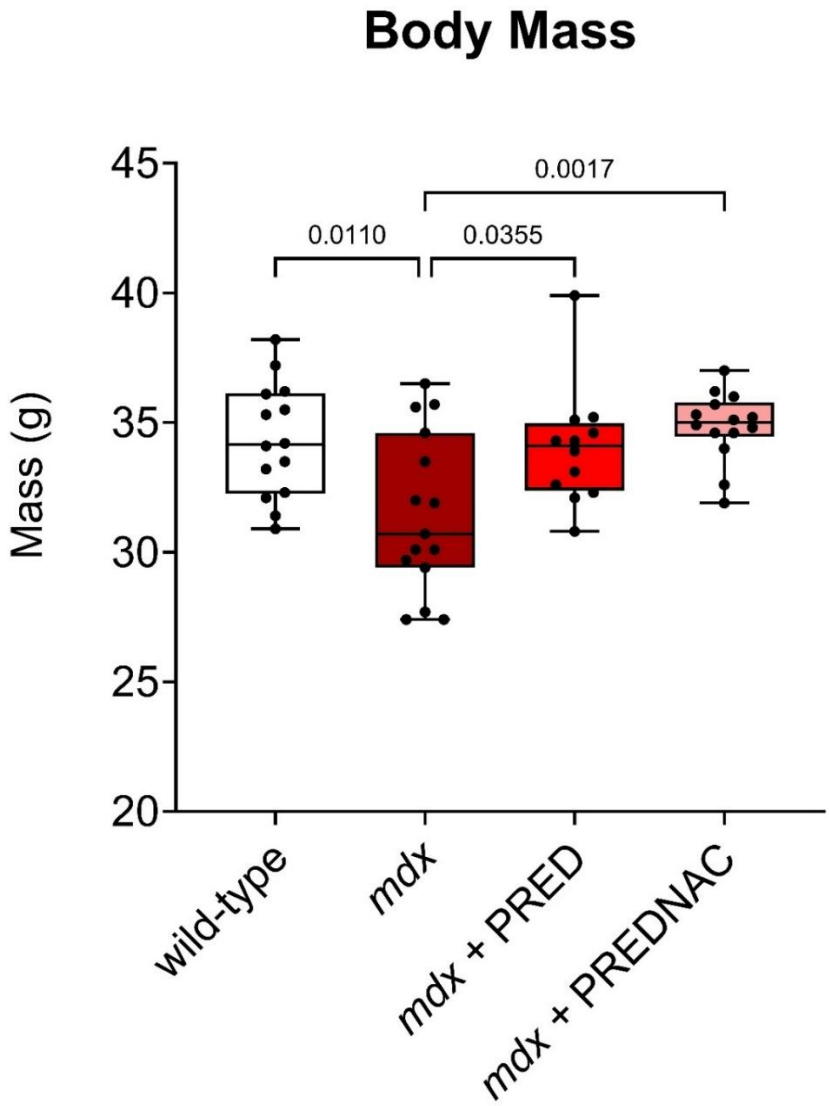

Figure 4.2: Body mass in wild-type (n = 14), mdx (n = 15), mdx + PRED (n = 12) and mdx +PREDNAC (n = 14) mice. Values are expressed as box and whisker plots (median, 25th–75th percentile and scatter plot) and were compared statistically using one-way ANOVA with Tukey's post hoc tests. Values of p < 0.05 are reported. Abbreviations: PRED, α-methylprednisolone; PREDNAC, α-methylprednisolone plus N-acetyl cysteine.

4.5.2 Baseline ventilation and Ventilatory Responsiveness to Hypercapnic-Hypoxia in conscious mice

Respiratory frequency, f_R, $\dot{V}_I$, metabolic $\dot{V}_{O_2}$, metabolic $\dot{V}_{CO_2}$ and the $\dot{V}_I/\dot{V}_{O_2}$ and $\dot{V}_I/\dot{V}_{CO_2}$ during baseline conditions (F_{IO_2} = 0.209) and HcHx (F_{IO_2} = 0.10 and F_{ICO_2} = 0.06) are illustrated in Figure 3. Baseline values were similar between groups across all parameters measured. In response to HcHx, tidal volume ($p < 0.0001$) and minute ventilation ($p = 0.0003$) increased in *mdx* mice to a greater extent than wild-type mice, but no differences were evident between wild-type and *mdx* mice in $\dot{V}_I/\dot{V}_{O_2}$ and $\dot{V}_I/\dot{V}_{CO_2}$. Neither chronic PRED nor PREDNAC treatment influenced integrated ventilatory performance in the *mdx* mouse model of DMD

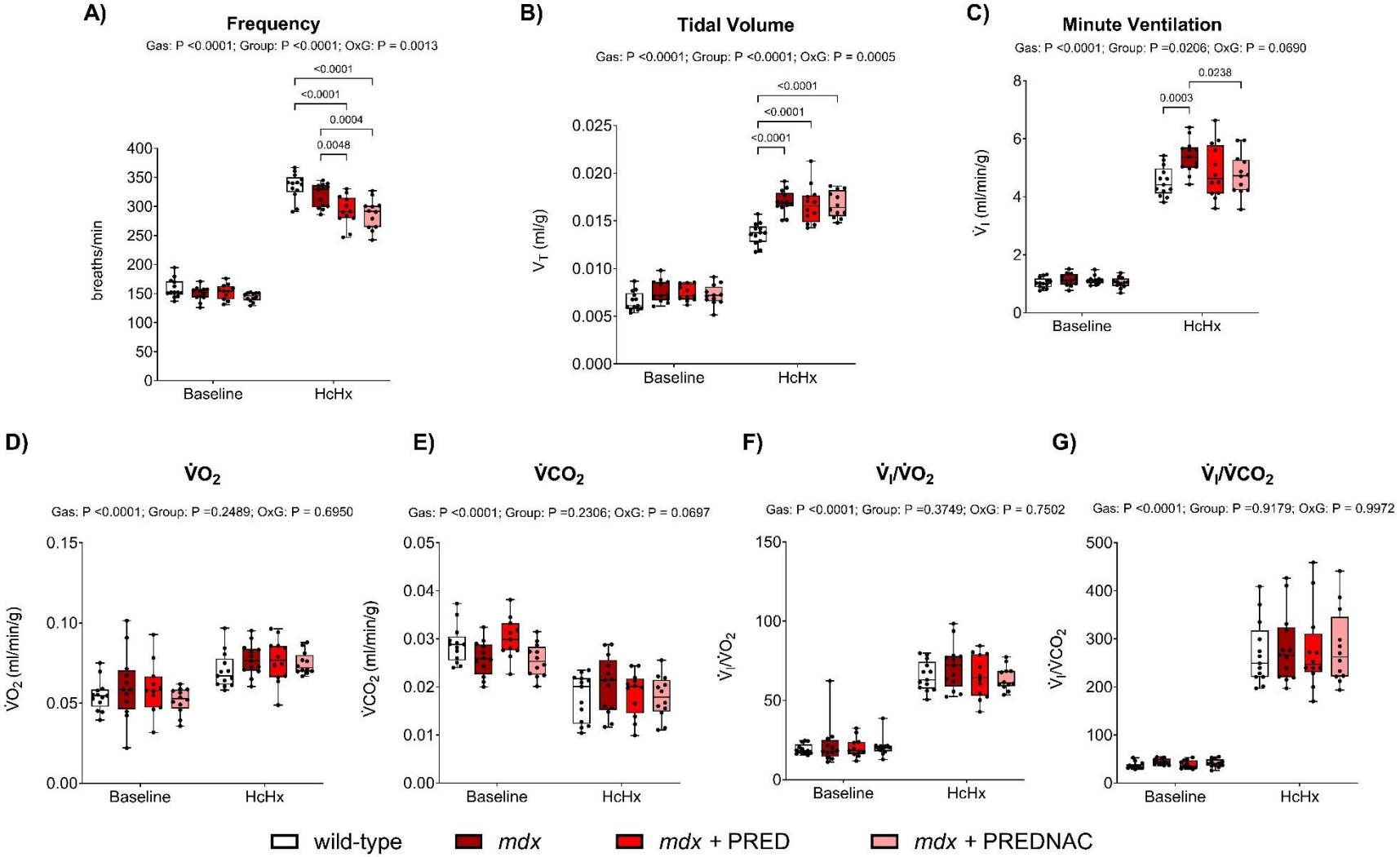
A)
Frequency
Gas: P <0.0001; Group: P <0.0001; OxG: P = 0.0013
breaths/min
<0.0001
<0.0001
0.0004
0.0048
Baseline
HcHx
B)
Tidal Volume
Gas: P <0.0001; Group: P <0.0001; OxG: P = 0.0005
V_T (ml/g)
<0.0001
<0.0001
<0.0001
Baseline
HcHx
C)
Minute Ventilation
Gas: P <0.0001; Group: P =0.0206; OxG: P = 0.0690
V̇_I (ml/min/g)
0.0238
0.0003
Baseline
HcHx
D)
V̇O2
Gas: P <0.0001; Group: P =0.2489; OxG: P = 0.6950
V̇O2 (ml/min/g)
Baseline
HcHx
E)
V̇CO2
Gas: P <0.0001; Group: P =0.2306; OxG: P = 0.0697
V̇CO2 (ml/min/g)
Baseline
HcHx
F)
V̇I/V̇O2
Gas: P <0.0001; Group: P =0.3749; OxG: P = 0.7502
V̇I/V̇O2
Baseline
HcHx
G)
V̇I/V̇CO2
Gas: P <0.0001; Group: P =0.9179; OxG: P = 0.9972
V̇I/V̇CO2
Baseline
HcHx
wild-type
mdx
mdx + PRED
mdx + PREDNAC

Figure 4.3: Assessment of breathing and metabolism during baseline conditions and exposure to hypercapnic hypoxia in conscious wild-type (n = 13), mdx (n = 13), mdx + PRED (n = 12) and mdx + PREDNAC (n = 12) mice. (A–C) Frequency (A), tidal volume (B) and minute ventilation (C) were determined from measurement of respiratory airflow. (D-G) The oxygen consumption (D) and carbon dioxide production (E) were measured, and the ventilatory equivalent for oxygen ($\dot{V}_I/\dot{V}_{O_2}$; F) and for carbon dioxide ($\dot{V}_I/\dot{V}_{CO_2}$; G) were determined offline. Data were compared statistically by two-way ANOVA (or mixed model when occasional data points were missing for technical reasons) with Tukey's multiple comparisons post hoc test (Prism v.10.3.1). Values of $p < 0.05$ are reported. Abbreviations: HcHx, hypercapnic hypoxia; PRED, α-methylprednisolone; PREDNAC, α-methylprednisolone plus N-acetyl cysteine; $\dot{V}_{CO_2}$, carbon dioxide production; $\dot{V}_{O_2}$, oxygen consumption.

4.5.3 Baseline and peak inspiratory pressure and EMG activity in anaesthetised mice

Representative original traces of inspiratory pressure and raw and integrated EMG activity before and during the tracheal occlusion manoeuvre are presented in Figure 4 (left-hand panel). Representative original traces of baseline conditions and the five successive maximum efforts (peak response) in wild-type (Figure 4A), *mdx* (Figure 4B), *mdx* + PRED (Figure 4C) and *mdx* + PREDNAC (Figure 4D) mice are presented in Figure 4 (middle and right-hand panels).

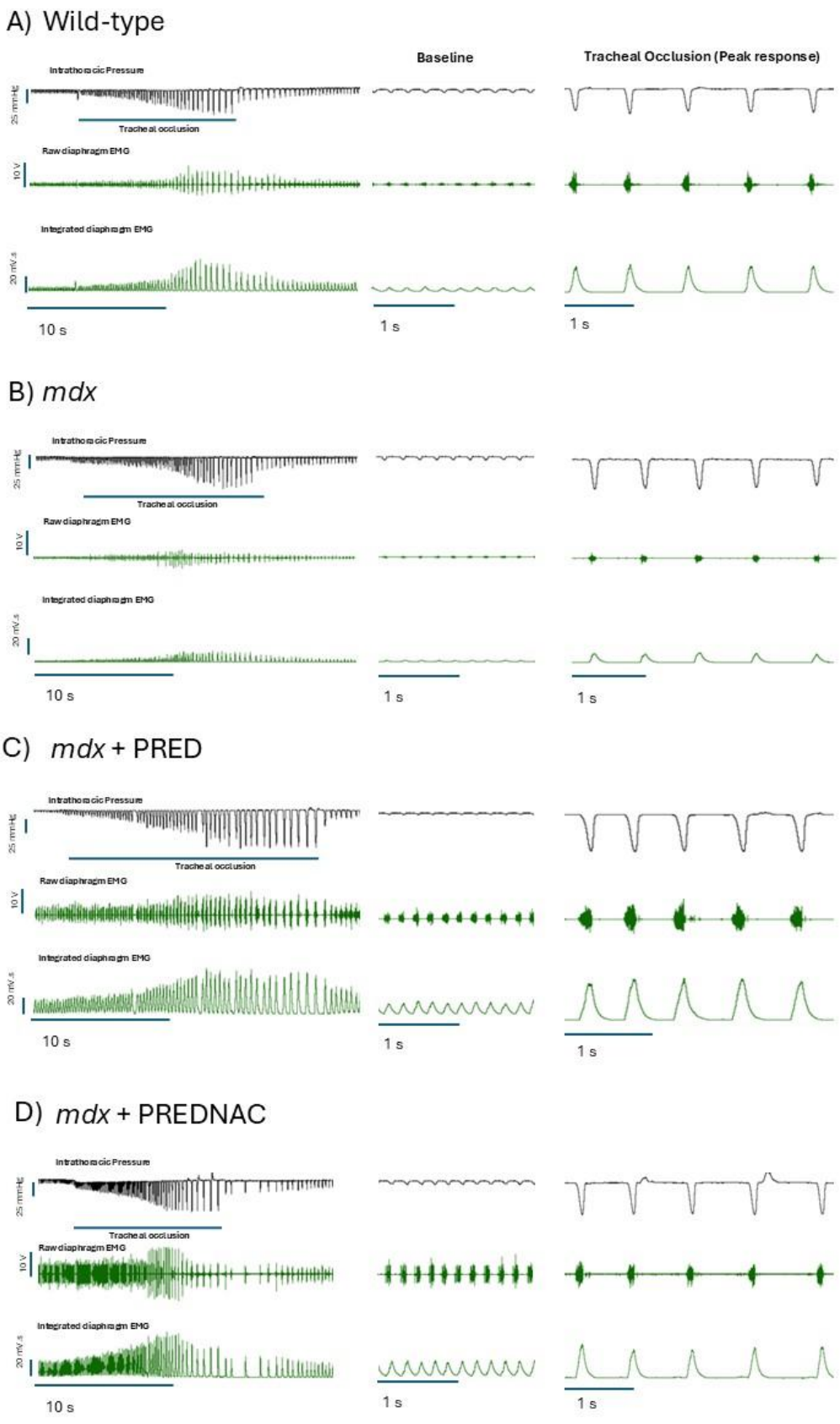
A) Wild-type
Baseline
Tracheal Occlusion (Peak response)
Intrathoracic Pressure
25 mmHg
Tracheal occlusion
Raw diaphragm EMG
10 V
Integrated diaphragm EMG
20 mV.s
10 s
1 s
1 s
B) mdx
Intrathoracic Pressure
25 mmHg
Tracheal occlusion
Raw diaphragm EMG
10 V
Integrated diaphragm EMG
20 mV.s
10 s
1 s
1 s
C) mdx + PRED
Intrathoracic Pressure
25 mmHg
Tracheal occlusion
Raw diaphragm EMG
10 V
Integrated diaphragm EMG
20 mV.s
10 s
1 s
1 s
D) mdx + PREDNAC
Intrathoracic Pressure
25 mmHg
Tracheal occlusion
Raw diaphragm EMG
10 V
Integrated diaphragm EMG
20 mV.s
10 s
1 s
1 s

Figure 4.4: Original traces of intrathoracic pressure and diaphragm raw and integrated EMG activities in anaesthetized wild-type (a), mdx (b), mdx + PRED (c) and mdx + PREDNAC (d) mice during baseline conditions and during tracheal occlusion evoking maximum EMG and peak pressure responses. The left panels show the entire trial. The middle panels show a portion of the baseline immediately preceding the airway occlusion. The right panels show the five successive peak responses during the tracheal occlusion. Abbreviations: PRED, α-methylprednisolone; PREDNAC, α-methylprednisolone plus N-acetyl cysteine.

Summary data for inspiratory pressure-generating capacity in baseline conditions and during protracted tracheal occlusion (peak response) are presented in Figure 5 for all groups. There were no differences in baseline inspiratory pressure generation across all groups. Inspiratory pressure was greater in *mdx* mice than in wild-type control mice. A paradoxical increase in inspiratory pressure generation was observed in *mdx* mice at 4 months of age ($p = 0.0001$) owing to diaphragm remodelling and compensation afforded by accessory muscles of breathing (O'Halloran et al., 2023). Neither PRED nor PREDNAC influenced peak inspiratory capacity in the *mdx* mouse model of DMD.

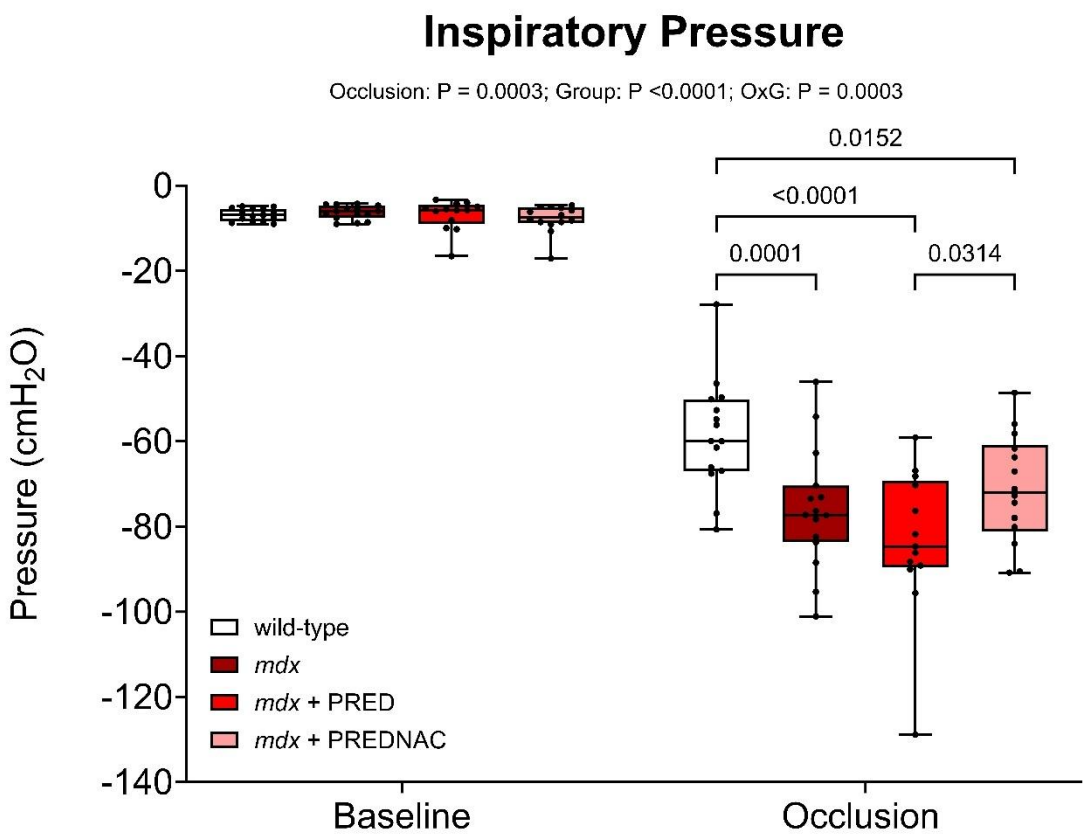

Figure 4.5: Inspiratory pressure generation during baseline and peak response during sustained tracheal occlusion in anaesthetized wild-type (n = 15), mdx (n = 15), mdx + PRED (n = 13) and mdx + PREDNAC (n = 14) mice. Summary data showing inspiratory pressure-generating capacity during baseline conditions and during tracheal occlusion (average of five successive greatest efforts). Values are expressed as box (median, 25th–75th percentile and individual data points) and whisker (minimum to maximum) plots. Data were compared statistically by two-way ANOVA (or mixed model when occasional data points were missing for technical reasons) with Tukey's multiple comparisons post hoc test (Prism v.10.3.1). Values of $p < 0.05$ are reported. Abbreviations: PRED, α-methylprednisolone; PREDNAC, α-methylprednisolone plus N-acetyl cysteine.

Summary data of the obligatory inspiratory muscles (diaphragm, external intercostals and parasternal intercostals) during baseline conditions and peak

responses during sustained tracheal occlusion are shown in Figure 6. There were no differences between groups in baseline conditions. There was a significant increase in diaphragm EMG activity in both drug treatment groups compared with *mdx* (p = 0.0008 for PRED and p = 0.0006 for PREDNAC). During peak activation, *mdx* parasternal EMG was significantly lower than wild-type (p = 0.0002), and this was recovered with PRED treatment (p = 0.015).

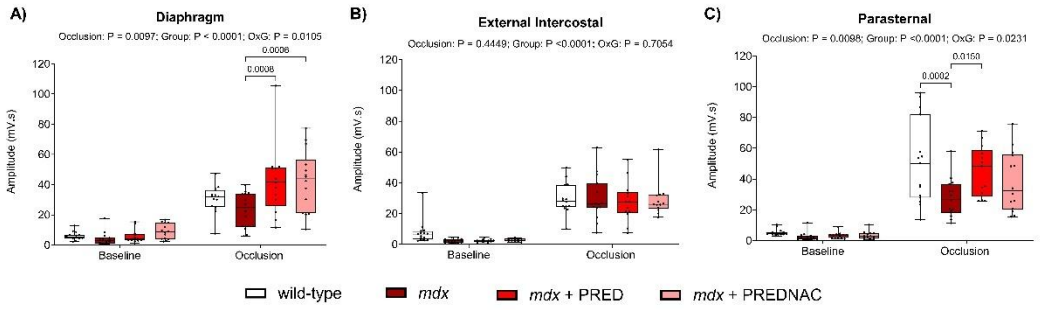

Figure 4.6: Diaphragm (a), external intercostal (b) and parasternal (c) respiratory EMG activities during baseline conditions and peak activation during tracheal occlusion in wild-type (n = 15), mdx (n = 15), mdx + PRED (n = 13) and mdx + PREDNAC (n = 14) mice. Values are expressed as box (median, 25th–75th percentile and individual data points) and whisker (minimum to maximum) plots. Data were compared statistically by two-way ANOVA (or mixed model when occasional data points were missing for technical reasons) with Tukey's multiple comparisons post hoc test (Prism v.10.3.1). Values of p < 0.05 are reported. Abbreviations: PRED, α-methylprednisolone; PREDNAC, α-methylprednisolone plus N-acetyl cysteine.

Summary data for accessory muscle EMGs (cleidomastoid, scalene, sternomastoid, trapezius and sternohyoid) during baseline conditions and peak responses during sustained tracheal occlusion are presented in Figure 7. There were no differences between groups in baseline conditions. Cleidomastoid

($p = 0.0278$) and sternohyoid ($p = 0.0044$) EMG activities were lower in *mdx* compared with wild-type mice. Drug treatments had no major effect on accessory EMG activities in *mdx* mice.

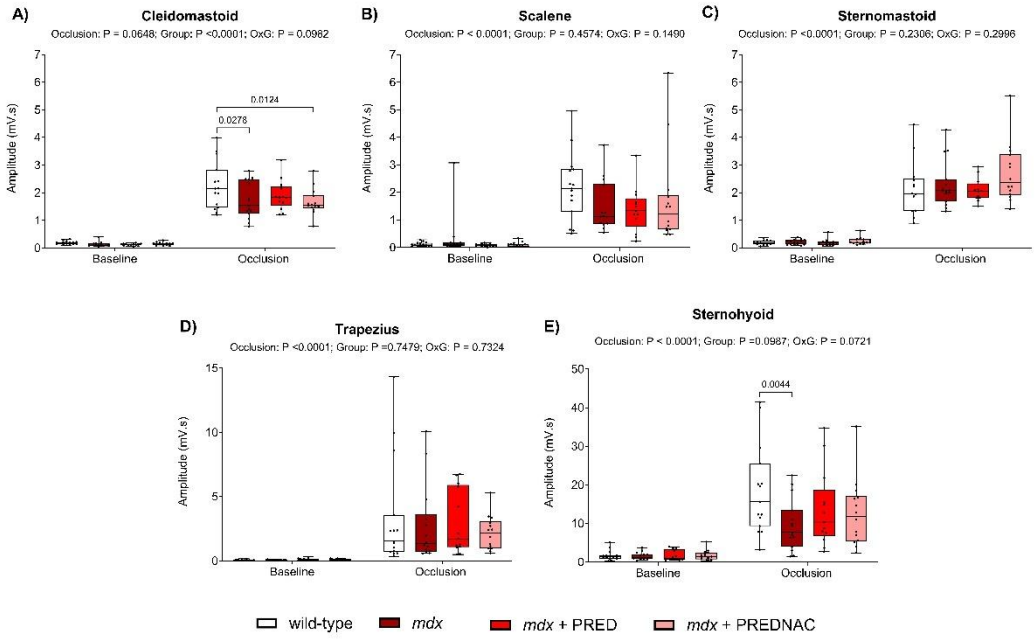

Figure 4.7: Cleidomastoid (a), scalene (b), sternomastoid (c), trapezius (d) and sternohyoid (e) respiratory EMG activity during baseline conditions and peak activation during tracheal occlusion in wild-type (n = 15), mdx (n = 15), mdx + PRED (n = 13) and mdx + PREDNAC (n = 14) mice. Values are expressed as box (median, 25th–75th percentile and individual data points) and whisker (minimum to maximum) plots. Data were compared statistically by two-way ANOVA (or mixed model when occasional data points were missing for technical reasons) with Tukey's multiple comparisons post hoc test (Prism v.10.3.1). Values of p < 0.05 are reported. Abbreviations: PRED, α-methylprednisolone; PREDNAC, α-methylprednisolone plus N-acetyl cysteine.

4.5.4 Respiratory parameters during baseline conditions, after vagotomy and during subsequent exposure to hypercapnic hypoxia in anaesthetized mice

Group data for respiratory parameters across the ventilatory range are shown in Figure 8 and Table 1. Respiratory frequency and minute ventilation tended to be significantly higher in *mdx* compared with wild-type mice. For the most part, drug treatments did not affect breathing parameters in *mdx* mice. Representative original traces of diaphragm raw and integrated EMG activity, tracheal airflow and tidal volume are presented in Figure 9 for all groups across a range of behaviours: baseline conditions, following bilateral vagotomy (increased central respiratory drive) and during exposure to HcHx (a further boost to central respiratory drive).

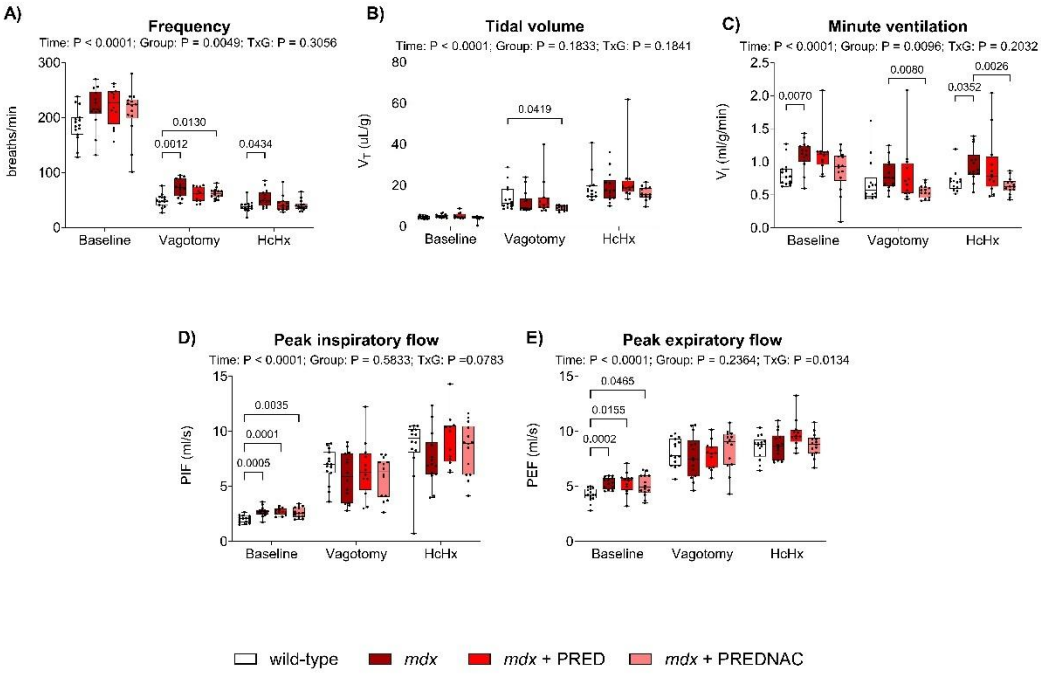

Figure 4.8: Summary data for respiratory frequency (a), tidal volume (b), minute ventilation (c), peak inspiratory flow (d) and peak expiratory flow (e) during baseline conditions, post-vagotomy and during hypercapnic hypoxia exposure in anaesthetized wild-type (n = 15), mdx (n = 15), mdx + PRED (n = 13) and mdx + PREDNAC (n = 14) mice. Values are expressed as box (median, 25th–75th

percentile and individual data points) and whisker (minimum to maximum) plots. Data were compared statistically by two-way ANOVA (or mixed model when occasional data points were missing for technical reasons) with Tukey's multiple comparisons post hoc test (Prism v.10.3.1). Values of $p < 0.05$ are reported. Abbreviations: f, respiratory frequency; HcHx, hypercapnic hypoxia; PEF, peak expiratory flow; PIF, peak inspiratory flow; PRED, α-methylprednisolone; PREDNAC, α-methylprednisolone plus N-acetyl cysteine; $\dot{V}_I$, minute ventilation; V_T, tidal volume.

Table 2: *Respiratory parameters during baseline conditions, following bilateral vagotomy and during exposure to hypercapnic hypoxia in anaesthetized wild-type, mdx, mdx + PRED and mdx + PREDNAC groups of mice.*

Baseline	**wild-type (n=15)**	***mdx* (n=15)**	***mdx* + PRED (n=13)**	***mdx* + PREDNAC (n=14)**	**ANOVA P-value**
Respiratory frequency (breaths/min)	187 ± 31	217 ± 37	220 ± 34	209 ± 45	0.0771
Tidal volume (µL/g)	4.4 ± 0.7	5.1 ± 0.8	5.1 ± 1.4	4.1 ± 1.1	**0.0400**
Minute ventilation (mL/g/min)	0.8 ± 0.2	1.1 ± 0.2	1.1 ± 0.3	0.9 ± 0.3	**0.0123**
Peak inspiratory flow (mL/s)	2.0 ± 0.3	2.7 ± 0.4	2.7 ± 0.3	2.6 ± 0.5	**0.0005**
Peak expiratory flow (mL/s)	4.2 ± 0.6	5.3 ± 0.5	5.3 ± 1.0	5.1 ± 1.0	**0.0090**
SpO_2 (%)	96.3 ± 3.3	96.6 ± 1.8	96.7 ± 1.0	96.9 ± 0.7	0.6540
$EtCO_2$ (%)	8.2 ± 1.2	8.5 ± 0.7	8.5 ± 1.2	9.1 ± 0.9	0.1206
Vagotomy					
Respiratory frequency (breaths/min)	49 ± 12	72 ± 16	61 ± 13	62 ± 9	**0.0005**
Tidal volume (µL/g)	13.9 ± 6.2	11.7 ± 5.3	13.9 ± 9.0	8.9 ± 1.2	0.0973
Minute ventilation (mL/g/min)	0.7 ± 0.3	0.8 ± 0.2	0.8 ± 0.5	0.6 ± 0.1	0.1000
Peak inspiratory flow (mL/s)	6.8 ± 1.5	5.9 ± 2.2	6.5 ± 2.6	5.8 ± 1.8	0.4084
Peak expiratory flow (mL/s)	8.1 ± 1.3	7.7 ± 1.9	7.8 ± 1.3	8.4 ± 1.8	0.5411
SpO_2 (%)	97.5 ± 1.0	97.1 ± 0.5	96.8 ± 0.9	97.1 ± 0.5	0.1764
$EtCO_2$ (%)	7.5 ± 1.2	8.1 ± 1.0	7.9 ± 1.5	8.9 ± 1.2	0.1462
HcHx					

Respiratory frequency (breaths/min)	39 ± 10	53 ± 16	43 ± 15	41 ± 10	**0.0319**
Tidal volume (µL/g)	19.2 ± 7.5	19.1 ± 7.3	22.3 ±12.8	16.0 ± 3.2	0.2496
Minute ventilation (mL/g/min)	0.7 ± 0.2	0.9 ± 0.3	0.9 ± 0.5	0.6 ± 0.1	**0.0209**
Peak inspiratory flow (mL/s)	8.6 ± 2.6	7.5 ± 2.4	5.8 ± 1.8	8.4 ± 2.3	0.3232
Peak expiratory flow (mL/s)	8.6 ± 1.1	8.7 ± 1.2	9.8 ± 1.3	8.8 ± 1.1	0.0561
SpO_2 (%)	50.9 ± 9.8	52.3 ± 8.5	54.6 ± 7.6	51.2 ± 6.4	0.6609
$EtCO_2$ (%)	>10	>10	>10	>10	

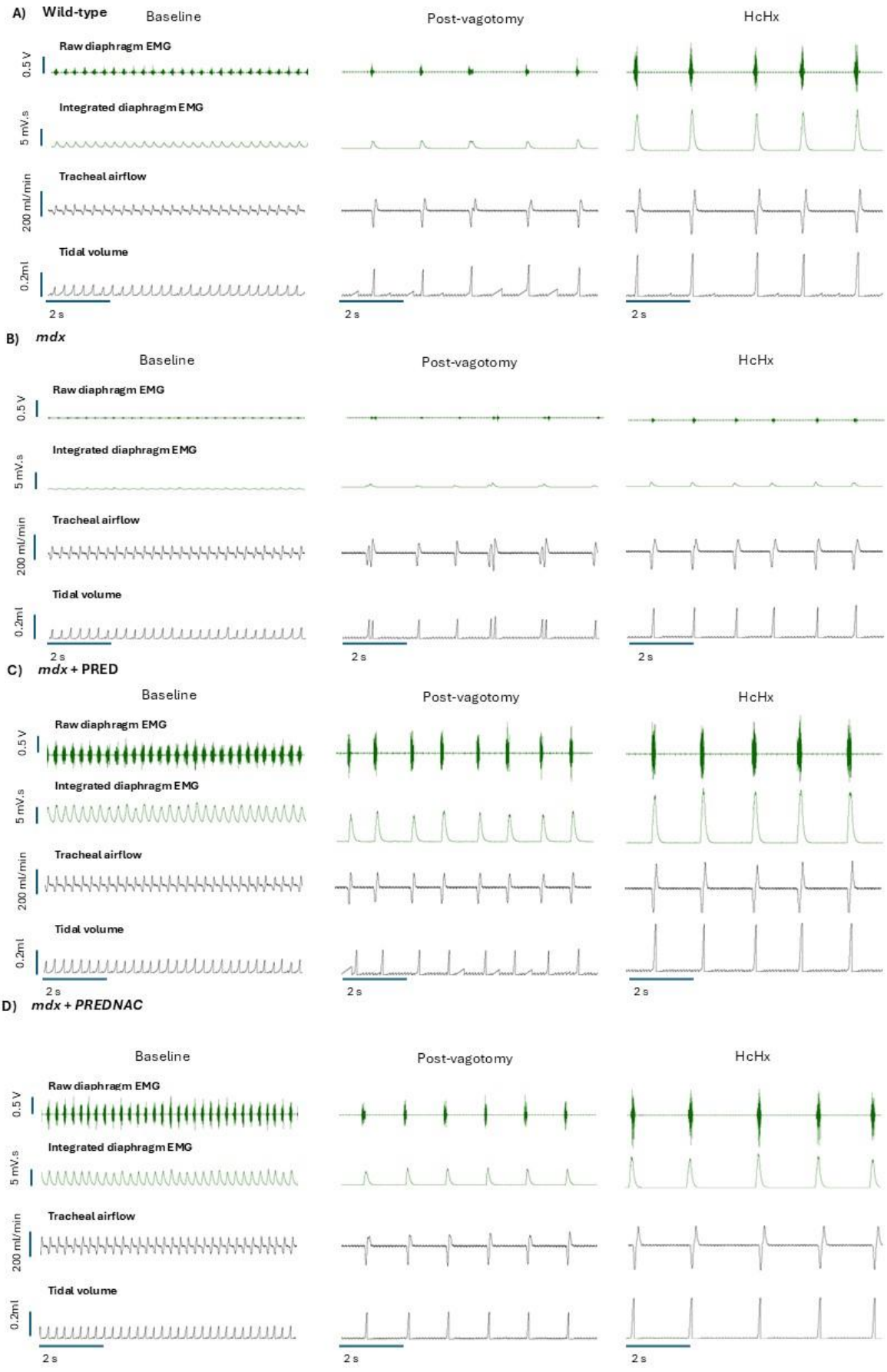
A) Wild-type
Baseline
Post-vagotomy
HcHx
Raw diaphragm EMG
0.5 V
Integrated diaphragm EMG
5 mV.s
Tracheal airflow
200 ml/min
Tidal volume
0.2ml
2 s
B) mdx
Baseline
Post-vagotomy
HcHx
Raw diaphragm EMG
0.5 V
Integrated diaphragm EMG
5 mV.s
Tracheal airflow
200 ml/min
Tidal volume
0.2ml
2 s
C) mdx + PRED
Baseline
Post-vagotomy
HcHx
Raw diaphragm EMG
0.5 V
Integrated diaphragm EMG
5 mV.s
Tracheal airflow
200 ml/min
Tidal volume
0.2ml
2 s
D) mdx + PREDNAC
Baseline
Post-vagotomy
HcHx
Raw diaphragm EMG
0.5 V
Integrated diaphragm EMG
5 mV.s
Tracheal airflow
200 ml/min
Tidal volume
0.2ml
2 s

Figure 4.9: Original traces of respiratory parameters across the ventilatory range in anaesthetized wild-type (a), mdx (b), mdx + PRED (c) and mdx + PREDNAC (d) mice. Diaphragm raw EMG activity, integrated diaphragm EMG activity, tracheal airflow and tidal volume in an anaesthetized mdx mouse during baseline conditions, following vagotomy and during hypercapnic hypoxia. Abbreviations: HcHx, hypercapnic hypoxia; PRED, α-methylprednisolone; PREDNAC, α-methylprednisolone plus N-acetyl cysteine.

4.5.5 Inflammatory cell infiltration and collagen deposition in diaphragm muscle

Representative histological images for diaphragm muscle from wild-type, *mdx*, *mdx* + PRED and *mdx* + PREDNAC groups are presented in Figure 10. Collagen deposition in the *mdx* diaphragm was significantly increased ($p < 0.0001$), and neither drug treatment significantly reduced diaphragm collagen deposition. The relative area of immune cell infiltration ($p < 0.0001$) and the density of centrally nucleated myofibres were significantly increased in the *mdx* diaphragm ($p < 0.0001$). PRED treatment alone did not significantly reduce immune cell infiltration or central nucleation. However, PREDNAC treatment significantly reduced immune cell infiltration ($p < 0.0001$) and central nucleation ($p = 0.0011$) in the *mdx* diaphragm.

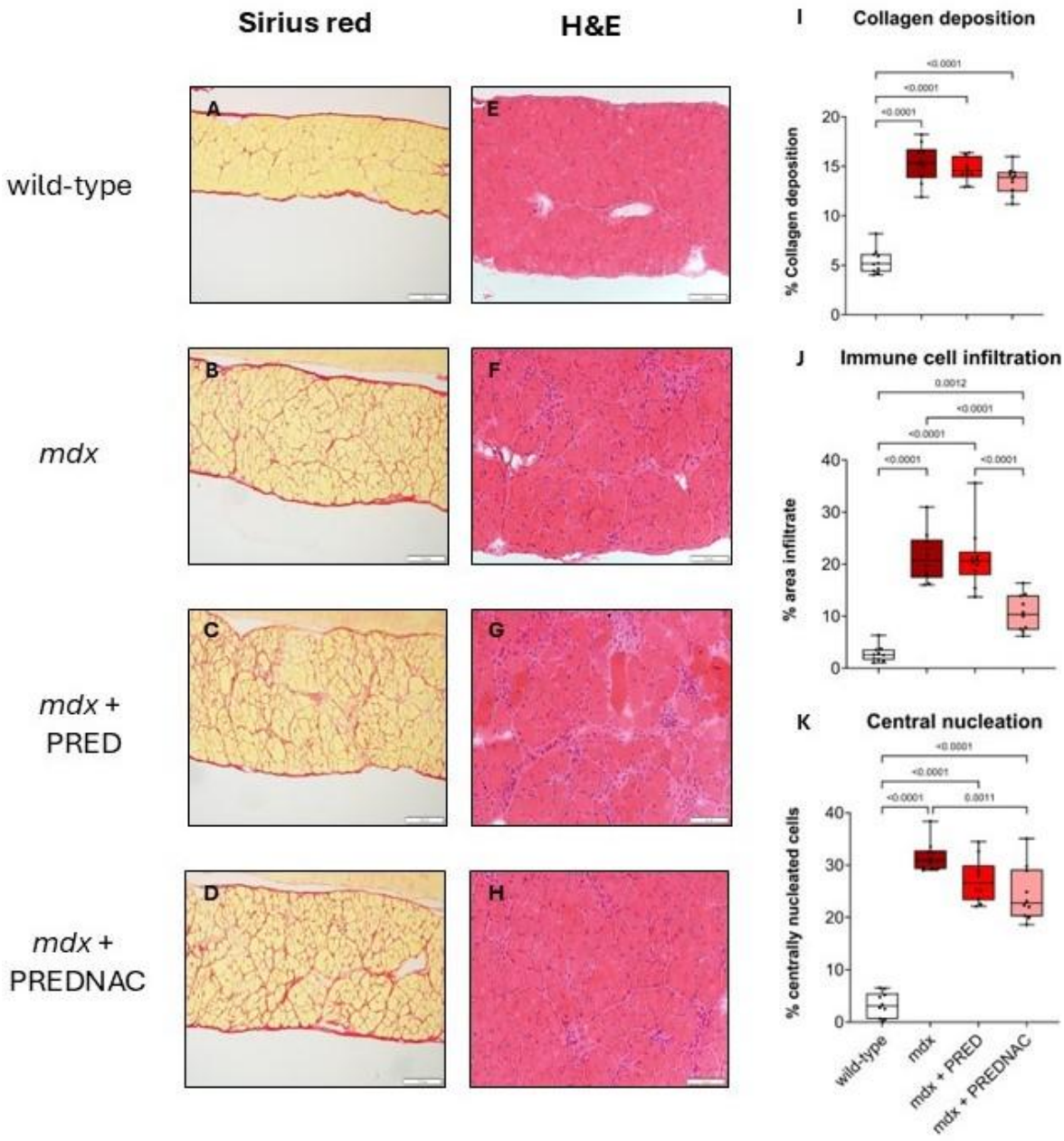

Figure 4.10: Assessment of collagen deposition and immune cell infiltration in diaphragm muscle from wild-type (n = 10), mdx (n = 10), mdx + PRED (n = 10) and mdx + PREDNAC (n = 10) mice. (A-H) Representative histological images of transverse sections of diaphragm muscle stained with Picrosirius Red (A-D) or Haematoxylin and Eosin (E-H). (I-K) Summary data showing the relative area of collagen deposition (I), relative area of infiltration of inflammatory cells (J) and relative density of centrally nucleated cells (K). Values are expressed as box and whisker plots (median, 25th–75th percentile and scatter plot) and were compared statistically using one-way ANOVA with Tukey's multiple

comparisons post hoc test (Prism v.10.3.1). Values of $p < 0.05$ are reported. Abbreviations: PRED, α-methylprednisolone; PREDNAC, α-methylprednisolone plus N-acetyl cysteine.

4.5.6 Diaphragm muscle contractile function ex vivo

Figure 11 shows summary data for diaphragm twitch time to peak, twitch half-relaxation time, twitch force, tetanic force, the force–frequency relationship and fatigue characteristics for wild-type, *mdx*, *mdx* + PRED and *mdx* + PREDNAC groups. Diaphragm force was significantly compromised in *mdx* mice, and this was not rescued by either of the two drug treatments.

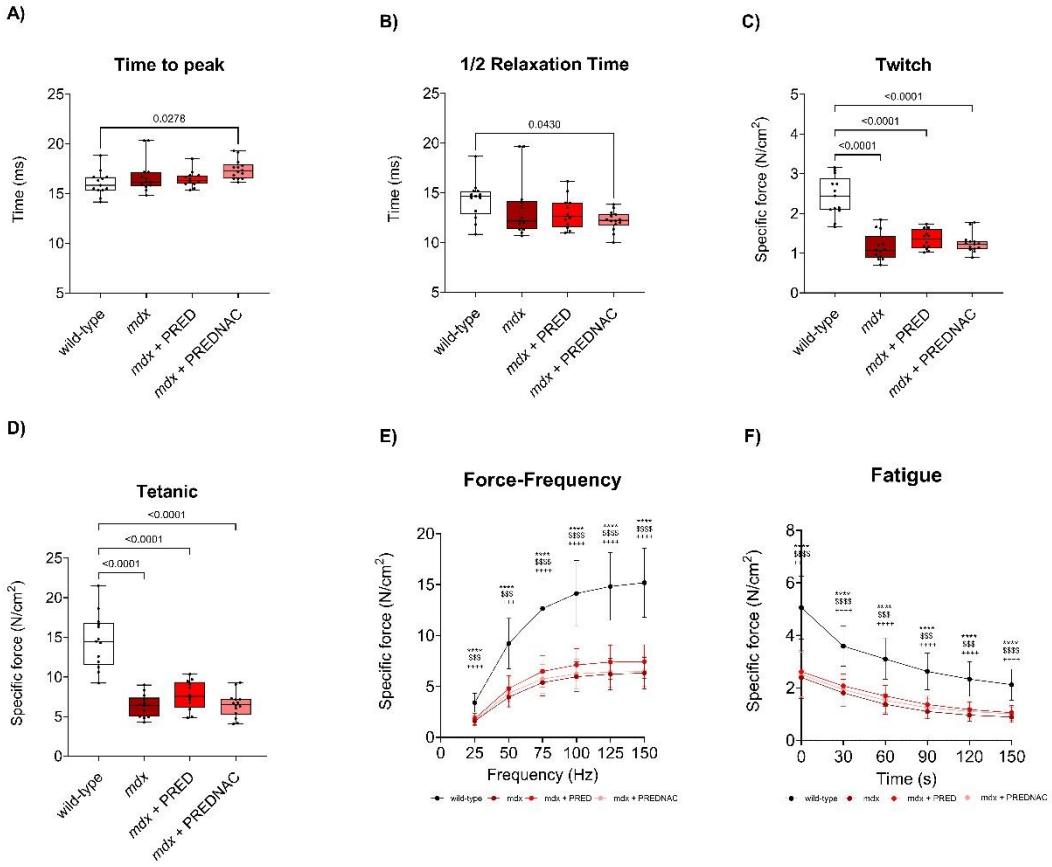

Figure 4.11: Ex vivo assessment of diaphragm time to peak (a), half-relaxation time (b), twitch force (c), tetanic force (d), force–frequency relationship (e) and

*fatigue characteristics (f), in wild-type (n = 13), mdx (n = 13), mdx + PRED (n = 12) and mdx + PREDNAC (n = 14) groups. Values are expressed as box and whisker plots (median, 25th–75th percentile and scatter plot) or mean ± SD (fatigue and force–frequency plots). Force and contractile kinetics data were compared statistically using a one-way ANOVA with Tukey's multiple comparison post hoc test. The fatigue and force–frequency relationships were compared by two-way ANOVA with Tukey's multiple comparisons post hoc test (Prism v.10.3.1). Values of p < 0.05 are reported for time to peak, half-relaxation time, twitch force and tetanic force. Force–frequency and fatigue data are shown as the mean ± SD and were compared statistically using two-way ANOVA with Tukey's post hoc test. * denotes mdx different from corresponding WT group; ** P < 0.01, *** P < 0.001, *** P < 0.0001. $ denotes mdx + PRED different from corresponding mdx group; $ P < 0.05, $$ P < 0.01, $$$ P < 0.001, $$$$ P<0.0001. + denotes mdx + PRED different from corresponding mdx group; + P < 0.05, ++ P < 0.01, +++ P < 0.001, ++++ P<0.0001.*

4.6 Discussion

The major findings of this study are as follows: (1) chronic PREDNAC treatment reduced immune cell infiltration and central nucleation in *mdx* diaphragm; (2) chronic PRED and PREDNAC increased peak *mdx* diaphragm EMG activity, and PRED alone increased parasternal intercostal EMG activity; (3) chronic PRED or PREDNAC did not restore force-generating capacity of the *mdx* diaphragm; (4) chronic PRED or PREDNAC did not affect *mdx* inspiratory pressure-generating capacity; and (5) chronic PRED or PREDNAC had no effect on ventilation and ventilatory responsiveness in *mdx* mice.

We gave PRED once weekly for 3 months to determine whether that would elicit beneficial effects on respiratory muscle quality and function without the

deleterious effects associated with chronic daily administration. In separate animals, we administered weekly PRED combined with daily NAC (a dietary antioxidant, anti-inflammatory and anti-fibrotic agent) to investigate whether this would further ameliorate dystropathology in the *mdx* diaphragm over the period of 1–4 months of age.

Structural remodelling within the diaphragm is evident very early in the *mdx* mouse model. This remodelling includes increased collagen deposition within the diaphragm (indicative of fibrosis), an increased number of centrally nucleated cells (marker of fibre regeneration) and infiltration of the muscle by immune cells (response to injury). We have previously described that at 1 month of age, collagen deposition in the diaphragm is equivalent in *mdx* and wild-type mice, but by 4 months of age there is a significant increase in collagen deposition in the *mdx* diaphragm and increased levels of the canonical profibrotic signalling factor transforming growth factor-β1 (O'Halloran et al., 2023; Quattrocelli et al., 2017). Both PRED and NAC work by anti-inflammatory actions. Daily PRED has been reported to be effective in reducing immune cell infiltration within skeletal muscle when administered over four weeks, but with prolonged daily use PRED can become ineffective and can even cause muscle atrophy (Quattrocelli et al., 2017).

In our study, weekly PRED alone had no effect on diaphragm fibrosis, immune cell infiltration and central nucleation in the *mdx* mouse model, indicating that the progression of the disease advances too rapidly for a single dose of PRED once weekly to be effective in ameliorating these effects. PREDNAC as a

combination therapy likewise did not significantly reduce collagen deposition in the *mdx* diaphragm. However, PREDNAC significantly decreased the relative area of immune cell infiltration and the relative density of centrally nucleated myocytes in the diaphragm. These reductions show that combined weekly glucocorticoid and daily antioxidant are effective in partly reducing the inflammation and injury-related regeneration in the diaphragm of the *mdx* mouse model of DMD. However, these improvements are not sufficient to offset muscle weakness and fibrosis.

Peak diaphragm muscle force is reduced in the *mdx* mouse model as early as 1 month of age (O'Halloran et al., 2023) and perhaps sooner. The present study confirms weakness in the diaphragm at 4 months of age. Diaphragm force was determined across a range of stimulus intensities, and our study demonstrates that neither PRED nor PREDNAC treatment rescues diaphragm muscle force in the *mdx* mouse model. This demonstrates that a weekly treatment regimen alone or in combination with daily antioxidant is not effective in ameliorating the loss of force-generating capacity in the *mdx* mouse model of DMD. This outcome was evident despite reduced inflammation within the *mdx* diaphragm with PREDNAC treatment, showing that the magnitude of the anti-inflammatory effect was not functionally relevant.

Peak EMG activity in the *mdx* mouse model is significantly reduced at 1 month of age and this reduced EMG activity persists to 16 months of age (O'Halloran et al., 2023). A reduction in respiratory EMG activity is evident as a reduction in the amplitude of motor unit action potentials owing to attrition of large motor units

and/or dysfunction in the neuromuscular junction. The present study revealed a reduction in *mdx* EMG activity compared with wild type within three of the eight respiratory muscles that were investigated. EMG activity was recovered in the parasternal intercostal muscle with PRED alone but not with PREDNAC. Diaphragm EMG activity was increased with both PRED and PREDNAC treatments compared with *mdx*, with values increasing more than wild type. The partial recovery of diaphragm and parasternal EMG activities is interesting. These two muscles carry a considerable burden of breathing and are likely to be the muscles most injured by contraction-induced injury in *mdx* mice. The anti-inflammatory effect of treatment in the diaphragm (and presumably parasternal) muscle might have improved neuromuscular integrity, owing to improvements in muscle quality, but this is speculative. Neither PRED nor PREDNAC influenced any of the accessory muscles of breathing, where all values were equivalent to *mdx* mice.

At 1 month of age, peak inspiratory pressure-generating capacity is reduced in *mdx* mice compared with wild-type mice (O'Halloran et al., 2023). Paradoxically, at 4 months of age, pressure generation is greater in *mdx* mice compared with wild-type counterparts (O'Halloran et al., 2023). The present study confirmed that *mdx* mice have a greater inspiratory pressure-generating capacity than wild-type mice. This adaptive response relates to diaphragm remodelling and compensation afforded by accessory muscles of breathing in early dystrophic disease (O'Halloran et al., 2023). Loss of this compensatory mechanism ensues in advanced dystrophic disease, underpinning the emergence of integrated respiratory system dysfunction (O'Halloran et al.,

2023). Neither PRED alone nor combined PREDNAC treatment affected inspiratory pressure-generating capacity (from baseline to peak activities) in the *mdx* mouse model of DMD despite the increase in EMG activity in the diaphragm.

The present study investigated baseline ventilation and ventilatory responsiveness to HcHx in conscious mice, and ventilation during baseline conditions, following bilateral vagotomy and subsequent exposure to HcHx in anaesthetized mice. Our results confirm previous work (O'Halloran et al., 2023) indicating that despite diaphragm injury and weakness, *mdx* mice maintain normal breathing and retain fully the ability to increase breathing in response to challenges across the ventilatory range in early disease. Weekly PRED or combined PREDNAC treatment had no effect on breathing and metabolism in *mdx* mice.

In summary, the PRED dosing strategy (once weekly 0.8 mg/kg i.p.) used in this study was ineffective in offsetting major facets of the disease, with no changes to diaphragm muscle structure or function. Co-administration of PREDNAC (once weekly PRED 0.8 mg/kg i.p. and 1% daily NAC in drinking water) caused a reduction in inflammation within the diaphragm muscle. However, diaphragm function was still impaired, indicating that the anti-inflammatory effect was not functionally relevant and was ultimately inadequate. PREDNAC also provoked an increase in diaphragm EMG activity; however, pressure-generating capacity was unaffected. It is evident that disease progression was too great to overcome by means of the current treatment strategy.

Our approach provided a comprehensive screening of respiratory performance in the *mdx* model, which is a strength. Breathing and chemoresponsiveness, in addition to integrated respiratory performance and diaphragm muscle force were assessed in all animals. Nevertheless, there are limitations of the study. It would have been useful to have concurrent information on limb muscle function to establish whether the lack of effect on the diaphragm reported in the study was specific to the respiratory muscle. We did not confirm the previous findings of (Quattrocelli et al., 2017). We studied one dose of PRED and NAC and chose a 3-month intervention for study, representing a dynamic period in the elaboration of a disease phenotype, but we acknowledge that different doses over different periods would be an added strength to the study. In our study, we did not investigate cross-sectional area or the thickness of the diaphragm because there was no increase in force in treated *mdx* diaphragms. We reason that there most probably was no difference in these parameters given the relationship between form and function. This differs from the findings of Quattrocelli, Barefield et al. (2017), who reported increased diaphragm cross-sectional area and thickness after weekly glucocorticoid treatment (but atrophy when used daily), but the two studies differ in several ways. We used the traditional *mdx* mouse, started treatment at 1 month of age for a period of 3 months using α-methylprednisolone at 0.8 mg/kg, and studied diaphragm but not limb muscle function. Quattrocelli, Barefield et al. (2017) used the more fibrotic D2.*mdx* model, started treatment at 6 months of age for a period of 1 month using prednisone at 1.0 mg/kg, and studied limb but not diaphragm muscle function.

Our study revealed that although weekly PRED has previously been shown to have beneficial effects in limb muscle, it is ineffective in exerting any functionally beneficial effect on the respiratory muscles. Previous studies investigating glucocorticoids and NAC in models of DMD have explored numerous dosing strategies and dose durations, and they provide a broad list of outcome measures that are not focused on the respiratory system but instead mostly on limb muscle form and function. Quattrocelli, Barefield et al., (2017) showed that prednisone or deflazacort treatment (1 mg/kg i.p.) once weekly for 4weeks in 6-month-old D2.*mdx* mice was effective in diminishing some of the harmful side-effects of the normal daily dosing regimen, showing improved grip strength, greater endurance to exercise and increased limb tetanic force. Hartel et al., (2001) showed that prednisone treatment (1 mg/kg, i.p.) daily for 8 weeks, starting at 4 weeks of age, reduced the levels of transforming growth factor-β1 and hydroxyproline concentrations, and increased collagen crosslinking in *mdx* diaphragm muscle. Keeling et al., (2007) showed that prednisolone (5 mg/kg, orally) twice weekly (consecutive days), for 2 years, resulted in improved survival and forelimb force-generating capacity. Concerning the potential benefits of NAC, Burns et al., (2019) showed that 1% NAC in the drinking water for 2 weeks rescued diaphragm function by increasing force-generating capacity and by reducing fibrosis and immune cell infiltration. Pinniger et al., (2017) showed that 2% NAC for 6 weeks improved *mdx* grip strength and force in the extensor digitorum longus muscle, with evidence of a reduction in muscle inflammation and oxidative stress. Terrill et al., (2012) found that 1% NAC treatment for 1 week prevented exercise-induced myofibre

necrosis, with a reduction in creatine kinase activity, in *mdx* mice. It is tempting to consider that a more aggressive dosing strategy might be effective (and required) for respiratory muscles, but the findings by Quattrocelli, Barefield et al., (2017) that daily dosing for a period of 1-month results in atrophic signalling in D2.*mdx* diaphragm suggest that this would be associated with diaphragm dysfunction. This suggests that studies exploring dosing regimens less frequent than daily but more frequent than weekly are worthy of pursuit.

4.7 Conclusion

The primary cause of death in patients with DMD is cardiorespiratory failure. This draws sharp focus to the need for optimal therapies to support respiratory system performance across the natural history of the disease. Our study reveals that weekly dosing with glucocorticoids might be suboptimal in support of breathing, suggesting that more frequent dosing might be required, perhaps owing to the higher duty cycle of respiratory muscles, which are rhythmically active throughout the day, in comparison to the limb muscles, which poses challenges for the determination of optimal glucocorticoid dosing in the clinic. Further studies examining the efficacy of different dosing strategies in preclinical models are warranted.

4.8 Author contributions

MNM: administration of PRED and PREDNAC; acquisition of whole-body plethysmography data; acquisition of diaphragm histology data; data and

statistical analysis and interpretation of data; preparation of figures and drafting of the manuscript. BTM: acquisition of force data; data and statistical analysis; preparation of figures; drafting of the manuscript. FMcD: supervision and critical review of the manuscript. KDO'H: acquisition of funding; experimental design; supervision; acquisition of EMG and pressure data; editing and critical review of the manuscript. Authors have approved the final version of the manuscript and agree to be accountable for all aspects of the work. All persons designated as authors qualify for authorship, and all those who qualify for authorship are listed.

4.9 Acknowledgements

We are grateful to staff of the Biological Services Unit, University College Cork for excellent service in the management of the mouse colony and animal care.

4.10 Conflict of Interest

The authors have no financial, professional or personal conflicts relating to this publication.

4.10 References

Aartsma-Rus, A., Van Deutekom, J. C. T., Fokkema, I. F., Van Ommen, G. B., & Den Dunnen, J. T. (2006). Entries in the Leiden Duchenne muscular dystrophy mutation database: An overview of mutation types and paradoxical cases that confirm the reading-frame rule. Muscle & Nerve, 34(2), 135–144. https://doi.org/10.1002/mus.20586

Broomfield, J., Hill, M., Guglieri, M., Crowther, M., & Abrams, K. (2021). Life Expectancy in Duchenne Muscular Dystrophy: Reproduced Individual Patient

Data Meta-analysis. Neurology, 97(23), e2304. https://doi.org/10.1212/WNL.0000000000012910

Burns, D. P., Canavan, L., Rowland, J., O'Flaherty, R., Brannock, M., Drummond, S. E., O'Malley, D., Edge, D., & O'Halloran, K. D. (2018). Recovery of respiratory function in mdx mice co-treated with neutralizing interleukin-6 receptor antibodies and urocortin-2. The Journal of Physiology, 596(21), 5175–5197. https://doi.org/10.1113/JP276954

Burns, D. P., Drummond, S. E., Bolger, D., Coiscaud, A., Murphy, K. H., Edge, D., & O'Halloran, K. D. (2019). N-acetylcysteine Decreases Fibrosis and Increases Force-Generating Capacity of mdx Diaphragm. Antioxidants, 8(12), 581. https://doi.org/10.3390/antiox8120581

Burns, D. P., Murphy, K. H., Lucking, E. F., & O'Halloran, K. D. (2019). Inspiratory pressure-generating capacity is preserved during ventilatory and non-ventilatory behaviours in young dystrophic mdx mice despite profound diaphragm muscle weakness. The Journal of Physiology, 597(3), 831–848. https://doi.org/10.1113/JP277443

Burns, D. P., Roy, A., Lucking, E. F., McDonald, F. B., Gray, S., Wilson, R. J., Edge, D., & O'Halloran, K. D. (2017). Sensorimotor control of breathing in the mdx mouse model of Duchenne muscular dystrophy. The Journal of Physiology, 595(21), 6653–6672. https://doi.org/10.1113/JP274792

Choi, M. H., Ow, J. R., Yang, N. Di, & Taneja, R. (2016). Oxidative Stress-Mediated Skeletal Muscle Degeneration: Molecules, Mechanisms, and Therapies. In Oxidative Medicine and Cellular Longevity (Vol. 2016). https://doi.org/10.1155/2016/6842568

Danon, M. J., & Carpenter, S. (1991). Myopathy with thick filament (myosin) loss following prolonged paralysis with vecuronium during steroid treatment. Muscle & Nerve, 14(11). https://doi.org/10.1002/mus.880141115

De Bruin, P. F., Ueki, J., Bush, A., Khan, Y., Watson, A., & Pride, N. B. (1997). Diaphragm thickness and inspiratory strength in patients with Duchenne

muscular dystrophy. Thorax, 52(5), 472–475. https://doi.org/10.1136/thx.52.5.472

Emery, A. E. (2002). The muscular dystrophies. The Lancet, 359(9307), 687–695. https://doi.org/10.1016/S0140-6736(02)07815-7

Evans, N. P., Misyak, S. A., Robertson, J. L., Bassaganya-Riera, J., & Grange, R. W. (2009). Immune-Mediated Mechanisms Potentially Regulate the Disease Time-Course of Duchenne Muscular Dystrophy and Provide Targets for Therapeutic Intervention. PM&R, 1(8), 755–768. https://doi.org/10.1016/j.pmrj.2009.04.010

Gao, Q. Q., & McNally, E. M. (2015). The Dystrophin Complex: Structure, Function, and Implications for Therapy. In Comprehensive Physiology (Vol. 5, Issue 3, pp. 1223–1239). Wiley. https://doi.org/10.1002/cphy.c140048

Hartel, J. V., Granchelli, J. A., Hudecki, M. S., Pollina, C. M., & Gosselin, L. E. (2001). Impact of prednisone on TGF-β1 and collagen in diaphragm muscle from mdx mice. Muscle and Nerve, 24(3). https://doi.org/10.1002/1097-4598(200103)24:3<428::AID-MUS1018>3.0.CO;2-E

Hoffman, E. P., Brown, R. H., & Kunkel, L. M. (1987). Dystrophin: The protein product of the duchenne muscular dystrophy locus. Cell, 51(6), 919–928. https://doi.org/10.1016/0092-8674(87)90579-4

Keeling, R. M., Golumbek, P. T., Streif, E. M., & Connolly, A. M. (2007). Weekly oral prednisolone improves survival and strength in male mdx mice. Muscle and Nerve, 35(1). https://doi.org/10.1002/mus.20646

Khirani, S., Ramirez, A., Aubertin, G., Boulé, M., Chemouny, C., Forin, V., & Fauroux, B. (2014). Respiratory muscle decline in duchenne muscular dystrophy. Pediatric Pulmonology, 49(5), 473–481. https://doi.org/10.1002/ppul.22847

Lewis, P., Sheehan, D., Soares, R., Coelho, A. V., & O'Halloran, K. D. (2016). Redox remodeling is pivotal in murine diaphragm muscle adaptation to chronic

sustained hypoxia. American Journal of Respiratory Cell and Molecular Biology, 55(1). https://doi.org/10.1165/rcmb.2015-0272OC

Maxwell, M. N., Marullo, A. L., Valverde-Pérez, E., Slyne, A. D., Murphy, B. T., & O'Halloran, K. D. (2024). Chronic N -acetyl cysteine treatment does not improve respiratory system performance in the mdx mouse model of Duchenne muscular dystrophy. Experimental Physiology, 109(8), 1370–1384. https://doi.org/10.1113/EP091862

Mhandire, D. Z., Burns, D. P., Roger, A. L., O'Halloran, K. D., & ElMallah, M. K. (2022). Breathing in Duchenne muscular dystrophy: translation to therapy. The Journal of Physiology, 600(15), 3465–3482. https://doi.org/10.1113/JP281671

O'Halloran, K. D., Maxwell, M. N., Marullo, A. L., Hamilton, C. P., Ó Murchú, S. C., Burns, D. P., Mahony, C. M., Slyne, A. D., & Drummond, S. E. (2023). Loss of compensation afforded by accessory muscles of breathing leads to respiratory system compromise in the mdx mouse model of Duchenne muscular dystrophy. The Journal of Physiology, 601(19), 4441–4467. https://doi.org/10.1113/JP285203

Passamano, L., Taglia, A., Palladino, A., Viggiano, E., D'Ambrosio, P., Scutifero, M., Cecio, M. R., Torre, V., De Luca, F., Picillo, E., Paciello, O., Piluso, G., Nigro, G., & Politano, L. (2012). Improvement of survival in Duchenne Muscular Dystrophy: Retrospective analysis of 835 patients. In Acta Myologica (Vol. 31, Issue OCTOBER).

Personius, K. E., & Sawyer, R. P. (2006). Variability and failure of neurotransmission in the diaphragm of mdx mice. Neuromuscular Disorders, 16(3), 168–177. https://doi.org/10.1016/j.nmd.2006.01.002

Pinniger, G. J., Terrill, J. R., Assan, E. B., Grounds, M. D., & Arthur, P. G. (2017). Pre-clinical evaluation of N -acetylcysteine reveals side effects in the mdx mouse model of Duchenne muscular dystrophy. The Journal of Physiology, 595(23), 7093–7107. https://doi.org/10.1113/JP274229

Quattrocelli, M., Barefield, D. Y., Warner, J. L., Vo, A. H., Hadhazy, M., Earley, J. U., Demonbreun, A. R., & McNally, E. M. (2017). Intermittent glucocorticoid steroid dosing enhances muscle repair without eliciting muscle atrophy. Journal of Clinical Investigation, 127(6). https://doi.org/10.1172/JCI91445

Redwan, A., Kiriaev, L., Kueh, S., Morley, J. W., Houweling, P., Perry, B. D., & Head, S. I. (2023). Six weeks of N-acetylcysteine antioxidant in drinking water decreases pathological fiber branching in MDX mouse dystrophic fast-twitch skeletal muscle. Frontiers in Physiology, 14. https://doi.org/10.3389/fphys.2023.1109587

Shortt, C. M., Fredsted, A., Chow, H. B., Williams, R., Skelly, J. R., Edge, D., Bradford, A., & O'Halloran, K. D. (2014). Reactive oxygen species mediated diaphragm fatigue in a rat model of chronic intermittent hypoxia. Experimental Physiology, 99(4). https://doi.org/10.1113/expphysiol.2013.076828

Smith, P. E. M., Edwards, R. H. T., & Calverley, P. M. A. (1989). Ventilation and Breathing Pattern during Sleep in Duchenne Muscular Dystrophy. Chest, 96(6), 1346–1351. https://doi.org/10.1378/chest.96.6.1346

Tenório, M. C. dos S., Graciliano, N. G., Moura, F. A., Oliveira, A. C. M. de, & Goulart, M. O. F. (2021). N-Acetylcysteine (NAC): Impacts on Human Health. Antioxidants, 10(6), 967. https://doi.org/10.3390/antiox10060967

Terrill, J. R., Radley-Crabb, H. G., Grounds, M. D., & Arthur, P. G. (2012). N-Acetylcysteine treatment of dystrophic mdx mice results in protein thiol modifications and inhibition of exercise induced myofibre necrosis. Neuromuscular Disorders, 22(5), 427–434. https://doi.org/10.1016/j.nmd.2011.11.007

Chapter 5. Neuromuscular and neuromechanical assessments of respiratory performance in the *mdx* mouse model of Duchenne muscular dystrophy across the natural history of disease

5.1 Publication information

In preparation for publication.

Keywords:

Duchenne muscular dystrophy; respiratory electromyogram spectrum parameters; mdx mouse; neuromechanical efficiency; neural respiratory drive; tension-time index

Key points

- Reliable temporal biomarkers of respiratory involvement in Duchenne muscular dystrophy (DMD) are needed.
- Several clinically relevant indices of respiratory neuromuscular performance were assessed across the natural history of disease (1-16-months of age) in the most commonly used preclinical model of DMD, the *mdx* mouse.
- Respiratory EMG activities are lower in *mdx* mice, evident in early disease. However, a remarkable compensation subserving respiratory system performance is evident. Several established indices of neuromuscular

and neuromechanical performance in *mdx* mice were equivalent to wild-type controls even in advanced disease.

- Studies in *mdx* mice >16 months of age or logistically convenient models of rapid neuromuscular disease progression are required to facilitate the study of ventilatory insufficiency, providing a platform to assess the efficacy of existing and emerging therapies for DMD.

5.2 Abstract

Duchenne muscular dystrophy (DMD) is a severe life-limiting X-linked neuromuscular disorder characterized by progressive skeletal muscle degeneration and respiratory failure. The mdx mouse, lacking dystrophin, is the most widely used preclinical model of DMD, yet the trajectory of respiratory dysfunction in this model remains incompletely defined.

We evaluated neural respiratory drive (NRD), neuromechanical efficiency (NME), tension-time index (TTI), inspiratory drive rate (IDR), and electromyographic (EMG) frequency spectrum parameters in the diaphragm, external intercostal, and parasternal muscles during baseline, following bilateral vagotomy and during subsequent hypercapnic hypoxia, and finally during sustained tracheal occlusion across the natural history of disease (aged 1–16 months).

Despite early and persistent reductions in EMG activity and frequency spectrum parameters in mdx mice, NRD and TTI in respiratory muscles were largely equivalent to controls, indicating preserved central drive and muscle endurance. NME was paradoxically increased in mdx mice, likely reflecting compensatory recruitment of accessory muscles rather than improved contractile efficiency of the major inspiratory muscles of breathing. The area under the pressure-time curve during sustained tracheal occlusion was reduced in mdx mice at 1 month of age, but equivalent to wild-type values at all other ages, demonstrating robust compensatory mechanisms that are effective even in advanced disease. No significant differences in inspiratory duty cycle, respiratory muscle effort, or TTI were observed between groups.

These findings reveal that despite profound diaphragm pathology, mdx mice maintain stable respiratory performance up to 16 months of age. We conclude that assessments of integrative respiratory morbidity in mdx mice should focus on animals aged ≥16 months or alternative models with accelerated disease progression. Our results underscore the need for refined translational models and highlight the importance of integrating EMG-based indices for early detection and monitoring of respiratory compromise in DMD.

5.3 Introduction

Duchenne muscular dystrophy (DMD) is a life-limiting X-linked neuromuscular disease, caused by mutations of the *DMD* gene that encodes for the protein dystrophin (E. P. Hoffman et al., 1987b). Dystrophin, which is completely absent in DMD, is part of the dystrophin glycoprotein complex that connects the F-actin of the cytoskeleton to the extracellular matrix via the sarcolemma, providing stability to the muscle membrane (Gao & McNally, 2015). Dystrophin deficiency results in skeletal muscle damage, immune cell infiltration, chronic inflammation and muscle wasting (Deconinck & Dan, 2007; Duan et al., 2021; McDouall et al., 1990; Schmalbruch, 1984). In DMD, there is a progressive decline in respiratory muscle strength and pulmonary function culminating in ventilatory insufficiency and consequential cardiorespiratory failure (De Bruin et al., 1997; Eagle et al., 2002; Ishikawa et al., 2011; Khirani et al., 2014; P. E. M. Smith et al., 1989).

Corticosteroids remain the most widely used therapeutic in the management of DMD. Corticosteroids such as prednisone/prednisolone/deflazacort are prescribed to patients with DMD with the intention of offsetting disease progression (Birnkrant et al., 2018). However, despite corticosteroid treatment and its early ambulatory benefits, respiratory function declines at a steady rate annually (Fauroux et al., 2015; Khirani et al., 2014). Respiratory involvement in DMD is poorly understood hampering its treatment (Trucco & O'Halloran, 2025). Spirometry and respiratory muscle testing as currently employed in DMD are not sufficient to delineate the trajectory of respiratory compromise from onset to end-stage disease (J. D. Finder, 2009; J. D. Finder et al., 2004; Hudson et al., 2025a; Sheehan et al., 2018). Complementary recordings of respiratory pressures and electromyography (EMG) can help chart the natural history of DMD by evaluating temporal progression of the disease (Fauroux et al., 2009, 2015; J. D. Finder, 2009; J. D. Finder et al., 2004; Hahn et al., 1997). A comprehensive battery of reliable and reproducible respiratory muscle tests could facilitate a pathology-based approach to the clinical management of respiratory morbidity in DMD, as opposed to the symptom-led approach currently undertaken.

Maximum inspiratory pressure (MIP) is a valuable parameter that can monitor disease progression, evaluate treatment efficacy, and predict patient outcome. In DMD patients, MIP declines at a rate of ~2.1 cmH_2O/year generally after the age of 10 years, which generally coincides with loss of ambulation and the beginning of wheelchair dependence (Fauroux et al., 2015; Khirani et al., 2014;

van Oosten et al., 2024; Whitelaw et al., 1975). Volitional and non-invasive assessment of MIP clinically assesses mouth pressure during a maximal inspiratory effort against an occluded mouthpiece (ATS/ERS Statement on Respiratory Muscle Testing, 2002). However, such volitional tests have limitations due to patients being unable to perform the manoeuvres correctly due to age or understanding (Fauroux et al., 2015; Hinton et al., 2007; Khirani et al., 2014).

Respiratory EMG can be used to assess the pattern and intensity of muscle activation. When used in conjunction with tests of mechanical function, together they provide indices of muscle contractile function (ATS/ERS Statement on Respiratory Muscle Testing, 2002). Routine monitoring of respiratory muscle function should be employed to guide respiratory management in DMD (J. D. Finder, 2009; J. D. Finder et al., 2004; Hudson et al., 2025b). Assessment of respiratory EMG is not utilised clinically in DMD despite a joint consensus for normal respiratory testing by the ERS and ATS that respiratory EMG can be used to assess the level and pattern of their activation to detect and diagnose neuromuscular pathology, and when coupled with tests of mechanical function, can assess the efficacy of contractile function (J. D. Finder, 2009; J. D. Finder et al., 2004; Hudson et al., 2025b; McManus et al., 2020).

EMG captures and displays the intricate, electrical activity produced by motor units as they regulate both voluntary and reflex muscle movements. EMG signals serve as a key diagnostic tool for various neuromuscular and neurological conditions, including myopathy and amyotrophic lateral sclerosis (Samanta et

al., 2022). Neuromuscular disorders such as DMD alter the morphology and physiology of the neuromuscular junction which are critical to motor unit health (Lovering et al., 2020; Ng & Ljubicic, 2020). Variations in EMG signal amplitude and spectral characteristics can help assess the balance between central and peripheral fatigue mechanisms in neuromuscular disorders (McManus et al., 2017). Myopathic conditions including DMD often show reduced low-frequency spectral content in EMG signals due to the presence of shorter-duration, polyphasic motor unit potentials resulting from muscle fibre degeneration and motor unit remodelling (Frascarelli et al., 1988; Kumar Bhoi et al., 2013; Ng & Ljubicic, 2020; Pandeya et al., 2023).

Neural respiratory drive (NRD) is a physiological index of the proportional activation of a muscle relative to maximum, used to infer the mechanical load on the respiratory muscles (Cavalcante et al., 2024; Jolley et al., 2009; MacBean et al., 2016; Murphy et al., 2011; Onofri et al., 2018; Reilly et al., 2011, 2016; Steier et al., 2017). NRD is expressed as EMG of the diaphragm during tidal breathing as a percentage of peak EMG activity obtained during a maximum inspiratory manoeuvre. Breath-by-breath calculation of NRD can be measured in real time (Cavalcante et al., 2024; Jolley et al., 2009; MacBean et al., 2016; Murphy et al., 2011; Onofri et al., 2018; Reilly et al., 2011, 2016; Steier et al., 2017). NRD has been used as a biomarker of disease severity in COPD (Jolley et al., 2009; Murphy et al., 2011), obesity hypoventilation syndrome (Onofri et al., 2018), hypertension (Cavalcante et al., 2024) and cystic fibrosis (Reilly et al., 2011, 2013, 2016).

Combining pressure and EMG provides a proxy measure for neuromechanical efficiency (NME) (also known as neuromechanical coupling). NME reflects the efficiency of converting neural activation to pressure generation (Bellani et al., 2013; Jansen et al., 2018; Lozano-Garcia et al., 2019; Lozano-García et al., 2021), reflecting the magnitude of inspiratory pressure that can be generated for each unit of diaphragm electrical activity (Bellani et al., 2013; Jansen et al., 2018). NME has been used to estimate breath-by-breath inspiratory effort and is recognised clinically as a useful index of diaphragm function and respiratory mechanics (Lozano-Garcia et al., 2019; Lozano-García et al., 2021), which can guide mechanical ventilatory support to minimise diaphragm dysfunction from ventilator over- and under-assist (Jansen et al., 2018, 2021; Tagliabue et al., 2019). NME is used to observe the level of neuromechanical uncoupling and related breathlessness observed in obstructive lung disease, such as COPD (O'Donnell et al., 2006) and neuromuscular disease (Lanini et al., 2001; Spinelli et al., 1992).

Another widely employed clinical measure in respiratory medicine is the tension-time index (TTI), which reflects the efficiency of the total work undertaken by all respiratory muscles. Elevated TTI is associated with inspiratory muscle fatigue (Bellemare & Grassino, 1982; Dassios & Dimitriou, 2019; Miller & Mayer, 2021). TTI is expressed as inspiratory pressure divided by maximum inspiratory pressure (P_{insp}/P_{MAX}) multiplied by the inspiratory time divided by total respiratory cycle time (T_i/T_{tot}) (Bellemare & Grassino, 1982; Restrepo et al., 2016). TTI has been used to investigate ventilator weaning, severity of lung disease in cystic

fibrosis (Hahn et al., 2008), and various neuromuscular diseases including DMD (García-Río et al., 2003; Hahn et al., 2009; Miller & Mayer, 2021).

Airway occlusion pressure ($P_{0.1}$) is a measure used in mechanically ventilated patients to determine their respiratory drive (Telias et al., 2018). $P_{0.1}$ is the pressure developed in the occluded airway 100ms after the onset of inspiration (Whitelaw et al., 1975). Although it has been used to measure patients' respiratory drive, $P_{0.1}$ is also incorporated in the measure of TTI in which P_{insp} is calculated by the equation $P_{insp} = 5 \times P_{0.1} \times Ti$ and has been assessed in patients with cystic fibrosis (Hahn et al., 2008) and DMD (García-Río et al., 2003; Hahn et al., 2009). The slope of the pressure generated reflects the rate of inspiratory muscle activation and the rate of increase in the electrical activity of the obligatory muscles will reflect the rate of activation of the individual muscles themselves also referred to as rise time, which has also been used as an indicator of drive (Telias et al., 2020).

One of the most widely studied models of DMD is the dystrophin deficient *mdx* mouse. Our research group has previously demonstrated compromised respiratory muscle form and function in the *mdx* mouse with pronounced structural remodelling, weakness and impaired respiratory control (Burns, Murphy, et al., 2019; Burns, Roy, et al., 2017; Mhandire et al., 2022; O'Halloran et al., 2023; Slyne et al., 2025). EMG activity of the obligatory muscles of breathing in the *mdx* mouse is reduced, which likely reflects impaired neuromuscular function pertinent to respiratory performance (Burns, Murphy, et al., 2019; O'Halloran et al., 2023; Personius & Sawyer, 2006; Slyne et al., 2025).

We have previously investigated inspiratory pressure and EMG activity in 1-, 4-, 8-, 12-, and 16-month-old wildtype and *mdx* mice (O'Halloran et al., 2023). Despite profound diaphragm muscle dysfunction, peak inspiratory pressure is preserved over a protracted period of the natural history of disease. Our work suggests that compensation is afforded by accessory respiratory muscles, including abdominal muscles, facilitated by the remodelled stiffened dystrophic diaphragm, as distinct from enhanced facilitation of respiratory motor drive in accessory motor pathways (O'Halloran et al., 2023).

In the current study, we re-analysed data from our previous study (O'Halloran et al., 2023) to assess several clinically relevant indices of respiratory neuromuscular performance including NRD (balance between respiratory muscle load and capacity), NME (inspiratory pressure related to electrical activation of the muscle), TTI (efficiency of the total work undertaken by respiratory muscles), IDR (inspiratory drive rate which indicates the rate of activation of the inspiratory muscles from the inspiratory pressure generation), frequency spectrum analysis (mean, median and max), total power (area under the curve of the frequency spectrum) and the pressure-time relationship during sustained peak activation in wild-type and *mdx* mice at 1, 4, 8,12, and 16 months of age. Our aim was to further characterise respiratory performance in the most widely used mouse model of DMD over the natural history of the disease. We hypothesized that clinically relevant indices of respiratory performance would be impaired in *mdx* mice especially in advanced disease, providing useful

translational biomarkers of DMD progression offering a platform for the assessment of novel therapeutics for respiratory compromise in DMD.

5.3 Methods

5.3.1 Ethical approval

Procedures on live animals were performed under project authorisations (AE19130/P117 and AE19130/P157) from the Health Products Regulatory Authority in accordance with Irish and European law with prior ethical approval by University College Cork (AEEC 2019/013 and AEEC 2021/019). Experiments were carried out in accordance with guidelines and requirements laid down by University College Cork's Animal Welfare Body and conformed to the principles and regulations described by Grundy (2015) as well as requirements for ethics and welfare reporting described by O'Halloran (2024).

5.3.1 Experimental animals

Breeding pairs for wild-type (C57BL/10ScSnJ) and *mdx* (C57BL/10ScSn-Dmd*mdx*/J) mice were purchased from The Jackson Laboratory (Bar Harbor, ME, USA) and colonies were established at University College Cork's specific pathogen-free facility. Studies were performed in male mice. Animals were housed in individually ventilated cages in temperature- and humidity-controlled rooms, operating on a 12 h light–12 h dark cycle with food and water available ad libitum.

5.3.2 Respiratory EMGs and inspiratory pressure recordings

In wild-type and *mdx* mice, anaesthesia was induced with 5% isoflurane in 60% O_2 (balance N_2) in an induction chamber. Mice were subsequently placed in the supine position and received 2% isoflurane in 60% O_2 (balance N_2) by nose-cone delivery. Mice were gradually transitioned from isoflurane to urethane anaesthesia (1.7 g kg^{-1} i.p. in total given in three injections) over a 25-min period. Body temperature was maintained at 37°C via a rectal probe and thermostatically controlled heating blanket (Harvard Apparatus, Holliston, MA, USA). Adequacy of depth of anaesthesia to permit surgical procedures was determined by an absent pedal withdrawal reflex and cardiac and respiratory frequency response to noxious pinch. Supplemental anaesthetic was administered over the course of the experimental protocol to ensure adequacy of depth of anaesthesia determined by the absence of palpebral and withdrawal reflexes and whisking, and stability of cardiorespiratory recordings. The final cumulative dose of urethane administered was 2.1–2.5 g kg^{-1} i.p. A pulse oximeter clip (MouseOx, Starr Life Sciences Corp., Oakmount, PA, USA) was placed on a shaved thigh for the measurement of peripheral capillary O_2 saturation (SpO_2). A mid-cervical tracheotomy was performed. All animals were maintained with a bias flow of supplemental O_2 (FiO_2 = 0.60) under baseline conditions. End-tidal carbon dioxide ($ETCO_2$) was measured from a side-arm of the tracheal cannula (MicroCapStar, CWE, Ardmore, PA, USA). Oesophageal pressure was measured using a pressure-tip catheter (Mikro-Tip, Millar Inc., Houston, TX, USA), which was positioned in the thoracic oesophagus through the

mouth. The catheter was advanced into the stomach to record positive pressure swings during inspiration and then withdrawn into the lower oesophagus where stable phasic sub-atmospheric pressure swings during inspiration were observed. Concentric needle monopolar recording electrodes (26G; Natus Manufacturing Ltd, Gort, Ireland) were inserted into the middle costal region of the diaphragm on the right-hand side for the continuous measurement of diaphragm EMG activity. In addition, concentric needle monopolar electrodes were inserted into an EIC, in the second to fourth rostro-ventral intercostal space, for the measurement of EIC EMG and into the PS (second or third space) for the measurement of PS EMG. EMG signals were amplified (×5000), filtered (500 Hz low cut-off to 5000 Hz high cut-off) and integrated (50 ms time constant; Neurolog system, Digitimer Ltd, Welwyn Garden City, UK). All signals were passed through an analog-to-digital converter (Powerlab r8/30; ADInstruments, Colorado Springs, CO, USA) and were acquired using LabChart 8 (ADInstruments) sampled at 20 kHz (EMG) or 1 kHz (other parameters).

5.3.3 Experimental protocol

Following instrumentation, animals were allowed to stabilise before baseline parameters were measured. Next, a pneumotachometer was connected to the tracheal cannula to record respiratory airflow for a period of 1–2 min. The pneumotachometer and $ETCO_2$ were disconnected and following a baseline period, animals were challenged with a single sustained tracheal occlusion for up to 30–40 s until peak inspiratory efforts to task failure (decline in pressure generation from the sustained peak nadir during occlusion) were observed in the

inspiratory pressure recordings during sustained maximum non-ventilatory efforts. Following recovery, animals were again instrumented for the measurement of $ETCO_2$ and tracheal airflow, and parameters were recorded during a newly established second baseline (pre-vagotomy) period. Subsequently, the vagi were sectioned bilaterally at the cervical level. Respiratory parameters were recorded under steady-state conditions for at least 10 min following vagotomy. Next, animals were challenged with hypercapnic hypoxia (FiO_2 = 0.15/ $FiCO_2$ = 0.06; 2 min) to examine the effects of chemostimulation on diaphragm, EIC and PS EMG activities and ventilatory parameters. Following the experimental protocol, anaesthetised mice were killed by cervical dislocation and death was confirmed by the absence of cardiac rhythm.

5.3.4 Data analysis

5.3.4.1 Neural respiratory drive

Respiratory EMG values were determined across all states (baseline, post-vagotomy and subsequent chemostimulation) and represented as a percentage of the maximum values determined during five consecutive peak efforts during the single sustained tracheal occlusion challenge to obtain the neural respiratory drive (NRD) index (%) as shown in the equation below.

$$NRD = \frac{EMG}{EMG_{MAX}} \times 100$$

5.3.4.2 Neuromechanical efficiency (NME)

Inspiratory pressure and respiratory EMG values were determined across all states and represented as pressure generated per μV. s^{-1} of integrated EMG activity ($cmH_2O.\mu V.s^{-1}$) to obtain values for neuromechanical efficiency (NME) as shown in the equation below.

$$NME = \frac{Pressure}{EMG}$$

5.3.4.3 Tension time index (TTI)

Inspiratory pressure, inspiratory time and total duty cycle were calculated across all behaviours and represented as the tension time index (TTI) as shown in the equation below.

$$TTI = \frac{P}{MIP} \times \frac{T_i}{T_{tot}}$$

5.3.4.4 Inspiratory drive rate (IDR) and EMG rise time

The slope of the inspiratory pressure generation and inspiratory integrated EMG for diaphragm, EIC and PS muscles was generated from onset to peak of the inspiratory time and represented as the inspiratory drive rate and EMG rise times.

5.3.4.5 Composite pressure-time relationship during sustained airway occlusion

Successive inspiratory efforts were measured for the full duration of the single sustained tracheal occlusion event generating maximum inspiratory effort until

task failure defined as the inability to sustain peak inspiratory pressure. Each inspiratory effort from the onset of airway occlusion to failure was measured and represented as a single point on a pressure-time plot. The area under the curve (AUC) of the cumulative pressure-time relationship was evaluated.

5.3.4.6 EMG signal processing and frequency analysis

EMG signals were sampled at 20 kHz using a custom acquisition system and stored as text files containing time and amplitude data. The analysis pipeline was implemented in MATLAB (MathWorks, Natick, MA) to systematically process all files from a target directory. Each recording contained data from up to three respiratory muscles: diaphragm, external intercostal, and parasternal intercostal.

Raw EMG signals underwent a digital filtering approach applied to isolate EMG frequency components: A 50 Hz notch filter (Q-factor = 35) removed power line interference, and a 4th-order Butterworth bandpass filter (30-1000 Hz) isolated the physiologically relevant EMG frequency range. Filter stability was automatically verified, with second-order section (SOS) implementations used as fallbacks when traditional implementations proved unstable.

5.3.4.7 Frequency Spectrum Analysis

Frequency content analysis was performed using Welch's method for power spectral density estimation. Mean frequency (power-weighted average frequency across the spectrum), median frequency (frequency dividing the

power spectrum into equal halves), maximum frequency, area under the curve (AUC), and total power across the frequency spectrum (30-1000 Hz) were calculated for each muscle at each age group with their corresponding power values. Hamming windows of 2048 samples was used (or maximum available length) with 50% overlap to generate smooth spectral estimates. Trapezoidal numerical integration was employed to calculate the area under the power spectral density curve.

5.4.6 Statistical analysis

Values are expressed as box and whisker plots (median, inter-quartile range (IQR) and individual data scatter plot) in graphs. Data were statistically compared using Prism 10.4.1 (GraphPad Software, San Diego, CA, USA). Data for inspiratory (oesophageal) pressure and EMG activities during baseline and tracheal occlusion, and EMG measures during baseline and stable peak levels in vagotomised mice and subsequent chemo-activation were statistically compared by two-way mixed ANOVA (time x genotype) with Šidák's multiple comparisons post hoc test. Exact P-values are reported for all comparisons. $P < 0.05$ was considered statistically significant.

5.5 Results

5.5.1 Neural respiratory drive

Original respiratory EMG recordings are shown across all behaviours in Figure 1. The overall level of EMG activity was significantly lower in *mdx* mice in all three

respiratory muscles across most behaviours. Figure 2 shows summary EMG data represented as neural respiratory drive (NRD) in anaesthetised wild-type and *mdx* mice during baseline, following bilateral vagotomy, and during subsequent exposure to hypercapnic hypoxia (HcHx). NRD for diaphragm (Figure 2A-E), EIC (Figure 2F-J), and PS (Figure 2K-O) are shown.

For NRD, there was a main effect of time ($p<0.0001$) across all age groups for all three muscles. There was a main effect of genotype for diaphragm at 16 months ($p=0.0031$). There was no interaction effect. Post hoc analyses revealed a significant difference between wild-type and *mdx* mice in diaphragm at 16 months during baseline ($p=0.0060$)

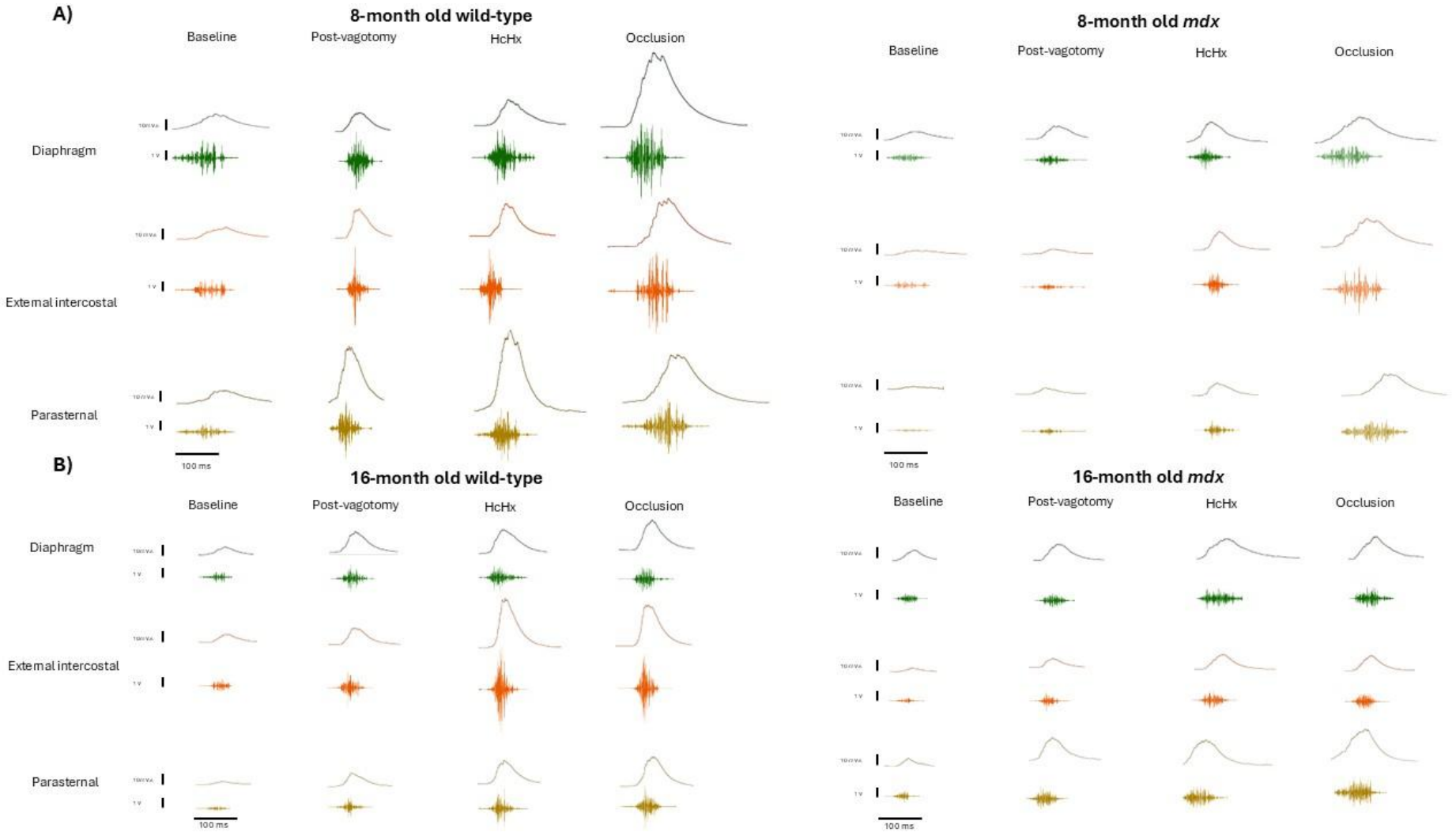
A)
8-month old wild-type
Baseline
Post-vagotomy
HcHx
Occlusion
Diaphragm
External intercostal
Parasternal
100 ms
8-month old mdx
Baseline
Post-vagotomy
HcHx
Occlusion
100 ms
B)
16-month old wild-type
Baseline
Post-vagotomy
HcHx
Occlusion
Diaphragm
External intercostal
Parasternal
100 ms
16-month old mdx
Baseline
Post-vagotomy
HcHx
Occlusion
100 ms

Figure 5.1 Original traces of individual raw EMG bursts with integrated signals in diaphragm, external intercostal, and parasternal in 8-month-old (A) and 16-month-old (B) wild-type and mdx mice during baseline, following bilateral vagotomy and during subsequent exposure to hypercapnic hypoxia (HcHx), and sustained tracheal occlusion. Note that electrical activation of the respiratory muscles increases successively across behaviours characterised by increased neural drive to maximum (occlusion). The pattern is similar in wild-type and mdx mice, but the overall level of electrical activation of the respiratory muscles is lower in mdx compared to wild-type

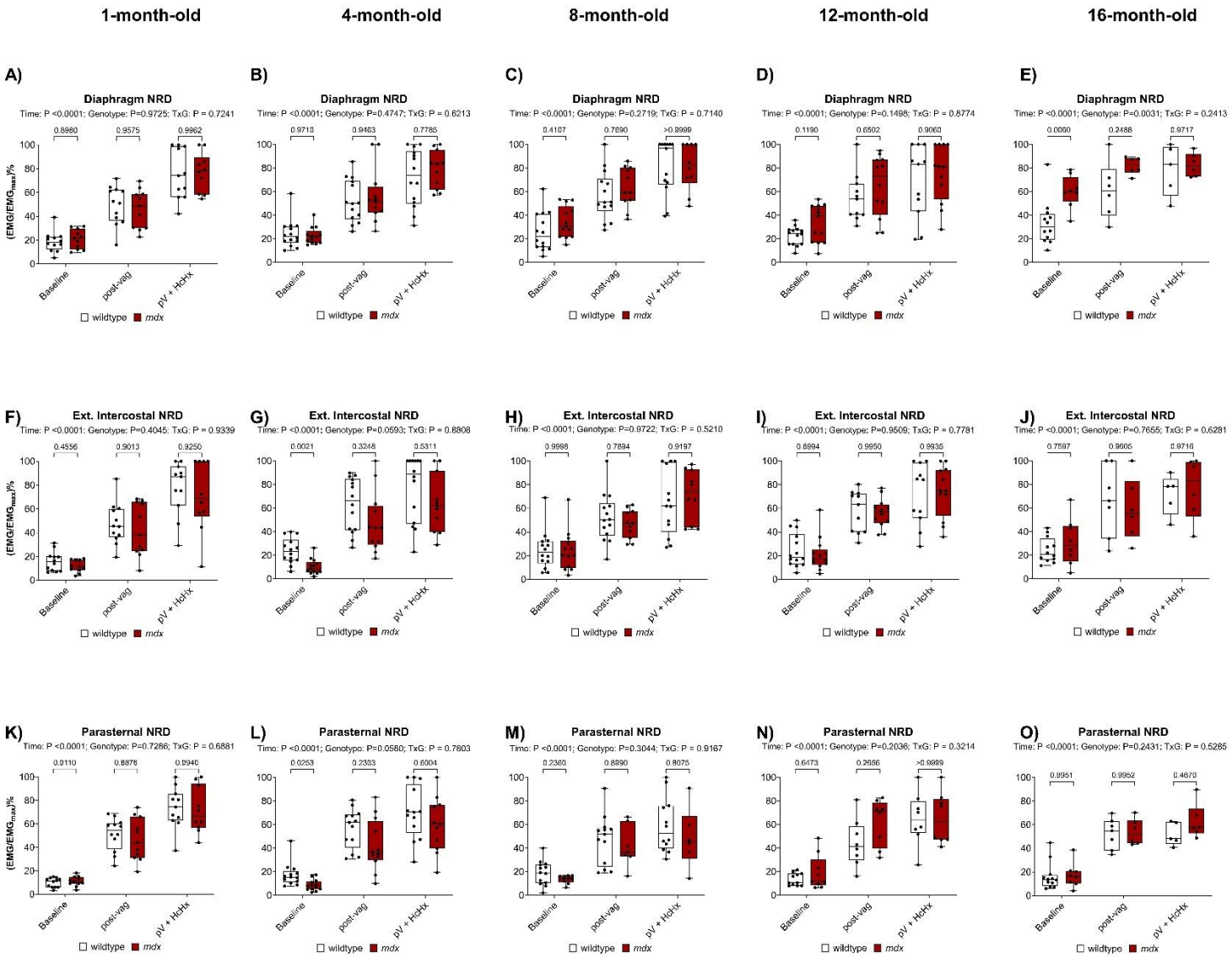
1-month-old
4-month-old
8-month-old
12-month-old
16-month-old
A)
Diaphragm NRD
Time: P <0.0001; Genotype: P=0.9725; TxG: P = 0.7241
0.8980
0.9575
0.9962
B)
Diaphragm NRD
Time: P <0.0001; Genotype: P=0.4747; TxG: P = 0.6213
0.9710
0.9463
0.7785
C)
Diaphragm NRD
Time: P <0.0001; Genotype: P=0.2719; TxG: P = 0.7140
0.4107
0.7890
>0.9999
D)
Diaphragm NRD
Time: P <0.0001; Genotype: P=0.1498; TxG: P = 0.8774
0.1190
0.6502
0.9060
E)
Diaphragm NRD
Time: P <0.0001; Genotype: P=0.0031; TxG: P = 0.2413
0.0060
0.2488
0.9717
F)
Ext. Intercostal NRD
Time: P <0.0001; Genotype: P=0.4045; TxG: P = 0.9339
0.4556
0.9013
0.9250
G)
Ext. Intercostal NRD
Time: P <0.0001; Genotype: P=0.0593; TxG: P = 0.8808
0.0021
0.3248
0.5311
H)
Ext. Intercostal NRD
Time: P <0.0001; Genotype: P=0.9722; TxG: P = 0.5210
0.9998
0.7884
0.9197
I)
Ext. Intercostal NRD
Time: P <0.0001; Genotype: P=0.9509; TxG: P = 0.7781
0.8994
0.9850
0.9935
J)
Ext. Intercostal NRD
Time: P <0.0001; Genotype: P=0.7655; TxG: P = 0.6281
0.7597
0.9605
0.9716
K)
Parasternal NRD
Time: P <0.0001; Genotype: P=0.7286; TxG: P = 0.6881
0.9110
0.8878
0.8940
L)
Parasternal NRD
Time: P <0.0001; Genotype: P=0.0580; TxG: P = 0.7803
0.0253
0.2333
0.6004
M)
Parasternal NRD
Time: P <0.0001; Genotype: P=0.3044; TxG: P = 0.9167
0.2360
0.8890
0.8075
N)
Parasternal NRD
Time: P <0.0001; Genotype: P=0.2036; TxG: P = 0.3214
0.6473
0.2656
>0.9999
O)
Parasternal NRD
Time: P <0.0001; Genotype: P=0.2431; TxG: P = 0.5285
0.9951
0.9952
0.4670
(EMG/EMGmax)%
Baseline
post-vag
pV + HcHx
wildtype
mdx

Figure 5.2: Respiratory muscle NRD during baseline, following bilateral vagotomy, and during subsequent exposure to hypercapnic hypoxia (HcHx) in anaesthetised wild-type and mdx mice. Group data for diaphragm (A-E), external intercostal (F-J) and parasternal intercostal (K-O) neural respiratory drive (NRD) during baseline, post-bilateral vagotomy, and during subsequent exposure to hypercapnic hypoxia (HcHx) in wild-type and mdx mice at 1, 4, 8, 12, and 16 months of age. Values are expressed as box (median, IQR and individual data points) and whisker (min to max) plots. Data were statistically compared by two-way mixed ANOVA with Šidák's multiple comparisons post hoc test. Absolute P-values for all comparisons are reported.

5.5.2 Frequency spectrum analysis

Filtered respiratory EMG recordings and respective frequency spectrum for diaphragm, EIC and PS in a 1-month-old wild type mouse are shown in Figure 3. Mean frequency, median frequency, maximum frequency, and area under the curve (AUC) were calculated for each muscle at each age group with their corresponding power values and are shown in Table 1.

For mean frequency, there was a main effect of time ($p<0.0001$) across all age groups for all three muscles. There was a genotype effect for diaphragm at 1, 4, 8, and 12 months ($p=0.0309$, $p=0.0071$, $p=0.0030$, $p=0.0003$), for EIC at 8 months ($p=0.0062$), and for PS at 1 month ($p=0.0023$). An interaction effect was seen for diaphragm at 8 and 16 months ($p=0.0004$, $p=0.0448$), and for PS at 1 month ($p=0.0268$). Post hoc analyses revealed a significant difference between wild-type and *mdx* mice in diaphragm at 4 months during baseline ($p=0.0003$), at 8

months during HcHx (p=0.0003), and at 12 months post vagotomy, HcHx, and occlusion (p=0.0108, p=0.0021, p=0.0061), and in EIC at 8 months during baseline and occlusion (p=0.0240, p=0.0408), and in PS at 1 month post vagotomy and occlusion (p=0.0057, p=0.0071), and at 8 months post vagotomy and during HcHx (p= 0.0154, p=0.0004).

For power at mean frequency, there was a main effect of time for diaphragm at 1, 8, and 12 months (p=0.0075, p=0443, p=0.0038), for EIC at 1, 4, and 8 months (p=0.0257, p=0029, p=0.0147), and for PS at 1 and 4 months (p=0.0028, p=0.0008). There was no genotype effect for diaphragm across all ages. There was a genotype effect for EIC at 1 and 16 months (p=0.0257, p=0.0089), and for PS at 8, 12, and 16 months (p=0.0199, p=0.0071, p=0.0131). An interaction effect was seen for diaphragm at 4, 8, and 12 months (p=0.0008, p=0.0014, p=0.0068), for EIC at 8 months (p=0.0024), and for PS at 1 month (p=0.0038). Post hoc analyses revealed a significant difference between wild-type and *mdx* mice in EIC at 1 month during occlusion (p=0.0111), and at 16 months during occlusion (p=0.0094), and in PS at 16 months of age post vagotomy (p=0.0457).

For median frequency, there was a main effect of time ($p<0.0001$) across all age groups for all three muscles. There was a genotype effect for diaphragm at 1, 4, 8, 12 months (p=0.0462, p=0.0305, p=0.0018, p=0.0003), for EIC at 8 months (p=0.0068), and for PS at 1 and 8 months (p=0.0012, p=0.0006). An interaction effect was seen for diaphragm at 8 months (p=0.0018) and for PS at 1 month (p=0.0009). Post hoc analyses revealed a significant difference between wild-

type and *mdx* mice in diaphragm at 4 months during baseline (p=0.0022), at 8 months during HcHx (p=0.0003), and at 12 months post vagotomy, during HcHx, and occlusion (p=0.0323, p=0.0030, p=0.0024), and for PS at 1 month during HcHx and occlusion (p=0.0447, p=0.0097) and at 8 months post vagotomy and during HcHx (p=0.0139, p=0.0008).

For power at median frequency, there was a main effect of time for diaphragm at 1 and 8 months (p=0.0071, p=0.0076), for EIC at 1, 4, 8, and 12 months (p=0.0175, p<0.0001, p=0.0219, p<0.0001), and for PS at 1, 4, and 16 months (p=0.0017, p<0.0001, p=0.0072). There was a main genotype effect for EIC at 8 and 16 months (p=0.0482, p=0.0278), and for PS at 1, 8, and 12 months (p=0.0464, p=0.0248, p=0.0084). An interaction effect was seen for diaphragm at 8 months (p<0.0001), for EIC at 8 months (p<0.0001), and for PS at 1, and 8 months (p=0.0393, p=0.0143). Post hoc analyses revealed a significant difference between wild-type and *mdx* mice in EIC 8 months during baseline (p<0.0001), and in PS at 8 months during occlusion (p=0.0117).

For diaphragm maximum frequency, there was a main time effect for diaphragm at 1, 4, 8, and 12 months (p=0.0492, p=0.0038, p=0.0423, p=0.0036), for EIC at 1, 4, 8, 12 months (p=0.0002, p=0.0226, p=0.0003, p=0.0007), and for PS 1, 4, 8, 16 months (p=0.0096, p=0.0021, p=0.0079, p=0.0053). There was a main genotype effect for diaphragm at 4, 8, and 12 months (p=0.0019, p=0.0271, p=0.0018), for EIC at 8 months (p=0.0025), and for PS at 8 months (p=0.0006). An interaction effect was seen for diaphragm at 1, 4, 8, and 12 months (p=0.0059, p<0.0001, p=0.0005, p<0.0001), for EIC at 8 and 16 months (p=0.0001, p=0.0468), and for

PS at 4 and 8 months (p=0.0006, p=0.0194). Post hoc analyses revealed a significant difference between wild-type and *mdx* mice in diaphragm at 4 months during baseline (p=0.0152), and at 12 months during HcHx and during occlusion (p=0.0020, p=0.0134), in EIC at 8 months during baseline and occlusion (p=0.0278, p=0.0045), and in PS at 8 months post vagotomy, during HcHx and occlusion (p=0.0004, p<0.0001, p=0.0481).

For power at maximum frequency, there was a main time effect for EIC at 4 and 12 months (p=0.0010, p=0.0251), and PS at 1 and 16 months (p=0.0008, p=0.0112). There was a main genotype effect for diaphragm at 16 months (p=0.0198), for EIC at 1 and 16 months (p=0.0019, p=0.0209), and for PS at 8 and 12 months (p=0.0164, p=0.0036). An interaction effect was seen for diaphragm, EIC and PS at 8 months (p<0.0001, p=0.0216, p=0.0147). Post hoc analyses revealed a significant difference between wild-type and *mdx* mice in EIC at 1 month during occlusion (p=0.0451), and in PS at 8 months during baseline and occlusion (p=0.0179, p=0.0240), and at 12 months during baseline (p=0.0256).

For diaphragm total power (AUC of the frequency spectrum), there was a main time effect for diaphragm at 1, 4, 8, and 12 months (p=0.0140, p=0.0061, p=0.0022, p=0.0348), for EIC at 1 and 8 months (p=0.0195, p=0.0006), and for PS at 4 and 8 months (p=0.0002, p=0.0022). There was a main genotype effect for diaphragm at 4, 8, and 16 months (p=0.0456, p=0.0197, p=0.0094), for EIC at 1, 12 and 16 months (p=0.0319, p=0.0153, p=0.0172), and for PS at 8 and 12 months (p=0.0029, p=0.0015). An interaction effect was seen for diaphragm at 4, 8, and 12 months (p=0.0038, p=0.0125, p=0.0032), for EIC at 1, 8 and 16 months

(p=0.0164, p=0.0116, p=0.0494), and for PS at 1 and 8 months (p=0.0105, p=0.0009). Post hoc analyses revealed a significant difference between wild-type and *mdx* mice in diaphragm at 4 and 8 months during occlusion (p=0.0437, p=0.0430), in EIC at 1 month during occlusion (p=0.0165), and at 16 months during baseline and occlusion (p=0.0475, p=0.0252), and in PS at 8 months during baseline, post vagotomy and occlusion (p=0.0170, p=0.0148, p=0.0041), and at 12 month during baseline (p=0.0244).

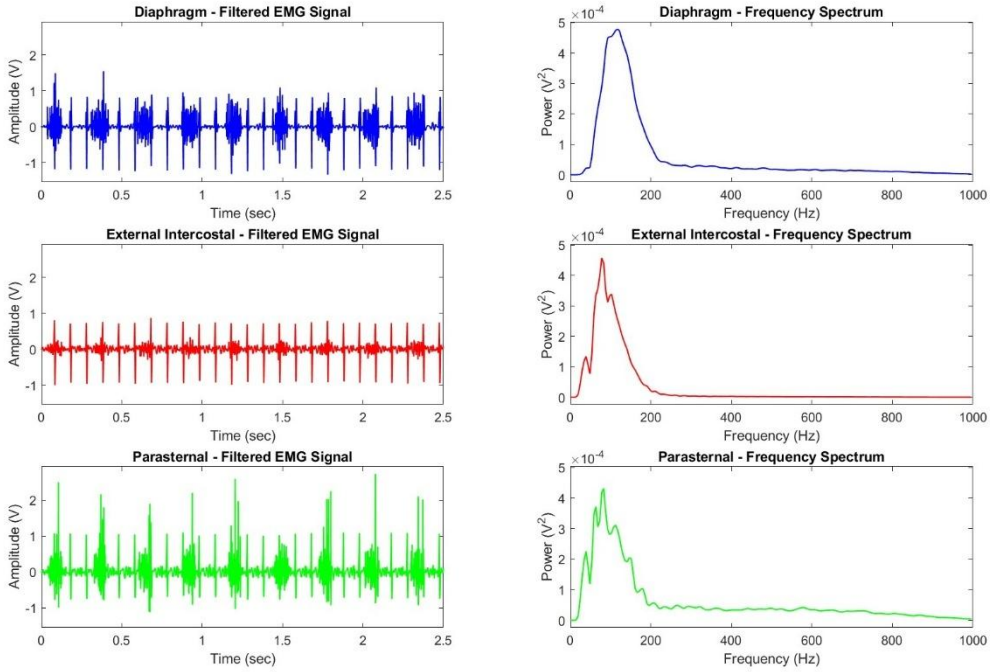

Figure 5.3: Original traces of filtered EMG signals with frequency spectrum in diaphragm, external intercostal, and parasternal in a 1-month-old wild-type mouse during baseline breathing. Mean frequency, median frequency, maximum frequency, and area under the curve (AUC) were calculated for each muscle at each age group with their corresponding power values.

Table 3: Frequency spectrum parameters of inspiratory muscle EMG activities recorded in urethane-anaesthetised wild-type and mdx mice. The data represent key spectral features including mean frequency, mean power, median frequency, median power, maximum frequency, maximum power, and total power, measured across three inspiratory muscles: diaphragm, external intercostal, and parasternal intercostal. Values are presented as mean ± standard deviation (SD) for each muscle at 1, 4, 8, 12, and 16 months. Statistical analysis results from two-way ANOVA assessing the effects of genotype, age, and their interaction are included for all muscles and parameters.

Two-way ANOVA	**Diaphragm**			**External intercostal**			**Parasternal**		
1 month old	**Time**	**Genotype**	**Time x Genotype**	**Time**	**Genotype**	**Time x Genotype**	**Time**	**Genotype**	**Time x Genotype**
mean frequency (Hz)	**<0.0001**	**0.0309**	0.4327	**<0.0001**	0.0591	0.2703	**<0.0001**	**0.0023**	**0.0268**
mean power (mV^2)	**0.0075**	0.953	0.1442	**0.0257**	**0.0043**	0.0519	**0.0028**	0.0696	**0.0038**
median frequency (Hz)	**<0.0001**	**0.0462**	0.1057	**<0.0001**	0.0756	0.0999	**<0.0001**	**0.0012**	**0.0009**
median power (mV^2)	**0.0071**	0.2552	0.427	**0.0175**	0.0867	0.0579	**0.0017**	**0.0464**	**0.0393**
max frequency (Hz)	**0.0492**	0.0518	**0.0059**	**0.0002**	0.5415	0.5374	**0.0096**	0.5282	0.4453
max power (mV^2)	0.2928	0.2838	0.5714	0.1174	**0.0019**	0.1125	**0.0008**	0.1776	0.2011
total power (mV^2)	**0.014**	0.4434	0.485	**0.0195**	**0.0319**	**0.0164**	0.0976	0.8778	**0.0105**
4 months old	**Time**	**Genotype**	**Time x Genotype**	**Time**	**Genotype**	**Time x Genotype**	**Time**	**Genotype**	**Time x Genotype**
mean frequency (Hz)	**<0.0001**	**0.0071**	0.4833	**<0.0001**	0.9991	0.551	**<0.0001**	0.4713	0.9988
mean power (mV^2)	0.1457	0.4796	**0.0008**	**0.0029**	0.9888	0.2129	**0.0008**	0.7241	0.6136
median frequency (Hz)	**<0.0001**	**0.0305**	0.2197	**<0.0001**	0.3659	0.4755	**<0.0001**	0.5712	0.9897
median power (mV^2)	0.3033	0.543	0.1917	**<0.0001**	0.2327	0.3475	**<0.0001**	0.0892	0.7828
max frequency (Hz)	**0.0038**	**0.0019**	**<0.0001**	**0.0226**	0.9885	0.2153	**0.0021**	0.1587	**0.0006**
max power (mV^2)	0.0784	0.661	0.0891	**0.001**	0.1332	0.743	0.3333	0.2026	0.8904
total power (mV^2)	**0.0061**	**0.0456**	**0.0038**	0.6955	0.0581	0.9858	**0.0002**	0.1653	0.6102
8 months old	**Time**	**Genotype**	**Time x Genotype**	**Time**	**Genotype**	**Time x Genotype**	**Time**	**Genotype**	**Time x Genotype**
mean frequency (Hz)	**<0.0001**	**0.003**	**0.0004**	**<0.0001**	**0.0062**	0.9449	**<0.0001**	**0.0004**	0.0877
mean power (mV^2)	**0.0443**	0.0619	**0.0014**	**0.0147**	0.495	**0.0024**	0.287	**0.0199**	0.0882
median frequency (Hz)	**0.0002**	**0.0018**	**<0.0001**	**<0.0001**	**0.0068**	0.2587	**<0.0001**	**0.0006**	0.2972

median power (mV^2)	**0.0076**	0.7086	**<0.0001**	**0.0219**	**0.0482**	**<0.0001**	0.8768	**0.0248**	**0.0143**
max frequency (Hz)	**0.0423**	**0.0271**	**0.0005**	**0.0003**	**0.0025**	**0.0001**	**0.0079**	**0.0006**	**0.0194**
max power (mV^2)	**0.037**	0.5603	**<0.0001**	0.1642	0.5626	**0.0216**	0.1559	**0.0164**	**0.0147**
total power (mV^2)	**0.0022**	**0.0197**	**0.0125**	**0.0006**	0.1984	**0.0116**	**0.0022**	**0.0029**	**0.0009**
12 months old	**Time**	**Genotype**	**Time x Genotype**	**Time**	**Genotype**	**Time x Genotype**	**Time**	**Genotype**	**Time x Genotype**
mean frequency (Hz)	**<0.0001**	**0.0003**	0.2089	**<0.0001**	0.8205	0.7289	**<0.0001**	0.1269	0.3223
mean power (mV^2)	**0.0038**	0.3941	**0.0068**	0.1308	0.4046	0.0576	0.0832	**0.0071**	0.0847
median frequency (Hz)	**<0.0001**	**0.0003**	0.059	**<0.0001**	0.8058	0.8593	**<0.0001**	0.2218	0.313
median power (mV^2)	0.8031	0.1983	0.6739	**<0.0001**	0.2225	0.6208	0.1494	**0.0084**	0.2275
max frequency (Hz)	**0.0036**	**0.0018**	**<0.0001**	**0.0007**	0.8475	0.9789	0.1231	0.1604	0.44
max power (mV^2)	0.748	0.2819	0.3448	**0.0251**	0.0788	0.5467	0.5119	**0.0036**	0.2559
total power (mV^2)	**0.0348**	0.06	**0.0032**	0.0682	**0.0153**	0.4615	0.3687	**0.0015**	0.8173
16 months old	**Time**	**Genotype**	**Time x Genotype**	**Time**	**Genotype**	**Time x Genotype**	**Time**	**Genotype**	**Time x Genotype**
mean frequency (Hz)	**0.0007**	0.1059	0.0448	**<0.0001**	0.2452	0.8933	**<0.0001**	0.7591	0.6226
mean power (mV^2)	0.1159	0.0634	0.0733	0.8186	**0.0089**	0.1513	0.2986	**0.0131**	0.0943
median frequency (Hz)	**0.0044**	0.0795	0.1819	**<0.0001**	0.3581	0.6055	**0.0002**	0.6819	0.9903
median power (mV^2)	0.2052	0.0528	0.5935	0.236	**0.0278**	0.3144	**0.0072**	0.0553	0.1192
max frequency (Hz)	0.0565	0.4561	0.1366	0.0573	0.0713	**0.0468**	**0.0053**	0.6521	0.0622
max power (mV^2)	0.1165	0.0198	0.2568	0.7353	**0.0209**	0.9931	**0.0112**	0.2529	0.2326
total power (mV^2)	0.1384	0.0094	0.1749	0.0987	**0.0172**	**0.0494**	0.2764	0.124	0.9317

6

1-month-old	**Diaphragm**			**External Intercostal**			**Parasternal**		
	Mean ± SD	**Mean ± SD**	**Adjusted P-value**	**Mean ± SD**	**Mean ± SD**	**Adjusted P-value**	**Mean ± SD**	**Mean ± SD**	**Adjusted P-value**
Baseline	**wild-type (n=12)**	***mdx* (n=11)**		**wild-type (n=12)**	***mdx* (n=11)**		**wild-type (n=12)**	***mdx* (n=11)**	
mean frequency (Hz)	178 ± 35	159 ± 40	0.6865	162 ± 27	135 ± 15	0.0468	164 ± 54	130 ± 23	0.2247
mean power (mV^2)	0.25 ± 0.31	0.20 ± 0.19	0.9842	0.12 ± 0.11	0.12 ± 0.08	0.9999	0.43 ± 0.38	1.53 ± 1.62	0.1856
median frequency (Hz)	123 ± 22	123 ± 17	>0.9999	108 ± 13	112 ± 18	0.9505	113 ± 24	107 ± 12	0.8751
median power (mV^2)	0.49 ± 0.45	0.29 ± 0.18	0.5965	0.49 ± 0.42	0.24 ± 0.20	0.3076	0.82 ± 0.57	1.90 ± 1.91	0.3353
max frequency (Hz)	98 ± 20	95 ± 14	0.9898	83 ± 15	95 ± 12	0.1691	87 ± 20	96 ± 7	0.4996
max power (mV^2)	0.57 ± 0.50	0.41 ± 0.30	0.8618	0.67 ± 0.57	0.28 ± 0.21	0.1735	1.12 ± 0.65	2.29 ± 2.29	0.4249

total power (mV^2)	52.56 ± 33.02	53.93 ± 39.65	>0.9999	65.54 ± 58.34	30.92 ± 22.13	0.2761	98.71 ± 42.31	199.92 ±206.51	0.4520
Vagotomy	**wild-type (n=12)**	***mdx* (n=11)**		**wild-type (n=12)**	***mdx* (n=11)**		**wild-type (n=12)**	***mdx* (n=11)**	
mean frequency (Hz)	214 ± 84	155 ± 29	0.1480	267 ± 100	197 ± 57	0.1884	243 ± 84	141 ± 18	**0.0057**
mean power (mV^2)	0.16 ± 0.17	0.24 ± 0.20	0.8098	0.08 ± 0.06	0.03 ± 0.02	0.1487	0.29 ± 0.26	0.93 ± 1.01	0.2394
median frequency (Hz)	132 ± 35	120 ± 10	0.7138	218 ± 111	130 ± 33	0.0843	166 ± 68	111 ± 10	0.0623
median power (mV^2)	0.39 ± 0.29	0.28 ± 0.20	0.8122	0.12 ± 0.08	0.19 ± 0.27	0.8985	0.50 ± 0.34	1.71 ± 1.68	0.1467
max frequency (Hz)	104 ± 11	98 ± 11	0.6600	89 ± 13	95 ± 16	0.8177	95 ± 8	96 ± 7	0.9854
max power (mV^2)	0.50 ± 0.32	0.33 ± 0.21	0.5151	0.27 ± 0.18	0.17 ± 0.20	0.7494	1.29 ± 0.73	2.03 ± 1.86	0.6657
total power (mV^2)	71.05 ± 45.01	60.72 ± 48.77	0.9771	50.99 ± 34.38	33.57 ± 41.64	0.7666	168.73 ± 85.24	187.58 ±158.61	0.9947
HcHx	**wild-type (n=10)**	***mdx* (n=10)**		**wild-type (n=10)**	***mdx* (n=10)**		**wild-type (n=10)**	***mdx* (n=10)**	
mean frequency (Hz)	260 ± 100	195 ± 51	0.3058	334 ± 95	247 ± 72	0.1362	272 ± 78	193 ± 69	0.1055
mean power (mV^2)	0.09 ± 0.06	0.22 ± 0.19	0.2467	0.12 ± 0.08	0.08 ± 0.07	0.7413	0.28 ± 0.23	0.27 ± 0.21	0.9999
median frequency (Hz)	199 ± 125	135 ± 25	0.4741	289 ± 114	188 ± 80	0.1385	193 ± 81	112 ± 17	**0.0447**
median power (mV^2)	0.35 ± 0.28	0.24 ± 0.15	0.8179	0.14 ± 0.08	0.14 ± 0.16	>0.9999	0.49 ± 0.31	1.54 ± 1.64	0.2749
max frequency (Hz)	101 ± 22	100 ± 14	>0.9999	119 ± 48	103 ± 30	0.8679	90 ± 16	91 ± 9	>0.9999
max power (mV^2)	0.58 ± 0.32	0.36 ± 0.20	0.4019	0.27 ± 0.14	0.24 ± 0.24	0.9979	1.43 ± 0.80	2.03 ± 1.94	0.8576
total power (mV^2)	99.80 ± 56.34	91.23 ± 80.08	0.9980	77.64 ± 54.47	82.83 ± 88.13	0.9998	237.29 ± 137.48	202.05 ±157.96	0.9747
Occlusion	**wild-type (n=12)**	***mdx* (n=11)**		**wild-type (n=12)**	***mdx* (n=11)**		**wild-type (n=12)**	***mdx* (n=11)**	
mean frequency (Hz)	339 ± 102	268 ± 85	0.2974	379 ± 105	335 ± 75	0.7013	413 ± 54	308 ± 80	**0.0071**
mean power (mV^2)	0.13 ± 0.09	0.06 ± 0.03	0.0860	0.21 ± 0.12	0.07 ± 0.05	**0.0111**	0.17 ± 0.09	0.17 ± 0.16	>0.9999
median frequency (Hz)	297 ± 131	203 ± 106	0.2577	348 ± 136	297 ± 96	0.7723	387 ± 78	252 ± 104	**0.0097**
median power (mV^2)	0.20 ± 0.12	0.19 ± 0.15	>0.9999	0.29 ± 0.22	0.08 ± 0.06	**0.0281**	0.28 ± 0.19	0.26 ± 0.23	0.9997
max frequency (Hz)	223 ± 182	95 ± 54	0.1394	250 ± 154	205 ± 135	0.9129	188 ± 144	143 ± 68	0.8173
max power (mV^2)	0.44 ± 0.29	0.42 ± 0.30	0.9996	0.62 ± 0.55	0.14 ± 0.07	**0.0451**	0.56 ± 0.44	0.76 ± 0.69	0.9036
total power (mV^2)	101.52 ± 55.53	73.11 ± 65.35	0.7391	143.10 ± 96.28	41.93 ± 30.44	**0.0165**	189.95 ± 144.94	143.44 ±127.87	0.8890

7

4-month-old	**Diaphragm**			**External Intercostal**			**Parasternal**		
	Mean ± SD	**Mean ± SD**	**Adjusted P-value**	**Mean ± SD**	**Mean ± SD**	**Adjusted P-value**	**Mean ± SD**	**Mean ± SD**	**Adjusted P-value**
Baseline	**wild-type (n=14)**	***mdx* (n=13)**		**wild-type (n=14)**	***mdx* (n=13)**		**wild-type (n=12)**	***mdx* (n=12)**	
mean frequency (Hz)	278 ± 88	147 ± 29	**0.0003**	167 ± 28	162 ± 36	0.9900	173 ± 20	154 ± 37	0.5098

mean power (mV^2)	0.08 ± 0.06	0.18 ± 0.20	0.4558	0.23 ± 0.17	0.35 ± 0.40	0.8380	0.32 ± 0.19	0.38 ± 0.43	0.9850
median frequency (Hz)	225 ± 92	114 ± 14	**0.0022**	115 ± 13	122 ± 12	0.4477	125 ± 11	112 ± 12	0.0510
median power (mV^2)	0.10 ± 0.09	0.17 ± 0.15	0.5947	0.58 ± 0.35	0.44 ± 0.42	0.8479	0.70 ± 0.28	0.56 ± 0.49	0.8610
max frequency (Hz)	86 ± 18	83 ± 22	0.9944	85 ± 22	92 ± 19	0.8905	104 ± 14	97 ± 16	0.7551
max power (mV^2)	0.26 ± 0.17	0.22 ± 0.20	0.9833	0.76 ± 0.42	0.51 ± 0.45	0.5061	0.86 ± 0.35	0.63 ± 0.54	0.6328
total power (mV^2)	47.77 ± 25.22	41.24 ± 41.89	0.9862	80.30 ± 45.39	56.80 ± 53.80	0.6769	95.35 ± 48.77	61.28 ± 55.42	0.4122
Vagotomy	**wild-type (n=14)**	***mdx* (n=12)**		**wild-type (n=14)**	***mdx* (n=12)**		**wild-type (n=12)**	***mdx* (n=12)**	
mean frequency (Hz)	315 ± 106	240 ± 94	0.2402	260 ± 85	237 ± 106	0.9612	265 ± 67	257 ± 87	0.9986
mean power (mV^2)	0.04 ± 0.03	0.13 ± 0.14	0.2259	0.09 ± 0.06	0.04 ± 0.03	0.0761	0.13 ± 0.12	0.08 ± 0.06	0.5878
median frequency (Hz)	250 ± 145	182 ± 89	0.4900	160 ± 54	154 ± 63	0.9982	154 ± 30	136 ± 17	0.3306
median power (mV^2)	0.19 ± 0.17	0.19 ± 0.19	>0.9999	0.29 ± 0.19	0.31 ± 0.33	0.9994	0.41 ± 0.34	0.15 ± 0.11	0.1067
max frequency (Hz)	94 ± 21	82 ± 26	0.6333	92 ± 28	103 ± 23	0.7579	107 ± 12	91 ± 19	0.1103
max power (mV^2)	0.30 ± 0.23	0.30 ± 0.29	>0.9999	0.58 ± 0.25	0.46 ± 0.42	0.9076	0.69 ± 0.43	0.49 ± 0.44	0.7385
total power (mV^2)	57.51 ± 37.22	52.20 ± 58.90	0.9983	86.06 ± 30.45	54.11 ± 48.00	0.2589	108.98 ± 82.60	78.21 ± 67.88	0.7986
HcHx	**wild-type (n=14)**	***mdx* (n=11)**		**wild-type (n=14)**	***mdx* (n=11)**		**wild-type (n=12)**	***mdx* (n=11)**	
mean frequency (Hz)	364 ± 85	264 ± 120	0.1224	292 ± 83	310 ± 128	0.9916	302 ± 70	292 ± 69	0.9938
mean power (mV^2)	0.07 ± 0.05	0.11 ± 0.10	0.7922	0.12 ± 0.09	0.05 ± 0.03	0.0591	0.14 ± 0.11	0.06 ± 0.05	0.2145
median frequency (Hz)	302 ± 142	213 ± 135	0.4164	212 ± 98	270 ± 144	0.7108	214 ± 82	217 ± 95	>0.9999
median power (mV^2)	0.15 ± 0.12	0.22 ± 0.24	0.8643	0.27 ± 0.19	0.08 ± 0.08	**0.0173**	0.34 ± 0.28	0.16 ± 0.14	0.2197
max frequency (Hz)	93 ± 18	81 ± 21	0.5618	94 ± 32	91 ± 18	0.9966	116 ± 22	87 ± 17	**0.0070**
max power (mV^2)	0.36 ± 0.25	0.34 ± 0.37	0.9997	0.52 ± 0.18	0.38 ± 0.45	0.8599	0.77 ± 0.53	0.42 ± 0.40	0.3014
total power (mV^2)	91.24 ± 59.55	53.13 ± 39.77	0.2635	88.60 ± 32.35	65.13 ± 60.85	0.7448	120.22 ± 88.10	59.83 ± 45.89	0.2329
Occlusion	**wild-type (n=14)**	***mdx* (n=13)**		**wild-type (n=14)**	***mdx* (n=12)**		**wild-type (n=13)**	***mdx* (n=13)**	
mean frequency (Hz)	424 ± 117	290 ± 140	0.0505	362 ± 91	390 ± 110	0.9324	387 ± 87	372 ± 109	0.9919
mean power (mV^2)	0.22 ± 0.22	0.08 ± 0.06	0.1787	0.11 ± 0.09	0.08 ± 0.05	0.7191	0.25 ± 0.24	0.22 ± 0.20	0.9979
median frequency (Hz)	404 ± 160	245 ± 172	0.0806	313 ± 126	363 ± 143	0.8278	349 ± 116	338 ± 150	0.9992
median power (mV^2)	0.26 ± 0.25	0.21 ± 0.20	0.9632	0.20 ± 0.15	0.08 ± 0.05	0.0719	0.27 ± 0.23	0.23 ± 0.24	0.9953
max frequency (Hz)	341 ± 263	94 ± 20	**0.0152**	119 ± 37	104 ± 16	0.6906	140 ± 33	301 ± 224	0.0953
max power (mV^2)	0.57 ± 0.51	0.33 ± 0.29	0.4651	0.38 ± 0.29	0.24 ± 0.15	0.4414	0.79 ± 0.64	0.65 ± 0.75	0.9793
total power (mV^2)	165.65 ± 137.10	55.80 ± 32.90	**0.0437**	89.11 ± 52.63	69.98 ± 50.78	0.8372	234.78 ±199.80	155.18 ±140.93	0.6891

8

8-month-old	Diaphragm			External Intercostal			Parasternal		
	Mean ± SD	Mean ± SD	Adjusted P-value	Mean ± SD	Mean ± SD	Adjusted P-value	Mean ± SD	Mean ± SD	Adjusted P-value
Baseline	**wild-type (n=15)**	***mdx* (n=14)**		**wild-type (n=15)**	***mdx* (n=14)**		**wild-type (n=14)**	***mdx* (n=10)**	
mean frequency (Hz)	243 ± 85	244 ± 83	>0.9999	241 ± 94	159 ± 41	**0.0240**	166 ± 34	142 ± 21	0.1668
mean power (mV^2)	0.07 ± 0.08	0.04 ± 0.03	0.5451	0.06 ± 0.06	0.11 ± 0.08	0.2584	0.24 ± 0.15	0.14 ± 0.18	0.5839
median frequency (Hz)	155 ± 60	191 ± 75	0.5384	141 ± 64	111 ± 17	0.3676	125 ± 21	101 ± 22	0.0586
median power (mV^2)	0.10 ± 0.09	0.05 ± 0.04	0.4045	0.06 ± 0.04	0.23 ± 0.09	**<0.0001**	0.45 ± 0.22	0.28 ± 0.26	0.4057
max frequency (Hz)	83 ± 15	103 ± 34	0.2449	72 ± 13	86 ± 12	**0.0278**	99 ± 18	85 ± 29	0.5335
max power (mV^2)	0.29 ± 0.30	0.09 ± 0.04	0.1003	0.35 ± 0.29	0.35 ± 0.13	>0.9999	0.58 ± 0.27	0.28 ± 0.16	**0.0179**
total power (mV^2)	25.70 ± 22.60	16.16 ± 6.16	0.5553	44.20 ± 33.61	29.88 ± 13.39	0.4678	68.97 ± 42.74	26.45 ± 13.50	**0.0170**
Vagotomy	**wild-type (n=16)**	***mdx* (n=14)**		**wild-type (n=16)**	***mdx* (n=14)**		**wild-type (n=15)**	***mdx* (n=11)**	
mean frequency (Hz)	323 ± 106	239 ± 100	0.1291	330 ± 141	241 ± 84	0.1578	232 ± 57	163 ± 53	**0.0154**
mean power (mV^2)	0.05 ± 0.04	0.07 ± 0.07	0.8303	0.03 ± 0.02	0.05 ± 0.05	0.6689	0.14 ± 0.10	0.11 ± 0.10	0.8883
median frequency (Hz)	278 ± 141	193 ± 103	0.2420	279 ± 176	175 ± 85	0.1749	164 ± 55	107 ± 33	**0.0139**
median power (mV^2)	0.09 ± 0.08	0.19 ± 0.18	0.2994	0.04 ± 0.03	0.19 ± 0.19	0.0832	0.51 ± 0.37	0.28 ± 0.24	0.2534
max frequency (Hz)	82 ± 17	108 ± 32	0.0889	77 ± 18	82 ± 16	0.9128	104 ± 19	74 ± 14	**0.0004**
max power (mV^2)	0.12 ± 0.08	0.23 ± 0.19	0.2311	0.27 ± 0.26	0.46 ± 0.38	0.4483	0.73 ± 0.46	0.39 ± 0.25	0.1196
total power (mV^2)	31.88 ± 20.17	32.01 ± 16.57	>0.9999	42.72 ± 27.67	55.11 ± 37.76	0.7880	129.22 ± 103.92	35.18 ± 20.82	**0.0148**
HcHx	**wild-type (n=14)**	***mdx* (n=12)**		**wild-type (n=14)**	***mdx* (n=12)**		**wild-type (n=13)**	***mdx* (n=9)**	
mean frequency (Hz)	386 ± 102	211 ± 87	**0.0003**	412 ± 130	307 ± 62	0.0553	261 ± 55	153 ± 48	**0.0004**
mean power (mV^2)	0.11 ± 0.10	0.07 ± 0.05	0.7033	0.07 ± 0.05	0.04 ± 0.03	0.5472	0.18 ± 0.18	0.08 ± 0.06	0.2518
median frequency (Hz)	348 ± 159	104 ± 23	**0.0003**	392 ± 171	243 ± 91	**0.0414**	183 ± 62	92 ± 25	**0.0008**
median power (mV^2)	0.12 ± 0.14	0.31 ± 0.27	0.1782	0.06 ± 0.04	0.06 ± 0.04	0.9986	0.41 ± 0.32	0.37 ± 0.34	0.9971
max frequency (Hz)	233 ± 207	82 ± 24	0.0683	245 ± 236	85 ± 28	0.0987	109 ± 19	65 ± 8	**<0.0001**
max power (mV^2)	0.13 ± 0.09	0.43 ± 0.29	**0.0183**	0.20 ± 0.17	0.31 ± 0.28	0.6961	0.64 ± 0.41	0.56 ± 0.42	0.9867
total power (mV^2)	92.82 ± 96.37	44.73 ± 13.39	0.3044	54.07 ± 40.52	45.65 ± 32.24	0.9653	129.77 ± 96.75	59.84 ± 53.68	0.1607
Occlusion	**wild-type (n=16)**	***mdx* (n=14)**		**wild-type (n=15)**	***mdx* (n=13)**		**wild-type (n=15)**	***mdx* (n=11)**	
mean frequency (Hz)	386 ± 103	306 ± 89	0.1213	450 ± 90	371 ± 61	**0.0408**	371 ± 105	297 ± 74	0.1677
mean power (mV^2)	0.15 ± 0.15	0.04 ± 0.02	**0.0417**	0.17 ± 0.15	0.07 ± 0.05	0.1210	0.34 ± 0.32	0.09 ± 0.09	0.0615
median frequency (Hz)	363 ± 127	247 ± 114	0.0529	435 ± 112	331 ± 101	0.0633	334 ± 138	241 ± 96	0.2025

median power (mV^2)	0.25 ± 0.23	0.06 ± 0.04	**0.0256**	0.18 ± 0.14	0.08 ± 0.08	0.1241	0.72 ± 0.69	0.07 ± 0.04	**0.0117**
max frequency (Hz)	166 ± 94	108 ± 31	0.1945	366 ± 247	106 ± 30	**0.0045**	258 ± 199	107 ± 46	**0.0481**
max power (mV^2)	0.45 ± 0.37	0.16 ± 0.11	**0.0334**	0.38 ± 0.36	0.16 ± 0.06	0.1491	1.14 ± 0.97	0.31 ± 0.26	**0.0240**
total power (mV^2)	121.49 ± 118.43	34.79 ± 21.41	**0.0430**	132.87 ± 113.76	66.13 ± 44.36	0.1890	268.88 ± 202.80	52.13 ± 34.27	**0.0041**

9

12-month-old	**Diaphragm**			**External Intercostal**			**Parasternal**		
	Mean ± SD	**Mean ± SD**	**Adjusted P-value**	**Mean ± SD**	**Mean ± SD**	**Adjusted P-value**	**Mean ± SD**	**Mean ± SD**	**Adjusted P-value**
Baseline	**wild-type (n=14)**	***mdx* (n=13)**		**wild-type (n=14)**	***mdx* (n=13)**		**wild-type (n=12)**	***mdx* (n=9)**	
mean frequency (Hz)	319 ± 119	220 ± 69	0.0564	200 ± 49	188 ± 51	0.9558	179 ± 52	239 ± 80	0.2543
mean power (mV^2)	0.06 ± 0.06	0.11 ± 0.11	0.5617	0.05 ± 0.04	0.10 ± 0.11	0.5138	0.28 ± 0.28	0.06 ± 0.06	0.1271
median frequency (Hz)	273 ± 159	171 ± 68	0.1540	120 ± 19	115 ± 15	0.9016	126 ± 21	187 ± 63	0.0782
median power (mV^2)	0.17 ± 0.19	0.12 ± 0.06	0.8613	0.24 ± 0.20	0.22 ± 0.17	0.9963	0.76 ± 0.76	0.09 ± 0.09	0.0604
max frequency (Hz)	90 ± 13	93 ± 27	0.9953	81 ± 13	88 ± 10	0.4773	98 ± 6	112 ± 45	0.8309
max power (mV^2)	0.29 ± 0.28	0.25 ± 0.18	0.9898	0.37 ± 0.24	0.27 ± 0.14	0.5547	0.94 ± 0.82	0.09 ± 0.08	**0.0256**
total power (mV^2)	45.89 ± 33.84	51.27 ± 39.81	0.9929	42.98 ± 30.52	28.27 ± 16.79	0.4342	96.17 ± 74.15	18.54 ± 19.10	**0.0244**
Vagotomy	**wild-type (n=12)**	***mdx* (n=12)**		**wild-type (n=12)**	***mdx* (n=12)**		**wild-type (n=10)**	***mdx* (n=8)**	
mean frequency (Hz)	331 ± 86	229 ± 56	**0.0108**	264 ± 85	265 ± 99	>0.9999	243 ± 109	330 ± 88	0.2806
mean power (mV^2)	0.05 ± 0.03	0.05 ± 0.02	>0.9999	0.04 ± 0.04	0.02 ± 0.01	0.6390	0.11 ± 0.08	0.04 ± 0.03	0.1695
median frequency (Hz)	276 ± 134	151 ± 21	**0.0323**	155 ± 63	146 ± 54	0.9949	182 ± 98	272 ± 106	0.2960
median power (mV^2)	0.14 ± 0.12	0.14 ± 0.10	>0.9999	0.17 ± 0.18	0.11 ± 0.09	0.8182	0.71 ± 0.85	0.06 ± 0.06	0.1894
max frequency (Hz)	95 ± 16	96 ± 29	>0.9999	81 ± 18	85 ± 11	0.9523	97 ± 10	159 ± 129	0.6172
max power (mV^2)	0.29 ± 0.19	0.23 ± 0.15	0.8955	0.32 ± 0.25	0.21 ± 0.14	0.6791	0.98 ± 1.00	0.11 ± 0.08	0.1176
total power (mV^2)	58.22 ± 41.98	51.74 ± 36.40	0.9908	60.04 ± 53.37	26.76 ± 12.65	0.2101	109.19 ± 87.89	22.88 ± 13.48	0.0724
HcHx	**wild-type (n=12)**	***mdx* (n=12)**		**wild-type (n=12)**	***mdx* (n=12)**		**wild-type (n=10)**	***mdx* (n=8)**	
mean frequency (Hz)	373 ± 109	214 ± 78	**0.0021**	317 ± 99	322 ± 109	>0.9999	278 ± 121	311 ± 60	0.9189
mean power (mV^2)	0.08 ± 0.06	0.04 ± 0.02	0.3087	0.08 ± 0.08	0.03 ± 0.02	0.3666	0.10 ± 0.07	0.03 ± 0.02	0.0964
median frequency (Hz)	342 ± 155	136 ± 71	**0.0030**	251 ± 138	256 ± 146	>0.9999	227 ± 153	240 ± 78	0.9990
median power (mV^2)	0.17 ± 0.16	0.10 ± 0.04	0.4582	0.14 ± 0.17	0.05 ± 0.04	0.3763	0.50 ± 0.56	0.05 ± 0.04	0.1755
max frequency (Hz)	94 ± 18	65 ± 9	**0.0020**	94 ± 18	80 ± 17	0.2359	91 ± 12	85 ± 32	0.9854
max power (mV^2)	0.32 ± 0.22	0.25 ± 0.15	0.8595	0.28 ± 0.21	0.17 ± 0.09	0.3709	0.79 ± 0.71	0.14 ± 0.09	0.0983
total power (mV^2)	83.78 ± 64.38	42.86 ± 32.28	0.2466	62.91 ± 44.47	28.47 ± 12.95	0.0905	143.22 ± 137.62	26.29 ± 17.64	0.0970

Occlusion	wild-type (n=14)	*mdx* (n=13)		wild-type (n=14)	*mdx* (n=13)		wild-type (n=12)	*mdx* (n=18)	
mean frequency (Hz)	442 ± 92	300 ± 112	**0.0061**	384 ± 81	360 ± 69	0.8843	355 ± 84	366 ± 74	0.9972
mean power (mV^2)	0.15 ± 0.10	0.08 ± 0.05	0.1622	0.10 ± 0.08	0.06 ± 0.04	0.4780	0.09 ± 0.07	0.07 ± 0.08	0.9615
median frequency (Hz)	430 ± 123	244 ± 124	**0.0024**	343 ± 116	313 ± 119	0.9445	306 ± 124	319 ± 99	0.9980
median power (mV^2)	0.19 ± 0.14	0.13 ± 0.08	0.5283	0.10 ± 0.07	0.06 ± 0.02	0.1876	0.22 ± 0.29	0.03 ± 0.02	0.2671
max frequency (Hz)	317 ± 230	95 ± 44	**0.0134**	251 ± 217	238 ± 189	0.9997	123 ± 55	156 ± 140	0.9562
max power (mV^2)	0.39 ± 0.33	0.22 ± 0.10	0.3403	0.22 ± 0.14	0.19 ± 0.07	0.9460	0.57 ± 0.58	0.21 ± 0.25	0.2943
total power (mV^2)	114.17 ± 84.60	45.47 ± 25.31	0.0546	68.90 ± 45.64	46.20 ± 22.07	0.4126	146.82 ± 151.29	49.64 ± 45.33	0.2416

10

16-month-old	Diaphragm			External Intercostal			Parasternal		
	Mean ± SD	Mean ± SD	Adjusted P-value	Mean ± SD	Mean ± SD	Adjusted P-value	Mean ± SD	Mean ± SD	Adjusted P-value
Baseline	**wild-type (n=12)**	***mdx* (n=10)**		**wild-type (n=12)**	***mdx* (n=10)**		**wild-type (n=12)**	***mdx* (n=10)**	
mean frequency (Hz)	244 ± 129	215 ± 71	0.9458	232 ± 99	197 ± 57	0.7699	158 ± 34	157 ± 50	>0.9999
mean power (mV^2)	0.05 ± 0.04	0.05 ± 0.03	0.9991	0.07 ± 0.07	0.03 ± 0.03	0.4252	0.28 ± 0.27	0.07 ± 0.04	0.1483
median frequency (Hz)	202 ± 139	153 ± 68	0.7507	149 ± 70	141 ± 45	0.9955	119 ± 16	112 ± 35	0.9565
median power (mV^2)	0.29 ± 0.39	0.10 ± 0.06	0.4839	0.20 ± 0.20	0.05 ± 0.04	0.141	0.31 ± 0.29	0.22 ± 0.18	0.9209
max frequency (Hz)	86 ± 15	103 ± 37	0.5766	93 ± 19	88 ± 8	0.9071	93 ± 27	73 ± 21	0.2349
max power (mV^2)	0.38 ± 0.41	0.18 ± 0.11	0.4593	0.30 ± 0.29	0.11 ± 0.09	0.2151	1.00 ± 1.07	0.37 ± 0.26	0.2512
total power (mV^2)	44.61 ± 33.41	25.44 ± 16.14	0.3746	36.68 ± 25.21	12.92 ± 9.20	**0.0475**	97.84 ± 96.58	45.17 ± 37.55	0.3526
Vagotomy	**wild-type (n=7)**	***mdx* (n=6)**		**wild-type (n=7)**	***mdx* (n=6)**		**wild-type (n=7)**	***mdx* (n=6)**	
mean frequency (Hz)	252 ± 102	240 ± 116	0.9994	286 ± 126	271 ± 102	0.9987	162 ± 25	191 ± 47	0.6514
mean power (mV^2)	0.09 ± 0.07	0.05 ± 0.03	0.7019	0.08 ± 0.06	0.04 ± 0.05	0.7152	0.28 ± 0.17	0.05 ± 0.03	**0.0457**
median frequency (Hz)	202 ± 115	192 ± 128	0.9998	239 ± 149	228 ± 104	0.9998	115 ± 19	112 ± 20	0.9992
median power (mV^2)	0.25 ± 0.24	0.13 ± 0.12	0.7076	0.15 ± 0.13	0.03 ± 0.03	0.2439	0.69 ± 0.57	0.21 ± 0.15	0.2466
max frequency (Hz)	91 ± 31	119 ± 49	0.6988	102 ± 15	85 ± 11	0.1684	86 ± 16	80 ± 21	0.9671
max power (mV^2)	0.39 ± 0.30	0.11 ± 0.05	0.1624	0.29 ± 0.23	0.13 ± 0.14	0.5506	0.96 ± 0.90	0.74 ± 0.68	0.9793
total power (mV^2)	60.68 ± 37.67	24.02 ± 15.02	0.1691	54.08 ± 39.16	14.73 ± 8.52	0.2089	107.68 ± 98.56	66.86 ± 54.53	0.8425
HcHx	**wild-type (n=5)**	***mdx* (n=5)**		**wild-type (n=5)**	***mdx* (n=5)**		**wild-type (n=5)**	***mdx* (n=5)**	
mean frequency (Hz)	283 ± 67	246 ± 87	0.9252	345 ± 139	318 ± 82	0.9938	261 ± 102	210 ± 32	0.8065
mean power (mV^2)	0.14 ± 0.10	0.04 ± 0.02	0.2891	0.12 ± 0.09	0.02 ± 0.01	0.2229	0.13 ± 0.12	0.08 ± 0.05	0.9326

median frequency (Hz)	232 ± 99	178 ± 100	0.8792	295 ± 194	282 ± 114	>0.9999	128 ± 12	117 ± 10	0.5818
median power (mV^2)	0.23 ± 0.13	0.04 ± 0.01	0.1454	0.13 ± 0.07	0.04 ± 0.03	0.3071	0.38 ± 0.36	0.26 ± 0.19	0.9574
max frequency (Hz)	103 ± 23	92 ± 27	0.945	103 ± 20	88 ± 43	0.9498	92 ± 11	71 ± 10	0.0627
max power (mV^2)	0.46 ± 0.41	0.10 ± 0.03	0.3817	0.28 ± 0.23	0.10 ± 0.08	0.6139	0.54 ± 0.49	0.67 ± 0.44	0.9891
total power (mV^2)	102.91 ± 90.80	29.56 ± 24.79	0.4707	66.95 ± 39.40	17.41 ± 12.71	0.2904	73.40 ± 58.79	73.03 ± 47.44	>0.9999
Occlusion	**wild-type (n=12)**	***mdx* (n=9)**		**wild-type (n=12)**	***mdx* (n=9)**		**wild-type (n=12)**	***mdx* (n=9)**	
mean frequency (Hz)	362 ± 123	255 ± 102	0.1554	420 ± 80	355 ± 111	0.4997	368 ± 108	353 ± 73	0.9926
mean power (mV^2)	0.07 ± 0.04	0.04 ± 0.02	0.3236	0.12 ± 0.09	0.02 ± 0.01	**0.0094**	0.11 ± 0.14	0.09 ± 0.09	0.9957
median frequency (Hz)	335 ± 153	205 ± 104	0.119	403 ± 114	316 ± 145	0.5001	321 ± 154	302 ± 104	0.9947
median power (mV^2)	0.10 ± 0.10	0.05 ± 0.04	0.5601	0.10 ± 0.08	0.05 ± 0.06	0.5163	0.22 ± 0.22	0.10 ± 0.10	0.3578
max frequency (Hz)	234 ± 198	131 ± 65	0.389	311 ± 267	106 ± 42	0.089	107 ± 47	132 ± 42	0.6472
max power (mV^2)	0.16 ± 0.09	0.11 ± 0.09	0.7011	0.29 ± 0.25	0.09 ± 0.08	0.0918	0.53 ± 0.60	0.41 ± 0.44	0.9699
total power (mV^2)	40.95 ± 17.98	27.78 ± 23.26	0.5711	109.78 ± 99.20	13.51 ± 5.09	**0.0252**	124.63 ± 136.37	72.16 ± 75.18	0.7374

11

5.5.3 Neuromechanical Efficiency (NME)

Figure 4 shows inspiratory pressure and respiratory EMG data represented as neuromechanical efficiency (NME) in anaesthetised wild-type and *mdx* mice during baseline, following bilateral vagotomy, during subsequent exposure to hypercapnic hypoxia (HcHx) and finally peak responses during sustained tracheal occlusion. NME for diaphragm (4A-E), EIC (4F-J), and PS (4K-O) are shown.

For NME there was a main time effect for diaphragm across all age groups ($p<0.0001$), for EIC at 4, 8, 12, and 16 months ($p<0.0001$, $p=0.0077$, $p<0.0001$, $p=0.0112$), and for PS across all age groups ($p<0.0001$, $p<0.0001$, $p<0.0001$, $p<0.0001$, $p=0.0007$). There was a main genotype effect for diaphragm at 1, 4, 8, 12 months ($p=0.0355$, $p=0.0082$, $p=0.0016$, $p=0.0111$), for EIC at 1, 4, and 16 months ($p=0.0248$, $p=0.0027$, $p=0.0020$), and for PS at 1, 4, 8, and 12 months ($p=0.0343$, $p=0.0138$, $p<0.0001$, $p=0.0250$). An interaction effect was seen for diaphragm at all age groups ($p=0.0115$, $p=0.0134$, $p<0.0001$, $p=0.0026$, $p=0.0049$), for EIC at 4 and 16 months ($p<0.0001$, $p=0.0148$), and for PS at 4, 8, 12, and 16 months ($p<0.0001$, $p=0.0014$, $p=0.0334$, $p=0.0241$). Post hoc analyses revealed a significant difference between wild-type and *mdx* mice in diaphragm at 1 month during occlusion ($p=0.0038$), at 4 months during baseline and occlusion ($p=0.0324$, $p=0.0005$), at 8 months of age during baseline and occlusion ($p=0.0286$, $p<0.0001$), at 12 months during occlusion ($p<0.0001$). There was a significant difference between wild-type and *mdx* mice for EIC at 4 months during baseline ($p<0.0001$) and at 16 months during occlusion ($p<0.0001$). Differences were also noted for PS at 1 month during baseline ($p=0.0094$), at 4 months during baseline ($p<0.0001$), at 8 months during baseline, post vagotomy, and occlusion ($p<0.0001$, $p=0.0033$, $p=0.0054$), and at 12 months during baseline ($p=0.0014$).

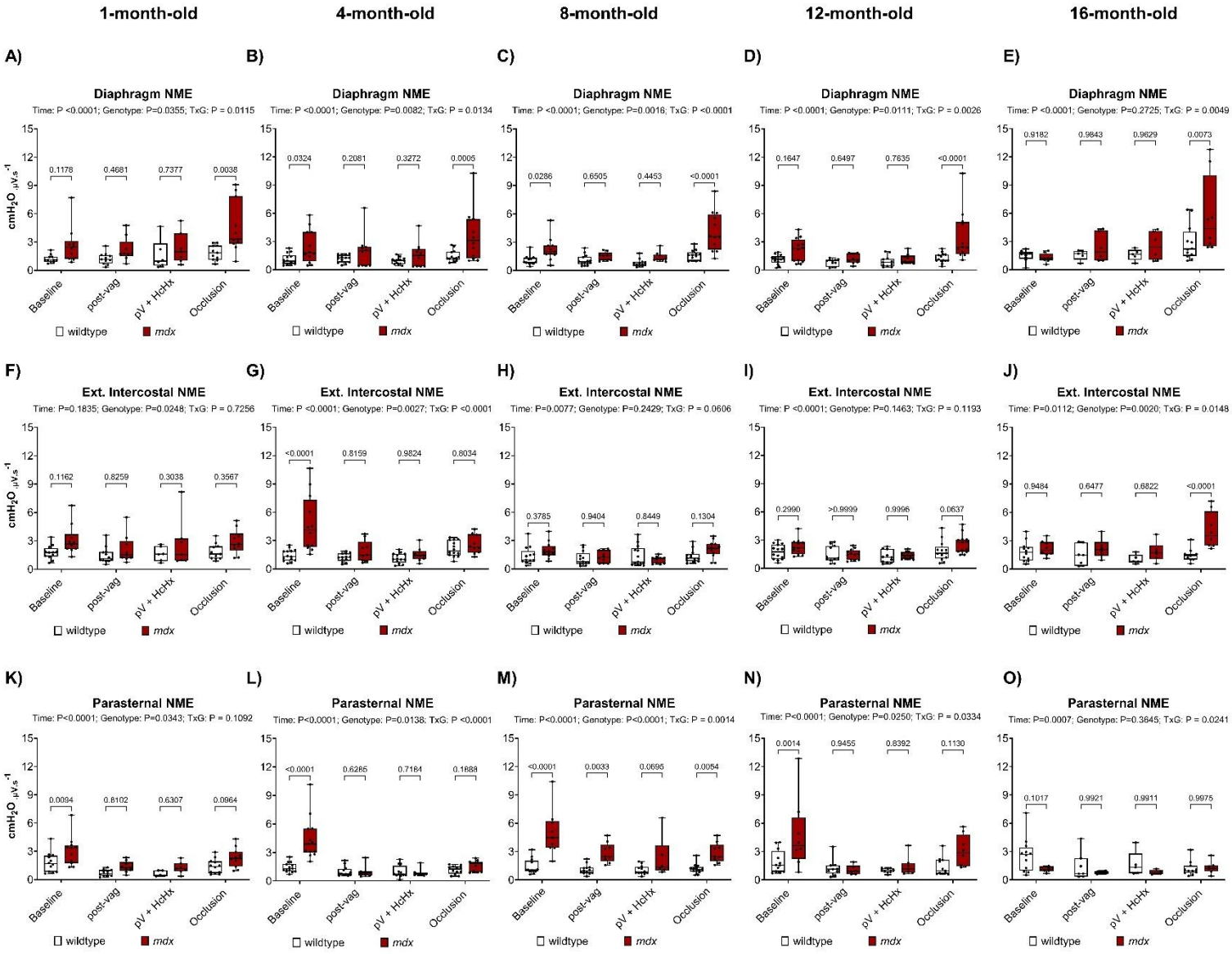
1-month-old
4-month-old
8-month-old
12-month-old
16-month-old
A)
B)
C)
D)
E)
Diaphragm NME
Time: P <0.0001; Genotype: P=0.0355; TxG: P = 0.0115
Time: P <0.0001; Genotype: P=0.0082; TxG: P = 0.0134
Time: P <0.0001; Genotype: P=0.0016; TxG: P <0.0001
Time: P <0.0001; Genotype: P=0.0111; TxG: P = 0.0026
Time: P <0.0001; Genotype: P=0.2725; TxG: P = 0.0049
0.1178
0.4681
0.7377
0.0038
0.0324
0.2081
0.3272
0.0005
0.0286
0.6505
0.4453
<0.0001
0.1647
0.6497
0.7635
<0.0001
0.9182
0.9843
0.9629
0.0073
F)
G)
H)
I)
J)
Ext. Intercostal NME
Time: P=0.1835; Genotype: P=0.0248; TxG: P = 0.7256
Time: P <0.0001; Genotype: P=0.0027; TxG: P <0.0001
Time: P=0.0077; Genotype: P=0.2429; TxG: P = 0.0606
Time: P <0.0001; Genotype: P=0.1463; TxG: P = 0.1193
Time: P=0.0112; Genotype: P=0.0020; TxG: P = 0.0148
0.1162
0.8259
0.3038
0.3567
<0.0001
0.8159
0.9824
0.8034
0.3785
0.9404
0.8449
0.1304
0.2990
>0.9999
0.9996
0.0637
0.9484
0.6477
0.6822
<0.0001
K)
L)
M)
N)
O)
Parasternal NME
Time: P<0.0001; Genotype: P=0.0343; TxG: P = 0.1092
Time: P<0.0001; Genotype: P=0.0138; TxG: P <0.0001
Time: P<0.0001; Genotype: P<0.0001; TxG: P = 0.0014
Time: P<0.0001; Genotype: P=0.0250; TxG: P = 0.0334
Time: P=0.0007; Genotype: P=0.3645; TxG: P = 0.0241
0.0094
0.8102
0.6307
0.0964
<0.0001
0.6285
0.7184
0.1888
<0.0001
0.0033
0.0695
0.0054
0.0014
0.9455
0.8392
0.1130
0.1017
0.9921
0.9911
0.9975
cmH2O µV.s-1
Baseline
post-vag
pV + HcHx
Occlusion
wildtype
mdx

Figure 5.4: Respiratory muscle NME during baseline, following bilateral vagotomy, during subsequent exposure to hypercapnic hypoxia (HcHx) and during sustained tracheal occlusion in anaesthetised wild-type and mdx mice. Group data for diaphragm (A-E), external intercostal (F-J) and parasternal intercostal (K-O) neuromechanical efficiency (NME) during baseline, post-bilateral vagotomy, subsequent exposure to hypercapnic hypoxia (HcHx) and during sustained tracheal occlusion in wild-type and mdx mice at 1, 4, 8, 12, and 16 months of age. Values are expressed as box (median, IQR and individual data points) and whisker (min to max) plots. Data were statistically compared by two-way mixed ANOVA with Šidák's multiple comparisons post hoc test. Absolute P-values for all comparisons are reported.

5.5.4 Tension-time index (TTI)

Figure 5 shows inspiratory time (5 A-E), total respiratory cycle time (5 F-J), and inspiratory pressure (5K-O) data in anaesthetised wild-type and *mdx* mice during baseline, following bilateral vagotomy, during subsequent exposure to hypercapnic hypoxia (HcHx) and finally for peak responses obtained during sustained tracheal occlusion.

For inspiratory time there was a main time effect at 1 and 8 months ($p=0.0003$, $p=0.0002$). There was a main genotype effect at 16 months ($p=0.0406$), and no interaction effect. Post hoc analyses revealed inspiratory time was equivalent between wild-type and *mdx* mice.

For total respiratory cycle time there was a main time effect at all ages ($p<0.0001$), a main genotype effect at 1 and 12 months ($p=0.0047$, $p=0.0001$), and an interaction effect at 8 and 12 months ($p=0.0427$, $p=0.00020$). Post hoc analyses revealed a significant difference between wild-type and *mdx* mice at 12 months during baseline, post vagotomy, HcHx, and occlusion ($p=0.0162$, $p=0.0323$, $p=0.0010$, $p=0.0206$) (Figure 5I).

For inspiratory pressure there was a main time effect at all ages ($p<0.0001$), a genotype effect at 1, and 12 months ($p=0.0243$, $p=0.0115$) and an interaction effect at 4 months ($p=0.0118$). Post hoc analyses revealed a significant difference between wild-type and *mdx* mice at 1 and 12 months post vagotomy ($p=0.0209$, $p=0.0285$).

Figure 6 shows the parameters that determine the TTI, which include inspiratory time divided by the total respiratory cycle time (i.e., inspiratory duty cycle) (6A-E), inspiratory pressure divided by the maximum inspiratory pressure (i.e. respiratory muscle effort) (6F-J), and the product of these two ratios which is TTI (6K-O).

For inspiratory duty cycle there was a main time effect for all age groups ($p<0.0001$, $p<0.0001$, $p<0.0001$, $p<0.0001$, $p=0.0158$), a genotype effect at 16 months ($p=0.0383$), and an interaction effect at 1 and 12 months ($p=0.0021$, 0.0014). Post hoc analyses revealed no significant differences between wild-type and *mdx* for inspiratory duty cycle.

For respiratory muscle effort there was a main time effect across all age groups ($p<0.0001$), a genotype effect at 8, 12, and 16 months ($p=0.0403$, $p=0.0483$, $p=0.0153$), and an interaction effect at 4 and 8 months ($p=0.0380$, $p=0.0219$). Post hoc analyses revealed no significant differences between wild-type and *mdx* for respiratory muscle effort.

For TTI there was a time effect for all age groups ($p<0.0001$, $p<0.0001$, $p<0.0001$, $p<0.0001$, $p=0.0277$), a genotype effect at 1 month ($p=0.0269$), and an interaction effect at 1 month ($p=0.0042$). Post hoc analyses revealed no significant differences between wild-type and *mdx* for TTI.

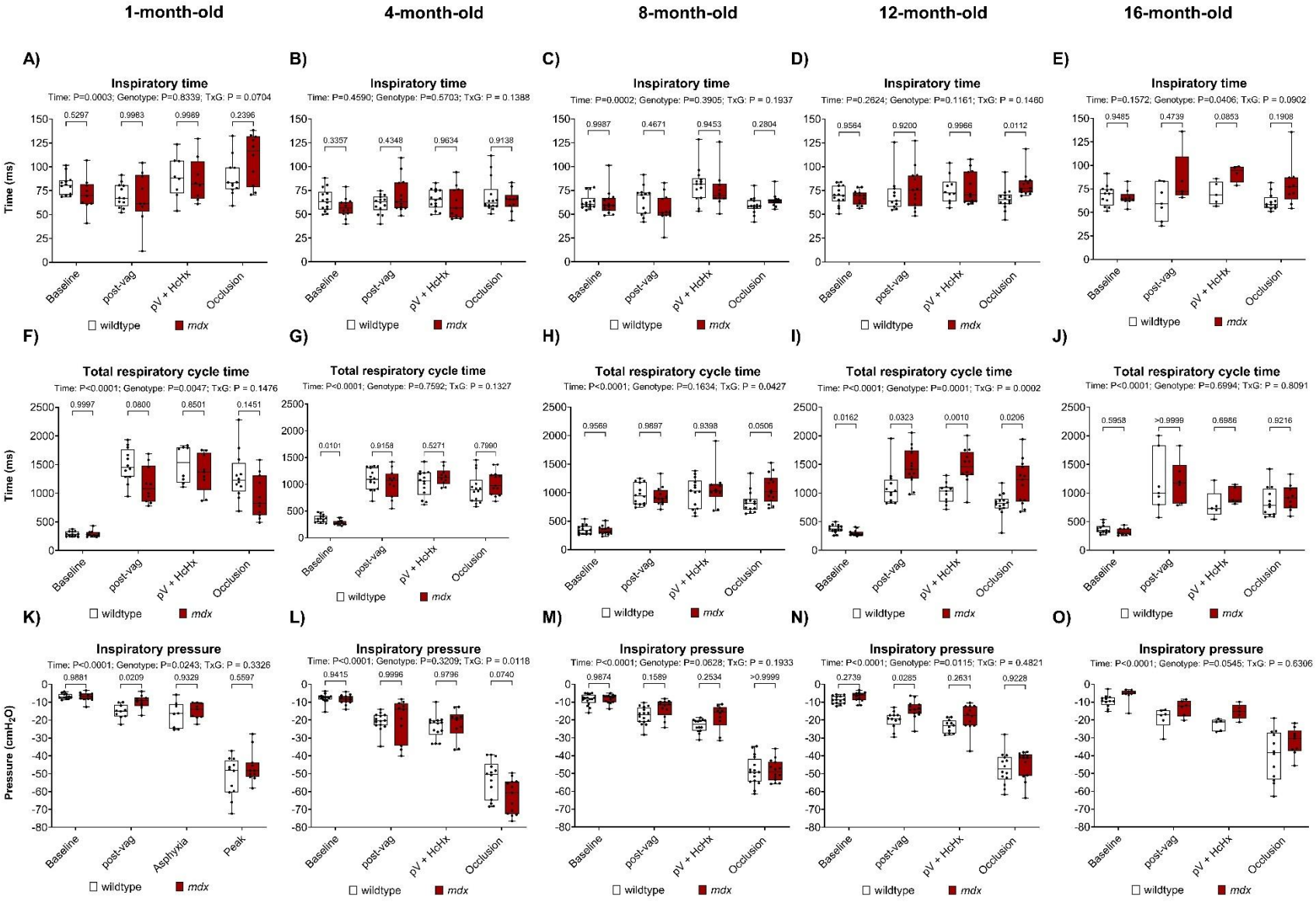
1-month-old
4-month-old
8-month-old
12-month-old
16-month-old
A)
B)
C)
D)
E)
Inspiratory time
Time: P=0.0003; Genotype: P=0.8339; TxG: P = 0.0704
Time: P=0.4590; Genotype: P=0.5703; TxG: P = 0.1388
Time: P=0.0002; Genotype: P=0.3905; TxG: P = 0.1937
Time: P=0.2624; Genotype: P=0.1161; TxG: P = 0.1460
Time: P=0.1572; Genotype: P=0.0406; TxG: P = 0.0902
0.5297 0.9983 0.9989 0.2396
0.3357 0.4348 0.9634 0.9138
0.9987 0.4671 0.9453 0.2804
0.9564 0.9200 0.9968 0.0112
0.9485 0.4739 0.0853 0.1908
Time (ms)
Baseline
post-vag
pV + HcHx
Occlusion
wildtype
mdx
F)
G)
H)
I)
J)
Total respiratory cycle time
Time: P<0.0001; Genotype: P=0.0047; TxG: P = 0.1476
Time: P<0.0001; Genotype: P=0.7592; TxG: P = 0.1327
Time: P<0.0001; Genotype: P=0.1634; TxG: P = 0.0427
Time: P<0.0001; Genotype: P=0.0001; TxG: P = 0.0002
Time: P<0.0001; Genotype: P=0.6994; TxG: P = 0.8091
0.9997 0.0800 0.8501 0.1451
0.0101 0.9158 0.5271 0.7990
0.9569 0.9697 0.9398 0.0506
0.0162 0.0323 0.0010 0.0206
0.5958 >0.9999 0.6986 0.9216
Time (ms)
Baseline
post-vag
pV + HcHx
Occlusion
wildtype
mdx
K)
L)
M)
N)
O)
Inspiratory pressure
Time: P<0.0001; Genotype: P=0.0243; TxG: P = 0.3326
Time: P<0.0001; Genotype: P=0.3209; TxG: P = 0.0118
Time: P<0.0001; Genotype: P=0.0628; TxG: P = 0.1933
Time: P<0.0001; Genotype: P=0.0115; TxG: P = 0.4821
Time: P<0.0001; Genotype: P=0.0545; TxG: P = 0.6306
0.9881 0.0209 0.9329 0.5597
0.9415 0.9996 0.9796 0.0740
0.9874 0.1589 0.2534 >0.9999
0.2739 0.0285 0.2631 0.9228
Pressure (cmH2O)
Baseline
post-vag
Asphyxia
Peak
pV + HcHx
Occlusion
wildtype
mdx

Figure 5.5: Inspiratory time, total respiratory cycle time, and inspiratory pressure during baseline, following bilateral vagotomy, during subsequent exposure to hypercapnic hypoxia (HcHx), and sustained tracheal occlusion in anaesthetised wild-type and mdx mice. Group data for inspiratory time(A-E), total respiratory cycle time (F-J) and inspiratory pressure (K-O) during baseline, post-bilateral vagotomy, subsequent exposure to hypercapnic hypoxia (HcHx), and sustained tracheal occlusion in wild-type and mdx mice at 1, 4, 8, 12, and 16 months of age. Values are expressed as box (median, IQR and individual data points) and whisker (min to max) plots. Data were statistically compared by mixed affect analysis with Šidák's multiple comparisons post hoc test. Absolute P-values for all comparisons are reported.

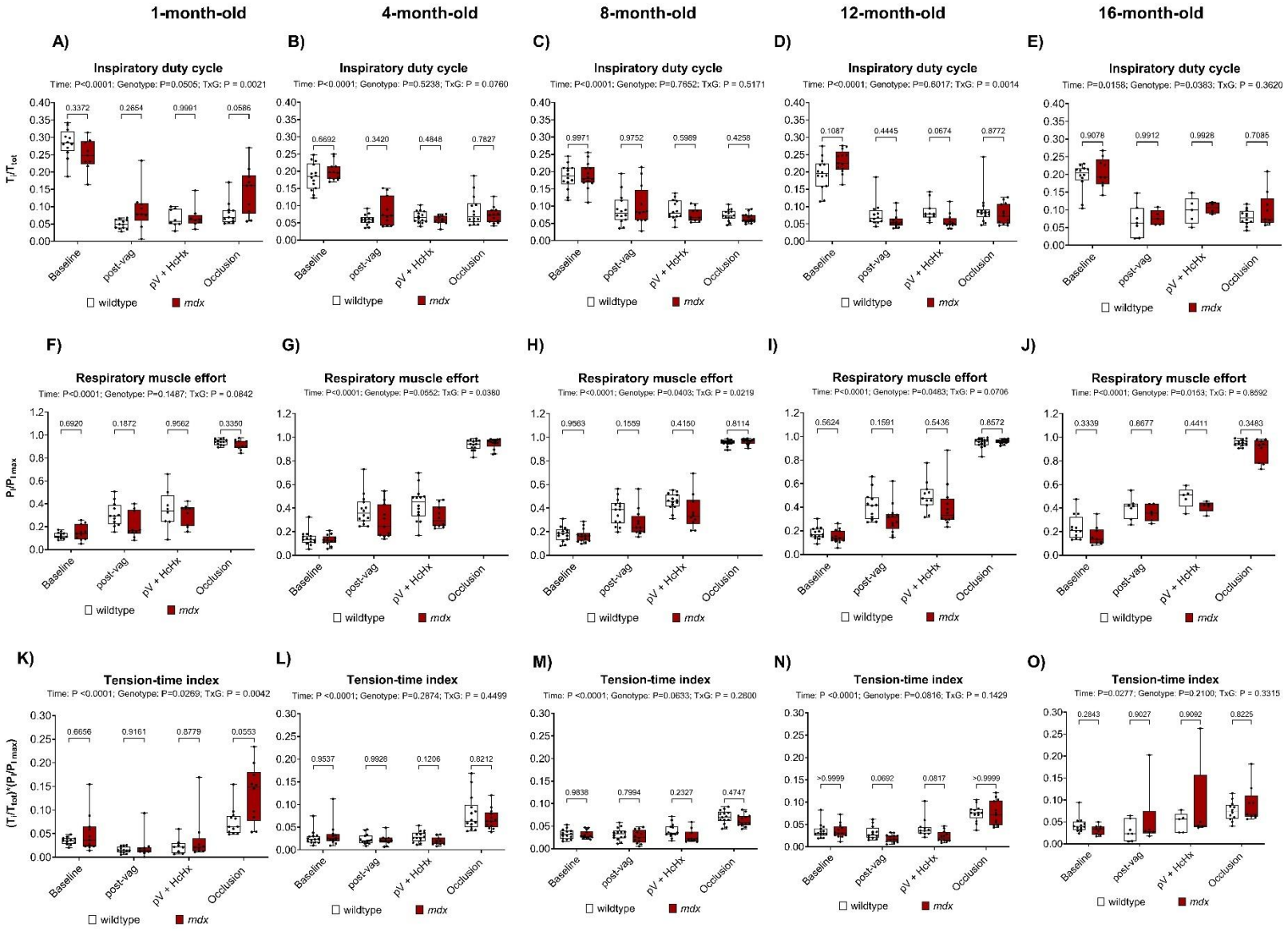
1-month-old
4-month-old
8-month-old
12-month-old
16-month-old
A)
B)
C)
D)
E)
Inspiratory duty cycle
Time: P<0.0001; Genotype: P=0.0505; TxG: P = 0.0021
Time: P<0.0001; Genotype: P=0.5238; TxG: P = 0.0760
Time: P<0.0001; Genotype: P=0.7652; TxG: P = 0.5171
Time: P<0.0001; Genotype: P=0.8017; TxG: P = 0.0014
Time: P=0.0158; Genotype: P=0.0383; TxG: P = 0.3620
T_I/T_tot
0.3372
0.2654
0.9991
0.0586
0.6692
0.3420
0.4848
0.7827
0.9971
0.9752
0.5989
0.4258
0.1087
0.4445
0.0674
0.8772
0.9078
0.9912
0.9928
0.7085
F)
G)
H)
I)
J)
Respiratory muscle effort
Time: P<0.0001; Genotype: P=0.1487; TxG: P = 0.0842
Time: P<0.0001; Genotype: P=0.0552; TxG: P = 0.0380
Time: P<0.0001; Genotype: P=0.0403; TxG: P = 0.0219
Time: P<0.0001; Genotype: P=0.0483; TxG: P = 0.0706
Time: P<0.0001; Genotype: P=0.0153; TxG: P = 0.8592
P_I/P_I max
0.6920
0.1872
0.9562
0.3350
0.9563
0.1559
0.4150
0.8114
0.5624
0.1591
0.5436
0.8572
0.3339
0.8677
0.4411
0.3483
K)
L)
M)
N)
O)
Tension-time index
Time: P <0.0001; Genotype: P=0.0269; TxG: P = 0.0042
Time: P <0.0001; Genotype: P=0.2874; TxG: P = 0.4499
Time: P <0.0001; Genotype: P=0.0633; TxG: P = 0.2800
Time: P <0.0001; Genotype: P=0.0816; TxG: P = 0.1429
Time: P=0.0277; Genotype: P=0.2100; TxG: P = 0.3315
(T_I/T_tot)*(P_I/P_I max)
0.6656
0.9161
0.8779
0.0553
0.9537
0.9926
0.1206
0.8212
0.9838
0.7994
0.2327
0.4747
>0.9999
0.0692
0.0817
>0.9999
0.2843
0.9027
0.9092
0.8225
Baseline
post-vag
pV + HcHx
Occlusion
wildtype
mdx

Figure 5.6: Inspiratory duty cycle, respiratory effort, and tension-time index (TTI) during baseline, post-bilateral vagotomy, during subsequent exposure to hypercapnic hypoxia (HcHx), and finally peak responses during sustained tracheal occlusion in anaesthetised wild-type and mdx mice. Group data for inspiratory duty cycle (A-E), respiratory muscle effort (F-J) and tension-time index (TTI) (K-O) during baseline, post-bilateral vagotomy, during subsequent exposure to hypercapnic hypoxia (HcHx), and finally peak responses during sustained tracheal occlusion in wild-type and mdx mice at 1, 4, 8, 12, and 16 months of age. Values are expressed as box (median, 25-75 percentile and individual data points) and whisker (min to max) plots. Data were statistically compared by two-way mixed ANOVA with Šidák's multiple comparisons post hoc test. Absolute P-values for all post-hoc comparisons are reported.

5.5.5 Inspiratory drive rate (IDR) and EMG rise time

Figure 7 shows the slope of inspiratory pressure (7A-E), integrated diaphragm EMG (7F-J), integrated EIC EMG (7K-O), and integrated PS EMG (7P-T) data in anaesthetised wild-type and *mdx* mice during baseline, following bilateral vagotomy, during subsequent exposure to hypercapnic hypoxia (HcHx) and for peak responses obtained during sustained tracheal occlusion.

For IDR there was a main time effect for all age groups ($p<0.0001$), a genotype effect at 1, 12, and 16 months ($p=0.0096$, $p=0.0021$, $p=0.0002$), and an interaction effect at 1 and 4 months ($p=0.0331$, $p=0.0086$). Post hoc analyses revealed a significant difference between wild-type and *mdx* during occlusion at all age groups ($p=0.0008$, $p=0.0052$, $p=0.0208$, $p=0.0007$, $p=0.0005$) (Figure 7A-E).

For diaphragm EMG rise time there was a main time effect across all ages ($p<0.0001$), a main genotype effect across all ages ($p=0.0013$, $p=0.0011$, $p=0.0023$, $p<0.0001$,

p=0.0013), and an interaction effect across all ages (p=0.0017, p=0.0282, p=0.0023, p=0.0033, p=0.0063). Post hoc analyses revealed a significant difference between wild-type and *mdx* at 1 month post vagotomy, HcHx and occlusion (p=0.0289, p=0.0192, p<0.0001), at 4 months during HcHx and occlusion (p=0.0325, p<0.0001), at 8 months during HcHx and occlusion (p=0.0113, p=0.0006), at 12 months post vagotomy, HcHx and occlusion (p=0.0447, p=0.0025, p<0.0001), and at 16 months during HcHx and occlusion (p=0.0124, p<0.0001) (Figure 7F-J).

For diaphragm EMG rise time there was a main time effect across all ages (p<0.0001), a main genotype effect at 1, 4, 12, 16 months (p=0.0047, p=0.0084, p=0.0055, p=0.0007), and an interaction effect at 1 and 16 months of age (p=0.0241, p=0.0066). Post hoc analyses revealed a significant difference between wild-type and *mdx* at 1 month of age post vagotomy and occlusion (p=0.0212, p=0.0017), at 4 months post vagotomy (p=0.0141), at 12 months during occlusion (p=0.0371), and at 16 months during occlusion (p<0.0001) (Figure 7K-O).

For PS EMG rise time there was a main time effect across all ages (p<0.0001), a main genotype effect at all ages (p=0.0039, p=0.0372, p=0.0016, p=0.0437, p=0.0389), and an interaction effect at 1, 8, and 16 months of age (p=0.0045, p=0.0090, p=0.0297). Post hoc analyses revealed a significant difference between wild-type and *mdx* at 1 month post vagotomy and occlusion (p=0.0025, p=0.0015), at 8 months post vagotomy, HcHx and occlusion (p=0.0024, p=0.0416, p=0.0005), at 12 months during occlusion (p=0.0141), and 16 months during occlusion (p=0.0013) (Figure 7P-T).

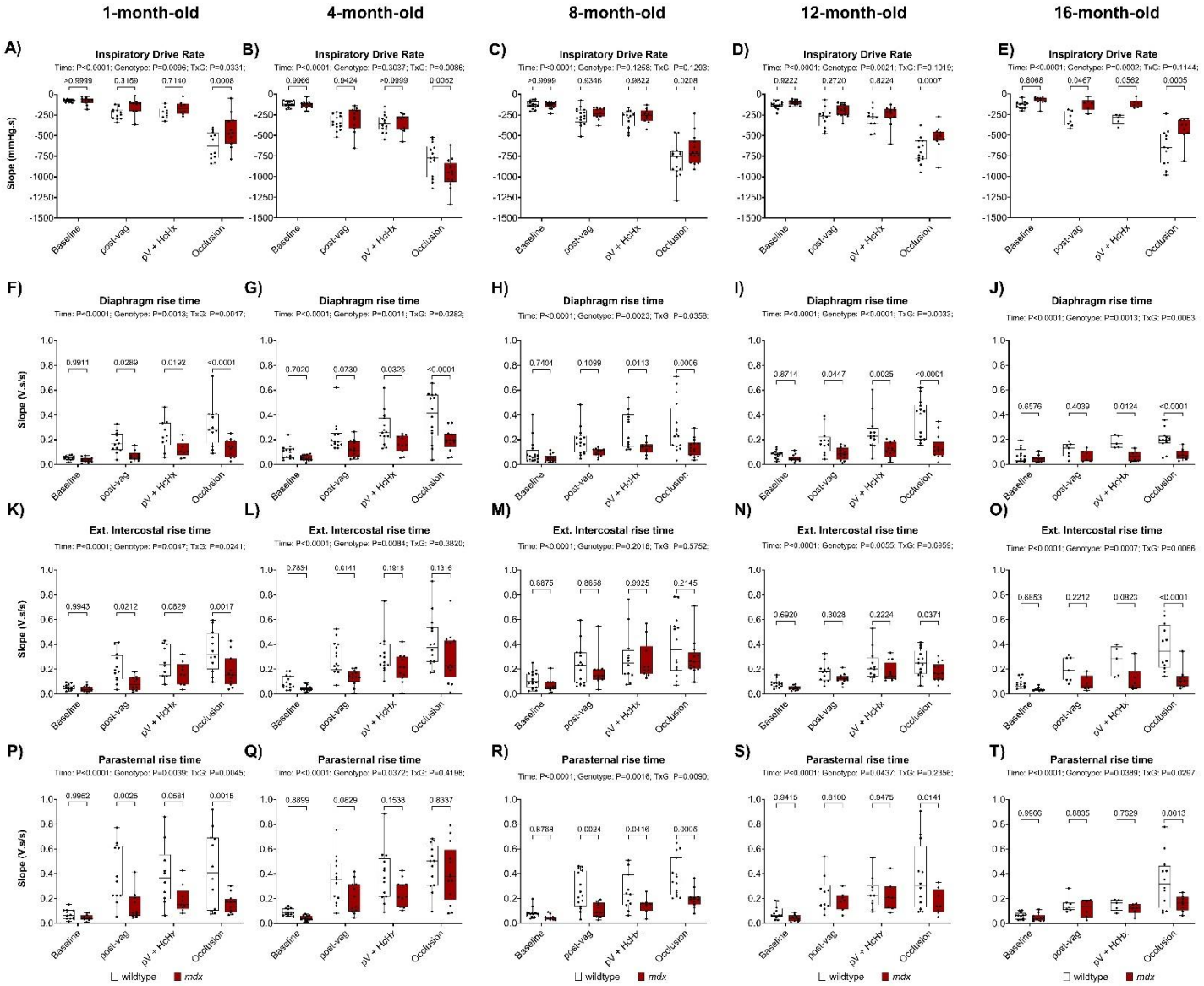
1-month-old
4-month-old
8-month-old
12-month-old
16-month-old
A)
B)
C)
D)
E)
Inspiratory Drive Rate
Slope (mmHg.s)
F)
G)
H)
I)
J)
Diaphragm rise time
Slope (V.s/s)
K)
L)
M)
N)
O)
Ext. Intercostal rise time
P)
Q)
R)
S)
T)
Parasternal rise time
Baseline
post-vag
pV + HcHx
Occlusion
wildtype
mdx

Figure 5.7: Slope of inspiratory pressure, and diaphragm, EIC, and PS integrated EMG recordings during baseline, post-bilateral vagotomy, during subsequent exposure to hypercapnic hypoxia (HcHx), and peak responses during sustained tracheal occlusion in anaesthetised wild-type and mdx mice. Group data for slope of inspiratory pressure (A-E), integrated diaphragm EMG (F-J), integrated EIC EMG (K-O), and integrated PS EMG (P-T), during baseline, post-bilateral vagotomy, during subsequent exposure to hypercapnic hypoxia (HcHx), and finally peak responses during sustained tracheal occlusion in wild-type and mdx mice at 1, 4, 8, 12, and 16 months of age. Values are expressed as box (median, 25-75 percentile and individual data points) and whisker (min to max) plots. Data were statistically compared by two-way mixed ANOVA with Šidák's multiple comparisons post hoc test. Absolute P-values for all post-hoc comparisons are reported.

5.5.6 Temporal pressure-time relationship during sustained tracheal occlusion from onset until task failure

Original inspiratory pressure recordings are shown across all behaviours in Figure 8. The black 'envelope' lines on the original traces represent the pressure-time relationship during sustained tracheal occlusion from onset until task failure.

Figure 9 shows data for area under the curve (AUC) of the pressure-time relationship determined during a single sustained tracheal occlusion from the first effort until task failure in anaesthetised wild-type and *mdx* mice. For pressure-time AUC there was no main age effect (p=0.1582), no main genotype effect (p=0.1037), but an interaction effect (p=0.0138).

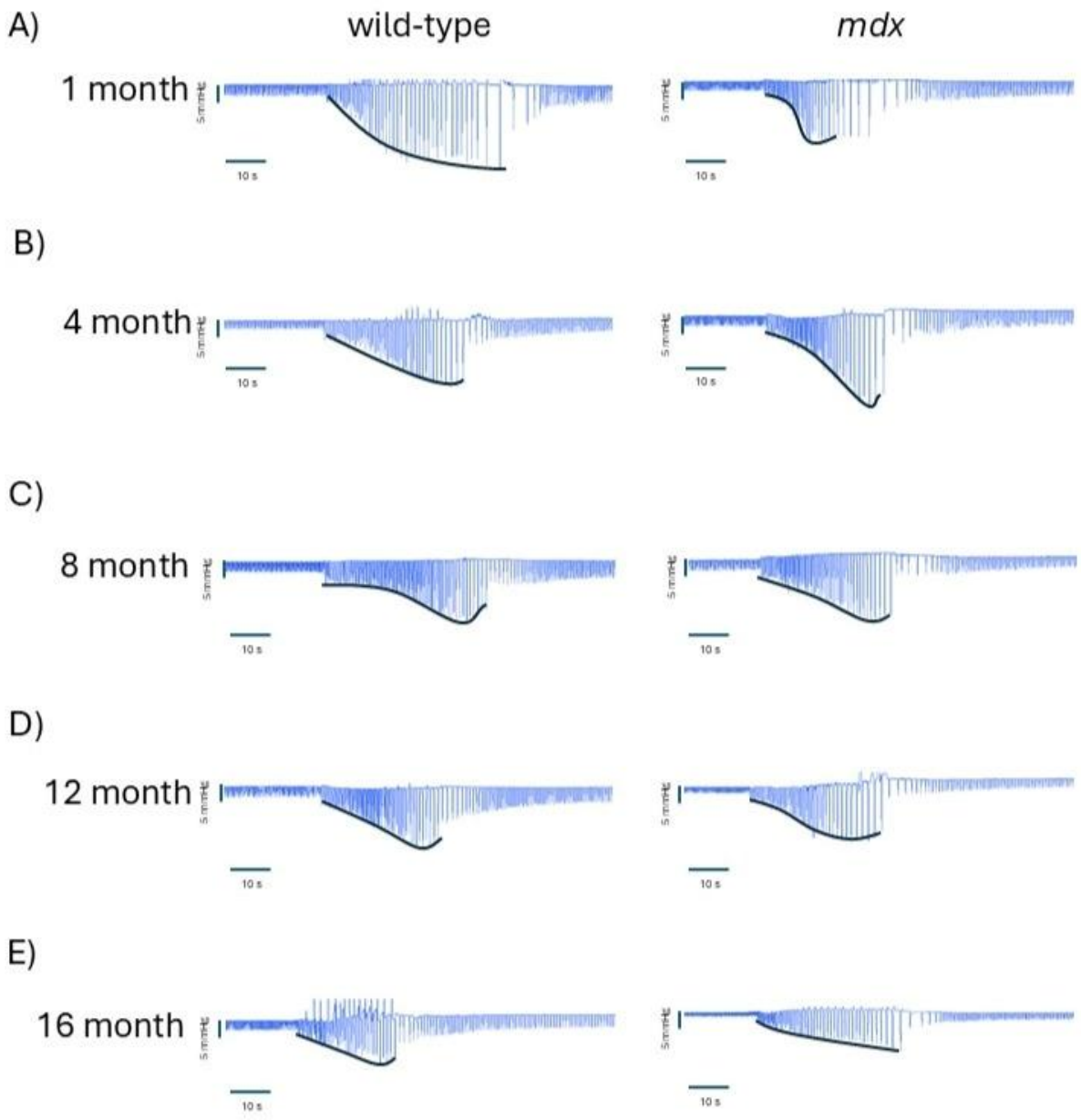

Figure 5.8: Original traces of inspiratory pressure during protracted airway occlusion for wild-type and mdx at 1 (A), 4 (B), 8 (C), 12 (D), and 16 (E) months of age. The black contour lines represent the pressure-time plots that were generated from which AUC was calculated.

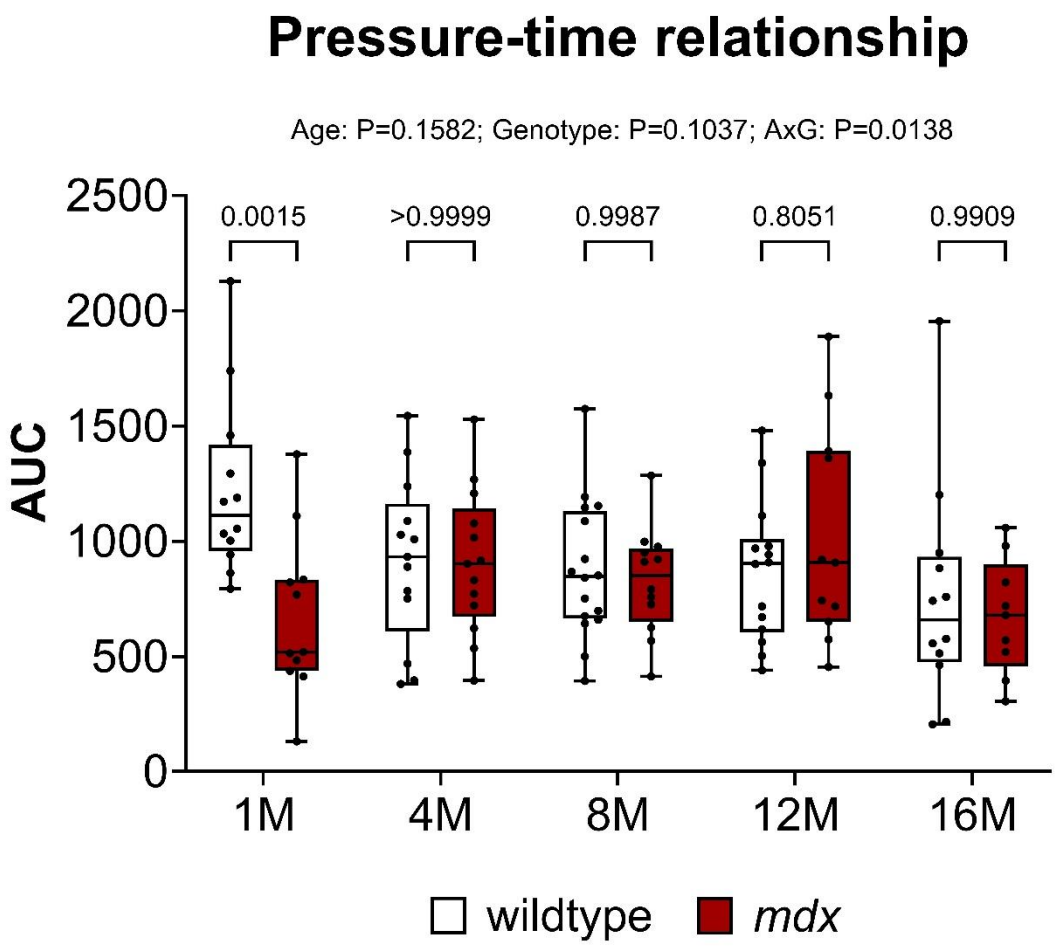

Figure 5.9: Pressure-time relationship during sustained tracheal occlusion from onset until task failure in anaesthetised wild-type and mdx mice. Group data for the area under the curve of the pressure-time relationship during a sustained tracheal occlusion in wild-type and mdx mice at 1, 4, 8, 12, and 16 months of age. Values are expressed as box (median, IQR and individual data points) and whisker (min to max) plots. Data were statistically compared by mixed two-way ANOVA analysis with Šidák's multiple comparisons post hoc test. Absolute P-values for all comparisons are reported.

5.6 Discussion

A comprehensive understanding of the respiratory phenotype across the natural history of disease in animal models of DMD is required to facilitate translational research focussed on novel therapeutics for respiratory insufficiency. The *mdx* mouse exhibits a distinct respiratory pathophysiology characterized by early-onset respiratory muscle histopathology and weakness as well as EMG deficits in primary inspiratory muscles, which persist and progress throughout the lifespan (O'Halloran et al., 2023; Slyne et al., 2025). The current study was motivated by the need to widen characterization of the respiratory phenotype in *mdx* mice to consider the extent to which the mouse model provides a platform for interventional studies. We focused on clinically relevant measures to characterise the potential utility of the *mdx* mouse as a translatable pre-clinical model of respiratory system dysfunction in DMD.

MIP is an important measure of respiratory muscle strength. Point measures of MIP are useful indirect indices of the peak strength of respiratory musculature. The trajectory of MIP across the natural history of disease in *mdx* mice demonstrates a paradoxical recovery phase in young *mdx* mice before progressive late-stage decline (O'Halloran et al., 2023; Slyne et al., 2025). In the present study, the pressure-time relationship during sustained occlusion was reduced in *mdx* mice at 1 month of age consistent with diaphragm weakness. However, this composite assessment of pressure-generating capacity was thereafter compensated and equivalent to wild-type through 16 months of age, indicating preserved capacity to sustain high demand respiratory work owing to sustained compensation by accessory muscles of breathing (O'Halloran et al.,2023; Slyne et al., 2025).

NRD is used to assess the mechanical load on the respiratory muscles (Cavalcante et al., 2024; Jolley et al., 2009; Murphy et al., 2011; Onofri et al., 2018; Reilly et al., 2011, 2016; Steier et al., 2017). Peak respiratory EMG activity is decreased in *mdx* mice, presenting in early disease, which complicates the use and interpretation of NRD since the reference maximum values for respiratory EMG activities are lower in *mdx* mice. Nevertheless, NRD was essentially equivalent across behaviours between wild-type and *mdx* mice with similar sequential increases in NRD with increased ventilatory demand suggesting preserved mechanisms of reflex motor recruitment of the respiratory musculature. The absolute levels of electrical activation, that is composite motor unit activity, in the respiratory EMGs are lower in *mdx* mice, suggesting impaired neural activation of muscle, which could relate to axonopathy which has been described in respiratory motor nerves in 12-month-old *mdx* mice (Dhindsa et al., 2020) and/or impaired neuromuscular transmission (Personius & Sawyer, 2006). Moreover, inspiratory drive rate derived from inspiratory pressure recordings were lower in *mdx* mice during maximal activation of the respiratory system during sustained tracheal occlusion, an effect seen across the natural history of the disease suggesting deficits in maximal central respiratory drive. 16-month-old *mdx* mice show an increased baseline NRD and although this is suggestive of a greater mechanical load necessitating a greater drive to breathe at baseline in *mdx*, this outcome arises due to the major decline in peak EMG activity in 16-month-old *mdx* mice i.e. absolute baseline EMG activity in *mdx* mice is less than wild-type. NRD has been assessed in COPD (Jolley et al., 2009; Murphy et al., 2011), obesity hypoventilation syndrome (Onofri et al., 2018), hypertension (Cavalcante et al., 2024) and cystic fibrosis (Reilly et al., 2011, 2013, 2016) but has not been used previously in DMD. Regular NRD testing could ostensibly facilitate progressive disease

monitoring and management in DMD but serious limitations in its use are revealed in our study in *mdx* mice, due to the complex nature of neuromuscular disease.

Continuous monitoring of skeletal muscles through intra-muscular EMG and its component frequency spectrum has been used for fatigue analysis. As a muscle becomes fatigued there is a shift towards lower frequencies of myoelectric signal power spectrum (Cifrek et al., 2009). Muscle fatigue during sustained contraction is characterised by decreases in muscle fibre conduction velocity, which directly changes the shape of the motor unit action potential (Yaar & Niles, 1992). With an increase in intra-muscular pressure during a certain level of contraction, the muscle becomes ischaemic when blood flow is stopped, and intracellular pH is decreased with the accumulation of metabolites resulting in the decrease in muscle fibre conduction velocity and the MUAP alteration and a decrease in median frequency (Brody et al., 1991). Reduction of the muscle fibre conduction velocity is one of the causes of signal power spectrum shift towards lower frequencies (Brody et al., 1991). During sustained tracheal occlusion, used in our study to elicit maximum respiratory EMG activation, for the most part MNF, MDF, and maximum frequency were equivalent between wild-type and *mdx* mice across 1-16 months indicating that despite the significant decrease in *mdx* respiratory EMG amplitudes, spectral features remain intact in the *mdx* mouse.

Similarly, comparisons can be drawn between combined EMG and frequency spectrum analysis and force. A decrease in muscle force can arise due to reduced EMG amplitude, and EMG spectrum shifts to the left (O'Halloran et al., 2023, Luttmann et al., 2000).

Pandeya et al., (2023) compared the frequency spectrum of wildtype and D2.*mdx* mice and showed greater power at higher frequency in the animals with muscular dystrophy

and fewer low frequency components, consistent with short-duration, polyphasic motor units, characteristic of myopathy which could be due to asynchronous activation of the damaged fibres. Frascarelli et al., (1988) showed in the biceps branchii of DMD boys that there was a greater amount of high frequency activity which in turn causes a shift in median frequency towards higher values. In the current study, this shift was not seen in the *mdx* diaphragm, EIC and PS muscles and MNF and MDF were shown to be equivalent indicating that the *mdx* mouse does not display the EMG spectral characteristics observed in the D2.*mdx* model and people with DMD.

Total power was calculated from AUC of the frequency spectrum. Total power has been used in place of the integral of the EMG signal as EMG rectification can alter the power spectrum of recorded EMG signals (Neto & Christou, 2010). Frascarelli et al., (1988) showed that the total power in biceps branchii muscles of DMD boys was lower than in controls. Despite significant reductions in *mdx* diaphragm EMG amplitude during maximal activation of the muscle at all age groups (1-16 months), total power was lower than wild-type values only at 4 and 8 months of age.

NME measures the efficiency of conversion of neural activation to pressure generation (Bellani et al., 2013; Jansen et al., 2018; Lozano-Garcia et al., 2019; Lozano-García et al., 2021). Apparent increases in *mdx* diaphragm NME during occlusion observed in our study most likely reflect accessory muscle contributions to preserved inspiratory pressure generation rather than improved efficiency in the diaphragm per se. Unlike the scenario in *mdx* mice, MIP declines in a linear fashion due to age-related decline in respiratory system performance compounded further by severity of disease in DMD (Fauroux et al., 2015; Khirani et al., 2014). The complexities of accessory muscle

compensation in the *mdx* mouse model obscure the potential utility of diaphragm or parasternal NME as a disease marker in *mdx* mice and most likely in DMD.

TTI is a critical measure of respiratory muscle function and risk of fatigue (Bellemare & Grassino, 1982; Dassios & Dimitriou, 2019; Miller & Mayer, 2021). Our study revealed that the *mdx* mouse differs substantively in TTI progression up to 16-months of age compared with progressive disease in human DMD. Surprisingly, TTI remains unchanged across all age groups and conditions in *mdx* mice. Moreover, no change in inspiratory duty cycle or respiratory muscle effort was observed. During increased respiratory demand, wild-type mice increase total respiratory cycle time to maintain low TTI values, which was strikingly evident during sustained occlusion with increased expiratory pause between powerful inspiratory efforts. A similar response was observed in *mdx* mice.

Hahn et al., (2009) measured $P_{0.1}$ (occlusion pressure at 0.1 seconds) and breathing patterns in 46 healthy males and 46 age-matched participants with DMD. TTI was significantly higher in DMD patients compared to age-matched controls (Hahn et al., 2009). Reduced MIP was a large contributor to the increase in TTI, consistent with the work of Mulreany and colleagues who investigated TTI in a smaller cohort of children with various neuromuscular diseases including children with DMD (Hahn et al., 2009; Mulreany et al., 2003). In patients with DMD, TTI increases beyond the threshold for fatigue and increases further, later in the disease, concurrent with the elaboration of major dysfunction (Khirani et al., 2014). TTI has emerged as a crucial measure in assessing respiratory function in DMD, offering a more comprehensive evaluation than single time point measurements of maximal inspiratory and expiratory pressures (Fauroux et al., 2015; Khirani et al., 2014). TTI has value due to its capacity to capture the

complex interplay of factors affecting respiratory muscle function, including increased respiratory load, decreased muscle strength, or a combination of both. It emerges as a robust predictor of respiratory failure in NMD patients, demonstrating strong inverse correlations with inspiratory vital capacity and peak inspiratory pressure (Miller & Mayer, 2021). Our study revealed that TTI is remarkably well maintained in *mdx* mice up to 16-months of age, notwithstanding that several other hallmark features of dystropathology are evident (e.g., diaphragm remodelling, weakness, and impaired EMG activity), again revealing a remarkably well-preserved respiratory capacity in *mdx* mice over much of the natural history of the disease.

As such, the *mdx* mouse model of DMD presents a conundrum for researchers interested in respiratory performance. There is profound diaphragm morbidity presenting early in the disease. Indeed, inspiratory pressure-generating capacity (O'Halloran et al., 2023) and pressure-time relationship (Fig. 9) are significantly impaired in 1-month-old *mdx* mice, consistent with diaphragm weakness, but respiratory performance is thereafter compensated and remarkably stable up to 16 months of age, with limited evidence of ventilatory insufficiency, and stability in several key clinically relevant indices of neuromuscular and neuromechanical performance. This raises concerns about the relevance of the model for human DMD or at least suggests that integrated respiratory assessments in *mdx* mice are best restricted to ≥16 months of age to end-stage disease (~22 months). This poses logistical challenges highlighting that alternative animal models are needed.

Other mouse models may better recapitulate the clinical respiratory phenotype such as the dystrophin-utrophin double knockout (*mdx*/*utrn*$^{-/-}$) mouse model of DMD (Hernández

Rodríguez et al., 2025). Further characterization of respiratory function in the latter and other models of DMD is necessary to fully capture disease trajectory, which also needs to be fully established in human DMD (Trucco & O'Halloran, 2025). Bridging this translational gap requires harmonization of electrophysiological biomarkers, manometry and imaging to provide a reliable and predictable platform for interventional trials.

5.7 Conclusion

Despite profound dystropathology of the major muscles of breathing, the *mdx* mouse shows remarkable compensation of respiratory system performance across much of the natural history of disease. We assessed several clinically relevant measures of respiratory neuromuscular and neuromechanical performance and found that these indices were generally equivalent in wild-type and *mdx* mice. As such, the *mdx* mouse, which is the most widely studied model of DMD, offers logistical challenges for the assessment of ventilatory insufficiency, a key hallmark of human DMD. Interventional studies focussed on breathing in *mdx* mice are best restricted to ≥16 months of age to end-stage disease (unless the focus relates to muscle form and function). Additional models that better recapitulate the progressive respiratory decline in human DMD are required, albeit that the natural history of respiratory compromise in DMD also remains to be fully characterized, revealing an opportunity for bi-directional translational research. Prioritizing EMG-integrated monitoring frameworks could enable earlier detection of respiratory decline and personalized therapeutic interventions in DMD management.

5.8 References

ATS/ERS Statement on respiratory muscle testing. (2002). American Journal of Respiratory and Critical Care Medicine, 166(4). https://doi.org/10.1164/rccm.166.4.518

Bellani, G., Mauri, T., Coppadoro, A., Grasselli, G., Patroniti, N., Spadaro, S., Sala, V., Foti, G., & Pesenti, A. (2013). Estimation of patient's inspiratory effort from the electrical activity of the diaphragm. Critical Care Medicine, 41(6). https://doi.org/10.1097/CCM.0b013e31827caba0

Bellemare, F., & Grassino, A. (1982). Effect of pressure and timing of contraction on human diaphragm fatigue. Journal of Applied Physiology, 53(5), 1190–1195. https://doi.org/10.1152/jappl.1982.53.5.1190

Birnkrant, D. J., Bushby, K., Bann, C. M., Apkon, S. D., Blackwell, A., Brumbaugh, D., Case, L. E., Clemens, P. R., Hadjiyannakis, S., Pandya, S., Street, N., Tomezsko, J., Wagner, K. R., Ward, L. M., & Weber, D. R. (2018). Diagnosis and management of Duchenne muscular dystrophy, part 1: diagnosis, and neuromuscular, rehabilitation, endocrine, and gastrointestinal and nutritional management. In The Lancet Neurology (Vol. 17, Issue 3). https://doi.org/10.1016/S1474-4422(18)30024-3

Brody, L. R., Pollock, M. T., Roy, S. H., De Luca, C. J., & Celli, B. (1991). pH-induced effects on median frequency and conduction velocity of the myoelectric signal. Https://Doi.Org/10.1152/Jappl.1991.71.5.1878, 71(5), 1878–1885. https://doi.org/10.1152/JAPPL.1991.71.5.1878

Burns, D. P., Murphy, K. H., Lucking, E. F., & O'Halloran, K. D. (2019). Inspiratory pressure-generating capacity is preserved during ventilatory and non-ventilatory

behaviours in young dystrophic mdx mice despite profound diaphragm muscle weakness. The Journal of Physiology, 597(3), 831–848. https://doi.org/10.1113/JP277443

Burns, D. P., Roy, A., Lucking, E. F., McDonald, F. B., Gray, S., Wilson, R. J., Edge, D., & O'Halloran, K. D. (2017). Sensorimotor control of breathing in the mdx mouse model of Duchenne muscular dystrophy. The Journal of Physiology, 595(21), 6653–6672. https://doi.org/10.1113/JP274792

Cavalcante, A. V. S. O. N., Fonseca, J. D., Cruz, H. R. A., Nascimento, V. F., Silva, J. P. S., Lins, C. A., Neto, S. C. G. B., & Lima, Í. N. D. (2024). Neural respiratory drive during maximal voluntary ventilation in individuals with hypertension: A case-control study. PLoS ONE, 19(6 June). https://doi.org/10.1371/journal.pone.0305044

Cifrek, M., Medved, V., Tonković, S., & Ostojić, S. (2009). Surface EMG based muscle fatigue evaluation in biomechanics. In Clinical Biomechanics (Vol. 24, Issue 4, pp. 327–340). https://doi.org/10.1016/j.clinbiomech.2009.01.010

Dassios, T., & Dimitriou, G. (2019). Determinants of inspiratory muscle function in healthy children. Journal of Sport and Health Science, 8(2), 183–188. https://doi.org/10.1016/j.jshs.2016.08.002

De Bruin, P. F., Ueki, J., Bush, A., Khan, Y., Watson, A., & Pride, N. B. (1997). Diaphragm thickness and inspiratory strength in patients with Duchenne muscular dystrophy. Thorax, 52(5), 472–475. https://doi.org/10.1136/thx.52.5.472

Deconinck, N., & Dan, B. (2007). Pathophysiology of Duchenne Muscular Dystrophy: Current Hypotheses. In Pediatric Neurology (Vol. 36, Issue 1). https://doi.org/10.1016/j.pediatrneurol.2006.09.016

Dhindsa, J. S., McCall, A. L., Strickland, L. M., Fusco, A. F., Kahn, A. F., & ElMallah, M. K. (2020). Motor axonopathies in a mouse model of Duchenne muscular dystrophy. Scientific Reports, 10(1). https://doi.org/10.1038/s41598-020-65824-1

Duan, D., Goemans, N., Takeda, S., Mercuri, E., & Aartsma-Rus, A. (2021). Duchenne muscular dystrophy. In Nature Reviews Disease Primers (Vol. 7, Issue 1). https://doi.org/10.1038/s41572-021-00248-3

Eagle, M., Baudouin, S. V., Chandler, C., Giddings, D. R., Bullock, R., & Bushby, K. (2002). Survival in Duchenne muscular dystrophy: Improvements in life expectancy since 1967 and the impact of home nocturnal ventilation. Neuromuscular Disorders, 12(10). https://doi.org/10.1016/S0960-8966(02)00140-2

Fauroux, B., Aubertin, G., Clément, A., Lofaso, F., & Bonora, M. (2009). Which tests may predict the need for noninvasive ventilation in children with neuromuscular disease? Respiratory Medicine, 103(4). https://doi.org/10.1016/j.rmed.2008.10.023

Fauroux, B., Quijano-Roy, S., Desguerre, I., & Khirani, S. (2015). The Value of Respiratory Muscle Testing in Children With Neuromuscular Disease. Chest, 147(2), 552–559. https://doi.org/10.1378/chest.14-0819

Finder, J. D. (2009). A 2009 perspective on the 2004 American thoracic society statement, “respiratory care of the patient with Duchenne muscular dystrophy.” Pediatrics, 123(SUPPL. 4). https://doi.org/10.1542/peds.2008-2952I

Finder, J. D., Birnkrant, D., Carl, J., Farber, H. J., Gozal, D., Iannaccone, S. T., Kovesi, T., Kravitz, R. M., Panitch, H., Schramm, C., Schroth, M., Sharma, G., Sievers, L., Silvestri, J. M., & Sterni, L. (2004). Respiratory care of the patient with duchenne muscular

dystrophy: ATS consensus statement. American Journal of Respiratory and Critical Care Medicine, 170(4). https://doi.org/10.1164/rccm.200307-885ST

Frascarelli, M., Rocchi, L., & Feola, I. (1988). EMG computerized analysis of localized fatigue in duchenne muscular dystrophy. Muscle & Nerve, 11(7), 757–761. https://doi.org/10.1002/mus.880110712

Gao, Q. Q., & McNally, E. M. (2015). The Dystrophin Complex: Structure, Function, and Implications for Therapy. In Comprehensive Physiology (Vol. 5, Issue 3, pp. 1223–1239). Wiley. https://doi.org/10.1002/cphy.c140048

García-Río, F., Pino, J. M., Ruiz, A., Díaz, S., Prados, C., & Villamor, J. (2003). Accuracy of noninvasive estimates of respiratory muscle effort during spontaneous breathing in restrictive diseases. Journal of Applied Physiology, 95(4), 1542–1549. https://doi.org/10.1152/japplphysiol.01010.2002

Hahn, A., Ankermann, T., Claass, A., Mann, M., Lindemann, H., & Neubauer, B. A. (2008). Non-invasive tension time index in relation to severity of disease in children with cystic fibrosis. Pediatric Pulmonology, 43(10), 973–981. https://doi.org/10.1002/ppul.20887

Hahn, A., Bach, J. R., Delaubier, A., Renardel-Irani, A., Guillou, C., & Rideau, Y. (1997). Clinical implications of maximal respiratory pressure determinations for individuals with Duchenne muscular dystrophy. Archives of Physical Medicine and Rehabilitation, 78(1). https://doi.org/10.1016/S0003-9993(97)90001-0

Hahn, A., Duisberg, B., Neubauer, B. A., Stephani, U., & Rideau, Y. (2009). Noninvasive Determination of the Tension-Time Index in Duchenne Muscular Dystrophy. American

Journal of Physical Medicine & Rehabilitation, 88(4), 322–327. https://doi.org/10.1097/PHM.0b013e3181909dfa

Hernández Rodríguez, M. Y., Biswas, D. D., Slyne, A. D., Lee, J., Scarrow, E., Abdelbarr, S. M., Daniels, H., O'Halloran, K. D., Ferreira, L. F., Gersbach, C. A., & ElMallah, M. K. (2025). Respiratory pathology in the mdx/utrn -/- mouse: A murine model for Duchenne Muscular Dystrophy (DMD). PLOS ONE, 20(2), e0316295. https://doi.org/10.1371/journal.pone.0316295

Hinton, V. J., Fee, R. J., Goldstein, E. M., & De Vivo, D. C. (2007). Verbal and memory skills in males with Duchenne muscular dystrophy. Developmental Medicine and Child Neurology, 49(2). https://doi.org/10.1111/j.1469-8749.2007.00123.x

Hoffman, E. P., Brown, R. H., & Kunkel, L. M. (1987). Dystrophin: The protein product of the duchenne muscular dystrophy locus. Cell, 51(6), 919–928. https://doi.org/10.1016/0092-8674(87)90579-4

Hudson, A. L., Jolley, C. J., Gandevia, S. C., & Butler, J. E. (2025a). Myths and methodologies: Invasive and non-invasive assessment of respiratory muscle activity in humans. Experimental Physiology. https://doi.org/10.1113/EP091526

Hudson, A. L., Jolley, C. J., Gandevia, S. C., & Butler, J. E. (2025b). Myths and methodologies: Invasive and non-invasive assessment of respiratory muscle activity in humans. Experimental Physiology. https://doi.org/10.1113/EP091526

Ishikawa, Y., Miura, T., Ishikawa, Y., Aoyagi, T., Ogata, H., Hamada, S., & Minami, R. (2011). Duchenne muscular dystrophy: Survival by cardio-respiratory interventions. Neuromuscular Disorders, 21(1). https://doi.org/10.1016/j.nmd.2010.09.006

Jansen, D., Jonkman, A. H., De Vries, H. J., Wennen, M., Elshof, J., Hoofs, M. A., Van Den Berg, M., De Man, A. M. E., Keijzer, C., Scheffer, G. J., Van Der Hoeven, J. G., Girbes, A., Tuinman, P. R., Marcus, J. T., Ottenheijm, C. A. C., & Heunks, L. (2021). Positive end-expiratory pressure affects geometry and function of the human diaphragm. Journal of Applied Physiology, 131(4). https://doi.org/10.1152/japplphysiol.00184.2021

Jansen, D., Jonkman, A. H., Roesthuis, L., Gadgil, S., Van Der Hoeven, J. G., Scheffer, G. J. J., Girbes, A., Doorduin, J., Sinderby, C. S., & Heunks, L. M. A. (2018). Estimation of the diaphragm neuromuscular efficiency index in mechanically ventilated critically ill patients. Critical Care, 22(1). https://doi.org/10.1186/s13054-018-2172-0

Jolley, C. J., Luo, Y. M., Steier, J., Reilly, C., Seymour, J., Lunt, A., Ward, K., Rafferty, G. F., Polkey, M. I., & Moxham, J. (2009). Neural respiratory drive in healthy subjects and in COPD. European Respiratory Journal, 33(2). https://doi.org/10.1183/09031936.00093408

Khirani, S., Ramirez, A., Aubertin, G., Boulé, M., Chemouny, C., Forin, V., & Fauroux, B. (2014). Respiratory muscle decline in duchenne muscular dystrophy. Pediatric Pulmonology, 49(5), 473–481. https://doi.org/10.1002/ppul.22847

Kumar Bhoi, A., Phurailatpam, D., & Tamang, J. S. (2013). Evaluation of Frequency Domain Features for Myopathic EMG Signals in Mat Lab. In Journal of Engineering Research and Applications www.ijera.com (Vol. 3). www.ijera.com

Lanini, B., Misuri, G., Gigliotti, F., Iandelli, I., Pizzi, A., Romagnoli, I., & Scano, G. (2001). Perception of dyspnea in patients with neuromuscular disease. Chest, 120(2). https://doi.org/10.1378/chest.120.2.402

Lovering, R. M., Iyer, S. R., Edwards, B., & Davies, K. E. (2020). Alterations of neuromuscular junctions in Duchenne muscular dystrophy. In Neuroscience Letters (Vol. 737). Elsevier Ireland Ltd. https://doi.org/10.1016/j.neulet.2020.135304

Lozano-Garcia, M., Estrada-Petrocelli, L., Moxham, J., Rafferty, G. F., Torres, A., Jolley, C. J., & Jane, R. (2019). Noninvasive Assessment of Inspiratory Muscle Neuromechanical Coupling during Inspiratory Threshold Loading. IEEE Access, 7, 183634–183646. https://doi.org/10.1109/ACCESS.2019.2960077

Lozano-García, M., Estrada-Petrocelli, L., Torres, A., Rafferty, G. F., Moxham, J., Jolley, C. J., & Jané, R. (2021). Noninvasive assessment of neuromechanical coupling and mechanical efficiency of parasternal intercostal muscle during inspiratory threshold loading. Sensors, 21(5). https://doi.org/10.3390/s21051781

MacBean, V., Hughes, C., Nicol, G., Reilly, C. C., & Rafferty, G. F. (2016). Measurement of neural respiratory drive via parasternal intercostal electromyography in healthy adult subjects. Physiological Measurement, 37(11). https://doi.org/10.1088/0967-3334/37/11/2050

McDouall, R. M., Dunn, M. J., & Dubowitz, V. (1990). Nature of the mononuclear infiltrate and the mechanism of muscle damage in juvenile dermatomyositis and Duchenne muscular dystrophy. Journal of the Neurological Sciences, 99(2–3). https://doi.org/10.1016/0022-510X(90)90156-H

McManus, L., De Vito, G., & Lowery, M. M. (2020). Analysis and Biophysics of Surface EMG for Physiotherapists and Kinesiologists: Toward a Common Language With

Rehabilitation Engineers. Frontiers in Neurology, 11. https://doi.org/10.3389/fneur.2020.576729

McManus, L., Hu, X., Rymer, W. Z., Suresh, N. L., & Lowery, M. M. (2017). Motor unit activity during fatiguing isometric muscle contraction in hemispheric stroke survivors. Frontiers in Human Neuroscience, 11. https://doi.org/10.3389/fnhum.2017.00569

Mhandire, D. Z., Burns, D. P., Roger, A. L., O'Halloran, K. D., & ElMallah, M. K. (2022). Breathing in Duchenne muscular dystrophy: translation to therapy. The Journal of Physiology, 600(15), 3465–3482. https://doi.org/10.1113/JP281671

Miller, K., & Mayer, O. H. (2021). Pulmonary function testing in patients with neuromuscular disease. Pediatric Pulmonology, 56(4), 693–699. https://doi.org/10.1002/ppul.25182

Mulreany, L. T., Weiner, D. J., McDonough, J. M., Panitch, H. B., & Allen, J. L. (2003). Noninvasive measurement of the tension-time index in children with neuromuscular disease. Journal of Applied Physiology, 95(3). https://doi.org/10.1152/japplphysiol.01087.2002

Murphy, P. B., Kumar, A., Reilly, C., Jolley, C., Walterspacher, S., Fedele, F., Hopkinson, N. S., Man, W. D. C., Polkey, M. I., Moxham, J., & Hart, N. (2011). Neural respiratory drive as a physiological biomarker to monitor change during acute exacerbations of COPD. Thorax, 66(7). https://doi.org/10.1136/thx.2010.151332

Neto, O. P., & Christou, E. A. (2010). Rectification of the EMG signal impairs the identification of oscillatory input to the muscle. Journal of Neurophysiology, 103(2), 1093–1103. https://doi.org/10.1152/jn.00792.2009

Ng, S. Y., & Ljubicic, V. (2020). Recent insights into neuromuscular junction biology in Duchenne muscular dystrophy: Impacts, challenges, and opportunities. In EBioMedicine (Vol. 61). Elsevier B.V. https://doi.org/10.1016/j.ebiom.2020.103032

O'Donnell, D. E., Hamilton, A. L., & Webb, K. A. (2006). Sensory-mechanical relationships during high-intensity, constant-work-rate exercise in COPD. Journal of Applied Physiology, 101(4). https://doi.org/10.1152/japplphysiol.01470.2005

O'Halloran, K. D., Maxwell, M. N., Marullo, A. L., Hamilton, C. P., Ó Murchú, S. C., Burns, D. P., Mahony, C. M., Slyne, A. D., & Drummond, S. E. (2023). Loss of compensation afforded by accessory muscles of breathing leads to respiratory system compromise in the mdx mouse model of Duchenne muscular dystrophy. The Journal of Physiology, 601(19), 4441–4467. https://doi.org/10.1113/JP285203

Onofri, A., Patout, M., Kaltsakas, G., Lhuillier, E., Mushemi-Blake, S., Arbane, G., Pengo, M. F., Marino, P., & Steier, J. (2018). Neural respiratory drive and cardiac function in patients with obesity hypoventilation syndrome following initiation of noninvasive ventilation. Journal of Thoracic Disease, 10. https://doi.org/10.21037/jtd.2017.12.129

Pandeya, S., Sanchez, B., Nagy, J. A., & Rutkove, S. B. (2023). Combining electromyographic and electrical impedance data sets through machine learning: A study in D2 -mdx and wild-type mice. Muscle & Nerve, 68(5), 781–788. https://doi.org/10.1002/mus.27963

Personius, K. E., & Sawyer, R. P. (2006). Variability and failure of neurotransmission in the diaphragm of mdx mice. Neuromuscular Disorders, 16(3), 168–177. https://doi.org/10.1016/j.nmd.2006.01.002

Reilly, C. C., Jolley, C. J., Elston, C., Moxham, J., & Rafferty, G. F. (2016). Blunted perception of neural respiratory drive and breathlessness in patients with cystic fibrosis. ERJ Open Research, 2(1). https://doi.org/10.1183/23120541.00057-2015

Reilly, C. C., Jolley, C. J., Ward, K., Macbean, V., Moxham, J., & Rafferty, G. F. (2013). Neural respiratory drive measured during inspiratory threshold loading and acute hypercapnia in healthy individuals. Experimental Physiology, 98(7). https://doi.org/10.1113/expphysiol.2012.071415

Reilly, C. C., Ward, K., Jolley, C. J., Lunt, A. C., Steier, J., Elston, C., Polkey, M. I., Rafferty, G. F., & Moxham, J. (2011). Neural respiratory drive, pulmonary mechanics and breathlessness in patients with cystic fibrosis. Thorax, 66(3). https://doi.org/10.1136/thx.2010.142646

Restrepo, R. D., Serrato, D. M., & Adasme, R. (2016). Assessing Respiratory System Mechanical Function. Clinics in Chest Medicine, 37(4), 615–632. https://doi.org/10.1016/j.ccm.2016.07.003

Samanta, K., Chatterjee, S., & Bose, R. (2022). Neuromuscular disease detection based on feature extraction from time–frequency images of EMG signals employing robust hyperbolic Stockwell transform. International Journal of Imaging Systems and Technology, 32(4), 1251–1262. https://doi.org/10.1002/ima.22709

Schmalbruch, H. (1984). Regenerated muscle fibers in duchenne muscular dystrophy: A serial section study. Neurology, 34(1). https://doi.org/10.1212/wnl.34.1.60

Sheehan, D. W., Birnkrant, D. J., Benditt, J. O., Eagle, M., Finder, J. D., Kissel, J., Kravitz, R. M., Sawnani, H., Shell, R., Sussman, M. D., & Wolfe, L. F. (2018). Respiratory

management of the patient with Duchenne muscular dystrophy. Pediatrics, 142. https://doi.org/10.1542/peds.2018-0333H

Slyne, A. D., Burns, D. P., Wöller, K., May, A., Dowd, R., Drummond, S. E., Jasionek, G., & O'Halloran, K. D. (2025). Obligatory and accessory respiratory muscle structure, function and control in early and advanced disease in the mdx mouse model of Duchenne muscular dystrophy Corresponding author. The Journal of Physiology, 1–40. https://doi.org/10.1113/JP288709#support-information-section

Smith, P. E. M., Edwards, R. H. T., & Calverley, P. M. A. (1989). Ventilation and Breathing Pattern during Sleep in Duchenne Muscular Dystrophy. Chest, 96(6), 1346–1351. https://doi.org/10.1378/chest.96.6.1346

Spinelli, A., Marconi, G., Gorini, M., Pizzi, A., & Scano, G. (1992). Control of breathing in patients with myasthenia gravis. The American Review of Respiratory Disease, 145(6). https://doi.org/10.1164/ajrccm/145.6.1359

Steier, J., Cade, N., Walker, B., Moxham, J., & Jolley, C. (2017). Observational study of neural respiratory drive during sleep at high altitude. High Altitude Medicine and Biology, 18(3). https://doi.org/10.1089/ham.2016.0097

Tagliabue, G., Ji, M., Suneby Jagers, J. V., Zuege, D. J., Kortbeek, J. B., & Easton, P. A. (2019). Distinct neural-mechanical efficiency of costal and crural diaphragm during hypercapnia. Respiratory Physiology and Neurobiology, 268. https://doi.org/10.1016/j.resp.2019.06.004

Telias, I., Damiani, F., & Brochard, L. (2018). The airway occlusion pressure (P0.1) to monitor respiratory drive during mechanical ventilation: increasing awareness of a not-

so-new problem. Intensive Care Medicine, 44(9), 1532–1535. https://doi.org/10.1007/s00134-018-5045-8

Telias, I., Junhasavasdikul, D., Rittayamai, N., Piquilloud, L., Chen, L., Ferguson, N. D., Goligher, E. C., & Brochard, L. (2020). Airway Occlusion Pressure As an Estimate of Respiratory Drive and Inspiratory Effort during Assisted Ventilation. American Journal of Respiratory and Critical Care Medicine, 201(9), 1086–1098. https://doi.org/10.1164/rccm.201907-1425OC

van Oosten, J. P., Akoumianaki, E., & Jonkman, A. H. (2024). Monitoring respiratory muscles effort during mechanical ventilation. In Current Opinion in Critical Care. Lippincott Williams and Wilkins. https://doi.org/10.1097/MCC.0000000000001229

Whitelaw, W. A., Derenne, J. P., & Milic-Emili, J. (1975). Occlusion pressure as a measure of respiratory center output cm conscious man. Respiration Physiology, 23(2). https://doi.org/10.1016/0034-5687(75)90059-6

Yaar, I., & Niles, L. (1992). Muscle fiber conduction velocity and mean power spectrum frequency in neuromuscular disorders and in fatigue. Muscle & Nerve, 15(7), 780–787. https://doi.org/10.1002/mus.880150706

Chapter 6. Summary and conclusion

6.1 Summary of Key Findings

This thesis comprehensively examined the efficacy of various therapeutic interventions targeting respiratory dysfunction in the dystrophin-deficient *mdx* mouse model of DMD. The primary focus was on evaluating the effects of acute intermittent hypoxia (AIH), chronic N-acetyl cysteine (NAC) supplementation, intermittent glucocorticoid (α-methylprednisolone, PRED) therapy, and a combined regimen of PRED and NAC (PREDNAC) on respiratory muscle performance, ventilatory parameters, and underlying muscle pathology.

The investigation into AIH revealed that, although *mdx* mice exhibited increased minute ventilation 60 minutes post-AIH, this was attributable to elevated metabolic CO_2 production rather than the manifestation of ventilatory long-term facilitation (LTF). Notably, neither wild-type nor *mdx* mice demonstrated LTF under the tested conditions, suggesting that the AIH protocol employed was insufficient to induce neuroplasticity in this context and that alternative approaches, such as isocapnic or hypercapnic AIH or repeated exposures, may be necessary to elicit LTF in dystrophic models or that other models of DMD need to be used. It is also important to acknowledge that eliciting LTF to counter ventilatory insufficiency in DMD may be counter-productive as increased neural drive may result in further contraction-induced muscle injury worsening outcomes. However, AIH may elicit beneficial changes in respiratory muscles, and this is worthy of pursuit.

Chronic NAC supplementation over three months did not yield improvements in diaphragm force-generating capacity, ventilatory function, or respiratory EMG activity in

mdx mice. Furthermore, NAC failed to reduce collagen deposition, immune cell infiltration, or alter transcriptional markers associated with inflammation and oxidative stress in the diaphragm. These findings indicate that NAC, as a standalone intervention, offers limited therapeutic benefit for respiratory muscle preservation in DMD.

The PREDNAC trial, which combined weekly α-methylprednisolone with daily NAC, similarly did not enhance diaphragm function, inspiratory pressure, or ventilatory performance in *mdx* mice. While PREDNAC reduced diaphragm inflammatory cell infiltrate, it did not rescue pressure, EMG deficits or ameliorate fibrosis, underscoring the limited efficacy of this combination therapy for respiratory muscle pathology.

Examination of the natural history of respiratory performance in the *mdx* mouse model by way of measurement of clinically relevant neuromuscular and neuromechanical indices showed that this model is not sufficient and does not match the respiratory trajectory of DMD, since it failed to show respiratory insufficiency and decline as late as 16-months into disease progression. Therefore, the model differs to the clinical scenario and poses logistical challenges since mice > 16months of age are required to study ventilatory insufficiency of end-stage disease.

6.2 Future studies

The findings from this thesis highlight several important avenues for future research in the field of DMD, particularly regarding respiratory dysfunction and therapeutic intervention. One of the most pressing needs is the adoption of preclinical models that more accurately recapitulate the rapid and progressive respiratory decline observed in human DMD. The current *mdx* mouse model, while valuable for studying early-stage

muscle pathology, maintains stable respiratory function until at least 16 months of age, which limits its utility for investigating interventions aimed at slowing or reversing respiratory deterioration within a practical experimental timeframe. Future studies should therefore explore alternative models, such as genetically modified mice with accelerated disease progression (*mdx/utrn*$^{-/-}$) or larger animal models (golden retriever), to better mirror the clinical trajectory of respiratory failure in DMD.

Additionally, the lack of respiratory efficacy observed with both antioxidant (NAC) and glucocorticoid (α-methylprednisolone) therapies—alone or in combination—suggests that targeting a single pathological pathway is insufficient to yield substantial improvements in respiratory muscle function. Future research should investigate combinatorial therapeutic strategies that simultaneously address oxidative stress, chronic inflammation, fibrosis, and neuromuscular transmission deficits. Approaches could include the use of next-generation corticosteroids with improved safety profiles, novel anti-fibrotic agents, or gene therapies that restore or compensate for dystrophin deficiency. Furthermore, the optimization of dosing regimens—such as daily versus intermittent steroid administration or repeated exposure protocols for interventions like AIH—warrants systematic evaluation to maximize therapeutic benefit while minimizing adverse effects.

Another critical area for future investigation is the refinement of clinical and preclinical outcome measures. Traditional assessments such as FVC and MIP measurements may not detect early or subtle changes in respiratory muscle performance. The integration of respiratory EMG analysis as a biomarker for neuromuscular compromise should be further validated both in animal models and patient populations to enhance early

detection and monitoring of disease progression. Additionally, the use of EMG as an independent biomarker or in tandem with other measures such as pressure could predict respiratory decline earlier in DMD boys, which could help delineate the temporal sequence of compensatory mechanisms and functional decline, informing the optimal timing for therapeutic intervention.

Finally, translating promising preclinical findings into clinical trials remains a major challenge. Future studies should prioritize the design of translational research protocols that bridge the gap between animal studies and human application, including the assessment of safety, tolerability, and efficacy of novel therapies in DMD patients. Collaborative, multi-centre trials and the use of standardized outcome measures will be essential for advancing new treatments and new biomarkers toward clinical adoption.

6.3 Critical Evaluation of Therapeutic Approaches

The *mdx* mouse can maintain stable respiratory performance up to 16 months of age, despite pronounced diaphragm pathology. This reveals that compensatory mechanisms, such as the large ventilatory reserve of the diaphragm, increased reliance on accessory respiratory muscles and altered mechanics associated with diaphragm stiffening, mask functional deficits in younger *mdx* mice. Consequently, the *mdx* model does not accurately replicate the progressive respiratory decline characteristic of human DMD, limiting its utility for preclinical studies aimed at early intervention for ventilatory insufficiency.

The lack of significant improvement with both antioxidant and glucocorticoid therapies—alone or in combination—highlights the complexity of dystrophic muscle pathology and

suggests that targeting a single pathway is insufficient to halt or reverse respiratory decline. The findings also emphasize the need for more sensitive clinical and preclinical biomarkers, such as EMG-based indices, to detect early neuromuscular compromise and guide therapeutic strategies.

6.4 Conclusions

In summary, the thesis demonstrates that neither AIH, NAC, PRED, nor their combination provide meaningful benefits to respiratory function in the *mdx* mouse model of DMD. The preserved inspiratory pressure observed in *mdx* mice, despite severe diaphragm weakness, underscores the importance of compensatory adaptations that delay overt respiratory failure. These results suggest that the *mdx* model, while valuable for studying certain aspects of muscle pathology, is limited in its capacity to model the natural history of respiratory decline seen in human DMD, particularly at early and mid-stages of disease progression.

Future research for respiratory muscle dysfunction should prioritize preclinical models that more closely mirror the accelerated respiratory deterioration observed in patients, as well as the exploration of combination therapies that target multiple pathological pathways, including oxidative stress, inflammation, and fibrosis. Recent success has been seen with Givinostat (Duvyzat™) which offers a multifactorial therapeutic approach for DMD by targeting key pathological processes such as fibrosis (reduced by 30-40% in *mdx* mice) and inflammation, while promoting muscle regeneration and function through Histone Deacetylase (HDAC) inhibition, improving muscle strength and histopathology. Micro-dystrophin gene therapy addresses DMD's genetic basis by delivering truncated

dystrophin to stabilize muscle membranes, with clinical trials showing improved motor function and dystrophin expression. Preclinical studies in *DKO* mice reveal partial diaphragm improvement and reduced fibrosis in respiratory muscles. While clinical data suggest potential respiratory benefits, further investigation in preclinical models is needed to comprehensively evaluate its efficacy on respiratory system performance and to optimize treatment strategies for translational applications.

Additionally, the integration of EMG-based biomarkers into clinical practice may enhance the early detection and monitoring of respiratory compromise, ultimately improving patient outcomes.

Overall, this work underscores the urgent need for novel therapeutic strategies and improved disease models to effectively address the respiratory complications of DMD and thereby facilitate the translation of preclinical findings into meaningful clinical advances.

Conference proceedings

1. Michael N. Maxwell, Anthony L. Marullo, Aoife D. Slyne, Eric F. Lucking, Ken D. O'Halloran (2022). Ventilatory effects of acute intermittent hypoxia in conscious dystrophic mice. *International Society for Arterial Chemoreception* meeting Lisbon, Portugal, June 2022.

2. Michael N. Maxwell & Ken D. O'Halloran (2022). Peak inspiratory pressure generation and diaphragm EMG activity in early and advanced dystrophic disease. *Europhysiology*, Copenhagen, Denmark, September 2022.

3. Michael N. Maxwell & Ken D. O'Halloran (2023). Neuromuscular coupling of obligatory respiratory muscles to inspiratory pressure is reduced in dystrophic (*mdx*) mice. *American Physiology Summit*, California, USA, April 2023.

4. Maxwell MN, Marullo AL, Slyne AD, Murphy BT, O'Halloran KD. Chronic N-acetyl cysteine treatment does not improve respiratory performance in the *mdx* mouse model of Duchenne muscular dystrophy. *UCC COMH Futures Conference*, Cork, Ireland, September 2023.

5. Maxwell MN, Marullo AL, Slyne AD, Murphy BT, O'Halloran KD. Chronic N-acetyl cysteine treatment does not improve respiratory performance in the *mdx* mouse

model of Duchenne muscular dystrophy. *PANAM Physiological Sciences Conference*, Puerto Varas, Chile, November 2023.

6. Maxwell MN, Marullo AL, Slyne AD, Murphy BT, O'Halloran KD. Characterisation of respiratory system performance in the dystrophic (*mdx*) mouse model of DMD and efficacy of chronic treatment with N-acetyl cysteine. *UCC Life Sciences Conference*, Cork, Ireland, December 2023.

7. Michael N. Maxwell, Ben T. Murphy, Fiona B. McDonald, Ken D. O'Halloran. PREDNAC DMD: Respiratory effects of combined chronic glucocorticoid and antioxidant intervention in the *mdx* mouse model of Duchenne muscular dystrophy.*16th Oxford conference: Breathing for life*, Virginia, USA, October 2024.

List of Publications during PhD training

1. **Maxwell MN**, Marullo AL, Slyne AD, Lucking EF, O'Halloran KD. Ventilatory Effects of Acute Intermittent Hypoxia in Conscious Dystrophic Mice. *Adv Exp Med Biol*. 2023; 1427:83-88. https://doi.org/10.1007/978-3-031-32371-3_9

2. **Maxwell MN**, O'Halloran KD. Alcohol and airway calibre: Does motor or muscle depression contribute to increased likelihood of obstruction? *Exp Physiol*. 2023 Mar;108(3):331-332. https://doi.org/10.1113/ep091055

3. **Michael N. Maxwell** & Ken D. O'Halloran (2023). Neuromuscular coupling of obligatory respiratory muscles to inspiratory pressure is reduced in dystrophic (*mdx*) mice. *Physiology* https://doi.org/10.1152/physiol.2023.38.S1.5732684

4. O'Halloran KD**, Maxwell MN**, Marullo AL, Hamilton CP, Ó Murchú SC, Burns DP, Mahony CM, Slyne AD, Drummond SE. Loss of compensation afforded by accessory muscles of breathing leads to respiratory system compromise in the

mdx mouse model of Duchenne muscular dystrophy. *J Physiol*. 2023 Oct;601(19):4441-4467. https://doi.org/10.1113/jp285203

5. **Maxwell MN**, Marullo AL, Valverde-Pérez E, Slyne AD, Murphy BT, O'Halloran KD. Chronic N-acetyl cysteine treatment does not improve respiratory system performance in the mdx mouse model of Duchenne muscular dystrophy. *Exp Physiol*. 2024 Aug;109(8):1370-1384. https://doi.org/10.1113/ep091862

6. Ben Murphy, **Michael Maxwell**, Anthony Marullo, Ken O'Halloran. Advanced Age Impairs the Neuromuscular Control of Peak Inspiratory Performance in Mice. *Physiology* https://doi.org/10.1152/physiol.2024.39.S1.2494

7. **Maxwell MN**, Murphy BT, McDonald FB, O'Halloran KD. Exploring the respiratory efficacy of combined chronic glucocorticoid and antioxidant interventions in the *mdx* mouse: The PREDNAC trial. *Exp Physiol*. 2025 May 26. https://doi.org/10.1113/EP092491

O’Halloran, Maxwell *et al*., 2023.

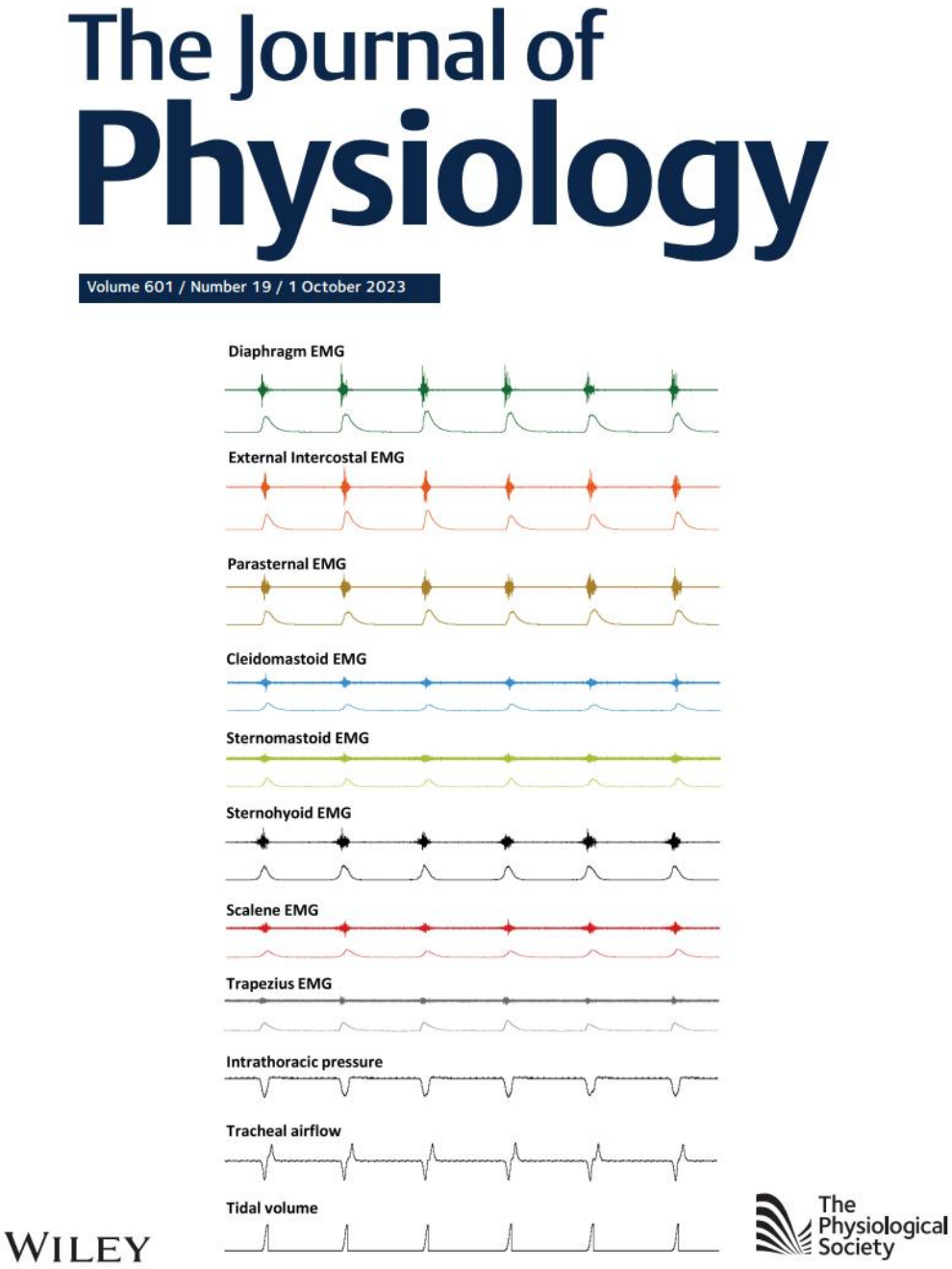

Maxwell *et al*., 2025